NICOLAUS COPERNICUS UNIVERSITY IN TORUŃ

Biotechnological potential of diacylglycerol acyltransferases from *Nannochloropsis oceanica* for boosting lipid production in diverse hosts.

Marta Saldat

Under the supervision of dr hab. Krzysztof Zienkiewicz, prof. NCU
and co-supervision of prof. Zhi-Yan (Rock) Du

A thesis submitted in fulfilment of the requirements for the degree of Doctor of Philosophy to Academia Copernicana Interdisciplinary Doctoral School

Nicolaus Copernicus University in Toruń
Toruń, January 2026

Acknowledgements

To my husband and my parents – thank you for believing in me even when I doubted myself, and for helping me through the toughest moments. I would not make it without you, Grzegorz. Mum and Dad, you are irreplaceable. To my kids, Helen and Marcel — I hope that one day you will fall in love with science, just as I did.

My sincere thanks go to dr hab. Krzysztof Zienkiewicz, prof. NCU and dr hab. Agnieszka Zienkiewicz, prof. NCU for their leadership, mentorship, and unwavering support. They were far more than supervisors; they were true mentors who shaped my scientific growth and encouraged my independence.

To all my lab colleagues – thank you for the science, the laughter, and the emotional support that kept me going. The international experience shared with colleagues from India, Thailand, Tunisia, and Iran was truly one of a kind, and it made this journey even more memorable and fulfilling. Vipul Svarup Bhatnagar, thank you for everything!

My thanks go to dr Ida Lager and dr Kamil Demski for being guardian angels during my internship abroad. Your kindness, generosity, and constant readiness to help made me feel safe, welcome, and supported far away from home. Your presence made my stay in Sweden truly beautiful and unforgettable.

I am truly grateful to all office workers at INCT and IDUB for their constant help with paperwork and administrative matters. Thank you for being supportive, responsive, and patient – your assistance saved me time, reduced stress, and made this PhD journey easier to manage.

Special thanks go to Lola, my supervisors' dog, for making all the meetings brighter and lighter. She always managed to break the ice, reduce tension, and bring smiles – turning stressful moments into easier ones.

Author's declaration

I, Marta Saldat, hereby declare that the research presented in this thesis constitutes my own original work, conducted at the Centre for Modern Interdisciplinary Technologies, Nicolaus Copernicus University in Toruń, between September 2020 and January 2026. This thesis is submitted in accordance with the regulations of the Doctoral School of *Academia Copernicana*.

I confirm that I have taken all reasonable measures to ensure the originality of this work. To the best of my knowledge, it does not breach Polish education laws, infringe upon any third-party intellectual property rights, or contain any unauthorised confidential material. This thesis has not been previously submitted, either in full or in part, for the award of any degree at this or any other institution.

AI tools were used exclusively to improve the readability and clarity of the text.

This work was supported by:

Polish National Science Centre (grant number: 2019/35/B/NZ9/01075)

Nicolaus Copernicus University Excellence Initiative – Research University (grant numbers: 4/2022/MD3, 4/2024/MD6, 20/2023/Grants4NCUStudents)

Abstract

This doctoral dissertation focuses on the analysis of the functional properties of type 2 diacylglycerol acyltransferases (DGATs type 2, also referred to as DGTTs) using the model oleaginous microalga *Nannochloropsis oceanica* CCMP1779, whose genome encodes an exceptionally rich repertoire of *DGTT* genes. Triacylglycerols (TAGs) represent the major form of carbon and energy storage in eukaryotic cells and play a key role in microalgal stress responses and metabolic flexibility. Despite the crucial role of DGTT enzymes in TAG biosynthesis, the functional basis for the extensive expansion of *DGTT* gene families in microalgae remains poorly understood.

This dissertation presents a comprehensive functional analysis of selected *DGTT* genes encoded by the genome of *N. oceanica* CCMP1779 (*NoDGTT*s) and addresses significant knowledge gaps related to their functional properties, degree of specialization, and potential applications in metabolic engineering across diverse experimental systems.

An integrated approach was employed, combining *in silico* analyses, molecular biology techniques (including heterologous gene expression and overexpression), microscopy, and analytical biochemistry, enabling systematic characterization of individual *NoDGTT* genes. Bioinformatic analyses revealed substantial structural diversity among NoDGTT isoforms, suggesting functional differentiation and distinct biotechnological potential in the context of sustainable lipid production. Functional characterization of individual NoDGTT enzymes was conducted using a genetically modified *Saccharomyces cerevisiae* H1246 strain deficient in TAG synthesis, allowing direct comparison of their capacities to promote TAG accumulation, independently of endogenous regulatory mechanisms present in microalgal cells. The results demonstrated pronounced functional differences among individual DGTT isoforms of *N. oceanica* CCMP1779 and enabled the establishment of a functional hierarchy within this enzyme family. Among the enzymes analyzed, NoDGTT12 emerged as the most efficient TAG-producing isoform. Detailed characterization of NoDGTT12 revealed a strong capacity to induce TAG biosynthesis in H1246 yeast, *N. oceanica* CCMP1779, and the model land plant *Arabidopsis thaliana*. Results obtained across these diverse experimental systems confirm that the activity of NoDGTT12 is an intrinsic property of the protein and is maintained across different cellular environments.

In summary, this dissertation significantly advances the current understanding of the functional organization of the TAG biosynthetic machinery encoded by the genome of *N. oceanica* CCMP1779. The findings provide new insights into the molecular mechanisms underlying induced TAG accumulation and identify *NoDGTT12* as a promising tool for the development of metabolic engineering strategies aimed at enhancing the production of high-energy lipids in eukaryotic cells.

Streszczenie

Niniejsza rozprawa doktorska dotyczy analizy funkcjonalnej acylotransferaz diacyloglicerolu typu 2 (DGAT typ 2, określanych również jako DGTT) z wykorzystaniem modelowej mikroalgi oleistej *Nannochloropsis oceanica* CCMP1779, której genom koduje wyjątkowo bogaty zestaw genów *DGTT*. Triacyloglicerol (TAG) stanowi główną formę magazynowania węgla i energii w komórkach eukariotycznych oraz odgrywa kluczową rolę w odpowiedzi mikroglonów na stres i ich elastyczności metabolicznej. Pomimo kluczowej roli enzymów DGTT w biosyntezie TAG, funkcjonalne podstawy tak rozległej ekspansji rodzin genów *DGTT* u mikroglonów pozostają nadal słabo poznane. Rozprawa przedstawia kompleksową analizę funkcjonalną wybranych genów *DGTT* kodowanych przez genom *N. oceanica* CCMP1779 (*NoDGTT*) oraz podejmuje próbę wypełnienia istotnych luk wiedzy dotyczących ich właściwości funkcjonalnych, stopnia specjalizacji oraz potencjału zastosowań w inżynierii metabolicznej w różnych systemach eksperymentalnych.

W niniejszej pracy zastosowano zintegrowane podejście obejmujące analizy *in silico*, techniki biologii molekularnej (w tym heterologiczną ekspresję genów oraz ich nadekspresję), mikroskopię oraz biochemię analityczną, co umożliwiło systematyczną charakterystykę poszczególnych genów *NoDGTT*. Analizy bioinformatyczne ujawniły znaczną różnorodność strukturalną izoform NoDGTT, sugerując ich funkcjonalne zróżnicowanie oraz odmienne możliwości zastosowań biotechnologicznych w kontekście zrównoważonej produkcji lipidów. Funkcjonalną charakterystykę poszczególnych enzymów NoDGTT przeprowadzono z wykorzystaniem genetycznie zmodyfikowanego szczepu *Saccharomyces cerevisiae* H1246, pozbawionego zdolności syntezy TAG, co umożliwiło bezpośrednie porównanie ich zdolności do promowania akumulacji TAG, niezależnie od endogennych mechanizmów regulacyjnych obecnych w komórkach mikroglonów.

Uzyskane wyniki wykazały wyraźne różnice funkcjonalne pomiędzy poszczególnymi izoformami DGTT *N. oceanica* CCMP1779 oraz pozwoliły na ustalenie hierarchii funkcjonalnej w obrębie tej rodziny enzymów. Spośród analizowanych enzymów NoDGTT12 wyłania się jako najbardziej efektywna izoforma produkująca TAG. Szczegółowa charakterystyka NoDGTT12 wykazała jego wysoką zdolność do indukowania biosyntezy TAG w drożdżach szczepu H1246, *N. oceanica* CCMP1779 oraz w modelowej roślinie lądowej *Arabidopsis thaliana*. Wyniki uzyskane w tak zróżnicowanych systemach eksperymentalnych potwierdzają, że aktywność NoDGTT12 jest właściwością wewnętrzną białka i pozostaje zachowana w odmiennych środowiskach komórkowych.

Podsumowując, niniejsza rozprawa istotnie pogłębia aktualny stan wiedzy na temat funkcjonalnej organizacji maszynerii biosyntezy TAG kodowanej przez genom *N. oceanica* CCMP1779. Uzyskane wyniki dostarczają nowych informacji na temat molekularnych mechanizmów leżących u podstaw indukowanej akumulacji TAG oraz identyfikują *NoDGTT12* jako obiecujące narzędzie do rozwoju strategii inżynierii metabolicznej ukierunkowanych na zwiększenie produkcji wysokoenergetycznych lipidów w komórkach eukariotycznych.

Abbreviations

ABRC	Arabidopsis Biological Resource Center
ampR	Ampicillin Resistance
APS	Ammonium Persulfate
ARE1	Acyl Transferase-Related Enzyme 1
ARE2	Acyl Transferase-Related Enzyme 2
BASTA	Glufosinate ammonium, common name
BF	Bright Field
BODIPY	Boron-dipyrromethene
BSA	Bovine Serum Albumin
CaMV	Cauliflower Mosaic Virus
Cas9	CRISPR-associated protein 9
CAT	Chloramphenicol Acetyltransferase
cDNA	Complementary strand of DNA
CFP	Cerulean Fluorescent Protein
CLSM	Confocal Laser Scanning Microscopy
CmR	Chloramphenicol Resistance
CRISPR	Clustered Regularly Interspaced Short Palindromic Repeats
DAG	Diacylglycerol
DGA1	Diacylglycerol Acyltransferase 1 (in *Saccharomyces cerevisiae*)
DGAT	Diacylglycerol Acyltransferase (type 1)
DGTT	Diacylglycerol Acyltransferase (type 2)
DMSO	Dimethyl Sulfoxide
DNA	Deoxyribonucleic Acid
dNTP	Deoxyribonucleotide Triphosphate
dsDNA	Double Strand DNA
DTT	Dithiothreitol
EB	Elution Buffer
EDTA	Ethylenediaminetetraacetic Acid
EF	Elongation Factor
EV	Empty Vector
FAME	Fatty Acid Methyl Ester
$FeCl_3$	Ferric Chloride
FFA	Free Fatty Acids
FID	Flame Ionization Detector
GAL1	Galactokinase
GC	Gas Chromatography
GFP	Green Fluorescent Protein
H_2SO_4	Sulfuric Acid
HEPES	4-(2-Hydroxyethyl)-1-Piperazineethanesulfonic Acid
HRP	Horseradish Peroxidase
K_2HPO_4	Dipotassium Phosphate
KanR	Kanamycin Resistance

KH_2PO_4	Monopotassium Phosphate
LB	Luria Broth
LD (buffer)	Laemli buffer + DTT
LD	Lipid Droplet
LiAc	Lithium Acetate
LRO1	Phospholipid:diacylglycerol Acyltransferase
MAG	Monoacylglycerol
MBOAT	Membrane Bound O-Acyltransferase
CFP	Cerulean Fluorescent Protein
MCS	Multiple Cloning Site
MgCl2	Magnesium Chloride
MnCl2	Manganese Chloride
MS (medium)	Murashige and Skoog medium
Na_2MoO_4	Sodium Molybdate
NaCl	Sodium Chloride
NaH_2PO_4	Monosodium Phosphate
$NaHCO_3$	Sodium Bicarbonate
$NaNO_3$	Sodium Nitrate
NCMA	National Center for Marine Algae and Microbiota
NoDGTT	*Nannochloropsis oceanica* DGTT
ori	Origin of Replication
PBS	Phosphate Buffered Saline
PCR	Polymerase Chain Reaction
PEG 3350	Polyethylene Glycol
PLATE solution	PEG, Lithium Acetate, Tris, and EDTA solution
PMSF	Phenylmethanesulfonyl Fluoride
PVDF	Polyvinylidene Fluoride
RNA	Ribonucleic Acid
RPM	Revolutions Per Minute
RT	Room Temperature
SC	Synthetic Complete medium
SC -URA	Synthetic Complete medium without Uracil
SD	Standard Deviation
SDS	Sodium Dodecyl Sulfate
PAGE	Polyacrylamide Gel Electrophoresis
ssDNA	Single strand DNA
TAE	Tris-Acetate-EDTA
TAG	Triacylglycerol
TBS	Tris-buffered Saline
TBST	Tris-buffered Saline with Tween-20
TFA	Total Fatty Acid
TMD	Transmembrane Domain
TLC	Thin Layer Chromatography
Tris	Tris(hydroxymethyl)aminomethane

Tris-HCl	Tris(hydroxymethyl)aminomethane Hydrochloride
UAS	Upstream Activating Sequence
Ura3 gene	Orotidine 5'-phosphate Decarboxylase coding gene
v/v	Volume per Volume
w/v	Weight per Volume
WB	Western Blot
WT	Wild Type
YPD	Yeast Peptone Dextrose
$ZnSO_4$	Zinc Sulfate

Table of contents

List of figures

List of tables

1. INTRODUCTION

1.1 Triacylglycerol as a central energy and carbon reservoir in living cells: a plant perspective

Triacylglycerols (TAGs), also known as triglycerides, are neutral lipids composed of three fatty acid chains esterified to a glycerol backbone (Figure 1).

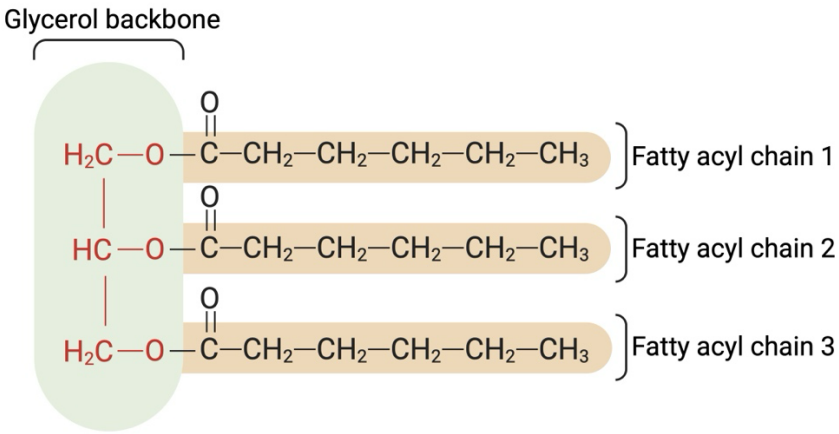

Figure 1. Structure of a TAG molecule showing a glycerol backbone esterified to three fatty acyl chains.

This simple yet highly efficient molecular structure enables dense storage of reduced carbon and chemical energy. Because fatty acids are highly reduced molecules, their oxidation yields substantially more energy per unit mass than carbohydrates or proteins. As a result, TAGs represent the most energy-rich form of biological fuel and are ideally suited for long-term storage in eukaryotic cells (Walther and Farese, 2012). Beside their role in energy storage, TAGs function as major cellular carbon reservoirs that link nutrient availability with metabolic homeostasis (Chapman et al., 2012). The ubiquity of TAG metabolism across animals, plants, fungi, and protists highlights its fundamental importance for life. Despite evolutionary divergence, the core pathways of TAG synthesis, storage, and degradation are highly conserved, reflecting strong selective pressure to maintain efficient energy management systems.

The following section is presented in the form of the review article of which I am a co-author. Although it focuses primarily on higher plants, it summarises fundamental mechanisms of TAG biosynthesis, lipid droplet (LD) formation, and regulatory integration that are conserved across photosynthetic eukaryotes. As such, it provides an essential conceptual framework for the analysis of TAG metabolism in microalgae presented in the subsequent chapters of this thesis.

Here, there and everywhere – the importance of neutral lipids in plant growth and development

dr hab. Agnieszka Zienkiewicz, prof. UMK,

mgr Marta Saldat,

dr hab. Krzysztof Zienkiewicz, prof. UMK✉

Centre for Modern Interdisciplinary Technologies, Nicolaus Copernicus University in Toruń, Toruń, Poland

https://doi.org/10.18388/pb.2021_409

✉ Corresponding author:kzienk@umk.pl

Key words: lipid droplets, triacylglycerol, neutral lipids, seed, pollen, leaf senescence.

Abbreviations: FFA – free fatty acids; DAG – diacylglycerol; DGAT – diacylglycerol acyltransferase; ER – endoplasmic reticulum; LD – lipid droplet; TAGs – triacylglycerol.

ABSTRACT

In plants, lipids serve as one of the major and vital cellular constituents. Neutral lipids reserves play an essential role in plant life cycle by providing carbon and energy equivalents for periods of active metabolism. The most common form of lipid storage are triacylglycerols (TAGs) packed into specialized organelles called lipid droplets (LDs). They have been observed in diverse plant organs and tissues, like oil seeds or pollen grains. LDs consist of a core, composed mostly of TAGs, enclosed by a single layer of phospholipids that is decorated by a unique set of structural proteins. Moreover, the recent advances in exploration of LDs proteome revealed a plethora of diverse proteins interacting with LDs. This is likely the result of a highly dynamic nature of these organelles and their involvement in many diverse aspects of cellular metabolism, tightly synchronized with plant developmental programs and directly related to plant-environment interactions. In this review, we summarize and discuss the current progress in understanding the role of LDs and their cargo during plant life cycle, with a special emphasis on developmental aspects.

INTRODUCTION

Lipids are a very diverse group of organic cellular compounds that are essential for a plethora of biological functions in prokaryotic and eukaryotic cells, including membrane structural organization, carbon and energy storage or cell signaling [1]. Such functional diversity of lipids is reflected in the variety of their structures. In plants, for the purposes of simplicity, the two most general levels of lipid classification are structural lipids and storage lipids. Internal structural lipids play a fundamental role in cell organization, being building blocks for cellular membranes [2,3]. This group of lipids is represented mostly by phospholipids, composed of two hydrophobic fatty acid "tails" esterified with glycerol and a hydrophilic "head" consisting of a phosphate group, as well as glycolipids comprised of a hydrophobic lipid "tails" and one or more hydrophilic sugar groups linked by a glycosidic bond [2].

Storage lipids in plants are represented mainly by triacylglycerols (TAGs), which at the chemical level are esters of glycerol backbone and three fatty acid tails. Such chemical structure and composition of TAGs indicates their predominant role in eukaryotic cells, namely, being a reservoir of cellular carbon and energy. In the following sections of this review, a more detailed focus will be given to this lipid class, with a special emphasis on their synthesis, metabolism and roles in diverse aspects of plant growth and development.

Most of our current knowledge on plant storage lipid metabolism in plant cells comes from studies on oilseeds, with *Arabidopsis thaliana* as the standard reference with respect to genetic and biochemical mechanisms governing TAGs synthesis and accumulation [4]. Consequently, reconstruction of these pathways in other plant species and plant cell types is mostly based on genome predictions and orthologous relationship to lipid metabolism-related genes. In plant cells, lipid synthesis starts in plastids, where fatty acids (FAs) are generated. FAs, usually as coenzyme A (CoA) conjugates (acyl-CoAs), are exported to the cytosol. They serve as essential acyl donors for synthesis of TAGs, which takes place in endoplasmic reticulum (ER) and is catalyzed by ER membrane residing enzymes [5] (Fig. 1).

Based on the orthology of the genes involved in TAG synthesis identified so far in plants, it has been shown that TAGs can be synthesized by several diverse pathways, of which the glycerol 3-phosphate (or Kennedy) pathway is the major one [4]. It starts with glycerol 3 phosphate (G-3-P), which is successively esterified with the acyl chain of acylo-CoAs. These reactions occur in a specific manner and are catalyzed by specific acyltransferases located in the ER membrane (Fig. 1). In the first reaction, catalyzed by glycerol-3-phosphate acyltransferase

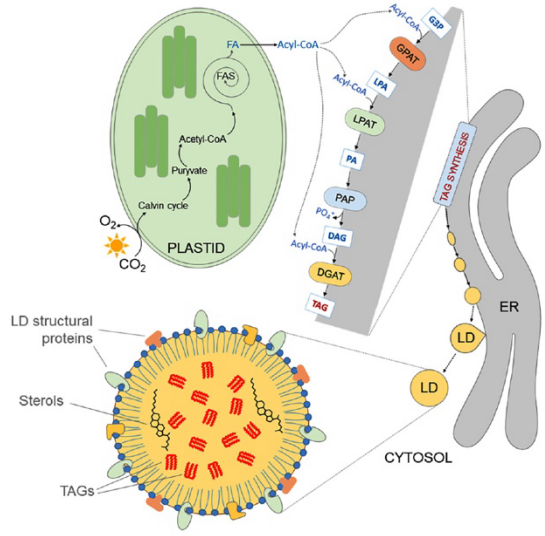

Figure 1. Major TAGs synthesis pathway and LDs formation process in plant cells. **Abbreviations**: CoA, coenzyme A; DAG, diacylglycerol; DGAT, acylCoA:diacylglycerol acyltransferase, ER, endoplasmic reticulum; FA, fatty acid; FAS, fatty acid synthase, G-3-P, glycerol-3-phosphate; GPAT, acyl-CoA:glycerol-3-phosphate acyl transferase; LD, lipid droplet; LPA, lysophosphatidic acid; LPAT, acyl-CoA:lysophosphatidic acid acyl transferase; PA, phosphatidic acid; PAP, phosphatidic acid phosphatase; TAG, triacylglycerol.

(GPAT), G-3-P is linked to acylo-CoA and lysphosphatidic acid (LPA) is generated. LPA after esterification with another acylo-CoA is converted into phosphatidic acid (PA). This reaction is catalyzed by lysophosphatidate acyltransferase (LPAT). PA can serve as a substrate for synthesis of phospholipids or TAGs. In the latter case, dephosphorylation of PA by phosphatidic acid phosphatase (PAP) leads to formation of diacylglycerol (DAG). DAGs are further converted into TAGs by acyl CoA:diacylglycerol acyltransferase (DGAT) and this reaction is considered a committed step of TAGs formation in eukaryotic cells [5,6]. TAGs synthesized at the ER membrane are then deposited in spherical organelles known in the literature under diverse terms, of which lipid droplets (LDs), oil bodies (OBs) and oleosomes are the most common [7-9]. For consistency and simplicity, the term lipid droplets (LDs) will be used in the following sections to describe them.

The assembly of LDs starts with deposition of TAGs in the ER bilayer in the form of lens. As TAGs concentration increases, membrane-packing defects caused by increasing volume of TAGs accumulating between the leaflets of the ER bilayer are recognized by amphiphatic helices of SEIPIN protein complex, which facilitates and controls the growth of LDs into the cytoplasm [10]. SEIPIN2 and SEIPIN3 proteins from *Arabidopsis thaliana* contain at their N-termini phenylalanine-acidic tract (FFAT) motifs, which serve to interact with *At*VAP27-1 protein. The interaction between these proteins is necessary for a proper formation of mature LDs, which finally detach from ER and localize to the cytosol [10]. Mature cytoplasmic LDs are spherical organelles composed of a phospholipid monolayer that surrounds a hydrophobic core of neutral lipids, mostly TAGs, with much smaller amounts of diacylglycerols (DAGs) and sterol esters [8,9]. The phospholipid monolayer of LDs is precisely spotted/speckled with specific proteins. These proteins are more or less tightly bound to the surface of LDs and play essential role in their biogenesis, trafficking and mobilization [9,11]. Large number of LDs-associated proteins has been identified in various proteomics analyses performed on LDs isolated from diverse plant tissues [8]. In order to better understand their function, LDs-associated proteins were divided into two main classes; class I includes proteins stably associating with ER membranes and recruited to the surface of LDs during their biogenesis, and class II which comprises proteins recruited to the LDs surface from the cytosol. The proteins from class I usually associate with the LDs membranes by their central hydrophobic domain, meanwhile their C- and N-termini face the cytosol. The LDs proteins of class II in turn may directly interact with other LDs-associating proteins or with LDs phospholipid monolayer through a lipid anchor [9].

Until recently LDs were considered as a simple storage compartment for TAGs, however their intense studies of the last two decades revealed that they represent highly dynamic structures, actively involved in diverse physiological processes, regulation of cellular energy homeostasis, remodeling of cellular membranes and numerous signaling pathways [12-14]. Moreover, they have been involved in diverse metabolic routes, functioning of multiple organelles as well as in many developmental programs. Below we provide a current view on the role of LDs in plant growth and development, with a special emphasis on their turnover and role in cellular metabolism in diverse types of plant cells.

SEED LIPID DROPLETS – THE BEGINNING OF AN ERA

In higher plants, the proper seed development and formation is a key to successful propagation of species. Seed formation is tightly associated with accumulation of storage compounds including starch, lipids and proteins in various parts of the seed. In oleaginous species, such as Arabidopsis, the main seed storage compounds are oils in the form of TAGs which are stored in LDs. These organelles are massively mobilized during first steps of seed germination and serve as a major carbon and energy source for a proper seedling growth prior to photosynthetic establishment.

The first basics of our current knowledge on the function and metabolism of LDs came from original studies in oilseeds, which were studied extensively decades before mammals and microbes. This includes the first efforts to characterize the proteins that specifically associate with seed LDs carried out at the end of the last century. This knowledge and advances made in the past 20 years to characterize these extraordinary organelles at molecular and cellular level showed that the function, stability and dynamics of seed LDs depends mainly on three major class I LDs-associated proteins – oleosins, caleosins, and steroleosins [5,8]. In Arabidopsis, five seed-specific types of oleosins were reported to be associated with LDs. The nomenclature of oleosins was designated based on their abundance in mature seed. Therefore, the most abundant oleosin is OLE1,

followed by OLE2, OLE3, OLE4 and OLE5 [15,16]. OLEs, as typical class I proteins, associate with the phospholipid monolayer of LDs through the hydrophobic central domain containing a proline knot motif. This domain is responsible for their anchoring in the TAGs matrix of LDs. Meanwhile, the hydrophilic C- and N-terminal domains of OLEs are exposed to the cytoplasm [17,18]. The analysis of Arabidopsis mutants demonstrated that loss of function of OLE1 leads to the accumulation of larger LDs, when compared to wild type seeds [15,19]. Interestingly, oleosins deficiency in *ole1 ole3* and *ole1 ole2* double mutants was correlated with even larger LDs than those observed in *ole1* seeds [15]. Thus, it has been proposed that oleosins are implicated in the control of the size and spatial distribution of LDs, by preventing their abnormal fusion during seed development [15,20]. Changes in the size and distribution patterns of LDs observed in oleosin mutants had small but significant impact on seed lipid content and composition [19,20]. Moreover, delay in seed germination was observed in the oleosin mutants, especially in *ole1 ole3* and *ole1 ole2*, which contained the lowest level of oleosins among all the analyzed mutants. In addition, after freezing treatment the seeds of *ole1 ole3* and *ole1 ole2* failed to germinate, unlike the wild type seeds [15]. These observations suggest that oleosins are essential not only for seeds performance but also for their freezing tolerance. Similar to oleosins, caleosins are considered as structural proteins of seed LDs. When compared to oleosins, caleosins possess larger hydrophilic N-terminal domain with a single EF-hand calcium binding motif, one central hydrophobic domain and hydrophilic C-terminus with a few potential phosphorylation sites [21-23]. Both, N- and C-termini of caleosin face the cytosol and contain heme-binding sites with conserved histidine residues. The ability of caleosins to bind calcium and the fact that they possess peroxigenase activity suggest that these proteins are probably not only simple structural proteins of LDs, but also might be involved in signaling events related to lipid metabolism. In Arabidopsis genome, eight genes encoding caleosins have been identified. These were divided into two types, L-caleosins (CLO4-CLO7) and H-caleosins (CLO1-3, CLO8), based on their molecular weight [24]. Two Arabidopsis caleosin-encoding genes – *CLO1* and *CLO2* are highly and specifically expressed during seed development, suggesting that their protein products could be implicated in the biogenesis of seed LDs [24]. Indeed, it was demonstrated that CLO1 is the most abundant caleosin present in the seeds LDs of *A. thaliana* [25]. Besides CLO1, recent analysis of LDs proteome from seeds showed also the presence of CLO2 in LDs fraction isolated at subsequent stages of their development, germination and seedling growth [26]. Trace amounts of two other caleosins – CLO3 and CLO5 were as well detected in the protein fraction of LDs isolated at two stages of seed development [26]. Interestingly, *At*CLO1 loss of function didn't affect seed germination rates, however it had an impact on LDs mobilization as the TAGs degradation in *Atclo1* mutant was delayed when compared to wild type plants [25]. Thus, it has been proposed that CLO1 plays a significant role in LDs degradation rather than in LDs formation. Steroleosins were the third, however minor, protein class identified in seed LDs proteome in *A. thaliana* [26,27]. Unlike oleosins and caleosins, steroleosins possess only two domains: an N-terminal hydrophobic region with a proline knob motif responsible for LDs-anchoring, and a soluble sterol-binding dehydrogenase/reductase domain [28]. Arabidopsis stereoleosin, known as HYDROXYSTEROID DEHYDROGENASE1 (*At*HSD1), has been identified in the proteome of LDs isolated from developing and mature seeds [26,29]. The overexpression of *AtHSD1* leads to reduced seed dormancy and seed yield when compared to wild type seeds [27,30]. No effect on fatty acids content or composition in the seeds of transgenic lines was detectable [27]. Interestingly, plants overexpressing *AtHSD1* are however hypersensitive to brassinosteroids (BR) [30]. These results, together with the fact that *AtHSD1* expression is induced by treatment with brassinolide (active BR), suggest that steroleosins might be implicated in the biosynthesis of BR and/or BR-mediated signaling pathways.

Mobilization of LDs during seed germination is associated with two main events: degradation of LDs-associated proteins and breakdown of the stored TAGs. In Arabidopsis, degradation of oleosins occurs via ubiquitin-proteasome pathway, however OLE2, OLE4 and OLE5 are degraded just prior to lipid hydrolysis, meanwhile degradation of OLE3 and OLE1 occurs at the onset of TAGs mobilization [16]. Recently, it has been demonstrated that plant UBX domain-containing protein PUX10 associates with Arabidopsis seed LDs and binds *via* its UBA domain to ubiquitinated oleosins and by its UBX domain to CELL DIVISION CYCLE 48 HOMOLOG A (CDC48A) protein [31,32]. CDC48A plays essential role in the ER-associated degradation (ERAD) of misfolded proteins [33]. This interaction has been suggested to be crucial for dislocation of oleosins from LDs and their degradation in the proteasome [31,32]. Unfortunately, there is no data available on caleosin and steroleosin degradation mechanisms during seed germination.

In turn, hydrolysis of TAGs (lipolysis) into FAs, DAGs and MAGs by TAGs lipases seems to be the major pathway of LDs breakdown in plants. SUGAR DEPENDENT1 lipase (SDP1) has been shown to play a prominent role in mobilization of TAGs from LDs in germinating Arabidopsis seeds [34,35]. *AtSDP1* loss of function leads to inhibition of TAGs breakdown and consequently hampers seedling development. The mobilization of TAGs starts when inactive form of AtSDP1 is translocated from the surface of peroxisomes into LDs surface *via* peroxules – dynamic extensions of peroxisomes [36]. FAs released from TAGs by the action of *At*SDP1 are then transported by an ATP-binding cassette (ABC) transporter (*At*PXA1) into peroxisomes where they enter β-oxidation process [37]. Until now, the analysis of diverse lipase mutants showed no significant differences in the TAGs breakdown rates during seed germination, compared to wild type plants. This fact strongly suggests that *At*SDP1 is the main TAGs lipase involved in LDs breakdown process. In addition to lipolysis, a specific autophagy-related pathway (lipophagy) may also be implicated in the hydrolysis of TAGs. Such scenario has been proposed recently based on the observations that LDs are commonly localized in the vacuolar lumen of cotyledon cells during early stages of seedling establishment [25]. Notably, the lack of LDs inside the vacuoles was observed in Arabidopsis caleosin *clo1* mutant and was correlated with a slower degradation of

TAGs during seed germination [25]. Therefore, it has been proposed that some portion of LDs might also be degraded by caleosin-dependent autophagy during seed germination. The molecular aspects of this process are currently under investigation in our laboratory.

LIPIDS IN POLLEN DEVELOPMENT – TWO FACES OF THE SAME COIN

Anthers with developing pollen grains are the second most active site in TAGs biosynthesis after the seed [38]. The central part of the anther is the loculus where microspores develop into pollen grains. The loculus is surrounded by several somatic layers. The most inner layer of the anther is tapetum, which synthesizes and secretes diverse compounds to the locular space, like nutrients, metabolites and pollen wall precursors to promote pollen development [39]. The latter group of compounds includes the specific lipidic cargo, which finally will form pollen wall and pollen coat (PC), also referred to as pollenkit or tryphine [40]. The secretion of lipidic material by tapetal cells occurs in a precisely synchronized manner, however the type of lipidic cargo and cellular structures involved in this process change during the course of pollen development [41] (Fig. 2A).

During early stages of microspore development, the tapetal cells secrete specific type of small cytosolic organelles of lipidic character termed pro-orbicules or Ubisch bodies. They have been discovered more than 150 years ago, however despite of such a long history their role in tapetal or pollen development has not yet been fully addressed. This is mainly due to their very small size and relatively strong association with the tapetal cell wall. Moreover, no Ubisch bodies have been found in the leading plant experimental models like *A. thaliana* or Brassica species, which strongly hampers their deeper biochemical or molecular characteristics. However, based on their histochemical and microscopic studies in other species, it has been suggested that Ubisch bodies seem to carry lipidic precursors of sporopollenin, which after polymerization becomes an impermeable barrier that protects developing pollen grains from physical, biological and chemical factors [40,42]. During later steps of pollen development, tapetum produces mostly lipidic components of the pollen coat, which are gradually deposited into the exine cavities (Fig. 2A–B). They are transported by two types of LDs – plastoglobuli and tapetosomes [38,40]. Plastoglobuli are synthesized by tapetal elaioplasts and have been characterized in depth in Brassica species [43,44]. They are surrounded by a membrane and carry sterol esters, which further serve as a matrix of the pollen coat. Interestingly, this is the only reported example of sterol esters occurring in a non-cytosolic location [43]. Beside sterol esters, the LDs from elaioplasts store also FFAs and membrane lipids and are equipped with specific plastid-lipid associated proteins of 31-36 kDa, depending on species [45]. In turn, tapetosomes are lipidic organelles specific to tapetal tissue and so far have also been observed and characterized mainly in Brassica species. Single tapetosome is of 2 to 3 µm in diameter and composed of many LDs, spatially associated with membranous matrix [44,46]. Such specific architecture of tapetosomes is most probably a reflection of a unique mechanism of their synthesis. During early stages of anther development, the secretory tapetal cells are rich in ER cisternae where TAGs synthesis takes place and numer-

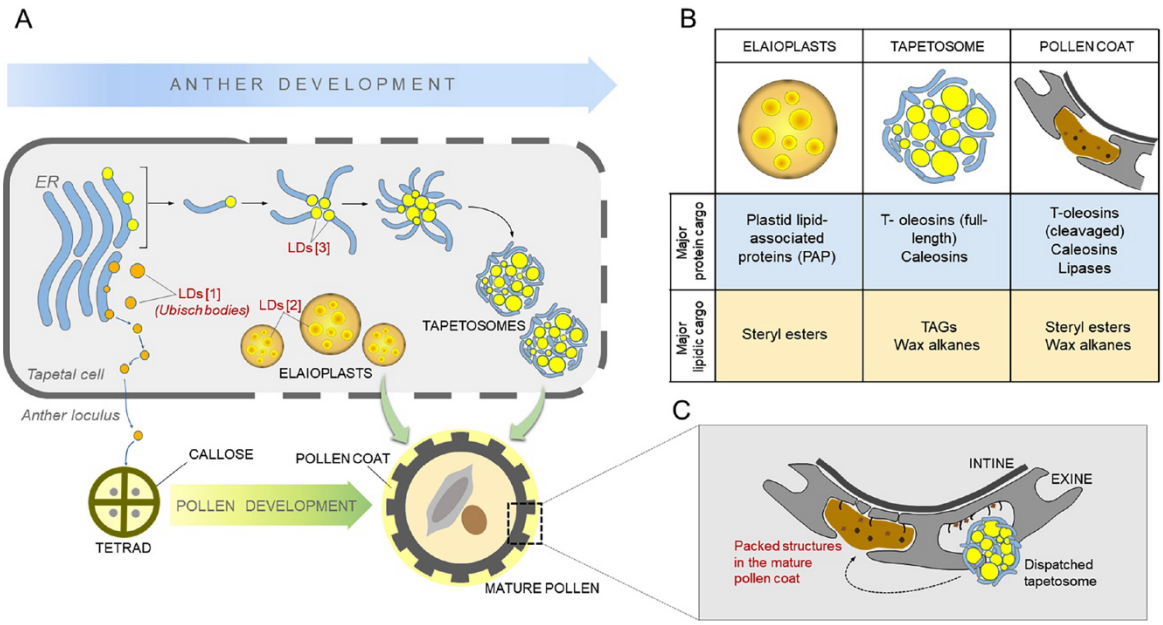

Figure 2. Neutral lipids produced by developing tapetal cells and their contribution to extracellular matrix of the pollen grain. A. Categories of LDs produced by tapetal cells during anther development and their target destinations onto developing pollen surface. B. Summary of protein and lipid cargos present in elaioplasts, tapetosomes and mature pollen coat. C. Morphological transformation of tapetosome during pollen wall development.

ous LDs are formed. This process seems to be analogical to LD synthesis in seeds [47]. However, unlike in seeds, LDs synthesis in tapetal cells is accompanied by intense production of numerous cisternae-like vesicles by the ER, which are linked together even after ER decomposition during tapetum degradation [48]. This spatial association is tough to be mediated by calreticulin and other binding proteins decorating the membrane of the cisternae-like vesicles [49]. As a result, mature tapetosome is a separate structure composed of numerous LDs embedded between a dense net of ER cisternae (Fig. 2A).

The lipidic cargo of tapetosomes includes TAGs stored in LDs as well as wax alkanes stored in ER, whereas major proteins associated with these structures contain oleosin domains, and thus are termed T-oleosins (Tapetal oleosins) [40]. T-oleosins are also known in the literature as glycine-rich proteins (GLRPs) [50] or oleo-pollenins [7]. In most of plant species, the process of pollen development and pollen coat formation is temporally correlated with tapetum degradation. As tapetum degenerates, both elaioplasts and tapetosomes are released into the anther locule targeting their lipidic and protein cargos to the pollen coat (Fig. 2A–B). The TAGs stored in LDs of tapetosomes are likely degraded as the majority of the lipids identified in the pollen coat seem to be derived from elaioplasts [40]. The pollen coat of mature pollen is composed of long- and short-chain lipids accompanied by oleosins and other specific proteins [51]. Importantly, once tapetosomes come into contact with the wall of developing pollen, T-oleosins undergo specific endoproteolytic cleavage at or near the junction between the oleosin-like domain and the remaining C-terminal domain, resulting in high variability with respect to the amino acid composition [40]. Early proteomics studies of the pollen coat in *A. thaliana* and several species of the genus Brassica revealed that pollen coat-associated T-oleosins form quite heterogenous group but their common feature is the presence of an oleosin-like domain [40]. This domain is also shared by oleosins from seeds and has been proposed to be responsible for their targeting to the tapetosomes and most probably to play a role in maintaining the structural integrity of these structures. In turn, the C-terminal domain released from the full length T-oleosins by endopeptidases after tapetal cell lysis becomes tightly associated with other pollen coat components. The cleavage itself is suggested to be one of the mechanisms enabling the change of tapetosome morphology to more compact once fused with the exine structures (Fig. 2C) [40].

Interestingly, beside T-oleosins the proteome of pollen coat from diverse plant species have been found to contain many other proteins, indicating more complex nature of this extracellular matrix. Among them, caleosins have been found in such diverse species like *A. thaliana* [52], *Brassica napus* [40], *Olea europaea* [53,54] or *Zea mays* [55]. Similar to T-oleosins, caleosins present in the pollen coat have been suggested to have tapetal origin [53,54]. Additionally, the presence of EF-hand Ca^{2+}-binding domain, several phosphorylation sites and lipid-binding domain suggests that pollen coat-associated caleosins might have a function in pollen-stigma signaling [40].

It is beyond doubt that both, lipid and lipid-associated protein components of the pollen coat have essential functions in pollen protection and pollination. It has been proposed that steryl esters delivered in LDs from elaioplasts form a waterproof barrier protecting mature pollen grain from its dehydration before reaching the receptive stigma and are directly involved in the adhesion of the pollen grain to the stigmatic surface [51]. Mutations affecting genes involved in their biogenesis lead to impaired development of tapetal elaioplasts and tapetosomes, and in consequence to deficient formation of pollen coat and strongly reduced pollen performance [56]. Moreover, disruptions in the synthesis of the pollen coat lipids, especially the long-chain ones, strongly affect pollen hydration [57,58]. The process of water uptake by the pollen is thought to be regulated not only by pollen coat lipids but also pollen coat proteins. Indeed, Mayfield and Preuss (2000) showed that mutation in the gene encoding one of the major pollen coat T-oleosins designated as GRP17-1 in *A. thaliana* results in a severe impairment of pollen hydration and consequently makes the mutants unable to pollinate [59]. More recent identification of extracellular lipases in the pollen coat proteome and their functional characteristics revealed that most probably they act together with T-oleosins to modify lipid composition at the pollen-stigma interface [52,60]. As the result, the permeability of the cuticle and the pollen coating changes, thus enabling the diffusion of water from the stigma to the desiccated pollen.

Regardless of the events occurring in the sporophytic tissues of the anther, microspores/pollen grains follow their own developmental program designed to prepare the mature pollen grains for delivering male gametes to the cells of female gametophyte. During the long period of pollen maturation, pollen grains of many plants accumulate storage lipids [38,53,54,61], likely to mobilize them during energy-demanding process of pollen tube growth [62]. The accumulation of lipids takes place mainly in the vegetative pollen cell and reaches the highest rates soon after the vacuolation stage of the microspore and leads to gradual increase of LDs number, with the maximum at pollen maturity [53,54,63]. Such pattern of lipid accumulation in developing pollen grains seems to be rather common for flowering plants, as it has been observed in such diverse species like Brassica [64], Arabidopsis [65], tobacco [66], olive [53,61] or lily [67]. The lipid synthesis and accumulation occurring during pollen development is crucial for normal pollen development as mutations of the key genes involved in TAG biosynthesis result in male sterility of plants. Zhang et al. (2009) showed that double knockout mutation in the genes encoding major TAG-producing enzymes – phosphatidyl:diacylglycerol acyltransferase 1 (PDAT1) and diacylglycerol acyltransferase 1 (DGAT1), results not only in a strong reduction of pollen LDs pool but also in abortion of around 50% of pollen grains soon after microspore mitosis. Interestingly, the abnormal pollen grains deficient in LDs had normal extracellular lipids. These results confirm that the precursors of extracellular pollen lipids are determined by the sporophytic tapetum and indicate that internal pollen lipids are determined by expression of the haploid genome of pollen [68].

In developing pollen, the synthesis of TAGs and LDs biogenesis likely takes place in specialized domains of ER. Indeed, pollen LDs were often found in the direct contact with ER cisternae [54]. Thus, the cellular mechanisms of LDs synthesis in pollen cells seems to be similar to those of oilseeds. This is suggested not only by their close spatial relationship with ER cisternae but also by the identification of pollen specific counterparts of seed LDs-associated proteins – oleosins and caleosins [53,67,69,70]. No pollen-specific steroleosin has been however found in LDs purified from pollen grains. Expression of oleosin-encoding genes has been confirmed in microspores/pollen grains of *A. thaliana* [69] and lily [67]. In turn, pollen specific caleosin proteins have been described in lily [70], olive [53,54] and more recently in cycas [71] and pine [72]. Our studies in olive showed also that the pollen specific caleosin is expressed mainly in the vegetative cell and that its levels gradually increase during pollen maturation, reaching the highest levels at pollen maturity, concurrently with the number of LDs [54]. These observations suggest that, similar to the seed caleosin, the pollen inner caleosin may also be involved in LDs biogenesis during pollen maturation. On the other hand, pollen oleosins and caleosins seem to be slightly different from their seed counterparts at molecular level as they are of different size. However, to date, no knockout mutants affected in these genes have been published to elucidate the function of the corresponding proteins in pollen development and performance.

By analogy to seeds, LDs stored in mature pollen serve most probably as a major energy and carbon source for a rapid pollen tube growth. This assumption is supported by a gradual decrease of LDs number just after pollen hydration and during pollen tube growth, likely illustrating the process of their mobilization [53,62]. As the rapid elongation of the pollen tube demands energy production and intense biosynthetic capacity [73], the TAGs stored in pollen LDs would serve not only as energy-rich substrate but also as building blocks for intense membrane synthesis [53,62,74]. The studies on LDs metabolism in germinating pollen and during pollen tube growth are however few and fragmentary. Our observations in olive showed that LDs mobilization in the pollen grain seems to be triggered just right after its hydration. This process begins from relocation of LDs into a close proximity to the aperture of hydrated pollen grain and their entering into the emerging pollen tube once the germination process starts [53,61,62]. During the whole course of pollen tube growth, the pool of LDs gradually decreases until their complete mobilization.

The cellular aspects of LDs mobilization in germinating pollen have been studied only in a few species. In olive growing pollen tubes LDs seem to spatially interact with ER structures [75], whereas in lily they were also found to be present in the vacuoles [70]. Such spatial distribution suggests that both, ER and vacuoles might be involved in LDs degradation. Interestingly, the fusion of LDs have been reported for germinating seeds of *A. thaliana* and suggested as one of the mechanisms of LDs mobilization [25]. The authors proposed also caleosin as the key player in this process. Our studies in olive growing pollen tubes indicated also that caleosin could be directly involved in LDs degradation in germinating pollen [53]. Our hypothesis is based on the presence of caleosin in both, the intracellular membranes and in the tonoplast, as well as on a gradual depletion of its pool during pollen tube growth, concurrently with decreasing number of LDs.

The molecular events accompanying LDs degradation during pollen germination and pollen tube growth are yet not fully deciphered. Studies on the enzymatic machinery directly involved in mobilization of pollen LDs are limited only to a few species, including *A. thaliana*, tobacco and olive. *At*SDP1L was the first identified putative TAG lipase of particularly high expression in mature pollen grains of *A. thaliana*, suggesting its involvement in LDs breakdown upon pollen germination [35]. More recently, Müller and Ischebeck (2018) showed that other TAG lipase – *At*OBL1 localizes to LDs in pollen tubes and its mutation results in a slower pollen tube growth *in vivo* in Arabidopsis [76]. LD-associated lipase, phospholipase A and lipoxygenase activities were also found on the surface of LDs present in germinating pollen and in growing pollen tubes of olive [62,77]. However, meanwhile phospholipase A activity was observed on the LDs surface at pollen maturity and after germination, the lipase activity and lipoxygenase protein were associated with LDs only when pollen germination is already in progress [62]. Thus, the proposed scenario of LDs mobilization during olive pollen germination is that phospholipase A is recruited to the pollen LDs prior to pollen maturity and promotes the fast access of lipase and lipoxygenase to the TAGs core of LDs after the water uptake by the pollen grain and during pollen germination. The biological rationale of such scenario is supported by the fact that the initiation of pollen germination and pollen tube growth occurs very fast, thus the localization of the lipid enzymatic machinery on the surface of LDs in mature pollen grain might guarantee the rapid mobilization of storage lipids as the pollen germination starts. Moreover, the differences in spatio-temporal recruitment of the enzymes involved in LDs breakdown observed between pollen grain and seed may results from their diverse energy demands, tightly connected with their biological role.

STORE OR NOT TO STORE – LIPID DROPLETS IN VEGETATIVE TISSUES

Until recently, it has been generally accepted that the cells of vegetative tissues, such as leaves or stems, do not have ability to accumulate TAGs. Nevertheless, the number of LDs significantly increases during Arabidopsis leaf senescence [78]. Moreover, the number of LDs in the leaf is regulated also by diurnal cycle, reaching the highest amount at the end of the night and the lowest at the end of the day [79]. Recently, it was demonstrated that lipid droplet-associated protein1 (LDAP1) and one of the caleosins isoform - CLO3, also known as RESPONSIVE TO DEHYDRATION20 (RD20), are the most abundant structural proteins of LDs from Arabidopsis leaves during senescence [78]. The Arabidopsis genome encodes three LDAPs proteins: LDAP1, LDAP2, LDAP3 [79]. Overexpression of all the LDAPs-encoding genes results in accumulation of LDs in the leaves at the end of the day, meanwhile the *LDAP*-disrupted lines were characterized by less abundant LDs in the leaves at

the end of the night [79]. Recently, it has been proposed that the LDAP proteins play a significant role in LDs biogenesis in the leaves. During initial steps of LDs formation, LDAP-interacting protein (LDIP) interacts with SEIPIN on the ER lumenal side, enabling the accumulation of TAGs between the leaflets of the ER bilayer [80]. As TAGs continues to accumulate, LDIP dissociates from the complex with SEIPIN and is translocated on the nascent LDs surface were it interacts with LDAP protein. Based on these data, it seems that interactions between LDIP and SEIPIN as well as between LDIP and LDAP proteins are essential for LDs biogenesis at ER and indicate that the machinery responsible for this process might be different from oil storing tissues/organs, like seed or pollen, where oleosins are the key players in the process of LDs formation [8,80].

Emerging evidences suggest that LDs accumulate not only in senescing leaves but also in response to biotic and abiotic stresses [81]. Indeed, under abiotic stresses, such as heat or cold, increased synthesis of TAGs and LDs formation is observed in leaves [79]. They accumulate TAGs under heat stress likely to remove the excess of toxic FFAs, such as α-linolenic acid (18:3) released from cellular membranes. Recently, it was demonstrated that HEAT INDUCIBLE LIPASE1 (HIL1) is implicated in the turnover of monogalactosyldiacylglycerol (MGDG), the major chloroplast membrane lipid under heat stress, which leads to the synthesis of 18:3-containing TAGs [82]. The ability of plants to resist freezing stress is as well associated with increased conversion of DAGs to TAGs and with up-regulation of *DGAT1* expression [83,84]. In Arabidopsis, a significant increase in the number of leaf LDs observed in response to cold was associated with a strong induction of *LDAP1* and *LDAP3* expression [79]. On the other hand, the higher accumulation of LDs in the leaf in response to high temperature was correlated with the increased expression of *LDAP1* but not of *LDAP2* and *LDAP3*. Thus, different proteins from LDAP family might participate in the formation of LDs under diverse stress conditions. Interestingly, the expression of *CLO3* – the leaf LDs specific caleosin, is as well strongly induced in response to abiotic stresses [85]. Moreover, the mutation in CLO3-encoding gene enhanced stomatal opening and led to reduced tolerance to drought [85]. It has been also shown that CLO3 plays an important role in the biosynthesis of oxylipins, which are directly implicated in plant response to pathogen attack [86,87]. The infection of Arabidopsis plants with the fungal pathogen *Colletotrichum higginisianum* induced the localization of α-dioxygenase 1 (α-DOX1) on the surface of leaf LDs and formation of 2-hydroperoxy-octadecatrienoic acid (2-HPOT) from α-linolenic acid released from TAGs. Then, CLO3 converts 2-HPOT into 2-hydroxy-octadecatrienoic acid (2-HOT), which has antifungal activity against *Colletrichum* spp. [87]. Additionally, the accumulation of LDs containing CYP71A12, CYP71A13 and PAD3 (PHYTOALEXIN DEFICIENT3) proteins was observed after *Pseudomonas syringae* pv tomato (Pst) DC3000 avrRpm1 infection of Arabidopsis leaves [88]. Three other proteins directly involved in plant resistance to herbivores and pathogens were also identified in the proteomic analyses of LDs isolated from Arabidopsis aging leaves. These were STRICTOSIDINE SYNTHASE (STR), 2-OXOGLUTARATE AND FE(II)-DEPENDENT OXYGENASE and NITRILE SPECIFIER PROTEIN5 (NSP5) [78]. Many pathogens are using stomata as a gate for penetration and plant infection [89]. Recently, it was reported that LDs localized in guard cells serve as energy source necessary to light-induced stomatal opening [90]. Interestingly, the studies of stomata in potato leaves before and after infection by *Phytophthora infestans* showed that the pathogen attack not only induces stomatal opening but is also accompanied by the degradation of TAGs in guard cells [91]. These recent observations open a new line of research directly connecting the metabolism of LDs and TAGs with plant defense response.

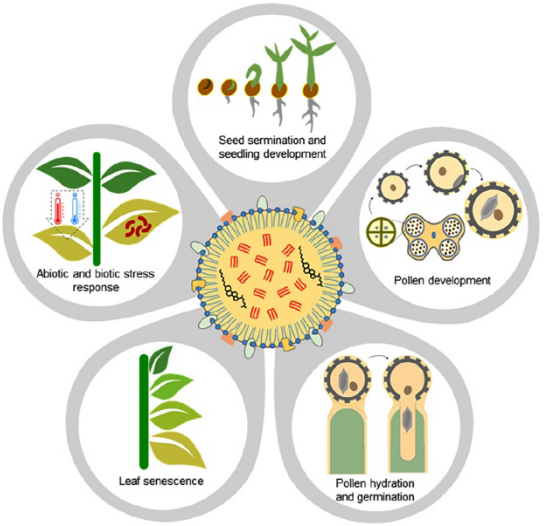

Figure 3. Schematic representation of plant developmental and physiological processes involving neutral lipids stored in LDs.

Overall, it seems likely that the dynamics and metabolism of LDs in the leaves is more intense than those of their seed or pollen counterparts. This is mainly due to the fact that in most of plants leaf is not a storage organ, but the major receptor of external stimuli, including biotic and abiotic factors. This in turn requires efficient cellular signaling systems and rapid responses at cellular level. Thus, leaf LDs might serve as a cellular mediator for diverse metabolic and signaling pathways involving lipids. Nevertheless, our understanding of LDs metabolism and function in leaves is still only fragmentary. Thus, upcoming research will be rather focused on LDs proteome in these organs, especially under stress conditions, in order to identify new specific LDs proteins and their role in LDs-mediated processes in plants.

CONCLUDING REMARKS AND FUTURE PERSPECTIVES

The present review outlines the essential role of neutral lipids in plant life cycles, starting from the earliest steps of seed germination, going through subsequent phases of plant growth and its interaction with environment, and ending up with sexual reproduction (Fig. 3). The studies of the last two decades revealed that plant LDs, beside common general structure, seem to be rather tissue/organ-spe-

cific in terms of their protein equipment and function. The recent advances in plant LDs proteome research strongly support this hypothesis and indicate much complex and more advanced role for these organelles than was previously thought. Similar to their animal and human counterparts, plant LDs have been re-discovered as dynamic cellular organelles and not simple oil storage depots. As in case of other cellular organelles, the life cycle of LDs, including their biogenesis, maturation, degradation and interactions with other organelles, is highly synchronized with developmental and physiological states of the plant. Regardless of the recent progress in deciphering the nature of plant LDs, many aspects of their lifecycle and role remain incompletely understood especially. This is especially true for non-seed tissues. Thus, the major challenges for upcoming research on plant LDs should include: 1) deeper mapping of proteomes and interactomes of LDs under diverse stresses, 2) gaining detailed knowledge related to the lifecycle of LDs in non-seed tissues, 3) matching the molecular mechanisms linking the lifecycle of LDs with plant developmental programs. Reaching the above goals will definitively lead to better understanding not only the role of LDs as metabolically important organelles but also to explore yet unknown pathways involving neutral lipids in plant cells.

REFERENCES:

1. Ridgway N, McLeod R (2016) Biochemistry of lipids, lipoproteins and membranes. Sixth edition. Elsevier, UK
2. Yuki N (2017) Plant Phospholipid Diversity: Emerging Functions in Metabolism and Protein–Lipid Interactions. Trends Plant Sci 22: 1027-1040
3. Mamode Cassim A, Gouguet P, Gronnier J, Laurent N, Germain V, Grison M, Boutté Y, Gerbeau-Pissot P, Simon-Plas F, Mongrand S. (2019) Plant lipids: Key players of plasma membrane organization and function. Prog Lipid Res 73: 1-27
4. Li-Beisson Y *et al.* (2013) Acyl-lipid metabolism. Arabidopsis Book 11: e0161
5. Chapman KD, Ohlrogge JB (2012) Compartmentation of triacylglycerol accumulation in plants. J Biol Chem 287: 2288-2294
6. Harris CA, Haas JT, Streeper RS, Stone SJ, Kumari M, Yang K, Han X, Brownell N, Gross RW, Zechner R, Farese RV Jr (2011) DGAT enzymes are required for triacylglycerol synthesis and lipid droplets in adipocytes. J Lipid Res 52: 657-567
7. Murphy DJ (2001) The biogenesis and functions of lipid bodies in animals, plants and microorganisms. Prog Lipid Res 40: 325-438
8. Huang AHC (2018) Plant Lipid Droplets and Their Associated Proteins: Potential for Rapid Advances. Plant Physiol 176: 1894-1918
9. Olzmann JA, Carvalho P (2019) Dynamics and functions of lipid droplets. Nat Rev Mol Cell Biol 20: 137-155
10. Greer MS, Cai Y, Gidda SK, Esnay N, Kretzschmar FK, Seay D, McClinchie E, Ischebeck T, Mullen RT, Dyer JM, Chapman KD (2020) SEIPIN Isoforms Interact with the Membrane-Tethering Protein VAP27-1 for Lipid Droplet Formation. Plant Cell 32: 2932-2950
11. van der Schoot C, Paul LK, Paul SB, Rinne PL (2011) Plant lipid bodies and cell-cell signaling: a new role for an old organelle? Plant Signal Behav 6: 1732-1738
12. Pyc M, Cai Y, Greer MS, Yurchenko O, Chapman KD, Dyer JM, Mullen RT (2017) Turning Over a New Leaf in Lipid Droplet Biology. Trends Plant Sci 22: 596-609
13. Peter KL, Kiran-Kumar S, Roberto EC (2020) Lipid droplets throughout the evolutionary tree. Prog Lipid Res 78: 101029
14. Herker E, Vieyres G, Beller M, Krahmer N, Bohnert M (2021) Lipid Droplet Contact Sites in Health and Disease. Trends Cell Biol 31: 345-358
15. Shimada TL, Shimada T, Takahashi H, Fukao Y, Hara-Nishimura I. (2008) A novel role for oleosins in freezing tolerance of oilseeds in *Arabidopsis thaliana*. Plant J 55: 798-809
16. Deruyffelaere C, Bouchez I, Morin H, Guillot A, Miquel M, Froissard M, Chardot T, D'Andrea S (2015) Ubiquitin-Mediated Proteasomal Degradation of Oleosins is Involved in Oil Body Mobilization During Post-Germinative Seedling Growth in Arabidopsis. Plant Cell Physiol 56: 1374-87
17. Napier JA, Beaudoin F, Tatham AS, Alexander LG, Shewry PR (2001) The seed oleosins: Structure, properties and biological role. Adv Bot Res 35: 111-138
18. Abell BM, Hahn M, Holbrook LA, Moloney MM (2004) Membrane topology and sequence requirements for oil body targeting of oleosin. Plant J 37: 461-470
19. Siloto RM, Findlay K, Lopez-Villalobos A, Yeung EC, Nykiforuk CL, Moloney MM (2006) The accumulation of oleosins determines the size of seed oilbodies in Arabidopsis. Plant Cell 18: 1961-1974
20. Miquel M, Trigui G, d'Andréa S, Kelemen Z, Baud S, Berger A, Deruyffelaere C, Trubuil A, Lepiniec L, Dubreucq B (2014) Specialization of oleosins in oil body dynamics during seed development in Arabidopsis seeds. Plant Physiol 164: 1866-1878
21. Chen JC, Tsai CC, Tzen JT (1999) Cloning and secondary structure analysis of caleosin, a unique calcium-binding protein in oil bodies of plant seeds. Plant Cell Physiol 40: 1079-1086
22. Naested H, Frandsen GI, Jauh GY, Hernandez-Pinzon I, Nielsen HB, Murphy DJ, Rogers JC, Mundy J (2000) Caleosins: Ca^{2+}-binding proteins associated with lipid bodies. Plant Mol Biol 44: 463-476
23. Shao Q, Liu X, Su T, Ma C, Wang P (2019) New insights into the role of seed oil body proteins in metabolism and plant development. Front Plant Sci 10: 1568
24. Shen Y, Liu M, Wang L, Li Z, Taylor DC, Li Z, Zhang M (2016) Identification, duplication, evolution and expression analyses of caleosins in Brassica plants and Arabidopsis subspecies. Mol Gen Genom 291: 971-988
25. Poxleitner M, Rogers SW, Lacey Samuels A, Browse J, Rogers JC (2006) A role for caleosin in degradation of oil-body storage lipid during seed germination. Plant J 47: 917-933
26. Kretzschmar FK, Doner NM, Krawczyk HE, Scholz P, Schmitt K, Valerius O, Braus GH, Mullen RT, Ischebeck T (2020) Identification of Low-Abundance Lipid Droplet Proteins in Seeds and Seedlings. Plant Physiol 182: 1326-1345
27. Baud S, Dichow NR, Kelemen Z, d'Andréa S, To A, Berger N, Canonge M, Kronenberger J, Viterbo D, Dubreucq B, Lepiniec L, Chardot T, Miquel M (2009) Regulation of HSD1 in seeds of Arabidopsis thaliana. Plant Cell Physiol 50: 1463-1478.
28. Lin LJ, Tai SS, Peng CC, Tzen JT (2002) Steroleosin, a sterol-binding dehydrogenase in seed oil bodies. Plant Physiol 128: 1200-1211
29. Jolivet P, Roux E, d'Andrea S, Davanture M, Negroni L, Zivy M, Chardot T (2004) Protein composition of oil bodies in *Arabidopsis thaliana* ecotype WS. Plant Physiol Biochem 42: 501-509
30. Li F, Asami T, Wu X, Tsang EW, Cutler AJ (2007) A putative hydroxysteroid dehydrogenase involved in regulating plant growth and development. Plant Physiol 145: 87-97
31. Deruyffelaere C, Purkrtova Z, Bouchez I, Collet B, Cacas JL, Chardot T, Gallois JL, D'Andrea S (2018) PUX10 Is a CDC48A Adaptor Protein That Regulates the Extraction of Ubiquitinated Oleosins from Seed Lipid Droplets in Arabidopsis. Plant Cell 30: 2116-2136
32. Kretzschmar FK, Mengel LA, Müller AO, Schmitt K, Blersch KF, Valerius O, Braus GH, Ischebeck T (2018) PUX10 Is a Lipid Droplet-Localized Scaffold Protein That Interacts with CELL DIVISION CYCLE48 and Is Involved in the Degradation of Lipid Droplet Proteins. Plant Cell 30: 2137-2160
33. Liu Y, Li J (2014) Endoplasmic reticulum-mediated protein quality control in Arabidopsis. Front Plant Sci 5: 162
34. Eastmond PJ (2006) SUGAR-DEPENDENT1 encodes a patatin domain triacylglycerol lipase that initiates storage oil breakdown in germinating Arabidopsis seeds. Plant Cell 18: 665-675

35. Kelly AA, Quettier AL, Shaw E, Eastmond PJ (2011) Seed storage oil mobilization is important but not essential for germination or seedling establishment in Arabidopsis. Plant Physiol 157: 866-875
36. Thazar-Poulot N, Miquel M, Fobis-Loisy I, Gaude T (2015) Peroxisome extensions deliver the Arabidopsis SDP1 lipase to oil bodies. Proc Natl Acad Sci 112: 4158-4163
37. Zolman BK, Silva ID, Bartel B (2001) The Arabidopsis pxa1 mutant is defective in an ATP-binding cassette transporter-like protein required for peroxisomal fatty acid beta-oxidation. Plant Physiol 127: 1266-1278
38. Piffanelli P, Ross JHE, Murphy DJ (1998) Biogenesis and function of the lipidic structures of pollen grains. Sex Plant Rep 11: 65-80
39. Goldberg RB, Beals TP, Sanders PM (1993) Anther development: basic principles and practical applications. Plant Cell 5: 1217-1229
40. Murphy DJ (2006) The extracellular pollen coat in members of the Brassicaceae: composition, biosynthesis, and functions in pollination. Protoplasma 228: 31
41. Parish RW, Li SF (2010) Death of a tapetum: A programme of developmental altruism. Plant Sci 178: 73-89
42. Huysmans S, El-Ghazaly G, Smets E (1998) Orbicules in angiosperms: Morphology, function, distribution, and relation with tapetum types. Bot Review 64: 240-272
43. Hernández-Pinzón I, Ross JH, Barnes KA, Damant AP, Murphy DJ (1999) Composition and role of tapetal lipid bodies in the biogenesis of the pollen coat of Brassica napus. Planta 208: 588-598
44. Wu SSH, Platt KA, Ratnayake C, Wang TW, Ting JTL, Huang AHC (1997) Isolation and characterization of neutral-lipid-containing organelles and globuli-filled plastids from *Brassica napus* tapetum. Proc Natl Acad Sci 94: 12711-12716
45. Kim HU, Wu SS, Ratnayake C, Huang AH (2001) Brassica rapa has three genes that encode proteins associated with different neutral lipids in plastids of specific tissues. Plant Physiol 126: 330-341
46. Hsieh K, Huang AH. 2005. Lipid-rich tapetosomes in Brassica tapetum are composed of oleosin-coated oil droplets and vesicles, both assembled in and then detached from the endoplasmic reticulum. Plant J 43: 889-899
47. Hsieh K, Huang AH (2004) Endoplasmic reticulum, oleosins, and oils in seeds and tapetum cells. Plant Physiol 136: 3427-3434
48. Suzuki T, Tsunekawa S, Koizuka C, Yamamoto K, Imamura J, Nakamura K, Ishiguro S (2013) Development and disintegration of tapetum-specific lipid-accumulating organelles, elaioplasts and tapetosomes, in *Arabidopsis thaliana* and *Brassica napus*. Plant Sci 207: 25-36
49. Hsieh K, Huang AHC (2007) Tapetosomes in brassica tapetum accumulate endoplasmic reticulum–derived flavonoids and alkanes for delivery to the pollen surface. Plant Cell 19: 582-596
50. de Oliveira DE, Franco LO, Simoens C, Seurinck J, Coppieters J, Botterman J, Van Montagu M (1993) Inflorescence-specific genes from *Arabidopsis thaliana* encoding glycine-rich proteins. Plant J 3:495-507
51. Rejón JD, Delalande F, Schaeffer-Reiss C, Alché JD, Rodríguez-García MI, Van Dorsselaer A, Castro AJ (2016) The Pollen Coat Proteome: At the Cutting Edge of Plant Reproduction. Proteomes 4: 5
52. Mayfield JA, Fiebig A, Johnstone SE, Preuss D (2001) Gene families from the *Arabidopsis thaliana* pollen coat proteome. Science 292: 2482-2485
53. Zienkiewicz K, Castro AJ, Alché Jde D, Zienkiewicz A, Suárez C, Rodríguez-García MI (2010) Identification and localization of a caleosin in olive (*Olea europaea* L.) pollen during *in vitro* germination. J Exp Bot 61: 1537-1546
54. Zienkiewicz K, Zienkiewicz A, Rodríguez-García MI, Castro AJ (2011) Characterization of a caleosin expressed during olive (*Olea europaea* L.) pollen ontogeny. BMC Plant Biol 11:122
55. Wu XL, Cai G, Gong FP, An SF, Cresti M, Wang W (2015) Proteome Profiling of Maize Pollen Coats Reveals Novel Protein Components. Plant Mol Biol Rep 33: 975-986
56. Ishiguro S, Nishimori Y, Yamada M, Saito H, Suzuki T, Nakagawa T, Miyake H, Okada K, Nakamura K (2010) The Arabidopsis FLAKY POLLEN1 gene encodes a 3-hydroxy-3-methylglutaryl-coenzyme A synthase required for development of tapetum-specific organelles and fertility of pollen grains. Plant Cell Physiol 51: 896-911
57. Preuss D, Lemieux B, Yen G, Davis RW (1993) A conditional sterile mutation eliminates surface components from Arabidopsis pollen and disrupts cell signaling during fertilization. Genes Dev 7: 974-985
58. Hulskamp M, Schneitz K, Pruitt RE (1995) Genetic evidence for a long--range activity that directs pollen tube guidance in arabidopsis. Plant Cell 7: 57-64
59. Mayfield JA, Preuss D (2000) Rapid initiation of Arabidopsis pollination requires the oleosin-domain protein GRP17. Nat Cell Biol 2: 128-130
60. Updegraff EP, Zhao F, Preuss D (2009) The extracellular lipase EXL4 is required for efficient hydration of Arabidopsis pollen. Sex Plant Reprod 22: 197-204
61. Rodríguez-García MI, M'Rani-Alaoui M, Fernández MC (2003) Behavior of storage lipids during development and germination of olive (*Olea europaea* L.) pollen. Protoplasma 221: 237-244
62. Zienkiewicz A, Zienkiewicz K, Rejón JD, Rodríguez-García MI, Castro AJ (2013) New insights into the early steps of oil body mobilization during pollen germination. J Exp Bot 64: 293-302
63. McCormick S (1993) Male Gametophyte Development. Plant Cell 5: 1265-1275
64. Charzynska M, Murgia M, Cresti M (1989) Ultrastructure of the vegetative cell of *Brassica napus* pollen with particular reference to microbodies. Protoplasma 152: 22-28
65. Zheng Y, Deng X, Qu A, Zhang M, Tao Y, Yang L, Liu Y, Xu J, Zhang S (2018) Regulation of pollen lipid body biogenesis by MAP kinases and downstream WRKY transcription factors in Arabidopsis. PLoS Genet 14: e1007880
66. Rotsch AH, Kopka J, Feussner I, Ischebeck T (2017) Central metabolite and sterol profiling divides tobacco male gametophyte development and pollen tube growth into eight metabolic phases. Plant J 92: 129-146
67. Jiang PL, Wang CS, Hsu CM, Jauh GY, Tzen JT (2007) Stable oil bodies sheltered by a unique oleosin in lily pollen. Plant Cell Physiol 48: 812-821
68. Zhang M, Fan J, Taylor DC, Ohlrogge JB (2009) DGAT1 and PDAT1 acyltransferases have overlapping functions in Arabidopsis triacylglycerol biosynthesis and are essential for normal pollen and seed development. Plant Cell 21(12): 3885-901.
69. Kim HU, Hsieh K, Ratnayake C, Huang AH. (2002) A novel group of oleosins is present inside the pollen of Arabidopsis. J Biol Chem 277(25): 22677-84
70. Jiang PL, Jauh GY, Wang CS, Tzen JT (2008) A unique caleosin in oil bodies of lily pollen. Plant Cell Physiol 49: 1390-1395
71. Pasaribu B, Fu JH, Jiang PL (2020) Identification and characterization of caleosin in *Cycas revoluta* pollen. Plant Signal Behav 15: 1779486
72. Pasaribu B, Chen CS, Liao YK, Jiang PL, Tzen JTC (2017) Identification of caleosin and oleosin in oil bodies of pine pollen. Plant Physiol Biochem 111: 20-29
73. Taylor LP, Hepler PK (1997) Pollen germination and tube growth. Ann Rev Plant Phys Plant Mol Biol 48: 461-491
74. Dorne AJ, Kappler R, Kristen U, Heinz E (1998) Lipid metabolism during germination of tobacco pollen. Phytochemistry 27: 2027-2031
75. Rodríguez-García MI, Fernández MC (1990) Ultrastructural evidence of endoplasmic reticulum changes during the maturation of the olive pollen grain (*Olea europaea* L., Oleaceae). Plant Syst Evol 171: 221-231
76. Müller AO, Ischebeck T (2018) Characterization of the enzymatic activity and physiological function of the lipid droplet-associated triacylglycerol lipase AtOBL1. New Phytol 217: 1062-1076
77. Rejón JD, Zienkiewicz A, Rodríguez-García MI, Castro AJ (2002) Profiling and functional classification of esterases in olive (*Olea europaea*) pollen during germination. Ann Bot 110: 1035-1045
78. Brocard L, Immel F, Coulon D, Esnay N, Tuphile K, Pascal S, Claverol S, Fouillen L, Bessoule JJ, Bréhélin C (2017) Proteomic analysis of lipid droplets from arabidopsis aging leaves brings new insight into their biogenesis and functions. Front Plant Sci 8: 894

79. Gidda SK, Park S, Pyc M, Yurchenko O, Cai Y, Wu P, Andrews DW, Chapman KD, Dyer JM, Mullen RT (2016) Lipid droplet-associated proteins (ldaps) are required for the dynamic regulation of neutral lipid compartmentation in plant cells. Plant Physiol 170: 2052-2071

80. Pyc M, Gidda SK, Seay D, Esnay N, Kretzschmar FK, Cai Y, Doner NM, Greer MS, Hull JJ, Coulon D, Bréhélin C, Yurchenko O, de Vries J, Valerius O, Braus GH, Ischebeck T, Chapman KD, Dyer JM, Mullen RT (2021) LDIP Cooperates with SEIPIN and LDAP to Facilitate Lipid Droplet Biogenesis in Arabidopsis. Plant Cell (*in press*)

81. Lu J, Xu Y, Wang J, Singer SD, Chen G (2020) The Role of Triacylglycerol in Plant Stress Response. Plants (Basel) 9: 472

82. Higashi Y, Okazaki Y, Takano K, Myouga F, Shinozaki K, Knoch E, Fukushima A, Saito K (2018) HEAT INDUCIBLE LIPASE 1 remodels chloroplastic monogalactosyldiacylglycerol by liberating α-linolenic acid in arabidopsis leaves under heat stress. Plant Cell 30: 1887-1905

83. Arisz SA, Heo JY, Koevoets IT, Zhao T, van Egmond P, Meyer AJ, Zeng W, Niu X, Wang B, Mitchell-Olds T, Schranz ME, Testerink C (2018) Diacylglycerol acyltransferase 1 contributes to freezing tolerance. Plant Physiol 177: 1410-1424

84. Tan WJ, Yang YC, Zhou Y, Huang LP, Xu L, Chen QF, Yu LJ, Xiao S (2018) Diacylglycerol acyltransferase and diacylglycerol kinase modulate triacylglycerol and phosphatidic acid production in the plant response to freezing stress. Plant Physiol 177: 1303-1318

85. Aubert Y, Vile D, Pervent M, Aldon D, Ranty B, Simonneau T, Vavasseur A, Galaud JP (2010) RD20, a stress-inducible caleosin, participates in stomatal control, transpiration and drought tolerance in *Arabidopsis thaliana*. Plant Cell Physiol 51: 1975-1987

86. Hanano A, Bessoule JJ, Heitz T, Blée E (2015) Involvement of the caleosin/peroxygenase RD20 in the control of cell death during Arabidopsis responses to pathogens. Plant Signal Behav 10: e991574

87. Shimada TL, Takano Y, Hara-Nishimura I (2015) Oil body-mediated defense against fungi: From tissues to ecology. Plant Signal Behav 10: p. e989036

88. Fernández-Santos R, Izquierdo Y, López A, Muñiz L, Martínez M, Cascón T, Hamberg M, Castresana C (2020) Protein profiles of lipid droplets during the hypersensitive defense response of arabidopsis against pseudomonas infection. Plant Cell Physiol 61: 1144-1157

89. Gudesblat GE, Torres PS, Vojnov AA (2009) Stomata and pathogens: Warfare at the gates. Plant Signal Behav 4: 1114-1116.

90. McLachlan DH, Lan J, Geilfus CM, Dodd AN, Larson T, Baker A, Hörak H, Kollist H, He Z, Graham I, Mickelbart MV, Hetherington AM (2016) The breakdown of stored triacylglycerols is required during light-induced stomatal opening. Curr Biol 26: 707-712

91. Yang LN, Liu H, Wang YP, Seematti J, Grenville-Briggs LJ, Wang Z, Zhan J (2021) Pathogen-mediated stomatal opening: a previously overlooked pathogenicity strategy in the oomycete pathogen phytophthora infestans. Front Plant Sci 12: 668797

1.2 Distinct regulatory principles of TAG metabolism in plants and microalgae

While studies in higher plants have provided a detailed and coherent framework for understanding TAG biosynthesis, LD biogenesis, and their integration with developmental programs, the regulatory logic governing storage lipid metabolism in unicellular photoautotrophs differs in several fundamental aspects.

In higher plants, TAG accumulation is largely confined to specialized tissues such as seeds and pollen and is tightly coordinated with organ differentiation and developmental timing (Zienkiewicz *et al*., 2010, 2011, 2022). These developmental programs ensure predictable patterns of carbon allocation and lipid storage during the plant life cycle. In contrast, microalgae lack dedicated storage organs and instead perform lipid synthesis, processing, storage, and mobilization within a single cell. Consequently, TAG metabolism in these organisms is not primarily linked to ontogenetic programs but is highly responsive to external environmental signals. In natural aquatic ecosystems, microalgae experience rapid and often unpredictable fluctuations in nutrient availability, light intensity, temperature, and salinity, which impose strong selective pressure for metabolic flexibility (Zienkiewicz *et al*., 2016; Huang *et al*., 2020; Shi *et al*., 2020). Under such conditions, the ability to dynamically redirect fixed carbon into neutral lipid pools represents an essential adaptive strategy.

Numerous physiological and transcriptomic studies demonstrate that TAG accumulation in microalgae is most commonly induced by abiotic stress, including nitrogen limitation, high irradiance, osmotic stress, and temperature shifts (Gargouri *et al*., 2017; Zienkiewicz *et al*., 2020; Xu *et al*., 2023). During stress, cell division is often limited, whereas photosynthetic carbon assimilation may continue, resulting in excess reductant and metabolic intermediates. Channeling this accumulated carbon into TAGs prevents metabolic imbalance, supports redox homeostasis, and protects the photosynthetic apparatus from photoinhibition and oxidative damage (Alboresi *et al*., 2016; Huang *et al*., 2020; Carro *et al*., 2022).

From a cellular perspective, TAGs in microalgae function not only as long-term energy reserves but also as transient metabolic buffers that enable rapid adjustment of carbon fluxes during transitions between growth and stress conditions. Stored TAGs can be efficiently mobilized upon stress relief, supplying fatty acids (FAs) and glycerol for membrane biogenesis, respiratory metabolism, and the reactivation of biosynthetic pathways (Lee *et al*., 2020; Zienkiewicz *et al*., 2020; Guéguen *et al*., 2021). This reversible mode of lipid storage distinguishes microalgal systems from most plant tissues and underlies their remarkable physiological plasticity. These functional differences are reflected at the molecular level in the organization and regulation of lipid biosynthetic pathways. Comparative genomic analyses reveal that many microalgal species possess unusually complex repertoires of terminal acyltransferases, particularly type 2 diacylglycerol acyltransferases (DGAT2, commonly referred to as DGTTs in algae), which are far more diversified than their counterparts in higher plants and animals (Wang *et al*., 2014; Li *et al*., 2016; Zienkiewicz *et al*., 2017). This expansion is accompanied by extensive sequence divergence, variation in membrane topology, and heterogeneous regulatory patterns, suggesting early functional differentiation among paralogous isoforms.

1.3 Physiological and regulatory specificity of TAG metabolism in microalgae

Similar to terrestrial plants, microalgal cells accumulate neutral lipids predominantly in the form of TAGs within LDs (Zienkiewicz *et al*., 2016; Zulu *et al*., 2018). These LDs consist of a TAG-rich hydrophobic core surrounded by a phospholipid monolayer decorated with characteristic structural and regulatory proteins (Zienkiewicz and Zienkiewicz, 2020). This conserved organization reflects the shared evolutionary origin of lipid storage systems in photosynthetic eukaryotes. Nevertheless, fundamental physiological and regulatory differences arise from the unicellular nature of microalgae.

In higher plants, intensive oil accumulation is largely restricted to specialized, non-photosynthetic tissues such as seeds and pollen, and is tightly coordinated with developmental programs (Zienkiewicz *et al*., 2010, 2011). In contrast, microalgae perform lipid synthesis, storage, remodeling, and mobilization within a single cell, which must simultaneously sustain photosynthesis, growth, and stress adaptation. As a consequence, TAG accumulation in microalgae is rarely linked to ontogenetic cues and instead occurs predominantly in response to environmental stimuli.

One of the most prominent drivers of TAG accumulation in microalgae is abiotic stress, including nutrient limitation, high or fluctuating light, temperature variation, and salinity stress. Under such conditions, TAGs function as central regulators of carbon and energy homeostasis rather than merely serving as passive storage compounds (Shi *et al*., 2020; Xu *et al*., 2023; Xin *et al*., 2024). In natural aquatic environments, where external conditions fluctuate rapidly and unpredictably, the ability to redirect excess fixed carbon into TAGs represents a flexible strategy for maintaining metabolic stability and cellular viability.
When cell division is inhibited by environmental stress, photosynthetically fixed carbon can continue to be assimilated and efficiently stored in the form of TAGs (Zienkiewicz *et al*., 2016; Huang *et al*., 2020; Song *et al*., 2022). This process prevents over-reduction of the photosynthetic electron transport chain and limits the accumulation of potentially toxic metabolic intermediates (Milrad *et al*., 2024). By acting as an inert yet readily mobilizable carbon sink, TAGs contribute to cellular redox balance and protect the photosynthetic apparatus from photodamage, particularly under high or variable light conditions (Alboresi *et al*., 2016; Gargouri *et al*., 2017; Carro *et al*., 2022).

From a physiological perspective, TAGs represent a dense and osmotically neutral energy reserve that can be rapidly mobilized when favorable conditions are restored (Lee *et al*., 2020; Zienkiewicz *et al*., 2020). During recovery from stress, stored TAGs are hydrolyzed to release FAs and glycerol, which fuel β- oxidation, membrane lipid remodeling, and the reactivation of growth-associated biosynthetic pathways (Guéguen *et al*., 2021; Young *et al*., 2021; Amari *et al*., 2024; Murison *et al*., 2025). This reversible mode of lipid storage enables microalgae to persist through adverse conditions and rapidly resume proliferation, providing a competitive advantage in dynamic aquatic ecosystems.

In addition to their metabolic functions, TAGs contribute to cellular organization through their association with LDs. The formation of LDs enables spatial segregation of neutral lipids from membrane systems, thereby minimizing interference with essential membrane-associated processes. Moreover, LDs act as dynamic organelles that interact with the endoplasmic reticulum (ER), chloroplasts, and mitochondria,

integrating TAG metabolism with cellular networks involved in lipid trafficking, stress signaling, and energy balance (Goold *et al*., 2015; Zienkiewicz *et al*., 2016, 2020).

Importantly, the stress-responsive and highly dynamic nature of TAG metabolism in microalgae imposes specific demands on the enzymatic machinery responsible for TAG synthesis. Rapid induction, precise regulation, and efficient substrate channeling require flexible and diversified acyltransferase systems capable of operating under fluctuating metabolic conditions. These requirements provide a physiological context for the expansion and functional diversification of DGATs, particularly DGTT family members, which will be discussed in detail in the following sections.

1.4 Exceptional expansion and functional diversification of DGAT/DGTT enzymes in microalgae

In microalgae, FA synthesis occurs predominantly in plastids, whereas TAG assembly takes place mainly at the ER, analogous to higher plants. TAG biosynthesis proceeds primarily through the Kennedy (glycerol phosphate) pathway, which involves the sequential esterification of glycerol-3-phosphate with fatty acyl-CoA molecules. The final and committed step of this pathway is catalyzed by DGAT, which converts diacylglycerol (DAG) into TAG and thereby exerts substantial control over metabolic flux into storage lipids.

Two major classes of membrane-associated DGAT enzymes, termed DGAT type 1 and DGAT type 2 (also referred to as DGTT in microalgae), are present in most eukaryotic organisms. These enzymes share low sequence similarity and appear to perform largely nonredundant functions in TAG biosynthesis. Phylogenetic analyses suggest that DGAT type 1 and DGAT type 2 originated independently and acquired similar catalytic functions through convergent evolution (Turchetto-Zolet *et al*., 2011). In most plants and animals, a single copy of each DGAT type 1 and DGAT type 2 gene is typically present, whereas yeast genomes usually contain only one DGAT type 2 gene. Similarly, most sequenced model microalgae harbor a single DGAT type 1 gene. In contrast to this conserved genomic organization, microalgae exhibit an exceptional expansion of type 2 DGAT genes. Many microalgal genomes encode multiple DGTT paralogs, often ranging from five to more than a dozen copies per species. This expansion represents a distinctive feature of algal lipid metabolism and sets microalgae apart from most other eukaryotic lineages. Comparative genomic analyses indicate that this proliferation is particularly pronounced in oleaginous taxa and correlates with their capacity for rapid and extensive TAG accumulation under stress conditions.

The unusually large number of DGTT genes in microalgae is thought to reflect their complex evolutionary history, shaped by endosymbiotic events, horizontal gene transfer, and lineage-specific gene duplication (Wang *et al*., 2014). *DGTT*s identified in algal genomes display substantial sequence divergence, even among paralogs within the same species. For example, among putative DGTT paralogs in *Chlorella* species, some cluster more closely with animal and fungal homologs, whereas others show stronger similarity to plant-type DGAT type 2 enzymes. Similarly, in *Ostreococcus tauri* and *Phaeodactylum tricornutum*, multiple DGTT genes have been identified that share limited sequence similarity with one another.

Nannochloropsis oceanica represents one of the most extreme cases reported to date, with up to twelve DGTT genes per genome. Phylogenetic analyses indicate that these paralogs are distributed throughout the DGTT tree rather than forming a single lineage-specific cluster (Zienkiewicz *et al*., 2016). Moreover, algal *DGTT*s do not group closely with their animal, plant, or fungal counterparts but instead cluster with *DGTT*s from other algae and oomycetes, suggesting closer relationships to heterologous algal homologs than to paralogs within the same species (Chen and Smith, 2012; Wang *et al*., 2014). Together, these observations support a heterogeneous evolutionary origin of algal DGTT families.

This complex evolutionary background is reflected in the functional diversity of DGTT enzymes. Studies in major microalgal model species demonstrate that DGTT genes respond differentially to nitrogen starvation and other environmental stresses, and no species has been identified in which all DGTT genes are uniformly induced under lipid-accumulating conditions (Zienkiewicz *et al*., 2016). In *N. oceanica* CCMP1779, only six out of twelve DGTT genes (*NoDGTT1 – NoDGTT6*) are strongly induced by nitrogen deprivation (Zienkiewicz *et al*., 2017, 2019), whereas other paralogs display weak, delayed, or even negative regulation.
For example, *NoDGTT8*, *NoDGTT11*, and *NoDGTT12* are downregulated during nitrogen starvation but become upregulated following nitrogen resupply (Zienkiewicz *et al*., 2020). These transcriptional patterns indicate that only a subset of DGTTs is directly involved in stress-induced TAG accumulation, whereas others may function during recovery, optimal growth, or alternative environmental conditions. Such regulatory diversification suggests that DGTT paralogs are embedded within distinct signaling and metabolic networks.

Functional studies further support this view. Heterologous expression analyses in TAG-deficient yeast strains demonstrated pronounced differences in catalytic efficiency among DGTT isoforms. In *N. oceanica* CCMP1779, expression of individual NoDGTT genes revealed that *NoDGTT5* exhibits the strongest activity, restoring TAG levels to approximately 53% of total FAs, whereas other isoforms display moderate or weak effects (Zienkiewicz *et al*., 2017). These findings demonstrate that DGTT expansion reflects functional specialization rather than simple genetic redundancy.

Genome-wide analyses across oleaginous microalgae consistently reveal extensive DGTT gene families, whereas DGAT type 1 and DGAT type 3 are usually represented by one or very few copies (Zienkiewicz *et al*., 2016; Bagnato *et al*., 2017). This organizational pattern suggests strong selective pressure favoring DGTT diversification in aquatic photoautotrophs. Structural divergence among DGTTs, including variation in transmembrane domains, loop regions, and predicted interaction surfaces, provides a mechanistic basis for differential regulation, substrate channeling, and integration with LD biogenesis pathways (Liu *et al*., 2016).
From an evolutionary and physiological perspective, expansion of DGTT families is closely linked to the stress-responsive lifestyle of microalgae. Rather than relying on a single dominant acyltransferase, these organisms deploy a distributed network of specialized isoforms that together provide flexibility, robustness, and regulatory precision. This organizational principle forms the molecular basis for both

natural stress adaptation and targeted metabolic engineering of TAG biosynthesis and represents a central theme of the present thesis.

1.5 Functional characterization of microalgal *DGTT* isoforms using heterologous expression systems

Although transcriptomic analyses have provided valuable insight into the regulation of DGTT genes under stress conditions, transcriptional induction alone does not necessarily reflect intrinsic enzymatic activity or quantitative contribution to TAG synthesis. Consequently, heterologous expression systems have been widely employed to dissect the catalytic properties, substrate preferences, and regulatory potential of individual *DGTT* isoforms in simplified and genetically tractable backgrounds.

In *N. oceanica* CCMP1779, the six DGTT-encoding genes most strongly induced by nitrogen starvation (*NoDGTT1* – *NoDGTT6*) were selected for early functional characterization using a TAG-deficient *Saccharomyces cerevisiae* strain H1266, which carries null mutations in three DGAT-related genes (*DGA1*, *LRO1*, and *ARE2*) and retains only approximately 1% of wild-type TAG-synthesizing activity (Sandager *et al*., 2002). Individual *NoDGTT* coding sequences were expressed under controlled promoters, and protein accumulation was confirmed for each construct.
Quantitative lipid analyses revealed pronounced differences in catalytic efficiency among DGTT isoforms. Among the tested enzymes, NoDGTT5 exhibited the strongest activity, restoring TAG levels to approximately 53% of TFAs. Yeast strains expressing NoDGTT2, NoDGTT3, and NoDGTT4 also accumulated substantially elevated TAG levels relative to control strains, whereas NoDGTT1 and NoDGTT6 produced only modest increases (Zienkiewicz *et al*., 2017). These results provided direct evidence that DGTT paralogs differ markedly in their intrinsic capacity to catalyze TAG formation.

Given its high activity in heterologous systems, *NoDGTT5* was subsequently overexpressed in its native host, *N. oceanica* CCMP1779. Constitutive expression driven by the elongation factor promoter resulted in a substantial increase in TAG content under optimal growth conditions, indicating that enhanced DGTT dosage can stimulate TAG synthesis independently of nutrient stress (Zienkiewicz *et al*., 2017). This finding demonstrated that terminal acyltransferase activity represents a key rate-limiting step in microalgal TAG biosynthesis and can be manipulated to redirect carbon flux toward storage lipids.
Furthermore, heterologous expression of *NoDGTT5* in higher plants under the cauliflower mosaic virus 35S promoter led to two- to three-fold increases in TAG accumulation in *Nicotiana tabacum* and *Arabidopsis thaliana* leaves and significantly elevated seed oil content (Zienkiewicz *et al*., 2017). These studies established *DGTT*s from *N. oceanica* CCMP1779 as powerful tools for metabolic engineering and demonstrated strong evolutionary conservation of DGTT catalytic mechanisms across photosynthetic eukaryotes.
Comparable functional divergence among DGTT family members has been reported in other microalgal species. In *Chlamydomonas reinhardtii*, only a subset of DGTT isoforms effectively complemented the TAG-deficient yeast phenotype (Sanjaya *et al*., 2013; Liu *et al*., 2016). Similarly, DGTTs from *Chlorella zofingiensis*, *Lobosphaera incisa*, and *Haematococcus pluvialis* display pronounced variability in TAG-synthesizing capacity when expressed in heterologous hosts (Zienkiewicz *et al*., 2018; Mao *et al*., 2019;

Ma *et al*., 2021). Together, these studies indicate that DGTT expansion is consistently associated with functional stratification across phylogenetically distant algal lineages.

Importantly, limited TAG accumulation observed for certain DGTT isoforms in yeast does not necessarily indicate a lack of physiological relevance in their native algal context. Several factors may constrain enzymatic performance in heterologous systems. First, substrate availability differs substantially between yeast and microalgae. *S. cerevisiae* predominantly synthesizes C16 and C18 FAs, whereas *N. oceanica* produces significant amounts of long-chain and polyunsaturated FAs, including eicosapentaenoic acid (C20:5). DGTTs adapted to such substrates may therefore exhibit reduced activity in yeast due to substrate mismatch (Liu *et al*., 2016; Mao *et al*., 2019; Ma *et al*., 2021).
Second, improper protein folding, membrane insertion, or targeting may compromise DGTT activity in heterologous hosts. DGTT enzymes are membrane-associated proteins that localize to specialized ER subdomains closely linked to LD biogenesis (Liu *et al*., 2016; Zienkiewicz *et al*., 2017). Differences in ER architecture and LD formation between algae and yeast may therefore influence enzyme functionality. Third, post-translational regulation and protein–protein interactions may be required for full catalytic competence *in vivo* and may be absent in simplified expression systems.

In addition, functional divergence within the DGTT family may extend beyond classical TAG synthesis. Neofunctionalization toward alternative acyltransferase activities has been reported in some microalgae, exemplified by the conversion of HpDGTT2 into a lysophosphatidic acid acyltransferase (Ma *et al*., 2021). Such findings suggest that some DGTT paralogs may participate in auxiliary lipid metabolic pathways rather than serving primarily as terminal TAG synthases.

Collectively, heterologous expression studies provide compelling evidence that DGTT paralogs differ substantially in catalytic efficiency, substrate utilization, and regulatory integration. These results support the view that DGTT gene family expansion reflects functional specialization rather than redundancy and establish a framework for systematic comparative analysis of individual isoforms. This framework forms the basis for the experimental strategies employed in the present thesis to resolve functional hierarchy within the NoDGTT family.

1.6 *Nannochloropsis oceanica* CCMP1779 as a model system for studying TAG biosynthesis

Species of the genus *Nannochloropsis* are widely recognized as some of the most efficient natural producers of TAGs among microalgae, combining high photosynthetic performance with an exceptional capacity to redirect fixed carbon into neutral lipid storage. Under nitrogen deprivation, high light, and other stress conditions, *Nannochloropsis* cells undergo pronounced metabolic reprogramming that results in TAG contents frequently exceeding 40–60% of dry cell weight, while maintaining relatively high carbon fixation rates compared with many other algal models (Rodolfi *et al*., 2009; Zienkiewicz *et al*., 2020; Xu *et al*., 2022) .
This remarkable lipid productivity is supported not only by enhanced *de novo* FA synthesis but also by extensive remodeling of chloroplast membrane lipids, which releases FAs that are efficiently recycled into TAGs (Simionato *et al*., 2013; Zienkiewicz *et al*., 2017). Lipidomic analyses further indicate that TAG

accumulation in *Nannochloropsis* follows defined temporal patterns, with early stress-induced TAG species enriched in saturated and monounsaturated FAs and later stages characterized by increased polyunsaturated lipid incorporation (Li *et al*., 2014) . These observations suggest coordinated regulation of precursor supply and terminal acyltransferase activity during stress progression.

A key determinant underlying the exceptional lipid productivity of *N. oceanica* CCMP1779 is the unusually large repertoire of genes encoding terminal TAG-synthesizing enzymes. Genomic analyses reveal that this strain encodes thirteen putative acyltransferases genes involved in TAG biosynthesis, including one DGAT type 1 and an expanded family of DGTT isoforms (Vieler *et al*., 2012; Li *et al*., 2016; Wei *et al*., 2017) . This represents one of the most extensive DGTT expansions described among sequenced microalgae and exceeds that reported for most other established model species.
Comparative analyses illustrate the exceptional nature of this expansion. *C. reinhardtii* contains nine DGTT genes alongside single DGAT type 1 and DGAT type 3 homologues (Liu *et al*., 2016; Bagnato *et al*., 2017), *P. tricornutum* encodes approximately five DGAT type 2 enzymes (Gong *et al*., 2013; Ding *et al*., 2023), and *Chlorella* species typically harbour three to six DGAT/DGTT genes depending on the strain (Guo *et al*., 2017; Kou *et al*., 2020). In contrast, the *DGTT* repertoire of *Nannochloropsis* represents an extreme case even among oleaginous microalgae.
This expanded acyltransferase network is thought to confer a high degree of metabolic flexibility, enabling precise regulation of TAG synthesis under diverse environmental conditions. Rather than relying on a single dominant enzyme, *Nannochloropsis* deploys a distributed system of DGTT isoforms that differ in expression dynamics, stress responsiveness, and functional contribution to TAG accumulation (Li *et al*., 2016; Zienkiewicz *et al*., 2017). Such an arrangement likely enhances both the robustness and magnitude of lipid production by enabling dynamic redistribution of metabolic flux among specialized enzymatic modules.

In addition to its exceptional lipid metabolism, *N. oceanica* CCMP1779 offers substantial practical advantages as a model system. Its relatively small genome, availability of high-quality genome annotations, established transformation protocols, and compatibility with modern genome editing technologies facilitate systematic functional analyses of lipid biosynthetic genes (Vieler *et al*., 2012; Li *et al*., 2016; Dhokane *et al*., 2023). Furthermore, its rapid growth, high biomass productivity, and tolerance to variable cultivation conditions support reproducible physiological and biochemical experimentation.
From a model biology perspective, the inducible and reversible nature of TAG accumulation in *Nannochloropsis* represents a major experimental advantage. Unlike seed plants, where lipid storage is developmentally fixed, TAG synthesis in *N. oceanica* can be precisely controlled through nutrient and light regimes, enabling time-resolved analyses of carbon partitioning, membrane remodeling, and LD biogenesis (Stavridou *et al*., 2024). This property facilitates direct investigation of regulatory transitions between growth and storage states.

Collectively, the combination of exceptional physiological TAG yields, an unusually expanded and diversified DGTT gene family, and advanced genetic accessibility firmly establishes *N. oceanica* CCMP1779 as a leading model for resolving functional hierarchy and specialization within microalgal TAG

biosynthesis pathways. These features provide a unique opportunity to integrate comparative genomics, heterologous expression, biochemical profiling, and native functional analyses, thereby enabling systematic dissection of DGTT function and regulation, as pursued in the present thesis.

1.7 Functional hierarchy and knowledge gaps within the expanded *NoDGTT* gene family

A defining genomic feature of *N. oceanica* CCMP1779 is the unusually extensive expansion of genes encoding DGTT enzymes. Comparative genome analyses consistently demonstrate that this strain encodes thirteen putative TAG-synthesizing acyltransferases, including one DGAT type 1 and an expanded family of DGTT isoforms, representing one of the largest DGTT repertoires reported among sequenced microalgae (Vieler *et al*., 2012; Li *et al*., 2016; Zienkiewicz *et al*., 2017). This degree of expansion clearly exceeds that observed in most other algal model systems and suggests strong lineage-specific selective pressures favoring diversification of terminal TAG synthesis machinery.

Phylogenetic analyses place *NoDGTT*s into multiple distinct clades, indicating that the family expanded through multiple rounds of gene duplication and divergence rather than through a single recent duplication event (Li *et al*., 2016). Many paralogs exhibit substantial variation in protein length, predicted transmembrane topology, and conserved motif composition, suggesting relaxed structural constraints and enabling functional differentiation. Such heterogeneity is consistent with the extensive structural diversification reported for *DGTT* families in other oleaginous microalgae.

At the cellular level, subcellular localization predictions and experimental evidence indicate that most NoDGTT isoforms are targeted to the ER, the principal site of TAG assembly and LD biogenesis (Liu *et al*., 2016; Wei *et al*., 2017; Zienkiewicz *et al*., 2017). Uniform ER localization supports their direct involvement in terminal TAG synthesis, whereas minor secondary targeting to other compartments observed for some isoforms may reflect auxiliary roles in lipid trafficking or turnover.

Among the expanded *DGAT/DGTT* repertoire, *NoDGAT1* and *NoDGTT5* represent the two isoforms for which functional evidence is most firmly established. Reverse genetic and overexpression studies demonstrate that DGAT1 plays a central role in bulk TAG accumulation, particularly under nitrogen deprivation, whereas DGTT5 functions as a stress-responsive acyltransferase closely linked to membrane lipid remodeling (Li *et al*., 2016; Wei *et al*., 2017; Zienkiewicz *et al*., 2017). These enzymes appear to operate within partially overlapping but non-identical functional regimes, suggesting hierarchical organization of TAG-synthesizing activities.

Despite these advances, the presence of more than ten additional *NoDGTT* paralogs raises fundamental questions regarding how TAG flux is distributed across this enzyme family. Transcriptomic analyses consistently reveal heterogeneous induction patterns under nutrient and environmental stresses, indicating that only subsets of isoforms are strongly engaged during TAG accumulation (Li *et al*., 2016; Poliner *et al*., 2018; Zienkiewicz *et al*., 2020). However, transcriptional regulation alone does not necessarily predict functional dominance at the protein or metabolic level.

Differences in enzyme stability, membrane topology, substrate specificity, and access to DAG and acyl-CoA pools may cause certain DGTTs to carry a disproportionate share of TAG flux even when expressed at comparable levels. Structural diversity within the NoDGTT family, manifested in variable protein length, transmembrane architecture, and predicted interaction surfaces, suggests that individual isoforms may be optimized for distinct physiological contexts, such as early versus late stress responses, recycling of specific membrane lipid pools, or channeling of particular acyl species into TAG (Liu *et al*., 2016; Zienkiewicz *et al*., 2017).

Genetic redundancy and compensatory mechanisms further complicate functional analysis. Studies in *C. reinhardtii* demonstrate that loss of individual DGTT genes can be masked by upregulation or enhanced activity of related paralogs, thereby complicating phenotypic interpretation (Lee *et al*., 2022). Given the even larger DGTT repertoire in *Nannochloropsis*, similar buffering effects are likely to occur, emphasizing the limitations of single-gene perturbation approaches. Moreover, the regulatory mechanisms coordinating DGTT activity with environmental stress signaling, membrane lipid remodeling, and LD biogenesis remain poorly defined. Although stress-induced TAG accumulation is tightly linked to ER dynamics and LD formation, it remains unclear how specific DGTT isoforms are recruited to these processes or whether distinct paralogs preferentially associate with specialized ER subdomains, LDs, or accessory proteins (Zienkiewicz *et al*., 2017).

Another unresolved aspect concerns functional specialization with respect to substrate utilization. Lipidomic analyses suggest that TAG species composition changes during stress progression, reflecting differential utilization of saturated, monounsaturated, and polyunsaturated FAs (Li *et al*., 2014). Whether individual NoDGTT isoforms preferentially channel FAs derived from *de novo* synthesis, chloroplast membrane remodeling, or cytosolic acyl-CoA pools remains largely unexplored. Finally, although heterologous expression studies demonstrate that many algal DGTTs retain catalytic activity across biological contexts, systematic cross-system validation remains limited. As a result, it is often difficult to disentangle intrinsic enzymatic properties from host-specific metabolic environments, thereby constraining functional interpretation.

Collectively, these unresolved issues highlight a critical gap between genomic expansion and functional understanding of DGTT enzymes in *N. oceanica*. Defining the functional hierarchy, specialization, and regulatory integration of individual NoDGTT isoforms is therefore central to elucidating the molecular logic of TAG biosynthesis in this genus. Addressing these questions forms the conceptual and experimental foundation of the present thesis.

1.8 Aims and scope of the present thesis

Previous functional studies of the expanded *DGTT* gene family in *N. oceanica* CCMP1779 focused primarily on the subgroup of six DGTT genes (*NoDGTT1 – NoDGTT6*) that are transcriptionally induced by nitrogen deprivation and were therefore presumed to play dominant roles in stress-induced TAG accumulation (Zienkiewicz *et al*., 2017). Using heterologous expression, native overexpression, and cross-kingdom validation, these studies identified NoDGTT5 as a highly efficient and biotechnologically valuable

TAG-synthesizing enzyme. However, the remaining six DGTT genes (*NoDGTT7 – NoDGTT12*), which do not display strong transcriptional induction under nitrogen deprivation, remained largely unexplored at the functional level.

The existence of this transcriptionally distinct subgroup raises fundamental questions regarding the functional organization of the DGTT family in *N. oceanica* CCMP1779. In particular, it remains unclear whether non-nitrogen-responsive DGTT isoforms represent redundant background activity, condition-specific regulators, or specialized enzymes contributing to TAG biosynthesis under alternative physiological states. Addressing this gap is essential for establishing a comprehensive model of DGTT-mediated lipid metabolism in this organism.

Against this background, the overarching aim of the present thesis is to functionally characterize the previously unexplored, non-nitrogen-responsive DGTT genes (*NoDGTT7 – NoDGTT12*) and to determine their contribution to TAG biosynthesis within the broader context of DGTT family diversification and specialization. By systematically extending earlier work on *NoDGTT1 – NoDGTT6*, this thesis seeks to elucidate whether functional hierarchy within the DGTT family is exclusively associated with nitrogen-responsive isoforms or whether additional high-performance enzymes are embedded within transcriptionally stable subgroups.

To achieve this aim, this work adopts a targeted, multi-system experimental strategy combining heterologous expression, native host manipulation, and plant-based validation. Particular emphasis is placed on resolving intrinsic catalytic properties independently of host-specific regulatory effects and on identifying isoforms with exceptional biotechnological potential.

The specific objectives of this research are as follows:

1. To perform comparative sequence and structural analyses of *NoDGTT7 – NoDGTT12* in order to identify conserved and divergent features that may underlie functional specialization within the non-nitrogen-responsive *DGTT* subgroup.
2. To functionally characterize *NoDGTT7 – NoDGTT12* through heterologous expression in the TAG-deficient yeast strain H1246, enabling quantitative comparison of their intrinsic TAG-synthesizing capacities under standardized metabolic conditions.
3. To identify high-performance *NoDGTT* candidates within this subgroup and to subject selected isoforms to detailed biochemical and lipidomic characterization in order to assess substrate preferences and effects on TAG composition.
4. To investigate the physiological impact of the most efficient isoform, in the native microalgal host through stable overexpression and phenotypic analysis under defined growth and stress regimes.
5. To evaluate the evolutionary conservation and functional robustness of the most efficient isoform through heterologous expression and complementation in *A. thaliana*, including analysis in the AS11 (*tag1-1*) mutant background, thereby enabling cross-kingdom validation of enzymatic performance.

In accordance with these objectives, this thesis is organized into seven main chapters. Chapter 1 introduces the biological, physiological, and evolutionary context of TAG metabolism, with particular emphasis on the diversification and functional expansion of DGAT/DGTT enzymes in microalgae. Chapter 2 details the experimental model organisms, reagents, equipment, and software used throughout the study. Chapter 3 describes the molecular, biochemical, and analytical methodologies applied in yeast, microalgal, and plant systems. Chapter 4 presents the results of *in silico* analyses and functional characterization of *Nannochloropsis oceanica* CCMP1779 *DGTT* isoforms, including heterologous expression in *S. cerevisiae* H1246, overexpression in *N. oceanica* CCMP1779, and complementation studies in *A. thaliana* AS11 (*tag1-1*). Chapter 5 discusses these findings in the context of DGAT/DGTT functional specialization, TAG biosynthesis, and physiological relevance, as well as their broader biotechnological implications. Chapter 6 summarizes the final conclusions and key take-home messages derived from this work. Chapter 7 contains the references cited throughout the thesis.

Collectively, this work extends previous functional studies of nitrogen-responsive DGTTs toward a comprehensive understanding of the expanded DGTT repertoire in *N. oceanica* CCMP1779. By elucidating the roles of non-nitrogen-responsive isoforms and establishing NoDGTT12 as a key contributor to TAG biosynthesis, this thesis advances current models of lipid metabolic regulation in microalgae and provides a rational foundation for future biotechnological exploitation of DGTT enzymes.

2. MATERIALS

2.1 Experimental model organisms

2.1.1 *Nannochloropsis oceanica* CCMP1779

Algae have emerged as promising candidates for biofuel production, primarily due to their capacity to accumulate significant amounts of lipids under adverse or stressful environmental conditions. Many microalgae are capable of producing lipids that can comprise 20 – 60% of their dry cell weight, predominantly in the form of TAGs, which serve as crucial precursors for biofuel (Zienkiewicz *et al*., 2016). To date, extensive screening has been conducted on thousands of algae species to evaluate their lipid profiles, resulting in the identification and characterization of several hundred oleaginous strains under both laboratory and outdoor culture conditions. Comprehensive databases, like *PhycoCosm* (*https://phycocosm.jgi.doe.gov*), integrate genomic data for over 100 microalgal species. Among these, the green alga *C. reinhardtii* has received the most comprehensive genetic analysis. However, it is not considered oleaginous due to its limited capacity for lipid accumulation. This limitation necessitates the exploration of alternative microalgal models with higher TAG productivity for targeted genetic manipulation and metabolic pathway optimization.

One of the most promising candidates is *Nannochloropsis* genus, which has attracted considerable attention for its exceptional biomass and lipid production capabilities. Even under normal growth conditions, *Nannochloropsis* species can accumulate approximately 10% of their dry weight as TAGs. Under stress conditions, such as nitrogen starvation, TAG accumulation can rise to as much as 60% of their dry weight (Van Vooren *et al*., 2012). Moreover, these small, unicellular green algae thrive in diverse environments, including marine, freshwater, and brackish waters, making them attractive sources for biofuel production. *Nannochloropsis* spp. are particularly suitable for lipid metabolism studies due to their relatively small genomes and the apparent expansion of gene families involved in lipid biosynthesis (Vieler *et al*., 2012; Wang *et al*., 2014; Zienkiewicz *et al*., 2016, 2020). Specifically, *N. oceanica* has emerged as an ideal experimental model for investigating lipid metabolism, thanks to several advantageous features: (1) rapid lipid production within hours, (2) ease of cultivation, (3) a well-characterized genome, (4) haploid genetics, and (5) straightforward DNA transformation techniques (Vieler *et al*., 2012; Zienkiewicz *et al*., 2017). Importantly, this marine oleaginous microalga offers also several benefits over not only other microalgal species but also traditional plant models like *A. thaliana*. These advantages include: (1) a unicellular, photosynthetic nature, (2) a brief life cycle ranging from 3 to 10 days, (3) highly controllable culture conditions, and (4) rapid manifestation of phenotypic or cellular responses to stress, often observable within hours. The combination of these attributes, along with a well-established molecular toolkit for *N. oceanica*, makes this microalga a highly suitable model for in-depth mechanistic studies of lipid metabolism, aimed at achieving the ideal “algal fuel cell”.

N. oceanica strain selected for this study was CCMP1779 and was purchased from the Bigelow National Center for Marine Algae and Microbiota (NCMA, East Boothbay, USA).

2.1.2 *Saccharomyces cerevisiae* H1246

S. cerevisiae (baker's yeast) has long been established as a premier model organism for the study of fundamental cellular processes relevant to higher eukaryotes. Its popularity in research is largely attributed to its eukaryotic cell structure, which shares many essential features with more complex organisms, including the presence of a nucleus, membrane-bound organelles, and highly conserved molecular pathways. These pathways encompass critical biological processes such as DNA replication, transcription, translation, cell cycle regulation, and metabolism, all of which are relevant to the understanding of eukaryotic biology at large (Peregrin-Alvarez *et al*., 2009; Vanderwaeren *et al*., 2022; Gaikani *et al*., 2024).

One of the most significant advantages of *S. cerevisiae* as a model organism is its fully sequenced genome, which was one of the first eukaryotic genomes to be completely sequenced in 1996 (Goffeau *et al*., 1996). This comprehensive genetic blueprint, combined with the ease of genetic manipulation, has paved the way for precise functional studies of individual genes and entire metabolic pathways. Genetic modifications in yeast are both straightforward and versatile, including techniques such as gene knockouts, overexpression systems, site-directed mutagenesis, and CRISPR-Cas9-based editing. This versatility allows researchers to systematically explore gene functions and interactions with exceptional precision. Furthermore, yeast is a highly efficient model for experimental studies due to its rapid growth rate, minimal nutritional requirements, and capacity for large-scale culture. Yeast cells can be propagated in both liquid and solid media, under aerobic or anaerobic conditions, making them amenable to various experimental setups. Additionally, their robustness and adaptability to diverse environmental conditions make them an attractive system for high-throughput screening and large-scale metabolic studies.
In recent years, *S. cerevisiae* has also emerged as a powerful tool for studying lipid metabolism, particularly due to its ability to be genetically engineered to modify lipid biosynthetic pathways. The *S. cerevisiae* H1246 strain used in this study is of particular interest in studies of TAG biosynthesis pathways. Unlike SCY62 strain (wild type) which retains functional copies of all the TAG synthesis-related genes, the H1246 (*MATα are1-Δ::HIS3 are2-Δ::LEU2 dga1-Δ::KanMX4 lro1-Δ::TRP1 ADE2 ura3*), generated in the SCY62 background, is a quadruple mutant with deletions in four key genes involved in TAG synthesis: Diacylglycerol Acyltransferase 1 (*DGA1,* a member of the DGAT2 family), Lecithin cholesterol acyltransferase Related Open reading frame (*LRO1*, a diglyceride acyltransferase), and the Acyl-coenzyme A: cholesterol acyl transferase-Related Enzymes *ARE1* and *ARE2* (Sandager *et al*., 2002). The H1246 strain thus produces neither TAGs nor LDs but is still viable, providing an excellent heterologous system to test the activity of enzymes such as DGATs (Zienkiewicz *et al*., 2016 and 2018).

The H1246 yeast strain utilized in this study was kindly provided as a gift from dr Magdalena Miklaszewska (University of Gdańsk, Poland).

2.1.3 *Arabidopsis thaliana* wild type (WT, ecotype Columbia, Col-0) and TAG-less mutant line (AS11, *tag1-1*)

A. thaliana is a well-established model organism extensively utilized in plant biology research due to its unique combination of advantageous traits: ease of genetic manipulation, a short life cycle (approximately 6 – 8 weeks), and a relatively simple and fully sequenced genome (Koornneef *et al*., 2010; Diaz, 2019). Its small size, rapid growth, and minimal cultivation requirements make it an ideal system for studying various aspects of plant biology, including genetics, development, biochemistry, and stress responses. Moreover, the extensive availability of genetic resources, mutant libraries, and comprehensive databases has further solidified its role as a critical model for functional genomics, agricultural biotechnology, and environmental science research.

One of the key strengths of *A. thaliana* as a model organism is the broad accessibility of genetically characterized lines, including mutants specifically designed to investigate lipid metabolism. Among these, the *A. thaliana* AS11 (*tag1-1*) line has proven particularly valuable for studying the mechanisms underlying TAG biosynthesis. The AS11 (*tag1-1*) line carries a semi-dominant mutation in a nuclear gene known as *TAG1*, which encodes a DGAT enzyme critical for TAG synthesis (Katavic *et al*., 1995). This mutation in the TAG1 gene results in notable disruptions in TAG biosynthesis. As a consequence, AS11 (*tag1-1*) plants exhibit several distinctive phenotypic traits compared to WT (Col-0) plants, including:

- reduced seed TAG content: the mutation significantly diminishes the overall TAG content within developing seeds,
- altered FA composition: AS11 (*tag1-1*) seeds exhibit decreased levels of very long-chain FAs, particularly eicosanoid acid (20:1) and oleic acid (18:1). Instead, α-linolenic acid (18:3) accumulates as the predominant FA present in TAGs,
- delayed seed development: altered lipid metabolism is associated with slower or impaired seed development compared to WT strains,
- modified TAG/DAG ratio: the AS11 (*tag1-1*) mutant consistently displays a lower TAG/DAG ratio during seed development, accumulating a higher proportion of DAG, which serves as the substrate for DGAT enzymes.

Through biochemical analyses, it has been demonstrated that AS11 (*tag1-1*) has no DGAT activity throughout seed maturation, which ultimately results in its reduced oil content phenotype. Further genetic analysis and cloning efforts identified the *TAG1* gene as being homologous to mammalian DGAT enzymes, confirming its function as a DGAT responsible for catalysing the final step of TAG synthesis (Katavic *et al*., 1995). Consequently, the combination of well-characterized genetic backgrounds, accessibility to genetic tools has made AS11 (*tag1-1*) not only an indispensable model for understanding lipid metabolism in plants, but also a perfect platform for heterologous expression and functional analysis of DGATs from diverse organisms (Zienkiewicz *et al*., 2017).

The AS11 (*tag1-1*) mutant line, along with its WT (Col-0) counterpart, were kindly provided as a gift from prof. Christoph Benning (Michigan State University, USA).

2.2 Laboratory equipment

TYPE	NAME	MANUFACTURER
Agarose gel electrophoresis	Sub-Cell GT Cell	Bio-Rad
Autoclave	Varioclav 135S	HP Labortechnik
Automatic pipette, adjustable	Research Plus 0.1 – 2.5 µl	Eppendorf
	Research Plus 2 – 20 µl	Eppendorf
	Research Plus 20 – 200 µl	Eppendorf
	Research Plus 100 – 1000 µl	Eppendorf
Centrifuge	Avanti J-26S XPI	Beckman Coulter
	MiniSpin plus	Eppendorf
	Avanti J-26S XPI Centrifuge with J-LITE JLA-10.500 fixed angle rotor	Beckman Coulter
	Optima XE Ultracentrifuge with SW 32 Ti swing-bucket rotor	Beckman Coulter
Chemiluminescence imaging system	ChemiDoc	Bio-Rad
Confocal microscope	FV 3000	Olympus
Electroporator	Gene Pulser Xcell Electroporation System	Bio-Rad
Freezers	-80 °C New Brunswick™	U725 Innova
	-20 °C Liebherr Premium	Liebherr
Gas chromatograph with flame ionization detector (GC-FID)	8860	Agilent
Gel documentation system for agarose gel	BioSpectrum 410	UVP
Heating block	ThermoMixer comfort	Eppendorf
Incubator	CLN32	Pol-Eko
Incubator shaker	ES-20	Biosan
Lamp for algae and plant culturing	FITO PANEL	Biogenet
Liquid scintillation counter	Hidex	300 SL
Magnifier/light microscope	DELTA	IPOS810
Mixer Mill	MM 400	Retsch
Multitube vortex	VXMTAL	Ohaus
Orbital shaker	Excella E10	New Brunswick Scientific
	SHHD1619AL	Ohaus
Oven	UN260	Memmert

pH meter	SevenExcellence	Mettler-Toledo
Polyacrylamide gel electrophoresis system	Mini-PROTEAN Tetra Cell	Bio-Rad
Power unit	PowerPac™ HC	Bio-Rad
Refrigerator	ADN 203/1S	Whirlpool
	SJ-FBA05DHXWE-EU	Sharp
Spectrophotometer	NanoDrop™ 2000	Thermo Scientific
	Spectroquant® Prove 100	Merck
Static image analyser	Camsizer M1	Microtrac
Tank blotting/transfer system	Mini Trans-Blot Cell	Bio-Rad
Thermocycler	Nexus Gradient GSX1	Eppendorf
TLC developing chamber	814019	Macherey-Nagel
TLC sprayer	TLC sprayer	CAMAG
Transilluminator	ETX-F26.M	Vilber
Vortex bath	Vortex Genie 2	Scientific Industries
Water bath with shaking	SWB16N	LaboPlay
Laboratory scale	PA224	Ohaus

2.3 Chemicals and enzymes

CHEMICAL	MANUFACTURER	CATALOG NO.
[^{14}C]-Glycerol	Larodan	ARC 0217-250
β-mercaptoethanol	Sigma-Aldrich	614920
Acetic acid	P.H.H. Stanlab Sp.J.	607-002-00-6
Acetone	Merck	8222512500
Acetonitrile	Honeywell	34967-2,5L
Agar	Sigma-Aldrich	102775038
Agarose	EURx	E0301
Amersham ECL Western Blotting Detection Reagent	Cytiva	RPN2209
Ammonium persulfate (APS)	Sigma	A3678
Ammonium sulphate	Chempur	11139720
Bio-Safe Coomassie Stain	Bio-Rad	1610787
Biotin (vit. B_7)	Sigma-Aldrich	1002922288
BODIPY™ 505/515	Invitrogen	D3921
Bromophenol blue	Chempur	115-39-9
Bovine Serum Albumine (BSA)	Sigma-Aldrich	A6003

Chloroform	Merck	1070242500
Cobalamin (vit. B_{12})	Sigma-Aldrich	103005003
Cobalt chloride	Chempur	115123407
Copper sulfate	Chempur	116582805
Diethyl ether	Honeywell	32203
Dimethoxypropane	Sigma-Aldrich	D136808
Dimethyl sulfoxide (DMSO)	Honeywell	41640
DL-Dithiothreitol, 98% (DTT)	Chemat	CM11990C
dNTP Mix	Thermo Scientific™	R0191
Ethylenediaminetetraacetic acid (EDTA)	Chempur	118798103
Ethyl alcohol 96%	Alpinus	2414124
Fatty Acid Methyl Esters Standard Mixture (FAME)	Sigma-Aldrich	SMB00937
Iron chloride, $FeCl_3$	Chempur	115123407
Galactose	Thermo scientific	150610010
Glucose	Chempur	114595600
Glufosinate ammonium (BASTA)	Thermo Scientific™	J66186.03
Glycerol	Honeywell	49770
Glycine	Glentham life science	56-40-6
HEPES	Duchefa Biochemie	H1504
Heptane	Honeywell	32287
Hexane	Honeywell	32293
Iodine	Merck	104761
Lithium acetate, LiAc	Sigma-Aldrich	L6883
Luria Broth (LB)	NZYTECH	MB14501
Methanol	Honeywell	34966-2,5L
Manganese chloride, $MnCl_2$	Merck	K52907927047
Murashige and Skoog (MS) Basal Salts with minimal organics	Sigma-Aldrich	M6899
Natural sea salt, pH=9-10	TropicMarin	25112
NEBuffer	New England Biolabs	B7001S
Paraformaldehyde	Polysciences	18814
Phosphate buffered saline (PBS)	Invitrogen	003002

Peptone	Millpore	70171
Perfect 100 bp ladder	EURx	E3134
Perfect 100-1000 bp ladder	EURx	E3141
Perfect™ Tricolor Protein Ladder	EurX	E3210
Petroleum ether	J.T. Baker	9265.2500
Phenylmethylsulfonyl fluoride (PMSF)	PanReac AppliChem	A0999.0005
Polyethylene glycol (PEG) 3350	Sigma-Aldrich	P4338
Potassium dihydrogen phosphate, KH_2PO_4	Eurochem BGD Sp z o o	7778-77-0
Potassium hydrogen phosphate, K_2HPO_4	Eurochem BGD Sp z o o	7758-11-4
Powdered milk	Spółdzielnia Mleczarska Gostyń	5900691-033217
Primuline	Sigma-Aldrich	206865
Protease inhibitors	Roche	12352204
Raffinose	Thermo Scientific	195675000
Salmon sperm carrier DNA	Invitrogen	15632011V
Silwet-77	Arysta	2200384
Sodium chloride, NaCl	P.H.H. Stanlab Sp.J.	7647-14-5
Sodium dihydrogen phosphate, NaH_2PO_4	Chempur	117991808
Sodium dodecyl sulfate (SDS)	Sigma-Aldrich	74255-250g
Sodium hydrogen carbonate, $NaHCO_3$	Chempur	118105307
Sodium hypochlorite	NTCE	CHLOROX S
Sodium molybdate, Na_2MoO_4	Chempur	118033700
Sodium nitrate $NaNO_3$	Sigma-Aldrich	221341
Sorbitol	Sigma-Aldrich	S1876
Sucrose	Chempur	17720907
Sulfuric acid, H_2SO_4	P.H.H. Stanlab Sp.J.	016-020-00-8
Tetramethylethylenediamine (TEMED)	Merck	1.10732.0100
Thiamine (vit. B_1)	Sigma-Aldrich	PHR1037-1g
Toluene	Honeywell	32249-12
Trifluoroacetic acid	Sigma-Aldrich	302031
Trifluoroacetic anhydrine	Sigma-Aldrich	91719
Tripentadecanoin	Merck	T4257
Tris base	Sigma-Aldrich	BP152-1

Tween 20	Sigma-Aldrich	P1379
Ultima Gold LSC Cocktail	Revvity	6013321
Yeast extract for microbiology	Sigma-Aldrich	92144
Yeast nitrogen base without amino acids	Sigma-Aldrich	Y0626
Yeast synthetic drop-out medium supplements without uracil	Sigma-Aldrich	Y1501
Zinc sulfate $ZnSO_4$	Chempur	112657501

ENZYME	MANUFACTURER	CATALOG NO.
AscI restriction enzyme	New England Biolabs	R0558
AseI restriction enzyme	New England Biolabs	R0526
BP Clonase™ II enzyme mix	Invitrogen	11789020
Color Perpetual Taq PCR Master Mix	EURx	E2745
DNase I	EURx	E1345
HpaI – restriction enzyme	New England Biolabs	R0105
LR Clonase™ enzyme mix	Invitrogen	11791020
Methanol	Honeywell	34966-2,5L
Phusion™ DNA Polymerase	Thermo Scientific™	F530
Phusion™ Plus DNA Polymerase	Thermo Scientific™	F631
Phusion™ Plus Master Mix	Thermo Scientific™	F631S
Proteinase K	Sigma-Aldrich	1.07393
RevertAid Reverse Transcriptase	Thermo Scientific™	EP0441
T4 DNA ligase	New England Biolabs	M0202S

2.4 Kits

KIT	KIT COMPONENTS	MANUFACTURER, CAT. NO.
CloneJET PCR Cloning Kit	• pJET1.2/blunt Cloning Vector • T4 DNA Ligase • 2X Reaction Buffer • DNA Blunting Enzyme	Thermo Scientific™, K1231
Monarch® DNA Gel Extraction Kit	• Gel Dissolving Buffer • DNA Wash Buffer • DNA Elution Buffer • DNA Cleanup Columns • Monarch Collection Tubes	New England Biolabs, T1020
NucleoSpin Plasmid EasyPure kit	• Resuspension Buffer A1 • Lysis Buffer A2 • Neutralization Buffer A3 • Wash Buffer AQ • Elution Buffer AE • RNase A	Macherey-Nagel, 740727

	• NucleoSpin® Plasmid EasyPure Columns • Collection Tubes	
Pierce™ Bradford Protein Assay Kit	• Pierce Bradford Assay Reagent • Albumin Standard ampules	Thermo Scientific™, 23200
Plasmid Miniprep DNA Purification Kit	• PL buffer • Cell R buffer • Lysis Blue buffer • Neutral B buffer • Wash PLX1 buffer • Wash PLX2 buffer • Elution buffer • DNA Binding Columns	EURx, E3500
TGX FastCast kit	• Resolver A solution • Resolver B solution • Stacker A solution • Stacker B solution	BioRad, 1610173
Universal RNA Purification Kit	• LG buffer • RL buffer • Wash DN1 buffer • Wash RBW buffer • DNR buffer • RNase-free water • Homogenization Columns • RNA Binding Columns	EURx, E-3598

2.5 Consumables

CONSUMABLE TYPE	MANUFACTURER	CATALOGUE NUMBER
3 MM Blotting paper, thickness 0.34 mm	Whatman	4928.1
Acid-washed glass beads (ø 425-600 µm)	Sigma	G8772
Culture tubes (14 ml)	Thermo Scientific	150268
DB-23 GC capillary column	Agilent	122-2332
Falcon tubes	NEST Biotech	• 15 ml – 601001 • 50 ml – 602052
Erlenmeyer flasks	Chemland	• 50 ml – 08-231.202.02 • 100 ml – 08-231.202.03 • 1000 ml – 08-231.202.09
Eppendorf tubes	Eppendorf	• 0.2 ml – 0030124359 • 1.5 ml – 0030120086 • 2.0 ml – 0030120094
Electroporator cuvettes	Bio-Rad	1652086
Glass pipettes	DWK	91704012

GC vials	Agilent	5182-0714
GC vials insert	Agilent	5181-1270
GS vials screw caps	Agilent	5182-0717
Immobilon®-P PVDF membranes	Millipore	IPVH00010
Kimble glass tubes	DWK	231751159
Open-top glass tubes	Brand	114106
Pellet pestles	DWK	7495211590
Petri dishes	Sarsted	82.1472.001
Pipette tips	Eppendorf	• 10 µl – 0030000811 • 200 µl – 0030000870 • 1000 µl – 0030000919
Plant pots	Grow world	BOX-00483
Polycarbonate centrifuge tubes	Beckman Coulter	355631
Polypropylene centrifuge bottles	Nalgene	3120-9500
Scintillation vials	Sarstedt	73.662.500
Seal-R-film™	Brand	701625
Soil	Plagron	Lightmix
Spectrophotometer cuvettes	Kartell™	0193800
Sterile filtering bottles	JetBiofil	FMC201500
TLC glass plate covered with silica gel layer	Macherey-Nagel	809013

2.6 Cells, vectors and antibodies

NAME	MANUFACTURER	CATALOGUE NUMBER
Agrobacterium tumefaciens GV3101	GoldBio Gold Biotechnology®	CC-207
One Shot™ TOP10 Chemically Competent *E. coli*	Invitrogen	C404010
Subcloning Efficiency™ DH5α Competent Cells *E. coli*	Invitrogen	18265017
pDONR™221 vector	Invitrogen	12536017
pJET1.2/blunt vector, CloneJET PCR Cloning Kit	Thermo Scientific™	K1231
pNOC-OX-CFP vector	Kindly provided as a gift by prof. Eric Poliner, Michigan State University (East Lansing, USA)	-
pUBC-CFP-Dest vector	Kindly provided as a gift by dr Anna Kasprowicz - Maluśki,	-

	Adam Mickiewicz University (Poznań, Poland)	
pYES2.1 Yeast Expression Vector, pYES2.1 TOPO™ TA Yeast Expression Kit	Invitrogen	K4150-01
Anti-GFP primary antibody produced in mouse	Sigma-Aldrich	G6539
Anti-mouse secondary antibody produced in rabbit, peroxidase stained	Sigma-Aldrich	A9044
Anti-GFP antibody produced in mouse, peroxidase stained	Miltenyi Biotec	130-091-833

2.7 Primers

TARGET SEQUENCE	(5‘) FORWARD AND REVERSE PRIMERS (3‘)
Elongation factor (EF) reference gene from *N. oceanica* CCMP1779	NoEF1F: TCAGATCCAAAACGGCTACTGC NoEF1R: GGTACGTCGGTCAATCTTTTCC
NoDGTT5 coding sequence	NoDGTT5F: ATGACGCCGCAAGCCGACATCACCAGCAAGACGA NoDGTT5R: CTCAATGGACAACGGGCGCGTCTCCC ACTCC
NoDGTT7 coding sequence	NoDGTT7F: ATGTTGCTGGCGTCGTCT NoDGTT7R: TCAGACGATGCGAAGCG
NoDGTT8 coding sequence	NoDGTT8F: ATGACATCCTCCCCACCA NoDGTT8R: TCACCTGACCACTAAGGTGG
NoDGTT11 coding sequence	NoDGTT11F: ATGGGTCTATTTGGCAG NoDGTT11R: CTAAAAGAAATTCAACGTCC
NoDGTT12 coding sequence	NoDGTT12F: ATGCATCCTCTAACAGGTGC NoDGTT12R: CTAATAAAGCTCCAGCTCCC
NoDGTT12 coding sequence flanked with *Asc*I and *Hpa*I restriction sites	NoDGTT12FAscI: GCGCGCGGCGCGCCATGCATCCTCTAACAGGTGC NoDGTT12RHpaI: GCGCGCGTTAACCTAATAAAGCTCCAGCTCCC
NoDGTT12 coding sequence flanked with attB1 and attB2 sites	NoDGTT12B1: GGGGACAAGTTTGTACAAAAAAGCAGGCTTA ATGCATCCTCTAACAGGTGC NoDGTT12B2a: GGGGACCACTTTGTACAAGAAAGCTGGGTG ATAAAGCTCCAGCTCCC
Genotyping of *A. thaliana* AS11 plants	As11A: CGACCGTCGGTTCCAGCTCATCGG As11B: GCGGCCAATCTCGCAGCGATCTTG As11C: TAAACAGTAGACTCATCATCG

2.8 Solutions, buffers and media

2.8.1 Antibiotics

ANTIBIOTIC	MANUFACTURER	CATALOGUE NUMBER
Carbenicillin	Duchefa-Biochemie	C0109.0025
Gentamycin	Duchefa-Biochemie	G0124.0025
Hygromycin B	Roth	CP12.2
Kanamycin	Duchefa-Biochemie	K0126.0025
Rifampicin	Duchefa-Biochemie	R0146.0025
Spectinomycin	Duchefa-Biochemie	S0188.0025

Streptomycin	Sigma-Aldrich	S6501

2.8.2 Solutions, buffers

SOLUTION/BUFFER TYPE	COMPOSITION (working concentration)
BODIPY™ 505/515 working solution	• 10 µM BODIPY™ 505/515 • 1x PBS buffer • Ultrapure water
EB buffer	• 200 mM Tris-HCl pH=7.5 • 250 mM NaCl • 25 mM EDTA • 0.5% (w/v) SDS • Distilled water
FAME solution	• Methanol/toluene (2:1 v/v) • 2.5% (v/v) H_2SO_4 (95-97%) • 2% (v/v) Dimethoxypropane
Fixative solution	• 4% (v/v) Paraformaldehyde • 1x PBS buffer
HEPES buffer	• 50 mM HEPES • 5 mM $MgCl_2$ • Distilled water
2x Laemmli buffer 100ml	• 100 mM Tris-HCl pH=6.8 • 4% (w/v) SDS • 0.2% (v/v) Bromophenol blue • 20% (v/v) Glycerol
LD buffer for SDS-PAGE	• 1.8x Laemmli buffer • 1 mM DTT
1x PBS buffer	• 1 tablet / 100 ml distilled water • (10 mM phosphate • 150 mM sodium chloride)
PLATE solution	• 40% (w/v) PEG3350 • 100 mM LiAc • 10 mM Tris-HCl (pH 7.5) • 0.4 mM EDTA • Ultrapure water
100 mM Potassium phosphate buffer pH=7.2	• 71.7 mM K_2HPO_4 • 28.3 mM KH_2PO_4 • Distilled water
Protein isolation buffer for *N. oceanica*	• 100 mM Tris-HCl pH=8.0 • 2 mM PMSF • 2% (v/v) β-mercaptoethanol • 4% (w/v) SDS • Ultrapure water
10x SDS Running buffer	• 0.25 M Tris-HCl • 1.92 M Glycine • 1% (w/v) SDS • Distilled water
50x TAE buffer	• 2.0 M Tris base • 1.0 M Acetic acid • 0.05 M EDTA • Distilled water
1x TAE buffer	• 40 mM Tris base

	• 20 mM Acetic acid • 1 mM EDTA • Distilled water
1x TE buffer	• 10 mM Tris-HCl pH=8 • 1 mM EDTA • Distilled water
10x TBS buffer	• 100 mM Tris • 1.5 M NaCl • Distilled water
1x TBST buffer	• 10 mM Tris • 150 mM NaCl • 0.1% (v/v) Tween 20 • Distilled water
TLC mobile phase	• 79% (v/v) Petroleum ether • 20% (v/v) Diethyl ether • 1% (v/v) Acetic acid
10x Transfer buffer for western blotting	• 0.25 M Tris • 0.5 M Glycine • Distilled water
1x Transfer buffer working solution	• 1x Transfer Buffer • 20% (v/v) EtOH • Distilled water
Yeast cell disruption buffer	• 20 mM Tris-HCl pH=7.9 • 10 mM $MgCl_2$ • 1 mM EDTA • 5% (v/v) Glycerol • 1 mM DTT • 30 mM Ammonium sulphate • 1x Protease inhibitors • Ultrapure water

2.8.3 Growing media

MEDIUM TYPE	COMPOSITION
½ MS + sucrose solid medium	• 0.22% (w/v) MS Basal Salts with minimal organics • 1% (w/v) Sucrose • 0.8% (w/v) Agar • Distilled water
½ MS – sucrose solid medium	• 0.22% (w/v) MS Basal Salts with minimal organics • 0.8% (w/v) Agar • Distilled water
½ MS + sucrose solid medium + BASTA	• 0.22% (w/v) MS Basal Salts with minimal organics • 1% (w/v) Sucrose • 0.8% (w/v) Agar • 20 µg/l BASTA • Distilled water
LB liquid medium	• 2.5% (w/v) LB broth • Distilled water
LB solid medium	• LB liquid medium • 1.5% (w/v) Agar
LB solid medium with antibiotic (carbenicillin or kanamycin)	• LB liquid medium • 1% (w/v) Agar • antibiotic to 50µg/ml
SC -URA liquid medium (non-	• 0.67% (w/v) Yeast nitrogen base without amino acids

inducible)	• 0.192% (w/v) Yeast synthetic drop-out medium supplements without uracil • 2% (w/v) Glucose • Distilled water
SC -URA liquid medium (inducible)	• 0.67% (w/v) Yeast nitrogen base without amino acids • 0.192% (w/v) Yeast synthetic drop-out medium supplements without uracil • 2% (w/v) Galactose • 1% (w/v) Raffinose • Distilled water
SC -URA solid medium	• SC -URA liquid medium • 1.5% (w/v) Agar
YPD liquid medium	• 1% (w/v) Yeast extract • 2% (w/v) Peptone • 2% (w/v) Glucose • Distilled water
YPD solid medium	• YPD liquid medium • 2% (w/v) Agar
F/2 medium	• For detailed recipe see point 2.8.4 (below) • + V: supplemented with vitamin • +Hyg: supplemented with hygromycin (100 µg/ml) • -N: lacking nitrogen source

2.8.3.1 F/2 medium for culturing *Nannochloropsis oceanica* CCMP1779

NAME	COMPONENT	STOCK SOLUTION CONCENTRATION	AMOUNT FOR 1L OF MEDIUM
Sea salt	Natural sea salt, pH=9-10	–	16.6 g
C-solution	$NaHCO_3$	0.5 M	40 ml
B-solution	Tris solution, pH=7.6	2 M	5 ml
N-solution	$NaNO_3$	0.88 M	2,5 ml
P-solution	NaH_2PO_4	0.21 M	1 ml
Fe-solution	Iron source (see recipe below)	–	1 ml
T-solution	Trace metals (see recipe below)	–	1 ml
V-solution	Vitamin stock (see recipe below)	–	1 ml
Agar*	Agar*	–	10 g*
Distilled water	–	–	to 1000 ml

Filter all the solutions in a sterile condition to separate, sterile bottles.

* Only for solid F/2 medium: add sea salt, agar and all the solutions, except V-solution. Autoclave and cool down to 55 °C. Add V-solution in a sterile condition.

Fe solution:

Component	Primary stock solution	
$FeCl_3$	6.5 g/L	0.04 M
EDTA, pH=8.0	45 g/L	0.15 M

Dissolve EDTA in 500 ml of distilled water and adjust to pH=8.0. Dissolve $FeCl_3$ separately and add into EDTA. Adjust pH=4.5 and add distilled water up to 1 L.

T-solution:

Component	Primary stock solution	Amount for 1L final solution
$CuSO_4$	9.8 g/L	5 ml
Na_2MoO_4	6.3 g/L	5 ml
$ZnSO_4$	22.0 g/L	5 ml
$CoCl_2$	10.0 g/L	5 ml
$MnCl_2$	180.0 g/L	5 ml

Take 5 ml of each trace metal solution and add 10 ml of 500 mM EDTA, pH=8.0. Carefully adjust to pH=4.5 and add distilled water up to 1 L.

V-solution:

Component	Primary stock solution	
Biotin (vit. B_7)	5 mg/L	3.77×10^{-3} M
Cobalamin (vit. B_{12})	5 mg/L	0.74×10^{-3} M
Thiamine (vit. B_1)	1 mg/L	4.09×10^{-3} M

Dissolve the vitamin in 750 ml of distilled water and add distilled water up to 1 L.

2.9 Software and services

NAME	MANUFACTURER
Agilent ChemStation software	Agilent Technologies, USA
BLAST software	NCBI, Bethesda, USA
DeepTMHMM – 1.0 software	Technical University of Denmark
DeepLoc – 2.0 software	Technical University of Denmark
DeltaOpticalDLTCamViewer	Delta Optical
Dimensions M1software	Microtrac
ExPASy software	Swiss Institute of Bioinformatics
Fiji software	*www.fiji.sc*
Genomed S.A (genotyping)	*www.genomed.pl*, Gdansk, Poland
ImageJ software	National Institutes of Health, USA
Oligo Evaluator™ software	Sigma-Aldrich
Olympus FluoView 3000 software	Olympus, Japan
PRALINE software	Centre for Integrative Bioinformatics VU Amsterdam
Protter software	Bernd Wollscheid lab
SnapGene software	*www.snapgene.com*

3. METHODS

The overall experimental workflow of this research is illustrated in Figure 2 and outlines the strategy used to investigate the potential of *N. oceanica* CCMP1779 DGAT-encoding genes to enhance TAG accumulation across three biological systems: *S. cerevisiae*, *N. oceanica*, and *A. thaliana*. In the *N. oceanica* CCMP1779 genome, two classes of *DGAT* genes are encoded: *DGAT* type 1 and *DGAT* type 2 (Zienkiewicz *et al*., 2017). The present study focuses specifically on *DGAT* type 2 genes, which, for clarity of nomenclature, will hereafter be named as DGTT-encoding genes. Each organism was selected to address specific questions related to TAG biosynthesis and accumulation, with methodologies tailored to maximize analytical accuracy and depth (details provided in the following sections). This study employed multiple genetic manipulation approaches, including heterologous expression and overexpression of NoDGTT-encoding genes, combined with a diverse set of analytical techniques. These techniques included microscopic analyses to assess cellular features of TAG accumulation; lipid extraction followed by quantitative and qualitative TAG profiling using GC-FID; and protein extraction coupled with chemiluminescent assays to detect *NoDGTT*s expression in the experimental models. Additionally, microsomal extractions were conducted to measure the *in vitro* enzymatic activity of NoDGTTs toward various substrates, further clarifying their functional roles in TAG synthesis. Together, these integrated experimental strategies provided a comprehensive framework for mechanistic characterization of selected *N. oceanica* DGTTs, offering unique advantages for functional studies.

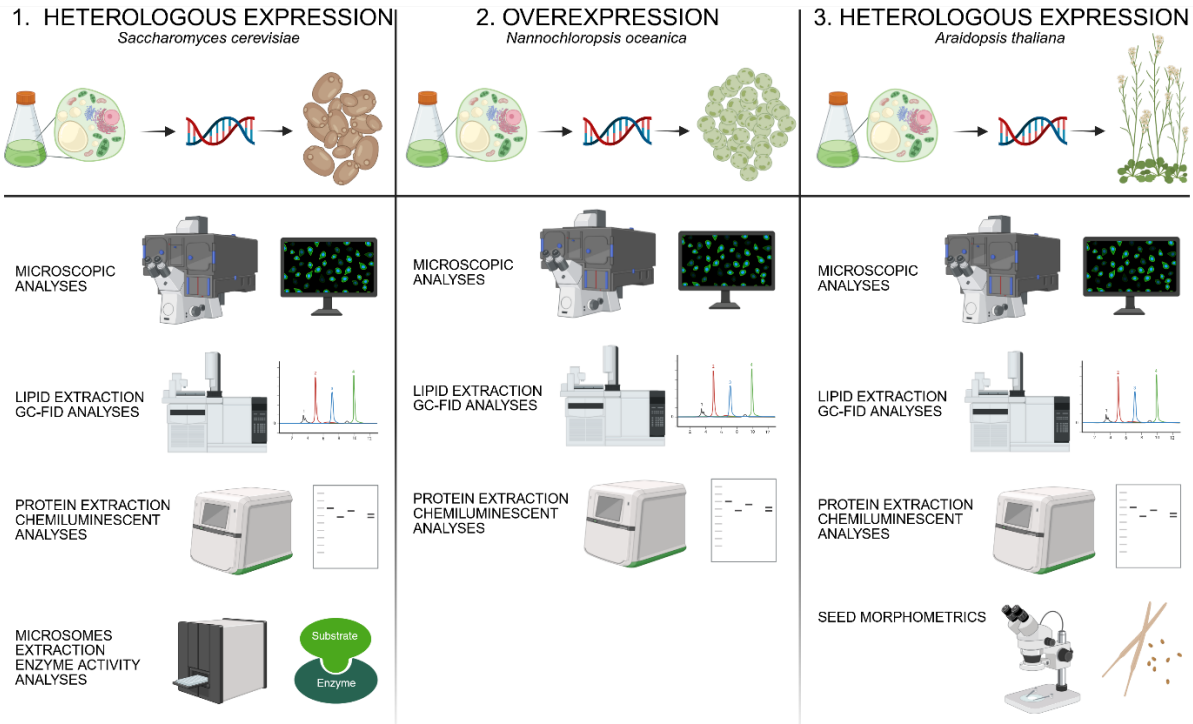

Figure 2. Overall workflow of the project. (1) Heterologous expression analysis of *NoDGTT*s in *S. cerevisiae* H1246 strain. (2) Overexpression of candidate *NoDGTT* in *N. oceanica* CCMP1779. (3) Heterologous expression analysis of candidate *NoDGTT* in *A. thaliana* WT (ecotype Columbia) and AS11 (*tag1-1*) lines.

3.1 Experimental procedures for *Saccharomyces cerevisiae* H1246

3.1.1 Culturing of *Saccharomyces cerevisiae* mutant strain H1246

S. cerevisiae strain H1246 was maintained in the laboratory on solid YPD standard medium (for composition see Section 2.8). The medium was sterilized by autoclaving at 121 °C for 15 min and subsequently poured into sterile Petri dishes under aseptic conditions. After solidification, yeast cells were streaked onto the agar surface using a sterile inoculating loop and incubated at 28 °C for 48 h to allow colony formation. Plates were then sealed with parafilm and stored at 4 °C for short-term preservation. All colonies were routinely refreshed and maintained regularly in the laboratory by restreaking onto fresh YPD plates every two weeks to ensure viability and prevent genetic drift.

3.1.2 Acquisition of *Nannochloropsis oceanica* CCMP1779 genes encoding DGTTs for transformation of H1246 yeast strain

The DGTT-encoding genes from the *N. oceanica* CCMP1779 genome were retrieved from the Joint Genome Institute *PhycoCosm* database, an integrative genomic platform dedicated to algal resources. All genome data and annotations were accessed based on the assembly and characterization previously described by Vieler *et al*. (2012). The nucleotide sequences of the *N. oceanica* CCMP1779 *DGTT* genes were translated into their corresponding amino acid sequences using the *ExPASy* tool and subsequently used for downstream analyses. These analyses included predictions of protein structural features, transmembrane domain detection and topology, as well as inference of subcellular localization for individual NoDGTT proteins. All predictions were performed using two online tools, *DeepLoc 2.0* and *Protter*, to compare outputs and increase confidence in the results.

Next, PCR primers were designed based on the gene sequences using the Oligo Evaluator™ online tool to specifically amplify the full coding sequences of the selected *N. oceanica* CCMP1779 *DGTT* genes. Complementary DNA (cDNA), obtained by reverse transcription of RNA extracted from *N. oceanica* CCMP1779, served as the template for primer binding, ensuring that amplification was restricted to transcribed regions and captured the full-length open reading frames for subsequent analysis, as described in Section 3.2.1. The quality of the cDNA was verified by assessing the expression of the *N. oceanica* CCMP1779 elongation factor-encoding gene (EF), used as a reference due to its high constitutive expression in algal cells (Zienkiewicz *et al*., 2017), as detailed in Section 3.2.3.

High-quality cDNA served as the template for PCR amplification of *NoDGTT* genes for subsequent ligation into the pJET1.2 vector. The composition of the master mix and PCR reaction conditions are provided in Table 1 and Table 2.

Table 1. Composition of PCR master mix for amplification of *NoDGTT*s sequences on *N. oceanica* CCMP1779 cDNA

COMPONENT	VOLUME/REACTION	FINAL CONCENTRATION
Phusion™ Plus Master Mix (2x)	10 µl	• 1 U of Phusion™ Plus DNA Polymerase • 1x Reaction Buffer (1.7 mM $MgCl_2$) • 0.2 mM of each dNTP
NoDGTTsF primer (see p. 2.7)	0.5 µl	10 mM
NoDGTTsR primer (see p. 2.7)	0.5 µl	10 mM
Molecular biology grade water	to 20 µl	–
Template DNA	2.0 µl	< 0.2 µg/20 µl
Total volume	20 µl	–

Table 2. Conditions of PCR reaction from Table 1.

STEP	TEMPERATURE	TIME	NUMBER OF CYCLES
Initial denaturation	98 °C	30 sec	1
Denaturation	98 °C	10 sec	30
Annealing*	*see below*	10 sec	
Extension	72 °C	30 sec	
Final extension	72 °C	5 min	1
Cooling	4 °C	indefinite	1

*Annealing temperature for *NoDGTT5* - 60 °C, for *NoDGTT7* - 60 °C, for *NoDGTT8* - 58 °C, for *NoDGTT11* - 50 °C, for *NoDGTT12* - 55 °C.

3.1.3 Ligation of *NoDGTT*s full-length coding sequences into pJET1.2/blunt vector

For bacterial cloning, the full-length DGTT coding sequences obtained from *N. oceanica* CCMP1779 were inserted into the pJET1.2/blunt vector (Figure 3) using a sticky-end cloning approach, following the manufacturer's protocol. The vector contains: (1) a T7 promoter commonly used to drive recombinant protein expression; (2) a multiple cloning site with various restriction enzyme recognition sequences; and (3) an ampicillin-resistance gene for selection and identification of successfully transformed cells.

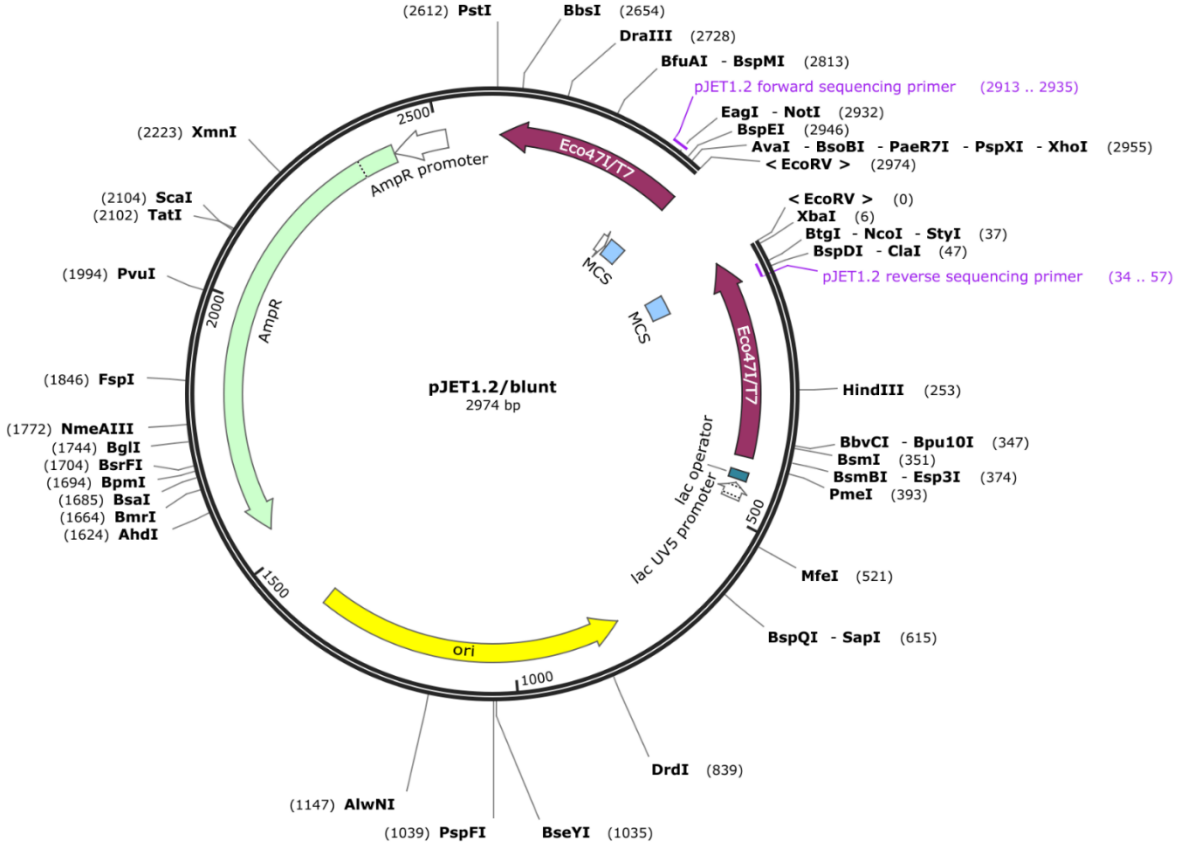

Figure 3. pJET1.2/blunt, circular vector map. Key features of the plasmid (1) AmpR (green arrow) – ampicillin resistance cassette for the positive selection of transformed *E. coli* carrying the plasmid, (2) ori – origin of replication (yellow arrow), responsible for the plasmid replication in transformed bacterial cells, (3) MCS – multiple cloning site (blue squares), containing recognition sites for specific restriction enzymes used for cloning purposes, (4) lac promoter and lac operator – commonly used to regulate gene expression of recombinant proteins, and (5) sequencing primer sites (indicated with purple font) – facilitate sequencing of inserted DNA fragments for their verification. Generated by SnapGene software.

The cloning procedure included both a blunting reaction and a ligation step. The blunting reaction was prepared on ice by combining the reagents listed in Table 3.

Table 3. Composition of blunting reaction mix for pJET1.2 vector

COMPONENT	VOLUME/REACTION	FINAL CONCENTRATION
2x reaction buffer	10 µl	1x
Non-purified PCR product	3 µl	0.45 pmol
Nuclease-free water	to 17 µl	–
DNA blunting enzyme	1 µl	–
Total volume	18 µl	–

The reaction mixture was gently mixed with a pipette tip, briefly centrifuged, and incubated for 5 min at 70 °C. Immediately after the blunting reaction, the ligation reaction was set up on ice by adding 1 µl of pJET1.2/blunt cloning vector (50 ng/µl) and 1 µl of T4 DNA ligase to the blunting mixture, bringing the final volume to 20 µl. The ligation mixture was then incubated at room temperature for 30 min.

Prior to transformation, Subcloning Efficiency™ DH5α *E. coli* competent cells were thawed on ice. A total of 5 ng of the DNA construct generated above was added to 100 µl of competent cells and mixed gently by flicking the tube. The samples were incubated on ice for 30 min, followed by heat shock at 42 °C for 30 sec in a heating block without shaking to facilitate transformation. The tubes were immediately returned to ice for 2 min, after which 900 µl of pre-warmed sterile LB medium was added to each tube. The cultures were placed horizontally in an incubator and shaken at 200 rpm for 1 h at 37 °C. Subsequently, 50 µl and 500 µl aliquots from each transformation reaction were spread onto pre-warmed selective LB agar plates (see section 2.8) supplemented with carbenicillin (50 µg/ml) and incubated overnight at 37 °C.

Cloning efficiency was assessed by colony PCR using Color Perpetual Taq PCR Master Mix according to the manufacturer's instructions. A 25 µl reaction mixture was prepared by combining the components listed in Table 4.

Table 4. Reaction mix for colony PCR after *E. coli* transformation with pJET1.2_*NoDGTT*s constructs

COMPONENT	VOLUME/REACTION	FINAL CONCENTRATION
Color Perpetual Taq PCR Master Mix (2x)	12.5 µl	• 1.25 U of Perpetual Taq DNA Polymerase • 1x Reaction Buffer (1.5mM MgCl2) • 0.2 mM of each dNTP
NoDGTTsF primer (see p. 2.7)	0.5 µl	10 mM
NoDGTTsR primer (see p. 2.7)	0.5 µl	10 mM
Molecular biology grade water	to 25 µl	–
Template DNA	cells from a single colony	–
Total volume	25 µl	–

A small portion of each individual colony was transferred to separate reaction tubes using sterile micropipette tips and briefly mixed to disperse the cells in the PCR master mix. The PCR was then performed using the cycling conditions provided in Table 5.

Table 5. Conditions of the colony PCR after transformation of *E. coli* with pJET1.2_*NoDGTT*s construct

STEP	TEMPERATURE	TIME	NUMBER OF CYCLES
Initial denaturation	95 °C	2 min	1
Denaturation	95 °C	30 sec	30
Annealing	*See below**	30 sec	
Extension	72 °C	30 sec	
Final extension	72 °C	7 min	1
Cooling	10 °C	indefinite	1

*Annealing temperature for *NoDGTT5* - 60 °C, for *NoDGTT7* - 60 °C, for *NoDGTT8* - 58 °C, for *NoDGTT11* - 50 °C, for *NoDGTT12* - 55 °C.

After confirming the presence of a PCR product of the correct size, selected *E. coli* transformant colonies were transferred from solid medium into 4 ml of liquid LB medium supplemented with carbenicillin (50 µg/ml). Following overnight incubation at 37 °C with shaking at 200 rpm, the cultures were used for pJET1.2/blunt plasmid DNA extraction. Plasmid purification was performed using the Plasmid Miniprep DNA Purification Kit according to the manufacturer's instructions. Briefly, 30 µl of Activation Buffer PL was applied to each spin column and left at room temperature while the bacterial samples were prepared.

From each overnight culture, 2 ml of the 3 ml inoculum was transferred to a 2.0 ml microcentrifuge tube and centrifuged at 12,000 × g for 2 min. The supernatant was discarded, and the remaining 1 ml of culture was added to the same tube and centrifuged again. After removing the supernatant, the tubes were inverted onto a paper towel to eliminate residual medium. The pellets were resuspended in 250 µl of Cell R buffer by gentle pipetting. Next, 250 µl of Lysis Blue buffer was added, and the tubes were inverted several times until the suspension turned uniformly blue. Lysis was followed by the addition of 350 µl of Neutralization and Neutral B binding buffer, with gentle inversion until the blue colour disappeared. Samples were centrifuged at 12,000 × g for 7 min, and 700 µl of the resulting clear supernatant was applied to the homogenization spin column and centrifuged at 11,000 × g for 1 min. The remaining supernatant was processed in the same manner until fully loaded. The DNA-binding column was then washed with 500 µl of Wash PLX1 buffer and centrifuged at 11,000 × g for 1 min, followed by discarding the flow-through. A sec wash with 650 µl of Wash PLX2 buffer was performed under the same conditions. The flow-through was discarded again, and the column was centrifuged for an additional 2 min at 11,000 × g to remove residual wash buffer. To elute the plasmid DNA, the column was placed into a clean 1.5 ml microcentrifuge tube, and 50 µl of Elution Buffer was applied directly to the membrane. After incubating for 2 min at room temperature, the tubes were centrifuged at 11,000 × g for 1 min to collect the purified plasmid DNA. DNA concentrations were measured using a NanoDrop™ 2000 spectrophotometer. To confirm insert accuracy, purified plasmid samples were sent for sequencing.

3.1.4 Cloning of *NoDGTT*s full-length coding sequences into the pYES2.1 TOPO™ vector

Samples containing correctly ligated NoDGTT coding sequences in the pJET1.2/blunt vector were further processed for subcloning into the pYES2.1 TOPO™ yeast expression vector (for convenience, referred to as pYES2.1 vector) for heterologous expression in the *Saccharomyces cerevisiae* H1246 strain. This procedure was performed using the pYES2.1 TOPO™ TA Yeast Expression Kit according to the manufacturer's instructions. In the first step, the NoDGTT coding sequences were re-amplified from the pJET1.2 plasmid DNA using Phusion™ Plus DNA Polymerase. A 20 µl PCR reaction was prepared using the specific primers listed in Section 2.7 and the components shown in Table 6. Amplification was carried out under the cycling conditions described in Table 7.

Table 6. Composition of PCR master mix for amplification of *NoDGTT*s sequences on pJET1.2 plasmid DNA

COMPONENT	VOLUME/REACTION	FINAL CONCENTRATION
Phusion™ Plus Master Mix (2x)	10 µl	• 1 U of Phusion™ Plus DNA Polymerase • 1x Reaction Buffer (1.7mM $MgCl_2$) • 0.2 mM of each dNTP
NoDGTTsF primer (see p. 2.7)	0.5 µl	10 mM
NoDGTTsR primer (see p. 2.7)	0.5 µl	10 mM
Molecular biology grade water	to 20 µl	–
Template DNA	2.0 µl	< 0.2 µg/20 µl
Total volume	20 µl	–

Table 7. Conditions of PCR reaction from Table 6.

STEP	TEMPERATURE	TIME	NUMBER OF CYCLES
Initial denaturation	98 °C	30 sec	1
Denaturation	98 °C	10 sec	30
Annealing	*see below**	10 sec	
Extension	72 °C	30 sec	
Final extension	72 °C	5 min	1
Cooling	4 °C	indefinite	1

*Annealing temperature for *NoDGTT5* - 60 °C, for *NoDGTT7* - 60 °C, for *NoDGTT8* - 58 °C, for *NoDGTT11* - 50 °C, for *NoDGTT12* - 55 °C.

The resulting PCR products were then cloned into the pYES2.1 TOPO™ vector, a reliable and optimized tool for yeast transformation and transgene expression (Figure 4).

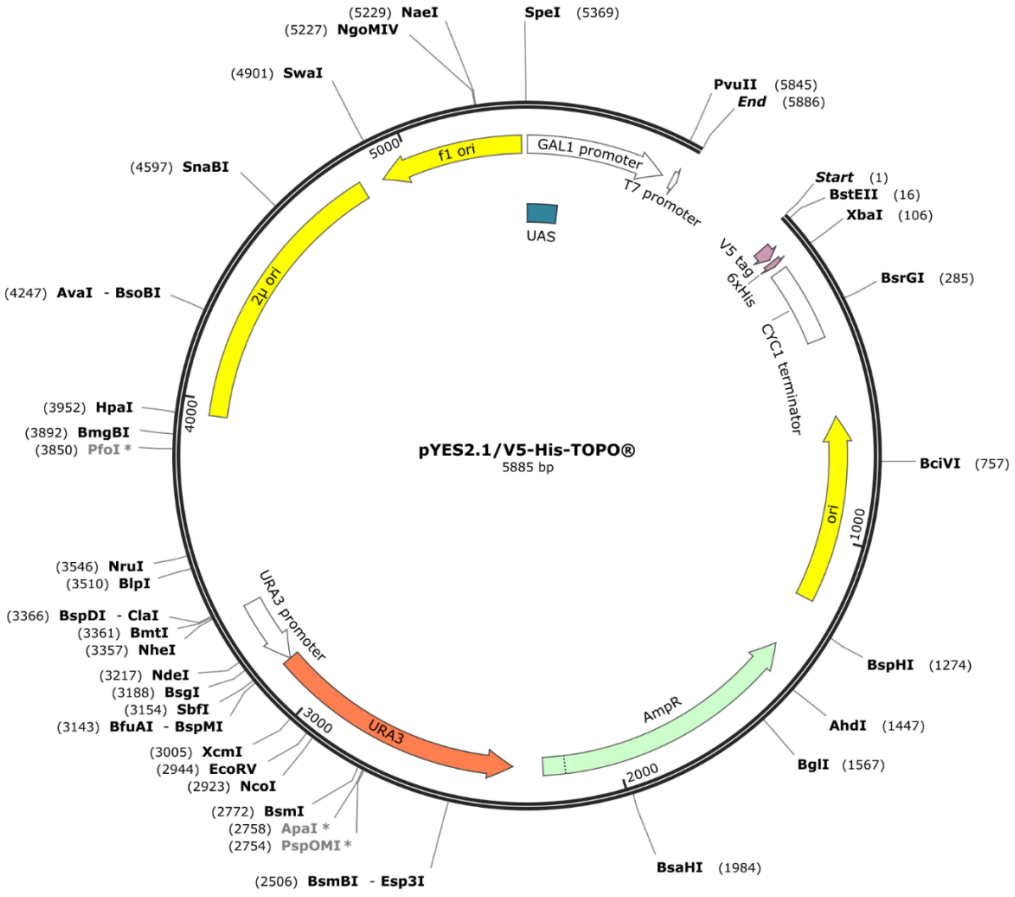

Figure 4. pYES2.1/V5-His-TOPO™, circular vector map. The key elements of the plasmid are: (1) AmpR (green arrow) – ampicillin resistance, allowing for the positive selection of transformed bacteria containing the plasmid. (2) ori – origin of replication (yellow arrow), responsible for plasmid replication in transformed bacterial cells, (3) URA3 gene (orange arrow) – selectable marker used for selection in *Saccharomyces cerevisiae*. (4) GAL1 promoter – galactose-inducible promoter that controls gene expression in yeast. (5) T7 promoter – for *in vitro* transcription or expression in *E. coli*. (6) UAS (blue square) – upstream activating sequence, regulating GAL1 promoter activity. (7) V5 tag – for detection of the protein expressed in yeast cells. (8) 6x His – polyhistidine tag for protein detection in yeast cells. (9) CYC1 terminator – transcription termination in yeast. Generated by SnapGene software.

Briefly, 1 µl of the fresh PCR product was mixed with 1 µl of the pYES2.1 TOPO™ vector, and sterile water was added to a final volume of 5 µl. The mixture was gently pipetted to mix and incubated at room temperature for 20 min. Next, the ligation mixture was placed on ice, and 2 µl of the TOPO™ Cloning reaction was gently combined with 50 µl of One Shot TOP10™ chemically competent *E. coli* that had been thawed on ice. The samples were incubated on ice for 30 min, followed by heat shock at 42 °C for 30 sec in a heating block without shaking. The tubes were immediately returned to ice for 2 min, after which 900 µl of pre-warmed sterile LB medium was added. The cultures were incubated horizontally at 37 °C with shaking at 200 rpm for 1 h. After recovery, 50 µl and 500 µl aliquots of each *E. coli* culture were spread onto pre-warmed selective LB agar plates supplemented with carbenicillin (50 µg/ml) and incubated overnight at 37 °C.

Cloning efficiency was assessed by colony PCR using Color Perpetual Taq PCR Master Mix according to the manufacturer's protocol, as described in Section 3.1.4. Plasmids containing the target inserts were isolated from transformed One Shot™ TOP10 cells using the Plasmid Miniprep DNA Purification Kit, following the manufacturer's protocol as described in Section 3.1.3, and stored at -20 °C.

3.1.5 PLATE ("*lazy bones*") transformation of H1246 yeast with *NoDGTT* full-length coding sequences

Yeast transformation with the pYES2.1 vector carrying the individual *NoDGTT5*, *NoDGTT7*, *NoDGTT8*, *NoDGTT11*, and *NoDGTT12* sequences began with inoculating 5 ml of liquid YPD medium with a single colony of the *S. cerevisiae* H1246 strain in 10 ml culture tubes. Each culture was sealed with parafilm and incubated overnight at 28 °C with shaking at 200 rpm. On the following day, 500 µl of each culture was centrifuged at maximum speed for 10 sec to pellet the yeast cells, and the supernatant was removed. The resulting pellets were then processed for transformation.

In parallel, DNA was prepared by:

1. denaturing 100 µg (10 µl) of double-stranded salmon sperm carrier DNA into single strands through two cycles of boiling at 95 °C for 1 min followed by cooling on ice for 1 min, and
2. mixing the denatured carrier DNA with 1 µg of the pYES2.1 construct carrying the respective *NoDGTT* sequence, dissolved in 5 µl of ultrapure water. The empty pYES2.1 vector served as a negative control.

The DNA mixtures were added to the yeast pellets and gently mixed with a pipette tip. Immediately afterward, 500 µl of PLATE solution (prepared as described in Section 2.8) was added to each sample, followed by vortexing for 10 sec. Next, 57 µl of DMSO was added to each tube and briefly vortexed. The samples were incubated at room temperature for 15 min and then heat-shocked at 42 °C for 15 min in a heat block. Following heat shock, samples were centrifuged at 10,000 rpm for 2 min, and the supernatant was discarded. The pellets were resuspended gently in 200 µl of TE buffer.

The yeast suspensions were immediately spread onto pre-warmed SC-URA selective plates, prepared as described in Section 2.8, and incubated at 28 °C for 72 h. Resulting H1246 transformant colonies were then transferred onto fresh SC-URA plates for further experiments.

3.1.6 Induction of transgene expression in H1246 yeast transformants

Expression of the transgenes carried by the pYES2.1 vector in H1246 transformants was regulated by the GAL1 promoter system. In this system, transgenic yeast are initially transferred from solid SC-URA selective medium into liquid SC-URA medium containing 2% glucose (Section 2.8). Glucose supports cell growth while simultaneously repressing the GAL1 promoter and preventing transgene expression. Once the cultures reach the desired density, they are transferred into liquid SC-URA medium containing 2% galactose and 1% raffinose as carbon sources, which activates the GAL1 promoter and induces transgene expression.

Accordingly, for each *NoDGTT* construct, as well as for the empty vector control, three single colonies of H1246 transformants were inoculated into separate Erlenmeyer flasks containing 50 ml of non-inducing SC-URA medium with 2% glucose (composition provided in Section 2.8). The cultures were grown overnight at 28 °C with shaking at 250 rpm.

The following day, the OD_{600} of each culture was measured using a spectrophotometer to determine the volume of overnight culture required to obtain an OD_{600} = 0.4 in 50 ml of inducing SC-URA medium. The necessary volume was calculated using the formula provided in the manufacturer's protocol:

$$\text{Volume (ml)} = (0.4 \times 50) / OD_{600}$$

To initiate transgene induction, the calculated volumes of each overnight culture were collected and centrifuged in 50 ml Falcon tubes at 1500 rpm for 5 min. The non-inducing medium was removed, and the cell pellets were resuspended in 50 ml of inducing SC-URA medium containing 2% galactose and 1% raffinose. The cultures were incubated for 48 h at 28 °C with shaking at 250 rpm.

After induction, the cultures were centrifuged at 1500 rpm for 5 min, the inducing medium was discarded, and the pellets were flash-frozen in liquid nitrogen and stored at -80 °C for further analyses. Parallel non-induced cultures were collected for microscopy, lipid extraction, and western blotting as controls.

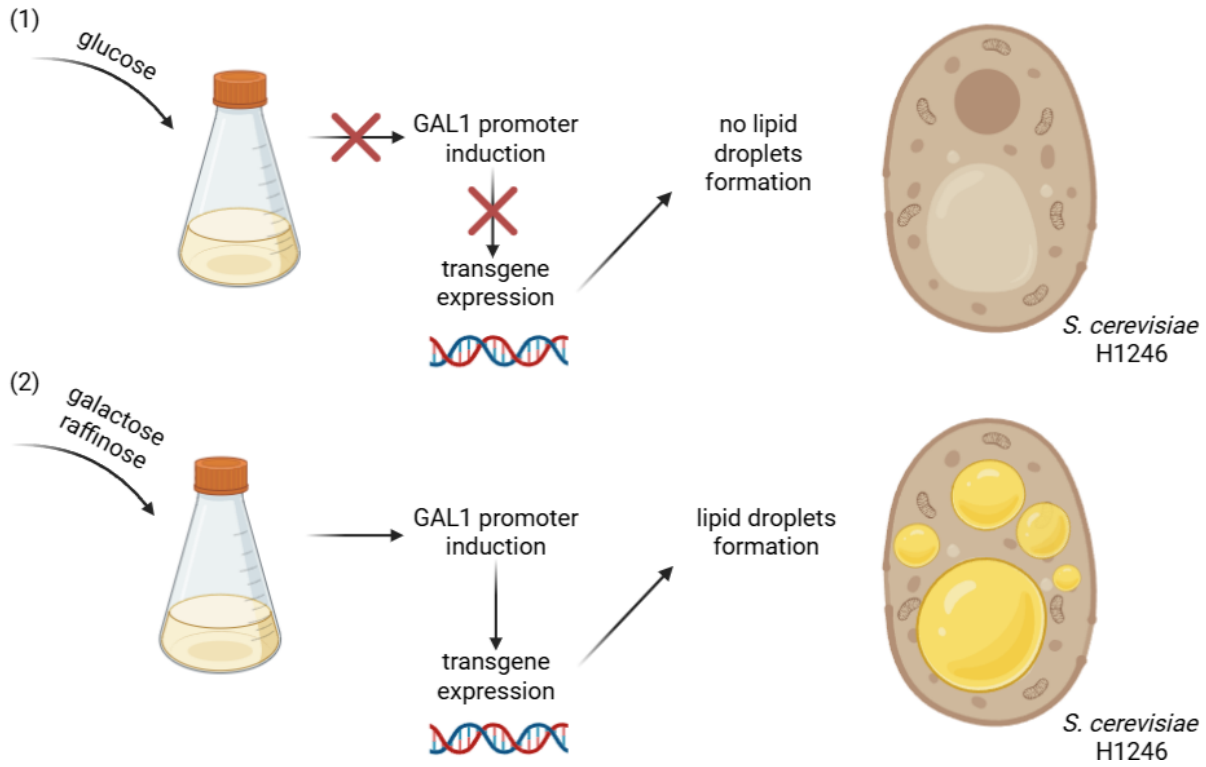

Figure 5. Transgene induction in yeast transformed with PLATE ("*lazy bones*") method. (1) Non-inducible medium contains 2% glucose, which does not induce GAL1 promoter in pYES2.1 vector, thus there is no transgene expression in *S. cerevisiae* H1246 strain. (2) The inducible medium contains 2% galactose and 1% raffinose, which induce GAL1 promoter and transgene expression, resulting in lipid droplets formation in *S. cerevisiae* H1246 strain.

3.1.7 Microscopic analysis of TAG accumulation in H1246 transformants by CLSM

For microscopic analysis, both non-induced and induced cultures were collected as described above and centrifuged for 2 min at 2500 rpm in 2 ml Eppendorf tubes. The supernatant was discarded, and the resulting pellet was resuspended in 500 µl of fixative solution (4% paraformaldehyde in 1× PBS, pH 7.2) to chemically fix the cells. Fixation was carried out overnight at 4 °C.

The following day, the samples were briefly centrifuged for 5 sec to pellet the cells. After discarding the fixative, the pellets were washed three times with 1× PBS (pH 7.2). Neutral lipids were visualized by staining the fixed yeast cells with BODIPY™ 505/515. The working solution was prepared by mixing 1 µl of the commercial stock with 500 µl of 1× PBS (pH 7.2). Then, 50 µl of fixed yeast suspension was combined with 150 µl of the BODIPY™ working solution and incubated for 30 min at room temperature in the dark.

After staining, samples were centrifuged for 2 min at 2500 rpm and the supernatant was discarded. The pellets were washed three times for 5 min each with 500 µl of 1× PBS (pH 7.2). Finally, the samples were resuspended in 100 µl of 1× PBS (pH 7.2) and immediately analysed *via* CLSM. Fluorescence derived from BODIPY™ 505/515 was detected with excitation at 505 and emission at 515 nm, utilizing a diode laser set to 0.1% intensity, with an excitation bandwidth of 505 nm and an emission bandwidth of 515 nm, and a gain setting of 1.0. Images were acquired using the CLSM and subsequently processed with Fiji software.

3.1.8 Extraction and analysis of lipids from H1246 transformants by GC–FID

For total lipid extraction, frozen yeast pellets prepared as described in Section 3.1.6 were transferred into Kimble glass tubes containing 0.5 ml of glass beads (ø 425–600 µm). Each sample was immediately covered with 1.5 ml of chloroform:methanol (2:1, v/v) and vortexed for 6 min in a multitube vortex at 2400 rpm. Subsequently, 0.5 ml of pure methanol was added, followed by an additional 1.5-min vortexing step. Next, 0.5 ml of ultrapure water was added, and samples were vortexed for another 1 min.

The tubes were centrifuged for 4 min at 4000 rpm at 4 °C. After phase separation, the lower chloroform phase was carefully collected using a glass pipette and transferred to an open-top glass tube. Solvents were evaporated under a gentle stream of gaseous N_2 in a fume hood, and the remaining lipid fractions were dissolved in 75 µl of chloroform. These lipid extracts were separated by thin-layer chromatography (TLC) and analysed according to the procedure described below.

Before use, TLC plates were dried at 200 °C for 2 h to remove residual moisture. For each sample, 50 µl of the chloroform-dissolved lipid fraction was divided into two equal 25 µl aliquots and spotted at the top and bottom of the silica gel–coated TLC glass plate, as shown in Figure 6.

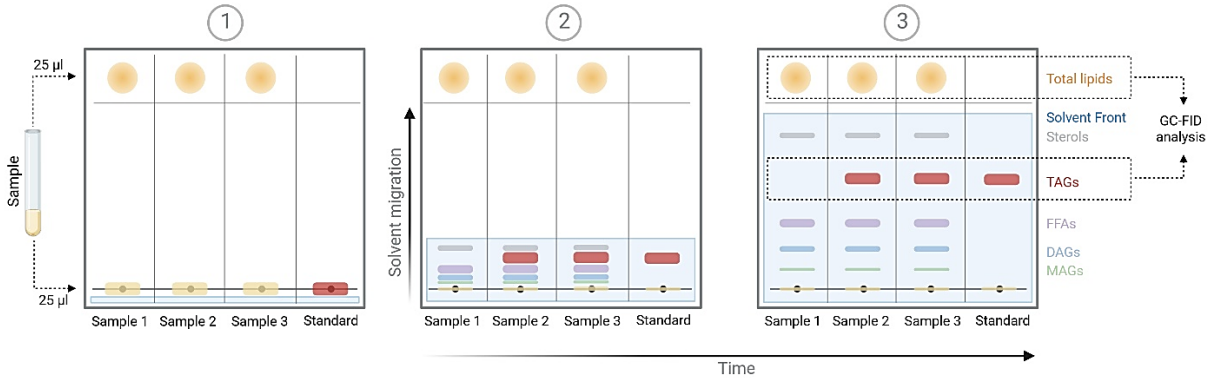

Figure 6. TLC workflow for TAG separation and quantification. Schematic representation of the TLC procedure used to separate and identify lipid classes in biological samples. (1) Sample application: A 25 µL aliquot of lipid extract from each sample is applied to both, top and origin of the TLC plate, whereas standard mixture is applied only to the origin of the TLC plate. (2) For chromatographic development the plate is placed in a developing chamber with a solvent system (blue), enabling lipids to migrate according to polarity and molecular interactions with the stationary phase. (3) Distinct lipid classes are separated, and TAGs (red) are visualized as discrete bands in a separate glass chamber saturated with iodine fumes. Total lipids and the identified TAG bands are excised and subjected to GC-FID for quantitative analysis, given as mol% of TAGs in total lipid pool.

Olive oil (2 µl dissolved in 200 µl of acetone) was used as a TAG standard to identify the TAG-corresponding band in each sample. The TLC plate was developed in a glass chamber containing 100 ml of the mobile phase described in Section 2.8, until the solvent front migrated to approximately two-thirds of the plate (Figure 6).

After development, the plate was air-dried under the fume hood and then placed in a glass TLC chamber saturated with iodine fumes to visualize the TAG bands. The TAG-corresponding spots were marked with a pencil, completely scraped off using metal blades, and transferred into fresh Kimble glass tubes. The same procedure was applied to all corresponding total-lipid spots collected from the upper portion of the TLC plate (Figure 6). Next, 1 ml of the fatty acid methyl esters (FAMEs) reagent (prepared as described in Section 2.8) and 200 µl of tripentadecanoin (used as an internal C15:0 TAG standard at a concentration

of 50 µg/ml in 80% v/v toluene) were added to each tube. The tubes were tightly closed, briefly vortexed, and incubated in a shaking water bath at 80 °C and 150 rpm for 1 h. After incubation, samples were cooled at room temperature for 10 min, followed by the addition of 1 ml of saturated NaCl solution and 1 ml of hexane. Each sample was vortexed twice for 5 sec and centrifuged for 10 min at 1500 rpm. The resulting upper hexane phase containing the extracted lipids was transferred to a clean open glass tube and evaporated to dryness under a stream of nitrogen in the fume hood.

The remaining lipid residue was dissolved in 25 µl of acetonitrile, vortexed, and transferred to GC vials for qualitative and quantitative analysis of lipid classes using GC-FID.

A GC equipped with a DB-23 capillary column (30 m × 0.25 mm, 0.25 µm film thickness) and an FID was used for qualitative and quantitative identification of FAMEs in the lipid fractions. The instrument was operated under the temperature conditions listed in Table 8.

Table 8. Temperature conditions used for qualitative and quantitative analysis of lipids by GC-FID

STEP	TEMPERATURE	RAMP	TIME
Initial hold	150 °C	–	1 min
Increase 150 °C --> 200 °C	200 °C	4 °C / min	12.5 min
Increase 200 °C --> 250 °C	250 °C	20 °C / min	2.5 min
Final hold	250 °C	–	3 min

To identify FAs, samples were analysed sequentially alongside a standard mixture of FAMEs with known retention times. The peak areas of the detected FAs were integrated using Agilent ChemStation software. For accurate quantification, peak areas were normalized to the molecular weight of each FA and to the concentration of the internal standard.

3.1.9 Identification of NoDGTT protein products in *Saccharomyces cerevisiae* H1246 transformants

3.1.9.1 Isolation of microsomal fraction from the *Saccharomyces cerevisiae* H1246 transformants

Because NoDGTT proteins are predicted to localize to the ER, the microsomal fraction, rich in ER-derived membranes, was isolated from H1246 yeast transformants for downstream analyses. All isolation steps were carried out on ice or at 4 °C to maintain protein integrity.

Yeast pellets collected as described in Section 3.1.6 were transferred into ice-cold Kimble glass tubes containing 1 ml of acid-washed glass beads (ø 425–600 µm) and immediately overlaid with 2 ml of ice-cold disruption buffer (Section 2.8). Samples were vortexed vigorously for 6 min at 4 °C using a multitube vortex to ensure efficient cell disruption. Following lysis, samples were centrifuged at 1500 × g for 15 min at 4 °C. The supernatants were transferred to chilled polycarbonate ultracentrifuge tubes, balanced, and centrifuged at 100,000 × g for 2 h at 4 °C in a swinging-bucket rotor. The resulting pellet — corresponding to the microsomal fraction — was gently resuspended in 50 µl of cold 100 mM potassium phosphate buffer (pH 7.2).

Total protein concentration was determined using the Bradford method. Briefly, 1 ml of Bradford reagent was mixed with 5 µl of each sample, incubated for 5 min, and the absorbance at 595 nm was measured. Protein concentrations were calculated using a BSA standard curve (Table 9). Microsomal protein samples were stored at -80 °C for further experiments.

Table 9. Standard curve of bovine serum albumin (BSA) for protein concentration determination

BSA CONCENTRATION [µg]	ABSORBANCE OD_{595}
2,5	0,179
5	0,439
10	0,818
15	0,694
20	0,917
25	1,059

3.1.9.2 Separation and immunoblotting of microsomal proteins

To detect the expression of the pYES-NoDGTT12-CFP (cerulean fluorescent protein) tagged protein in *S. cerevisiae* H1246 cultures by immunoblotting, microsomal protein samples were first separated by sodium dodecyl sulfate - polyacrylamide gel electrophoresis (SDS-PAGE) and subsequently transferred onto a polyvinylidene difluoride (PVDF) membrane as described below.

For protein separation, SDS-PAGE was performed using a 10% polyacrylamide gel, cast with the TGX FastCast kit, according to the manufacturer's protocol.

- Resolving gel preparation: The resolving gel acrylamide solution was prepared by combining 3 ml of Resolver A and B solutions. To this mixture, 30 µl of TEMED and 3 µl of 10% APS were added and mixed thoroughly. The solution was then carefully dispensed into the cassette, filling up to 1 cm below the bottom of the comb teeth.
- Stacking gel preparation: The stacking gel solution was prepared by combining 1 ml of Stacker A and B solutions. 10 µl of TEMED and 2 µl of 10% APS were added to the mixture, which was mixed thoroughly before being gently applied over the resolving gel to prevent mixing of the layers. The gel was allowed to polymerize for 30 min.
- Sample preparation: Prior to SDS-PAGE, 5 µl of LD buffer was added to 20 µl of each protein sample. The samples were then incubated at 95 °C for 10 min in a heat block to ensure complete protein denaturation before loading.

25 µl of each prepared sample was loaded onto the polyacrylamide gel and immersed in a tank filled with SDS Running Buffer (composition listed in section 2.8). The Perfect™ Tricolor Protein Ladder was used as a molecular weight marker. SDS-PAGE was conducted using a vertical polyacrylamide gel electrophoresis system at 90 V for 30 min, followed by 140 V for 1 h.

The western blotting technique was used to transfer, analyse, and visualize proteins from polyacrylamide gel to a PVDF membrane. After electrophoresis, the gel was carefully arranged into a blotting sandwich as shown in Figure 7. All layers were soaked in transfer buffer (composition listed in Section 2.8) and assembled in the blotting cassette in the following order: fiber pad, filter paper, gel, Immobilon®-P PVDF membrane, filter paper, and fiber pad. The PVDF membrane was pre-treated by soaking in 96% ethanol for 20 sec, followed by immersion in ultrapure water for 2 min to displace the ethanol, and finally equilibrated in transfer buffer. The assembled cassette was placed in the blotting tank filled with transfer buffer, and the transfer was carried out for 1 h at 100 V.

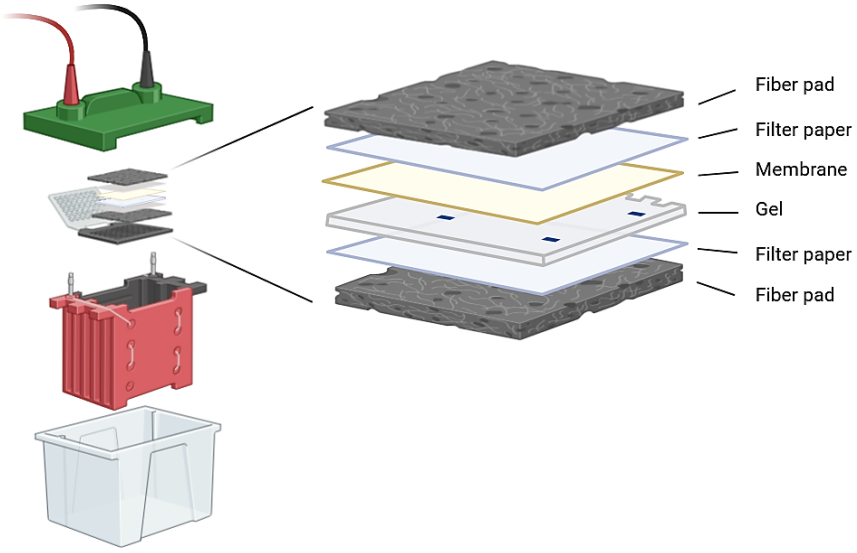

Figure 7. Western blot transfer setup. From the top left to the bottom: electrode module, transfer sandwich, transfer cassette, buffer tank.

The membrane with transferred proteins was then blocked by incubation in 5% whole milk powder dissolved in 1x TBST buffer (prepared as described in section 2.8) at room temperature for 2 h, followed by washing in 1x TBST buffer for 10 min. The membrane was subsequently incubated overnight at 4 °C with mouse anti-His antibody (1:5000) diluted in 1% whole milk powder in 1x TBST buffer with gentle shaking at 60 rpm on an orbital shaker. On the following day, the membrane was washed three times with 1x TBST buffer for 15 min each and then incubated with the secondary anti-mouse antibody, HRP stained (1:50 000) for 1 h at room temperature with gentle shaking at 60 rpm. The membrane was then washed three times for 15 min each in ultrapure water.

For signal detection, the Amersham ECL Western Blotting Detection Reagent was used according to the manufacturer's protocol. Equal volumes of Detection Solution 1 and 2 were mixed to provide sufficient volume to cover the entire membrane. The mixed detection reagent was applied to the membrane, followed by a 5 min incubation at room temperature in the dark. Excess reagent was gently removed using a paper towel, and the membrane was wrapped in a layer of transparent plastic foil, ensuring all air bubbles were removed. The membrane, with the protein side facing up, was placed in the Bio-Rad ChemiDoc Imaging System to capture a digital image at chemiluminescent wavelength.

To visualize total proteins separated by SDS-PAGE, the gel post-transfer was stained with Bio-Safe Coomassie Stain according to the manufacturer's protocol. The gel was first washed with ultrapure water three times for 15 min each to remove residual buffer. Subsequently, 50 ml of Coomassie solution was applied to the gel and incubated for 1 h at room temperature. The gel was then rinsed with ultrapure water for 30 min. All staining and washing steps were performed at room temperature on an orbital shaker set to 60 rpm.

3.1.10 *In vitro* characterization of NoDGTT12 acyl-CoA specificity

To characterize the enzymatic activity of NoDGTT12 toward various acyl-CoA substrates (16:0-CoA, 18:0-CoA, 18:1-CoA, 18:2-CoA, 18:3-CoA, 20:4-CoA, 20:5-CoA, and 22:1-CoA), *in vitro* NoDGTT assays were

performed following previously optimized protocols (Jeppson *et al*., 2019). The objective of these assays was to determine the acyl-donor preference of NoDGTT12 in order to inform the design of TAG production systems with desired FA profiles.

Radiolabelled [^{14}C]-*sn*-1,2-18:1-DAG substrate was prepared as described by Jeppson *et al*. (2019) through acylation of [^{14}C]-glycerol with the mixed anhydride of 18:1 FAs (Sánchez *et al*., 1973), yielding [^{14}C]-18:1 TAG. The resulting radiolabelled di-18:1-DAG was dissolved in dimethyl sulfoxide (DMSO) to a final concentration of 20 mM.

Microsomal fractions isolated from H1246 yeast transformants expressing NoDGTT12, corresponding to 40 µg of total protein, were diluted in 86 µl of 50 mM HEPES buffer. Then, 4 µl of the DAG substrate (20 nmol) in DMSO was added in a gradual, stepwise manner to the microsomal suspension during vigorous vortexing for 10 sec. The enzymatic reaction was initiated by adding 5 nmol of the respective acyl-CoA substrate (16:0-CoA, 18:0-CoA, 18:2-CoA, 18:3-CoA, 20:5-CoA, or 22:1-CoA) in 10 µl of water containing 0.1 mg of FA–free BSA.

Reactions were incubated at 30 °C with shaking at 1250 rpm for 20 min and terminated by adding 120 µl of 0.15 M acetic acid followed by 500 µl of methanol:chloroform (1:1, v/v). Samples were vortexed thoroughly and centrifuged for 2 min at maximum speed. The lower chloroform phase was collected into open-top glass tubes. A 50 µl aliquot (representing one-fifth of the chloroform phase) was transferred into scintillation vials and mixed with 5 ml of Ultima Gold LSC Cocktail for radioactivity measurement.

The remaining lipids were evaporated under a nitrogen stream, resuspended in 50 µl of chloroform, vortexed, and separated by TLC using a heptane:diethyl ether:acetic acid (70:30:1, v/v) solvent system. Following development, TAG bands were visualized in iodine fumes. The plate was lightly misted with water, TAG regions were marked with a pencil, and the silica corresponding to the TAG band was scraped into scintillation vials. The remaining silica from each track was collected in separate vials. 5 ml of Ultima Gold LSC Cocktail was added to each vial, and radioactivity was measured using a liquid scintillation counter.

3.2 Experimental procedures for *Nannochloropsis oceanica* CCMP1779

3.2.1 Culturing of *Nannochloropsis oceanica* CCMP1779

N. oceanica 1779 CCMP strain was cultured under sterile conditions in an enriched seawater F/2 medium (see point 2.8). Algal cultures were grown in 1000 ml Erlenmeyer flasks, on the horizontal shaker in 200 ml of F/2 medium at 130 rpm speed, at 22 °C under light intensity of 60 µmol/m^2s^{-1} for 3 days. The cultures under optimal conditions served as 1) controls for other experimental approaches, and 2) starting point of stress treatments, as described below.

200 ml N-repleted cultures of *N. oceanica* CCMP1779 grown for 3 days were aliquoted into 50 ml Falcon tubes and centrifuged for 5 min, at 4500 rpm to pellet the cells. The supernatant was discarded, and the pellet was resuspended in 15 ml of a sterile F/2 medium lacking nitrogen source (N-) (for recipe see point 2.8) by thorough mixing. After centrifugation (conditions as above), the obtained pellet was resuspended in 50 ml of fresh sterile N- F/2 medium. The resulting algal suspension was then added to 150 ml of a N- F/2 medium in the 1000 ml Erlenmeyer sterile flasks and cultured on the horizontal shaker at 130 rpm speed at 22 °C under the light intensity of 60 µmol/m^2s^{-1}. Samples of 50 ml were collected after 24, 48

and 72 hours into 50 ml Falcon tubes. In each case, algal cultures were centrifuged for 5 min at 4500 rpm. The resulting supernatant was discarded, and the pellet was gently resuspended in a small amount of the medium remaining at the bottom of the tube and transferred into a 2.0 ml Eppendorf tube by using a 1000 µl pipet. Afterwards, the suspension was centrifuged for 2 min at 14 000 rpm, and the supernatant was carefully and completely discarded. Two tungsten carbide homogenizer beads ø 3mm were added into each Eppendorf tube and the samples were frozen immediately in liquid nitrogen and stored at -80°C for further tests.

For the light stress *N. oceanica* 1779 CCMP strain was first cultured under optimal conditions. After 3 days of growth, the light intensity increased from 60 µmol/m^2s^{-1} to 600 µmol/m^2s^{-1}. Samples of 50 ml were collected 0 h, 24 h, 48 h and 72 h, as described previously.

3.2.2 Isolation of total RNA from *Nannochloropsis oceanica* CCMP1779 and cDNA synthesis

Total RNA was extracted from liquid cultures *N. oceanica* CCMP1779, as a matrix for cDNA reverse transcription. Just before RNA extraction, the deeply frozen samples containing *N. oceanica* CCMP1779 pellet and tungsten carbide beads were homogenized into a fine powder using a cryogenic mill. The homogenization was carried out at the speed of 30x/sec for 2 min. The homogenized samples were then proceeded to RNA extraction protocol by using Universal RNA Purification Kit, according to the manufacturer's protocol. Briefly, 200 µl of LG buffer and 100 µl of RL buffer were immediately added to the frozen sample, followed by vigorous vortexing until the homogenous liquid suspension was obtained. The sample was then transferred into a new 1.5 ml Eppendorf tube and centrifuged for 4 min at max speed of 14 000 rpm. The resulting supernatant was then carefully transferred into a fresh 1.5 ml Eppendorf tube and 200 µl of RL buffer were added to each tube. After gentle mixing by pipetting, each sample was transferred into a homogenization spin-column with a receiver tube and centrifuged at 11 000 x *g* for 2 min. In the next step, the resulting flow-through was mixed with the 0.6 volume of pure (99.9 %) high grade ethanol by pipetting. The resulting mixture was then transferred into the binding spin-columns and centrifuged at 11 000 x g for 1 min for RNA binding. The flow-through was discarded and 400 µl of WASH DN1 buffer was added into each column, followed by centrifugation at 11 000 x g for 1 min. The resulting flow-through was discarded and 50 µl of DNR buffer with 1U DNase I was added directly onto the column in order to eliminate DNA remains. After 20 min of incubation at RT, 400 µl of WASH RBW buffer was added to each sample, followed by centrifugation for 1 min at 11 000 x g. The spin-column was then placed in a fresh 1.5 ml collection Eppendorf tube and 50 µl of RNase-free water was added directly onto a column in each sample. RNA was eluted from the column by centrifugation at 11 000 x g for 1 min, quantified by using NanoDrop™ 2000 Spectrophotometer and stored at -80°C for further necessities.

The synthesis of first strand cDNA was carried out by RevertAid Reverse Transcriptase and performed according to the manufacturer's protocol. The composition of reaction mixture is given in Table 10.

Table 10. Composition of reaction mix for the synthesis of first strand cDNA synthesis on *N. oceanica* total RNA

Component	Volume/reaction	Final concentration
Total RNA	10 µl	1 µg
Oligo$(dT)_{18}$ primer	1.66 µl	0.5 µg

Molecular biology grade water	to 12.5 µl	–
5x Reaction buffer	4 µl	1 x
dNTP Mix (10 mM each)	2 µl	1 mM
RevertAid Reverse Transcriptase	1 µl	200 U

The mixture was gently vortexed, centrifuged briefly and incubated in the heating block at 42 °C for 60 min. The reaction was terminated by increasing the temperature up to 70°C for 10 min. The reverse transcription products were stored at -20°C for further experiments.

3.2.3 PCR reactions for *Nannochloropsis oceanica* CCMP1779 cDNA template quality-check

Each time the quality of the obtained cDNA was validated with an expression profiling of *N. oceanica* CCMP1779 elongation factor-encoding gene (EF) a reference, due to its high constitutive expression in the algal cells (Zienkiewicz *et al*., 2017). A PCR mix was prepared using Color Perpetual Taq PCR Master Mix, according to the manufacturer's protocol. The reaction mix of 25 µl was prepared using specific primers (point 2.7) and in quantities given in Table 11.

Table 11. Composition of master mix for PCR reactions using cDNA from *N. oceanica* CCMP1779

Component	Volume/reaction	Final concentration
Color Perpetual Taq PCR Master Mix (2x)	12.5 µl	• 1.25 U of Perpetual Taq DNA Polymerase • 1x Reaction Buffer (1.5mM $MgCl_2$) • 0.2 mM of each dNTP
NoEF1F primer	0.5 µl	10 mM
NoEF1R primer	0.5 µl	10 mM
Template DNA	2.0 µl	< 0.25 µg/25 µl
Molecular biology grade water	to 25 µl	–
Total volume	25 µl	–

PCR reaction was carried out in thermal cycler using the conditions given in Table 12.

Table 12. Conditions for PCR reactions from Table 11.

Step	Temperature	Time	Number of cycles
Initial denaturation	95 °C	2 min	1
Denaturation	95 °C	30 sec	30
Annealing	55 °C	30 sec	
Extension	72 °C	30 sec	
Final extension	72 °C	7 min	1
Cooling	10 °C	indefinite	1

The following verification gel electrophoresis was performed in 1% agarose in 1x TAE buffer (point 2.8), using Perfect 100-1000 bp ladder in order to validate the PCR product.

3.2.4 Overexpression of *NoDGTT*12 in *Nannochloropsis oceanica* CCMP1779

To overexpress *NoDGTT12* in *N. oceanica* CCMP1779, the pNOC-OX-*CFP* destination vector (Figure 8) was used following the cloning strategy described by Poliner *et al*. (2018) (Figure 9).

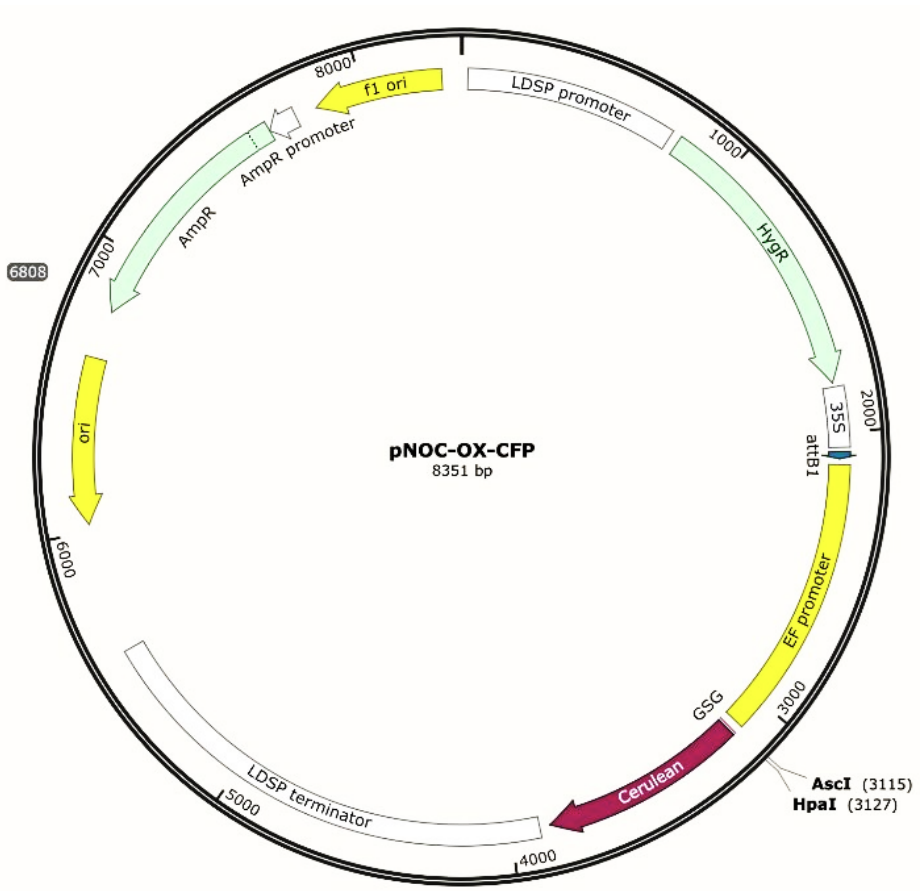

Figure 8. pNOC-OX-*CFP*, circular vector map. Key features of the plasmid (1) AmpR and HygR (green arrows) – ampicilin and hygromycin resistance, allowing for the positive selection of transformed algae containing the plasmid. (2) ori and f1 ori (yellow arrows) – origin of replication, responsible for plasmid replication in transformed algal cells, (3) 35 S promoter (white rectangle) – strong and constitutive promoter of the cauliflower mosaic virus (CaMV). (4) attB1 – *att*B cloning site for Gateway Cloning™ technique (5) Cerulean (red arrow) – for visualization of gene expression. (6) UAS (blue square) – upstream activating sequence, regulating GAL1 promoter activity. (7) LDSP promoter and terminator (white rectangles) – regulate expression of plasmid elements (8) Multiple cloning sites (AscI, HpaI) – facilitate insertion of target DNA sequences. Generated by SnapGene software.

The pNOC-OX-*CFP* vector utilizes the 35S promoter, a widely used regulatory element for high-level transgene expression in recombinant systems. The vector also contains an ampicillin resistance gene for bacterial selection, a hygromycin resistance gene for selection of transformed microalgal cells, and a CFP tag for visualization of protein expression in *N. oceanica* CCMP1779.

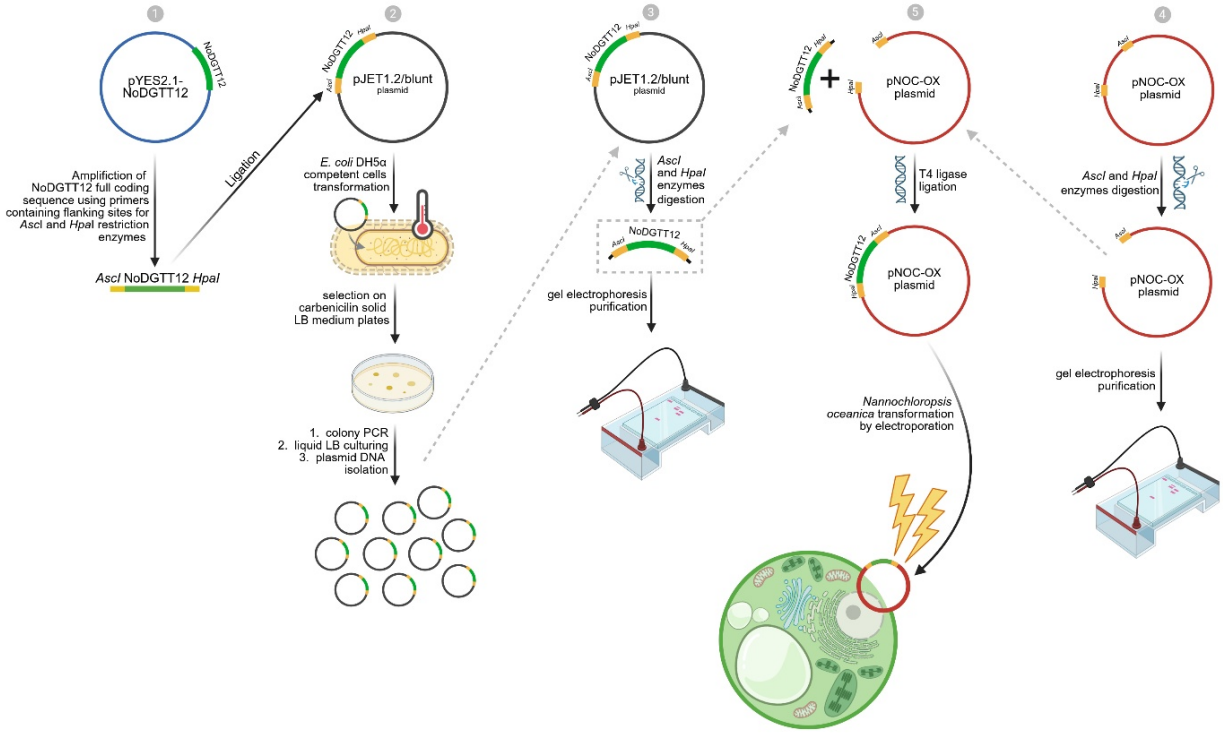

Figure 9. Experimental workflow for *N. oceanica* CCMP1779 transformation with pNOC-OX vector for overexpression of *NoDGTT12* gene. (1) Amplification of *NoDGTT12* with *Asc*I and *Hpa*I sites for restriction enzymes, (2) Ligation and cloning of the *NoDGTT12* sequence into pJET1.2/blunt vector, *E. coli* DH5α transformation and plasmid DNA isolation. (3) Restriction enzyme digestion and agarose gel electrophoresis purification of obtained plasmid fragment. (4) Restriction enzyme digestion and agarose gel electrophoresis purification of pNOC-OX vector. (5) Ligation of *NoDGTT12* full sequence with pNOC-OX vector and *N. oceanica* CCMP1779 transformation.

3.2.4.1 Cloning of *NoDGTT*s full-length sequences into the *pNOC*-OX-*CFP* vector

In the first step, the *NoDGTT12* sequence was amplified from the *NoDGTT12*- pYES2.1 vector (see section 3.1.4) using primers containing flanking sites for *Asc*I and *Hpa*I restriction enzymes required for subsequent cloning steps (see point 2.7). Amplification was carried out using Phusion™ Plus DNA Polymerase according to the manufacturer's protocol. The reaction mixture, with a total volume of 20 µl, is provided in Table 13 and conditions for the PCR reaction are given in the Table 14.

Table 13. Composition of PCR reaction mix for cloning of *NoDGTT12* sequence with flanking sites for *Asc*I and *Hpa*I restriction enzymes

COMPONENT	VOLUME/REACTION	FINAL CONCENTRATION
Phusion™ Plus Master Mix (2x)	10 µl	• 1 U of Phusion™ Plus DNA Polymerase • 1x Reaction Buffer (1.7mM MgCl2) • 0.2 mM of each dNTP
NoDGTT12F AscI primer	0.5 µl	10 mM
NoDGTT12R HpaI primer	0.5 µl	10 mM
Molecular biology grade water	to 20 µl	–
Template DNA	2.0 µl	< 0.2 µg/20 µl
Total volume	20 µl	–

Table 14. Conditions for PCR reaction from Table 13.

STEP	TEMPERATURE	TIME	NUMBER OF CYCLES
Initial denaturation	98 °C	30 sec	1
Denaturation	98 °C	10 sec	30
Annealing	60 °C	10 sec	
Extension	72 °C	30 sec	
Final extension	72 °C	5 min	1
Cooling	4 °C	indefinite	1

PCR products containing *NoDGTT12* sequence and *Asc*I and *Hpa*I flanking sites were then ligated into the backbone pJET1.2/blunt vector using the CloneJET PCR Cloning Kit according to the manufacturer's protocol. The ligation reaction mixture was prepared on ice (composition detailed in Table 15), briefly vortexed, and centrifuged before being incubated for 20 min at room temperature. The resulting ligation mixture was used directly for transformation.

Table 15. Composition of reaction mixture for ligation of pJET1.2 vector and *NoDGTT12* sequence flanked with sites for cutting with *AscI* and *HpaI* sites

COMPONENT	VOLUME/REACTION	FINAL CONCENTRATION
2x reaction buffer	10 µl	1x
PCR product	4 µl	0.6 pmol
Nuclease-free water	to 19 µl	–
T4 DNA ligase	1 µl	5 U
Total volume	20 µl	–

The cloning was performed *via* transformation of Subcloning Efficiency™ DH5α competent E. coli cells, following the procedure described in Section 3.1.3. For each transformation reaction, 100 µl and 500 µl aliquots were plated onto pre-warmed selective LB agar plates containing carbenicillin (50 µg/ml) and incubated overnight at 37 °C. The resulting colonies were screened for cloning efficiency using colony PCR with Color Perpetual Taq PCR Master Mix according to the manufacturer's protocol (see Section 3.1.3). The composition of the reaction mixture is listed in Table 4. Cells from individual colonies were transferred into PCR tubes using sterile micropipette tips and briefly mixed to disperse the cells in the master mix. PCR amplification was performed under the cycling conditions specified in Table 5.

Plasmid DNA from correctly identified colonies, containing the *NoDGTT12* sequence cloned into the pJET1.2/blunt vector, was extracted using the Plasmid Miniprep DNA Purification Kit, listed under section 2.4 and following the manufacturer's protocol. DNA concentration was measured using a NanoDrop™ 2000 Spectrophotometer, and the samples were subsequently sent for sequencing.

Only samples confirmed to be correct through sequencing were processed for cloning into the *pNOC-OX-CFP* vector.

For this purpose, plasmid DNA was digested with *Asc*I and *Hpa*I restriction enzymes according to the manufacturer's protocol. The composition of the restriction digest mixture is detailed in Table 16.

Table 16. Composition of restriction digest mixture for pNOC-OX-*CFP* vector

COMPONENT	VOLUME/REACTION	FINAL CONCENTRATION
Restriction enzyme *Hpa* I	2 µl	10 U
Restriction enzyme *Asc* I	1 µl	10 U
10x buffer rCutSmart	5 µl	1x
DNA	Calculated from the sample concentration	1 µg
Nuclease-free water	to 50 µl	–
Total volume	50 µl	–

The components were gently mixed by pipetting, centrifuged briefly, and incubated at 37 °C for 2 h in a thermal cycler. To terminate the reaction, enzymes were heat-inactivated by incubation at 80 °C for 20 min. Following digestion, the entire sample containing digested plasmid DNA was separated by gel electrophoresis under conditions described in section 3.1.3. and purified using the Monarch® DNA Gel Extraction Kit (point 2.4), according to the manufacturer's protocol.

Gel purification involved carefully cutting out the band containing the DNA fragment of the desired length from the agarose gel using a metal blade and transferring it to a 2.0 ml Eppendorf tube. The gel slice was weighed, and four volumes of Monarch Buffer BY were added per volume of gel slice. The mixture was incubated at 50 °C for 10 min with occasional vortexing every 2 min to fully dissolve the gel fragments. During this time, the Monarch DNA-binding Spin Column S1A (provided with the kit) was inserted into a Monarch Spin Collection Tube. The dissolved gel containing the plasmid DNA was loaded onto the column and centrifuged at 11,000 rpm for 1 min. The flow-through was discarded, and the process was repeated until the entire sample was filtered through the column. The column was then washed twice with 200 µl of Monarch Buffer WZ, with each wash involving loading, centrifugation (1 min at 11,000 rpm), and discarding the flow-through. The DNA-binding column was subsequently transferred to a clean 1.5 ml Eppendorf tube, and 10 µl of Monarch Buffer EY was applied directly to the column for DNA elution. After a 1 min incubation, the tube was centrifuged for 1 min at 11,000 rpm, and the DNA concentration was measured.

The pNOC-OX-*CFP* vector was digested in the same manner as the previously prepared *NoDGTT1*2-pJET1.2/blunt vector, using *Asc*I and *Hpa*I restriction enzymes according to the manufacturer's protocol. The composition of the restriction digest mixture is provided in Table 16. The components were gently mixed by pipetting, briefly centrifuged, and incubated at 37 °C for 2 h in a thermal cycler. To terminate the digestion reaction, enzymes were heat-inactivated at 80 °C for 20 min. The digested DNA was then separated by gel electrophoresis (see section 3.1.3) and purified using the Monarch® DNA Gel Extraction Kit as previously described.

The ligation reaction between the linearized pNOC-OX-*CFP* "backbone" vector and the *NoDGTT12* sequence was prepared on ice by combining the components listed in Table 17.

Table 17. Composition of reaction mixture for ligation of pNOC-OX-*CFP* vector and *NoDGTT12* sequence

COMPONENT	VOLUME/REACTION	FINAL CONCENTRATION
10x T4 ligase buffer	2 µl	1x
Linearized pNOC-OX-*CFP* vector DNA	Calculated from the sample concentration	100 ng
NoDGTT12 insert DNA	Calculated from the sample concentration	70 ng
Nuclease-free water	to 20 µl	–
T4 DNA ligase	1 µl	400 U
Total volume	50 µl	–

The mixture was gently pipetted up and down, briefly centrifuged, and incubated at 16 °C overnight in a thermal cycler. The reaction was terminated by heat inactivation of the ligase at 65 °C for 10 min and then immediately chilled on ice.

Bacterial transformation of One Shot™ TOP10 Chemically Competent *E. coli* cells with pNOC-*NoDGTT12-CFP* construct was conducted as already described under point 3.1.4. The efficiency of the transformation was assessed by colony PCR as described in section 3.1.4. The *pNOC-OX-CFP* vector carrying the target genes was subsequently isolated from bacterial cells (section 3.1.3) and stored at -20 °C.

3.2.4.2 Transformation of *Nannochloropsis oceanica* CCMP1779 with *pNOC-NoDGTT12-CFP* construct

For genetic transformation of *N. oceanica* CCMP1179 cells with the pNOC-*NoDGTT12-CFP* constructs, algal cultures were grown for 3 days under N+ conditions as described in section 3.2.1. Subsequently, 50 ml of the culture was transferred into a Falcon tube and centrifuged at 3000 × g for 10 min at 4 °C. The supernatant was discarded, and 25 ml of cold 375 mM sorbitol was added to the remaining *N. oceanica* CCMP1779 pellet to provide an osmotic protective medium. The pellet was thoroughly resuspended by pipetting and centrifuged under the same conditions. This washing step with sorbitol was repeated five times, and the final pellet was resuspended in 200 µl of sorbitol in an Eppendorf tube to achieve the cell concentration at 10^6 cells.

In parallel, the pNOC-*NoDGTT12-CFP* and pNOC-OX-*CFP* (empty vector, as a control) were linearized with the *AseI* enzyme using the mixture detailed in Table 18.

Table 18. Composition of reaction mix for digestion with *Ase I*

COMPONENT	VOLUME/REACTION	FINAL CONCENTRATION
pNOC-OX construct	Calculated from the sample concentration	Max 5 µg
Ase I restriction enzyme	2 µl	2 U
10x NEBuffer	5 µl	1x
Nuclease-free water	to 50 µl	–
Total volume	50 µl	–

The mixture was incubated at 37 °C for 10 h in a heating block without shaking, followed by heat inactivation at 65 °C for 10 min. The digested DNA was then separated by gel electrophoresis and purified using the Monarch® DNA Gel Extraction Kit, as previously described.

Single-stranded carrier DNA was prepared by two cycles of boiling at 95 °C for 1 min in a heat block and followed by incubation on ice for 1 min. Subsequently, 1.5 µg of linearized transforming DNA was added

to 30 µg of single-stranded carrier DNA (2.5 µl), mixed by vortexing, and transferred to the Eppendorf tube containing the *N. oceanica* CCMP1779 cell suspension kept on ice. The mixture was then transferred to a sterile 0.2 cm gap electroporation cuvette and subjected to electroporation using an electroporation system under the following parameters: 2.2 kV field strength, 500 Ohm resistance, and 50 µF capacitance. Immediately following electroporation, the sample was transferred from the cuvette to a 15 ml Falcon tube containing 5 ml of F/2 medium with nitrogen source and vitamins (N+ V+) for recovery. The cultures were incubated on a horizontal shaker at 130 rpm, 22 °C, with a light intensity of 60 µmol/m²s⁻¹ for 48 h. After the recovery period, 5 ml of autoclaved F/2 medium supplemented with 1% agar and 5 µl of hygromycin B (see section 2.8) was added to the recovered *N. oceanica* CCMP 1779 liquid culture. The mixture (thereafter termed as "top-agar culture") was gently but swiftly flicked to ensure even distribution. For top-agar culture, 10 ml of this suspension was immediately poured onto a Petri dish containing solid F/2 medium N+ V+ with hygromycin and spread uniformly by gentle orbital movements. After 30 min, required for solidification of the top-agar, the Petri dish was sealed with parafilm and incubated at room temperature under continuous light (60 µmol/m²s⁻¹).

Colonies of *N. oceanica* CCMP1779 transformed with the pNOC-*NoDGTT12-CFP* construct appeared after around 14 to 21 days. These colonies were transferred to fresh plates containing solid F/2 medium N+ V+ supplemented with hygromycin for further selection. Only cultures expressing the pNOC-*NoDGTT12-CFP* construct with hygromycin resistance were able to grow on the medium containing this antibiotic.

The selected positive colonies were then transferred individually into separate 50 ml flasks, each containing 10 ml of liquid F/2 medium supplemented with hygromycin (100 µg/ml). Each flask was labelled with a unique identification number corresponding to the respective colony from which it originated. The cultures were grown for 3 to 7 days under standard conditions at 22 °C, with continuous light of 60 µmol/m²s⁻¹ and gentle shaking at 130 rpm. After the cultivation period, the cells were harvested and collected for subsequent analyses including: 1) CLSM to visualize the expression of the cerulean-tagged pNOC-*NoDGTT12-CFP* construct, LD staining and chloroplast organization, 2) lipid extraction for GC-FID analysis, and 3) western blotting to confirm the presence and integrity of the overexpressed NoDGTT12 protein. Each sample was appropriately labelled to maintain correspondence between the original colonies and the subsequent experimental analyses.

3.2.4.3 Confirmation of *NoDGTT12* overexpression in *Nannochloropsis oceanica* CCMP1779 transformants

3.2.4.3.1 Protein extraction from *Nannochloropsis oceanica* CCMP1779 transgenic and non-transgenic cultures

For protein isolation, 50 ml of transgenic and non-transgenic *N. oceanica* CCMP1179 cultures grown as described previously (section 3.2.1) was transferred into 50 ml Falcon tubes. The samples were centrifuged at 3000 rpm for 7 min. After centrifugation, the supernatant was discarded, and 4 ml of sterile water was added to each tube containing the pellet. The pellet was thoroughly resuspended by mixing, and the resulting suspension was split into two 2 ml aliquots which were then transferred to 2.0 ml Eppendorf tubes. The tubes were briefly centrifuged, and the supernatant was carefully removed. The remaining pellet was immediately frozen in liquid nitrogen. Additionally, two tungsten carbide

homogenizer beads (ø 3 mm) were added to each tube. The prepared samples were either processed immediately or stored at -80 °C for later use.

For protein extraction, 100 µl of protein isolation buffer (section 2.8) was added to each homogenized sample. The tubes were immediately vortexed vigorously until the pellet was completely resuspended in the buffer. The resulting suspension was then transferred to a fresh 1.5 ml Eppendorf tube and incubated at 80 °C for 3 min in heating block. Following incubation, the samples were centrifuged at 13,000 rpm for 3 min, and the supernatant containing total protein was carefully collected and transferred to a new 1.5 ml Eppendorf tube. The total protein concentration for each sample was estimated using the Bradford method. For this, 1 ml of Bradford solution and 5 µl of sample were mixed in a spectrophotometer cuvette. After 5 min of incubation, the absorbance at OD_{595} nm was measured using a spectrophotometer. The measured absorbance values were compared against a standard curve prepared with known concentrations of BSA to determine the protein concentration of each sample (Table 9). The protein samples were stored at -80 °C for further experiments.

3.2.4.3.2 Detection of NoDGTT12-CFP protein construct by immunoblotting

To detect the expression of the pNOC-NoDGTT12-CFP tagged protein in *N. oceanica* CCMP1779 cultures by immunoblotting, protein samples were first separated by SDS-PAGE and subsequently transferred onto a PVDF membrane as described previously under point 3.1.9.2.

The membrane with transferred proteins was then blocked by incubation in 5% whole milk powder dissolved in 1x TBST buffer (prepared as described in section 2.8) at room temperature for 2 h, followed by washing in 1x TBST buffer for 10 min. The membrane was subsequently incubated overnight at 4 °C with primary mouse anti-GFP antibody solution (1:1000) diluted in 1% whole milk powder in 1x TBST buffer) with gentle shaking at 60 rpm on an orbital shaker. On the following day, the membrane was washed three times with 1x TBST buffer for 15 min each and then incubated with the secondary anti-mouse antibody, HRP stained (1:50 000) for 1 h at room temperature with gentle shaking at 60 rpm. The membrane was then washed three times for 15 min each in ultrapure water.

For signal detection, the Amersham ECL Western Blotting Detection Reagent was used, as explained in section 3.1.9.2.

3.2.4.3.3 Analysis of *Nannochloropsis oceanica* CCMP1179 transformants by CLSM

For CLSM analysis of the most robustly growing algal cultures, 2 ml of each culture was centrifuged at 2500 rpm for 2 min, and the supernatant was discarded. The resulting cell pellet was washed three times with 1x PBS buffer (pH 7.2) to remove residual medium. To visualize lipid droplets, BODIPY™ 505/515 dye was applied at a final concentration of 10 µg/ml in 1x PBS buffer. Staining was performed by incubating the samples at room temperature for 1 h, followed by two additional washes with 1 x PBS to eliminate excess dye. Samples were immediately examined using a CLSM.

Fluorescence derived from BODIPY™ 505/515 was detected utilizing a diode laser set to 0.1% intensity, with an excitation bandwidth of 505 nm and an emission bandwidth of 515 nm, and a gain setting of 1.0. Detection of the CFP-tagged pNOC-NoDGTT12-CFP fusion construct was carried out using a diode laser operating at 3% intensity, an excitation bandwidth of 435 nm and an emission bandwidth of 485 nm, with a gain of 1.0. Chlorophyll autofluorescence was captured by exciting the samples at 640 nm and detecting

emission at 700 nm, employing a diode laser with 0.5% intensity, an excitation bandwidth of 640, and an emission bandwidth of 700 nm, with a gain setting of 1.0. For each sample, observations were made on a total of 30 randomly selected *N. oceanica* CCMP1779 cells. Images were acquired using CLSM and subsequently processed with Fiji software.

3.2.4.4 Extraction and analysis of lipids from *Nannochloropsis oceanica* CCMP1779 transformants

For total lipid extraction, selected *N. oceanica* CCMP1179 liquid cultures expressing the *pNOC-NoDGTT12-CFP* construct were scaled up to a volume of 200 ml and cultivated in selective F/2 N+ medium supplemented with hygromycin for 3 to 7 days under standard conditions described previously. Non-transgenic *N. oceanica* CCMP1779 cultures grown under identical conditions and volume served as controls, as well as algae transformed with empty *pNOC*-OX-*CFP* vector.

The cultures were divided into four aliquots and transferred into 50 ml Falcon tubes, followed by centrifugation at 3000 rpm for 7 min using a centrifuge equipped with a swinging-bucket rotor. The supernatant was discarded, and 500 µl of sterile water was added to each Falcon tube. The algal pellet was resuspended by gentle pipetting, and the resulting suspension was transferred to 1.5 ml Eppendorf tubes. The tubes were briefly centrifuged, and the supernatant was carefully removed with a pipette.

The remaining *N. oceanica* CCMP1779 pellet was immediately subjected to lipid extraction following the protocol described by Zienkiewicz *et al*. (2020). The pellet was covered with 1 ml of a chloroform:methanol mixture (2:1, v/v) and transferred into Kimble glass tubes with 0,5 ml of glass beads (ø 425-600 µm). The samples were vortexed for 10 sec, and then 250 µl of 0.9% NaCl was added to each tube. After additional vortexing (5 sec, repeated twice), the samples were centrifuged at 3000 rpm for 3 min using a centrifuge equipped with a swinging-bucket rotor. The resulting lower lipidic phase was carefully collected using a glass pipette and transferred to an open-top glass tube. The solvent was evaporated under a stream of nitrogen gas within a fume hood, and the residual lipid phase was resuspended in 75 µl of chloroform. The extracted lipids were subsequently separated by TLC and analysed according to the procedure described below.

The TLC plates were dried at 200 °C for 2 h to remove any moisture. Prior to the TLC, 50 µl of chloroform-dissolved lipidic fraction from each sample was split into two equal parts of 25 µl spotted at the top and the bottom of the TLC glass plate covered with silica gel layer, as shown on Figure 6.

Olive oil (2 µl dissolved in 200 µl of acetone) was used as a TAG standard for identification of TAG-corresponding band in each sample. The plate was developed in a glass chamber containing 100 ml of mobile phase described in section 2.8, until the front of the separation reached over 2/3 of the plate (Figure 6).

Afterwards, TLC plate was dried under the hood and sprayed with 1% (w/v) acetone solution of primuline for visualization of TAGs under UV light (instead of iodine vapours) and further proceeded as described under point 3.1.8

A GC fitted with a DB-23 capillary column (30 m × 0.25 mm, 0.25 µm film thickness) and an FID were utilized as explained in detail under point 3.1.8.1.

3.3 Experimental procedures for *Arabidopsis thaliana*

3.3.1. Heterologous expression of NoDGTT12-encoding gene in *Arabidopsis thaliana*

3.3.1.1 Gateway cloning™ of *NoDGTT12* for *Agrobacterium tumefaciens* GV3101 transformation

For heterologous expression the *DGTT12* from *N. oceanica* CCMP1779 in *A. thaliana,* a Gateway cloning™ strategy (Figure 10) followed by *A. tumefaciens* GV3101-mediated transformation using the floral dip method (Zhang *et al*., 2006) was employed.

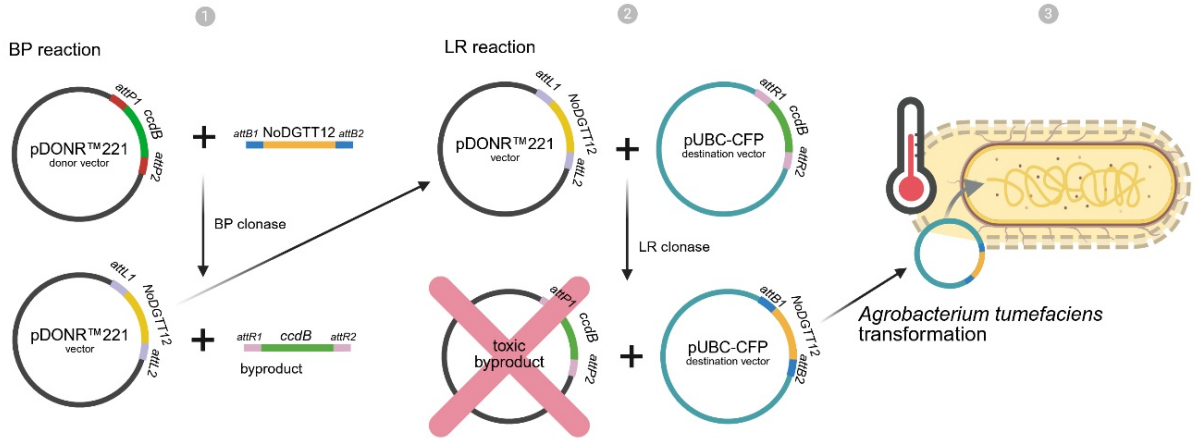

Figure 10. Schematic representation of Gateway cloning™ strategy. (1) BP reaction and creating the entry clone. (2) LR reaction with destination vector integration. (3) *A. tumefaciens* transformation.

Gateway cloning™ is a versatile and efficient technique for transferring DNA fragments between vectors through site-specific recombination. This method relies on the transfer of DNA between *attB*, *attP*, *attL*, and *attR* sites *via* recombination reactions, enabling rapid and accurate generation of expression constructs. The Gateway cloning™ process involves three primary steps: the BP reaction (entry clone creation), the LR reaction (integration into a destination vector), and final expression in the target system To obtain the NoDGTT12 coding sequence for transformation, *N. oceanica* CCMP 1779 was cultured under light stress conditions as described in section 3.2.1. Following cultivation, cells were harvested, homogenized, and RNA was extracted according to the procedure outlined in section 3.2.2. cDNA synthesis was performed using the extracted RNA, and the quality of the template was verified by PCR amplification of a reference EF-encoding gene, as described in section 3.2.3. The *NoDGTT12* gene was then amplified on pYES2.1-*NoDGTT12* template using primers containing *attB* flanking sites (see section 2.7). The PCR reaction, prepared according to the protocol in Table 19, was carried out using Phusion™ DNA Polymerase under conditions specified in Table 20.

Table 19. Composition of PCR reaction mix for amplification of *NoDGTT12* sequence flanked with *attB* sites

COMPONENT	VOLUME/REACTION	FINAL CONCENTRATION
5X Phusion™ HF Buffer	4 µl	1x Reaction Buffer
10 mM dNTPs	0.4 µl	200 µM of each dNTP
NoDGTT12B1 primer	0.5 µl	5 mM
NoDGTT12B2a primer	0.5 µl	5 mM
Molecular biology grade water	to 20 µl	–
pYES2.1-*NoDGTT12* template	2.0 µl	< 0.2 µg/20 µl
Total volume	20 µl	–

Table 20. Conditions of PCR reaction from Table 19.

STEP	TEMPERATURE	TIME	NUMBER OF CYCLES
Initial denaturation	98 °C	30 sec	1
Denaturation	98 °C	10 sec	30
Annealing	55 °C	30 sec	
Extension	72 °C	60 sec	
Final extension	72 °C	5 min	1
Cooling	4 °C	indefinite	1

The resulting PCR products flanked with *attB* sites were then recombined with the pDONR™221 donor vector containing *attP* sites using the BP reaction. This recombination, catalysed by BP Clonase™ enzyme mix, generated an entry clone with the *NoDGTT12* gene flanked by *attL* sites (Figure 10). The BP reaction was performed at room temperature for 1 h using the mixture listed in Table 21.

Table 21. Composition of BP reaction mixture (Gateway cloning™)

COMPONENT	VOLUME/REACTION	FINAL CONCENTRATION
*att*B-PCR product	6 µl	≥ 10 ng/µl
pDONR™221 Vector	1 µl	15 ng
TE buffer, pH=8.0	1 µl	to 8 µl
BP Clonase™ II enzyme mix	2 µl	1x

The BP reaction was terminated by adding 1 µl of 2 µg/µl Proteinase K solution and incubated at 37 °C for 10 min. Transformation of the BP reaction mixture into One Shot™ TOP10 Chemically Competent *E. coli* cells was performed as follows: 2 µl of the cloning reaction was added to the competent cells, mixed gently, and incubated on ice for 30 min. The cells were then heat-shocked at 42 °C for 30 sec, immediately transferred back to ice for 2 min, and 900 µl of pre-warmed LB medium was added. After incubation at 37 °C for 1 h with shaking (200 rpm), 50 µl and 500 µl aliquots were plated onto selective LB agar plates containing kanamycin (50 µg/ml) and incubated overnight at 37 °C.
The pDONR™221 vector used as the entry clone carries a kanamycin resistance gene for positive selection of transformed bacteria (Figure 11).

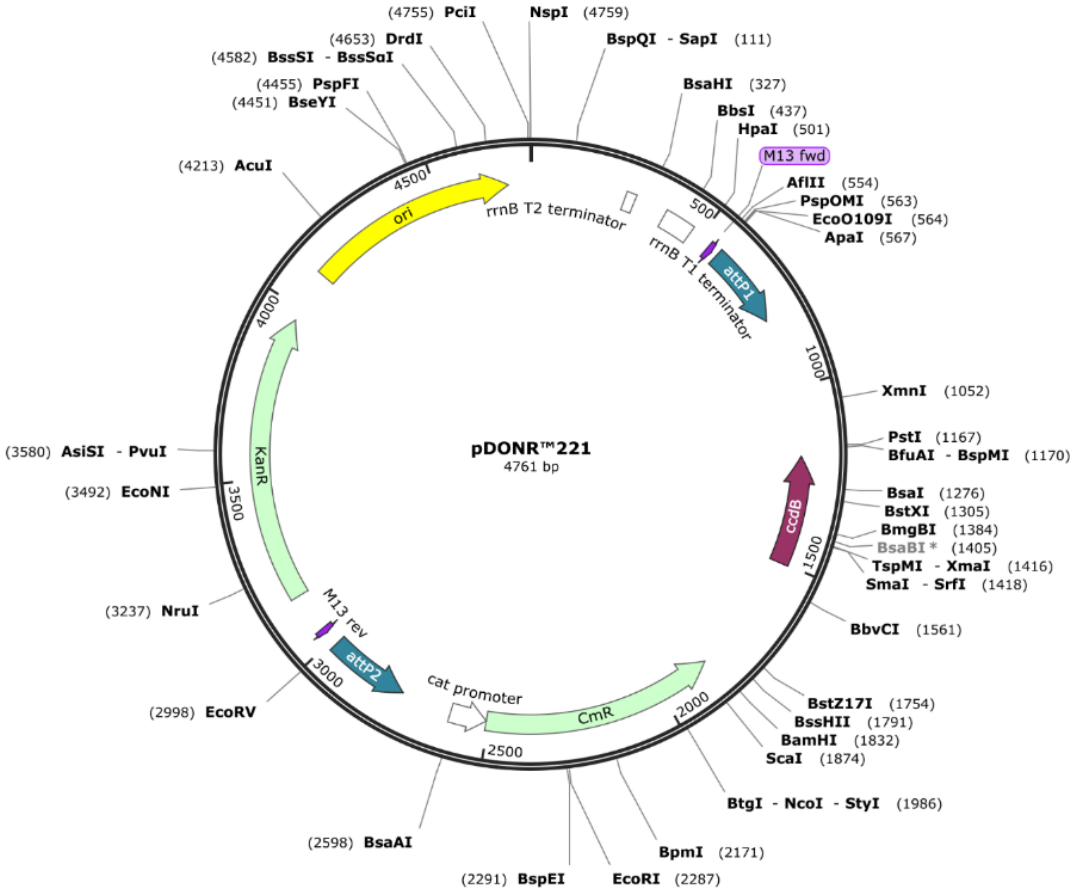

Figure 11. pDONR™221 vector, circular vector map. Key features of the plasmid (1) KanR, CmR (green arrows) – kanamycin and chloramphenicol resistance, allowing for the positive selection of transformed bacteria containing the plasmid. (2) ccdB Gene (purple arrow) – allowing for the negative selection of cells retaining the plasmid without recombination. (3) attP sites (blue arrows) – specific recombination sites for Gateway Cloning strategy (4) ori – origin of replication (yellow arrow), responsible for plasmid replication in transformed bacterial cells (5) cat promoter (white arrow) – chloramphenicol acetyltransferase (CAT) promoter that controls gene expression in yeast. (6) rrnb terminator (white squares) – facilitates transcription termination. (7) Restriction enzyme sites – labelled around the circular plasmid with their positions. Generated by SnapGene software.

Efficiency of cloning was verified by colony PCR using Color Perpetual Taq PCR Master Mix following the manufacturer's protocol (section 3.1.3). Correctly transformed plasmids were extracted using the Plasmid Miniprep DNA Purification Kit (section 2.4) and sequenced. Only samples confirmed to be correct were used for the subsequent LR reaction. The LR reaction, which facilitates integration of the *NoDGTT12* sequence into the destination vector *pUBC-CFP*-Dest, was performed using the LR Clonase™ enzyme mix. The reaction mixture, prepared as listed in Table 22, was incubated at room temperature for 1 h. The reaction was terminated by adding 1 µl of 2 µg/µl Proteinase K solution and incubating at 37 °C for 10 min.

Table 22. Composition of LR reaction mixture (Gateway cloning™)

COMPONENT	VOLUME/REACTION	FINAL CONCENTRATION
Entry clone	6 µl	≥ 10 ng/µl
pUBC-CFP vector	1 µl	15 ng
TE buffer, pH=8.0	1 µl	to 8 µl
LR Clonase™ II enzyme mix	2 µl	1x

Transformed One Shot™ TOP10 Chemically Competent *E. coli* cells were prepared by thawing on ice. 2 µl of the LR reaction mixture was added to the competent cells and mixed gently. The transformation protocol included 30 min of incubation on ice, a 42 °C heat shock for 30 sec, cooling on ice for 2 min, and the addition of 900 µl of pre-warmed sterile LB medium. The cultures were incubated horizontally for 1 h at 37 °C with shaking (200 rpm). Aliquots of 50 µl and 500 µl were spread onto LB agar plates containing streptomycin (50 µg/ml) and incubated overnight at 37 °C. Cloning efficiency was verified by colony PCR using the Color Perpetual Taq PCR Master Mix following the manufacturer's protocol (section 3.1.3).

The *pUBC-CFP*-Dest vector containing the *NoDGTT12* sequence was extracted from transformed *E. coli* cells using the NucleoSpin Plasmid EasyPure kit (see point 2.4). 6 ml of overnight culture was aliquoted into three Eppendorf tubes, centrifuged at 14,000 × g for 30 sec, and the supernatant was discarded. 50 µl of Buffer A1 was added to each tube, mixed by vigorous vortexing, and pooled into a single tube. The pooled suspension was treated with 250 µl of Buffer A2 and mixed gently by inverting the tube 5 times, followed by incubation at room temperature for 2 min. After adding 350 µl of Buffer A3, the mixture was inverted until it turned colourless and centrifuged at 14,000 × g for 3 min. The supernatant was applied to a NucleoSpin Plasmid EasyPure column fitted into a Collection Tube (2 ml). After centrifugation at 2,000 × g for 30 sec, the flow-through was discarded, and the column was washed with 450 µl of Buffer AQ. After centrifugation at 14,000 × g for 1 min, the column was transferred to a fresh Eppendorf tube. To elute the DNA, 30 µl of preheated Buffer AE (70 °C) was added directly to the column, incubated at 70 °C for 2 min, and centrifuged at 11,000 × g for 1 min. The purified plasmid DNA was subsequently used for *A. tumefaciens* transformation.

3.3.1.2 Transformation of *Agrobacterium tumefaciens* GV3101 with *pUBC-NoDGTT12-CFP* construct

Transformation of *A. tumefaciens* GV3101 is the first step in the floral-dip method for *A. thaliana* AS11 (*tag1-1*) transformation. The GV3101 strain is resistant to rifampicin due to a resistance gene located on a helper plasmid carried by this strain. Rifampicin is used to select only bacteria that contain this helper plasmid, which is also required for T-DNA transfer to plants. Gentamicin is used to eliminate any contaminating bacteria that may be present after transformation and helps maintain culture purity. The *pUBC-CFP* vector used for transformation carries spectinomycin and BASTA resistance genes, which enable positive selection of transformed colonies (Figure 12).

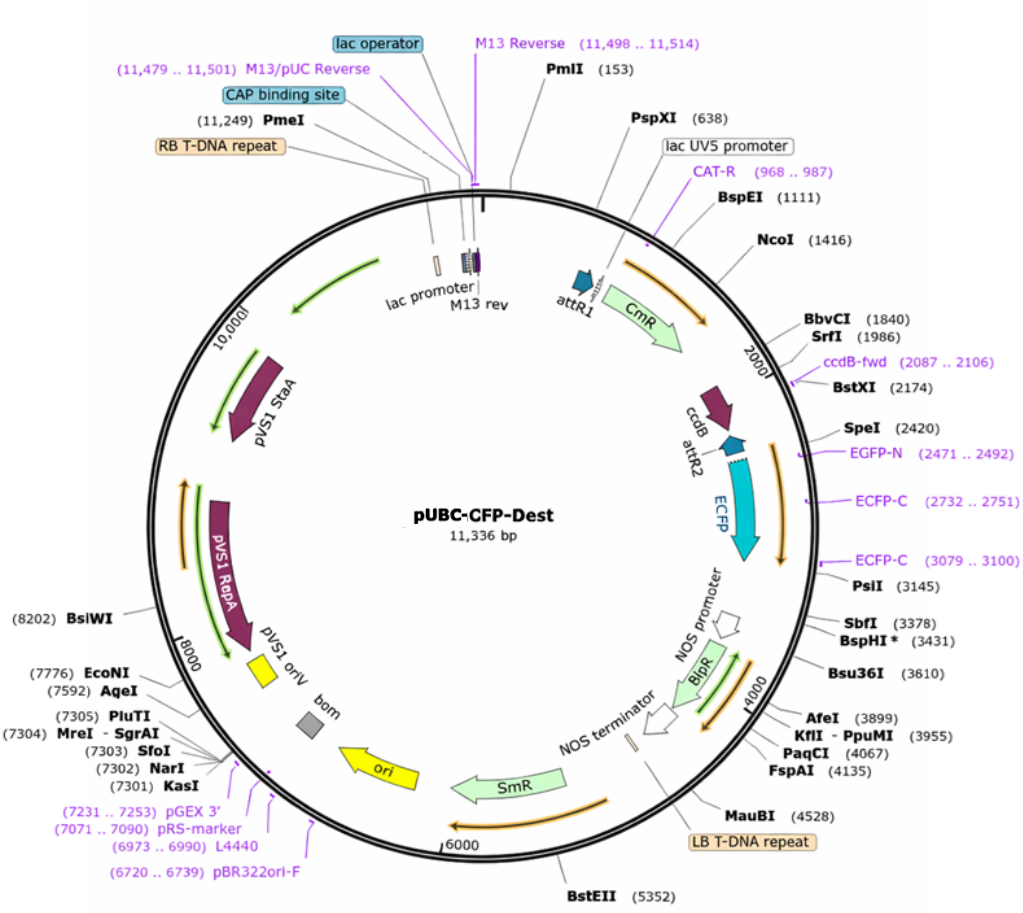

Figure 12. pUBC-*CFP*-DEST, circular vector map. Key features of the plasmid include: (1) NOS promoter (white arrow) – promoter driving reporter gene expression. (2) attR1 and attR2 sites (blue arrows) – Gateway™ recombination sites for site-specific cloning. (3) ccdB gene (purple arrow) – negative selection marker for selection of correct recombinants. (4) CmR (green arrow) – chloramphenicol resistance cassette for bacterial selection. (5) CFP (turquoise arrow) – cerulan fluorescent protein reporter gene. (6) NOS terminator (white arrow) – transcriptional terminator sequence. (7) pVS1 replicon (yellow square) – replication/maintenance functions for *Agrobacterium*. (8) ori (yellow arrow) and bom (grey square) – replication origin and mobilization region for propagation in *E. coli*. (9) SmR (green arrow) – streptomycin resistance marker for bacterial selection. (10) LB and RB T-DNA border repeats (yellow rectangle) – sequences enabling T-DNA transfer and integration into the plant genome. Plasmid map generated using SnapGene software.

Building on the selection strategy described above, *A. tumefaciens* GV3101 competent cells were thawed on ice, and 2 µg of the pUBC-*NoDGTT12-CFP* plasmid DNA were added. The suspension was then flash-frozen in liquid nitrogen for 5 min. The empty *pUBC-CFP* vector was used as a control. Following freezing, the cells were transferred immediately to 37 °C and incubated for 5 min. Subsequently, 1 ml of LB medium was added, and the tubes were incubated with shaking at 28 °C for 4 h to allow recovery and expression of the antibiotic resistance markers. After incubation, the cells were pelleted by centrifugation at 5000 rpm for 5 min, and the supernatant was discarded. The pellet was resuspended in 100 µl of LB and spread onto LB agar plates containing gentamicin, rifampicin, and spectinomycin (5 µl/ml of each antibiotic). Plates were incubated at 28 °C for 3 days to allow the growth of transformants. To assess transformation efficiency, colony PCR was performed. Individual *A. tumefaciens* GV3101 colonies were suspended in 50 µl of ultrapure water and incubated at 95 °C for 30 min, followed by a 10 min incubation on ice. From this lysate, 2 µl were used as template for colony PCR. Cloning efficiency was evaluated using the Color

Perpetual Taq PCR Master Mix according to the manufacturer's instructions, as described previously (see point 3.1.3).

3.3.1.3. Transformation of *Arabidopsis thaliana* AS11 (*tag1-1*) with *pUBC-NoDGTT12-CFP* construct

3.3.1.3.1 Verification of *Arabidopsis thaliana* AS11 (*tag1-1*) lines prior to floral-dip transformation

Before performing the floral-dip transformation, it was essential to verify the identity of the *A. thaliana* AS11 (*tag1-1*) mutant line to ensure that the plants used were true mutants and not wild type contaminants.

Seeds of AS11 (*tag1-1*) were sown in soil and grown under controlled growth conditions (150 µE m^{-2} s^{-1} light intensity, 16-h light/8-h dark cycle, 22 °C day/18 °C night) until they reached the rosette stage. At this developmental stage, leaf tissue was collected for genomic DNA extraction. Genotyping PCR was then performed using allele-specific primers designed to distinguish the *tag1-1* T-DNA insertion from the WT allele.

For DNA extraction from *A. thaliana* tissue for genotyping, 250 µL of EB buffer was poured to a 1.5 ml microcentrifuge tube and 100 µg of plant tissue, not exceeding one leaf, was placed in the tube. The sample was thoroughly grounded using a pellet pestle and then centrifuged at 13,000 x g for 3 min at room temperature. 250 µL of isopropanol was added into a separate tube, and the supernatant from the centrifuged sample was carefully transferred to the isopropanol-containing tube. The sample was gently mixed by tilting and incubated at -20 °C for 30 min to allow DNA precipitation. After incubation, the sample was centrifuged at 13,000 x g for 7 min at room temperature, and the resulting supernatant was discarded. 250 µL of cold 70% ethanol was added to wash the obtained DNA pellet, followed by centrifugation for 3 min at 13,000 x g. The ethanol wash was repeated once more under the same conditions. The supernatant was again discarded with care to remove as much liquid as possible. The pellet was then allowed to air-dry on the benchtop for 30 min and then resuspended in 20 µL of TE buffer (pH 8.0). The isolated DNA was stored at -20 °C until further use.

The genotyping PCR reaction mix was prepared using Color Perpetual Taq Polymerase. The reaction compositions are provided in Tables 23a and 23b. The PCR was performed using a thermal cycler under conditions specified in Tables 24a and 24b.

Table 23a. Reaction mix for *A. thaliana* genotyping PCR reaction 1

COMPONENT	VOLUME/REACTION	FINAL CONCENTRATION
Color Perpetual Taq PCR Master Mix (2x)	12.5 µl	• 1.25 U of Perpetual Taq DNA Polymerase • 1x Reaction Buffer (1.5mM MgCl2) • 0.2 mM of each dNTP
As11A primer	0.5 µl	10 mM
As11B primer	0.5 µl	10 mM
Template DNA	2.0 µl	< 0.25 µg/25 µl
Molecular biology grade water	to 25 µl	–
Total volume	25 µl	–

Table 23b. Reaction mix for *A. thaliana* genotyping PCR reaction 2

COMPONENT	VOLUME/REACTION	FINAL CONCENTRATION
Color Perpetual Taq PCR Master Mix (2x)	12.5 µl	• 1.25 U of Perpetual Taq DNA Polymerase • 1x Reaction Buffer (1.5mM MgCl2) • 0.2 mM of each dNTP
As11C primer	0.5 µl	10 mM
As11B primer	0.5 µl	10 mM
Template DNA	2.0 µl	< 0.25 µg/25 µl
Molecular biology grade water	to 25 µl	–
Total volume	25 µl	–

Table 24a. Conditions of the PCR reaction 1 for *A. thaliana* genotyping

STEP	TEMPERATURE	TIME	NUMBER OF CYCLES
Initial denaturation	94 °C	2 min	1
Denaturation	95 °C	30 sec	30
Annealing	62 °C	30 sec	
Extension	72 °C	30 sec	
Final extension	72 °C	7 min	1
Cooling	10 °C	indefinite	1

Table 24b. Conditions of the PCR reaction 2 for *A. thaliana* genotyping

STEP	TEMPERATURE	TIME	NUMBER OF CYCLES
Initial denaturation	94 °C	2 min	1
Denaturation	95 °C	30 sec	30
Annealing	55 °C	30 sec	
Extension	72 °C	30 sec	
Final extension	72 °C	7 min	1
Cooling	10 °C	indefinite	1

To analyse the PCR products, gel electrophoresis was carried out using a 1% agarose gel in 1x TAE buffer. A Perfect™ 100 bp DNA Ladder was included to estimate the PCR product size.

Successful confirmation of the mutant genotype was required before proceeding with the floral-dip transformation to ensure that only verified AS11 (*tag1-1*) plants were used in subsequent transformation experiments.

3.3.1.3.2 Floral-dip transformation of *Arabidopsis thaliana* AS11 (*tag1-1*)

A single colony of transformed *A. tumefaciens* GV3101 was selected and cultured in 5 ml of LB medium supplemented with gentamicin, spectinomycin, and rifampicin (5 µl/ml of each) in a shaking incubator at 28 °C and 250 rpm. After 8 h, this starter culture was scaled up to 250 ml using the same antibiotic-supplemented medium and incubated under the same conditions for an additional 12 h, until the culture reached an OD_{600} of approximately 0.8. The culture was transferred to 500 ml polypropylene bottles and centrifuged at 6000 rpm for 10 min. The supernatant was discarded, and the resulting pellet was gently and thoroughly resuspended in 500 ml of freshly prepared inoculation medium containing 5% sucrose and 0.05% Silwet-77 in ultrapure water. This suspension was poured into a small plastic tray, and the stems and flowers of flowering-stage *A. thaliana* AS11 (*tag1-1*) plants were carefully dipped into the medium for 10 sec.

Following dipping, the labelled pots were placed horizontally in a closed container and incubated overnight in a humid, dark environment. After 24 h, the lids were removed and the pots were placed upright. The treated plants were then grown in soil under controlled growth conditions (150 µE m^{-2} s^{-1} light intensity, 16-h light/8-h dark cycle, 22 °C day / 18 °C night) until seed maturation.
Mature seeds were harvested, passed through a sieve to remove debris, and stored in labelled plastic containers at room temperature for subsequent experiments.

3.3.2 Selection of positive *Arabidopsis thaliana* AS11 (*tag1-1*) transformants

To select *A. thaliana* AS11 (*tag1-1*) plants transformed with *A. tumefaciens* GV3101 carrying the NoDGTT12 coding sequence, glufosinate ammonium (BASTA) spraying was performed on 10-day-old seedlings. In the initial step, transformed *A. thaliana* AS11 (*tag1-1*) seeds were sterilized using a water solution containing 30% sodium hypochlorite and 0.2% Tween20. A total of 7 ml of the sterilization solution was added to a 15 ml Falcon tube containing 0.5 ml of seeds. The mixture was incubated at room temperature for 15 min, gently mixing by rolling the tube every 2 min.
After sterilization, the seeds were washed thoroughly with tap water five times and subjected to stratification in the dark at 4 °C for 48 h. Following stratification, the seeds were evenly distributed in pots and grown for 10 days in soil tyndallized at 60 °C for 8 h. Plants were grown under controlled conditions with a light intensity of 150 µmol/m^2s^{-1}, a 16-h light/8-h dark cycle, and a temperature regime of 22 °C during the day and 18 °C at night. After 10 days, the seedlings were sprayed with BASTA solution at a concentration of 17 mg/l and allowed to grow for an additional 3 days. To ensure effective selection, the plants were sprayed again with 17 mg/l BASTA solution on days 3 and 6 following the initial treatment. Positively selected plants were transferred to new pots and grown in soil as described above. The plants were cultivated until seeds reached maturity.

3.3.3 Detection of *NoDGTT12* expression in *Arabidopsis thaliana* AS11 (*tag1-1*) transformants by immunoblotting

3.3.3.1 Detection of *NoDGTT12* expression in first generation (F1) of *Arabidopsis thaliana* AS11 (*tag1-1*) transformants carrying *NoDGTT12-CFP* construct

To confirm the expression of *NoDGTT12-CFP* construct in *A. thaliana* AS11 (*tag1-1*) transformants, immunoblotting to CFP protein was performed on the F1 generation of transformants, cultivated as described under point 3.3.2. Total protein was isolated from the rosette leaves of transformed *A. thaliana* AS11 (*tag1-1*) plants. Approximately 100 mg of leaf material was transferred into a 2.0 ml cryotube containing three tungsten carbide homogenizer beads (ø 3 mm). The tubes were immediately deep-frozen in liquid N_2 and homogenized using a cryogenic ball mill set to 30x/sec for 2 min.
The frozen material was ground into a fine powder prior to protein extraction. To each homogenized sample, 100 µl of protein isolation buffer (prepared according to Section 2.8) was added. The tubes were vortexed vigorously until the pellet was fully resuspended in the buffer. The resulting suspension was transferred to a new 1.5 ml Eppendorf tube and incubated at 80 °C for 3 min. After heating, the samples were centrifuged at 13,000 rpm for 3 min, and the supernatant was carefully collected and transferred to a fresh 1.5 ml Eppendorf tube.

The protein concentration in the samples was determined as described in section 3.1.10. Samples were then stored at -20 °C until further use.

SDS-PAGE protein separation and transfer were performed as previously described under point 3.1.9.2. Following protein transfer, the membrane was processed for antibody incubation and signal detection. After the transfer, the gel was stained with Bio-Safe Coomassie Stain to visualize total proteins. The procedures were performed as outlined in section 3.1.9.2.

3.3.3.2 Detection of *NoDGTT12* expression in second generation (F2) of *Arabidopsis thaliana* AS11 (*tag1- 1*) transformants carrying *NoDGTT12-CFP* construct

To confirm the stable expression of the algal transgene *NoDGTT12* in transgenic *A. thaliana* AS11 (*tag1- 1*) plants across the generations, the F2 generation of transformants was cultivated and analysed, as described previously (see point 3.3.2). Approximately 0.5 ml of seeds from F1 plants with confirmed presence of NoDGTT12-CFP fusion protein were sterilized in a 15 ml Falcon tube containing a sterilization solution composed of 30% sodium hypochlorite and 0.2% Tween20. The sterilization mixture was added to the Falcon tube and incubated at room temperature for 15 min, gently mixing by rolling the tube every 2 min. After sterilization, the seeds were washed thoroughly with sterile water five times and stratified in the dark at 4 °C for 48 h. Following stratification, the seeds were evenly distributed on solid ½ MS + sucrose + BASTA medium and grown for 7 days. After the initial growth period, the seedlings were transferred to pots containing soil and cultivated under a light intensity of 150 µmol/m²s⁻¹, with a 16-hour light/8-hour dark cycle and temperature conditions of 22 °C during the day and 18 °C at night until seeds reached maturity. To identify plant lines exhibiting the highest levels of NoDGTT12-CFP fusion protein, total protein was isolated from rosette leaves and analysed by western blotting to CFP antigen, as outlined in section 3.3.3.1. Seeds from these selected lines were harvested for lipid isolation and further analysis.

3.3.4 Quantitative and qualitative analysis of lipid from seeds and seedlings of F2 generation *Arabidopsis thaliana* AS11 (*tag1-1*) transformants

To evaluate the lipid content and composition of *A. thaliana* AS11 (*tag1-1*) plants expressing *NoDGTT12-CFP* fusion construct during seed germination and early seedling development, a series of lipid extractions were performed. Five sample types were prepared for analysis:

1) 30 mature dry seeds,
2) ~500 µl of seeds after 24 h of germination,
3) ~500 µl of seeds after 48 h of germination,
4) ~500 µl of seeds after 72 h of germination,
5) ~500 µl of seeds after 96 h of germination.

Seeds were surface-sterilized and evenly distributed on solid ½ MS -SUC medium (see point 2.8), as described previously. Germination was carried out under controlled conditions: 150 µmol m^{-2} s^{-1} light intensity, a 16/8 h light–dark cycle, and temperatures of 22 °C (day) and 18 °C (night). For lipid extraction, each sample was transferred into a Kimble glass tube, to which 1 ml of FAME solution and 200 µl of tripentadecanoin (15:0), used as an internal TAG standard, were added. Tubes were tightly sealed, briefly vortexed, and incubated in a shaking water bath at 80 °C and 150 rpm for 1 h. After incubation, samples were cooled to room temperature for 10 min. Subsequently, 1 ml of saturated NaCl

solution and 1 ml of hexane were added to each tube. Samples were vortexed twice for 5 sec and centrifuged at 1500 rpm for 10 min. The upper hexane phase, containing the extracted lipids, was carefully transferred into a new open glass tube and evaporated to dryness under a stream of nitrogen in a fume hood. The dried lipid fraction was then dissolved in 25 µl of acetonitrile, vortexed, and transferred into GC vials for qualitative and quantitative lipid analysis using GC-FID. To identify FAs, samples were analysed like described previously (see point 3.1.9).

3.3.5 Microscopic analysis of TAG accumulation in *Arabidopsis thaliana* AS11 (*tag1-1*) plants

To enable microscopic analysis of *Arabidopsis thaliana* AS11 (*tag1-1*) seeds the seed coat first had to be removed to expose the internal structures. *S*eeds were immersed in water overnight at 4 °C in darkness to soften the seed coat and facilitate its removal. The seed coat was carefully removed under a light microscope, after which the cotyledons were transferred to a 1.5-ml Eppendorf tube containing 1× PBS and kept on ice. The PBS was then removed, 1 ml of 4% PA was added, and the cotyledons were incubated for 1 h on ice. The fixative was removed, seeds were washed with 1x PBS 3 times and stored in 1x PBS at 4 °C for further tests. To visualize lipid droplets, cotyledons were stained with BODIPY™ 505/515 and analysed as described under point 3.1.7.

3.3.6. Analysis of seeds morphology and morphometrics of *Arabidopsis thaliana* plants

To examine the morphology, seeds *of A. thaliana* – WT, AS11 (*tag1-1*), and AS11 (*tag1-1*) complemented with *NoDGTT12* – were briefly rinsed with 96% (v/v) ethanol to remove surface contaminants and subsequently air-dried. Around 50 µl of seeds were then mounted onto glass microscope slides without the use of mounting medium to preserve their native morphology. Microscopic observations were performed using a stereoscopic light microscope. Images of the seeds were captured under uniform lighting conditions to ensure consistency across samples. Morphometric analysis was performed using a static image analyser equipped with dedicated software. Seeds from separate lines were placed in 52 test tubes, and ~500 µl of seeds was dispensed onto a glass plate using compressed air at a pressure of 10 kPa to ensure even dispersion. The entire prepared area was scanned, and only whole grains were selected for measurement. The results were filtered using the circularity parameter. Circularity (C) represents particle roundness, calculated from the particle's perimeter and area. A perfect circle or sphere has a circularity value of 1, while all other shapes have circularity values < 1. This parameter was used to exclude measurements of overlapping grains. The following parameters were analysed: length, width, and area calculated from the equivalent diameter. All parameters were selected to ensure comparability with results obtained from sieve analysis, a method commonly used in the agricultural industry. Mean values and standard deviations were calculated, and data were subsequently used for comparative analyses.

4. RESULTS

4.1 *In silico* analysis of DGTT-encoding genes from *Nannochloropsis oceanica* CCMP1779

In order to elucidate the structural characteristics of DGTT enzymes in *N. oceanica* CCMP1779, twelve putative DGTT-encoding genes (designated *NoDGTT1* through *NoDGTT12*) were identified and analysed at both the nucleotide and amino acid levels. The complete nucleotide sequences of each gene were obtained from the Joint Genome Institute *PhycoCosm* database, and the corresponding open reading frames were translated *in silico* by using *ExPASy* online tool to deduce the primary amino acid sequences (Supplementary table 1). These proteins exhibited a broad range of predicted molecular weights, spanning from approximately 38.07 kDa (NoDGTT7) to 122.4 kDa (NoDGTT4). Computational analyses of transmembrane domains (TMDs) using two complementary *in silico* tools: Deep TMHMM1.0 and Protter (Table 25) were used. While DeepTMHMM employs machine-learning–based sequence classification to predict the likelihood of membrane-spanning regions and their orientation, Protter provides a graphical representation of protein topology, mapping predicted transmembrane helices onto the sequence with explicit delineation of cytosolic and luminal regions.

Table 25. NoDGTTs structural features and TMDs analysed *in silico*. (DeepTMHMM – 1.0) "Sequence" axis indicates amino acid position 0–400. "Probability" axis indicates likelihood of class assignment. Red color: transmembrane regions, pink color: ER internal region, blue color: cytoplasmic site of ER. (Protter) Orange bar indicates the ER lipid bilayer with intra~ and extracellular sites of the membrane. Circles with letters represent amino acids in the protein sequence. Blue numbers indicate transmembrane segments passing through the ER membrane.

Name	DeepTMHMM – 1.0 prediction	Protter prediction
NoDGTT1 43.97 kDa	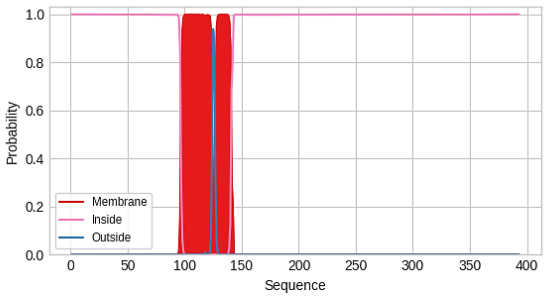	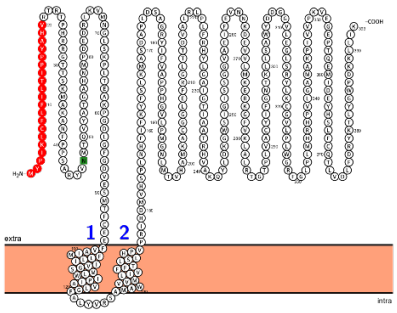
NoDGTT2 53.81 kDa	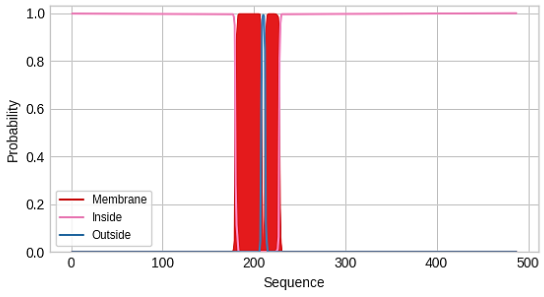	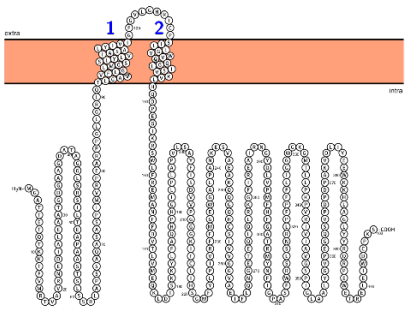

NoDGTT3
44.45 kDa

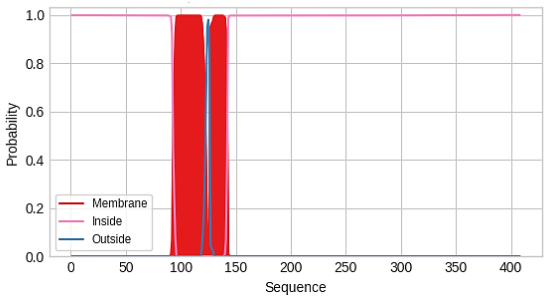

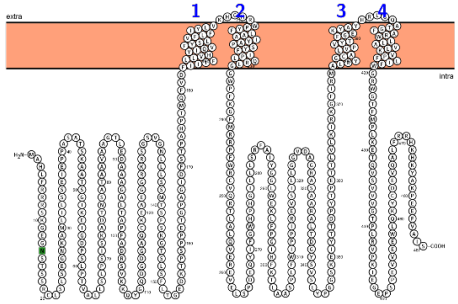

NoDGTT4
122.4 kDa

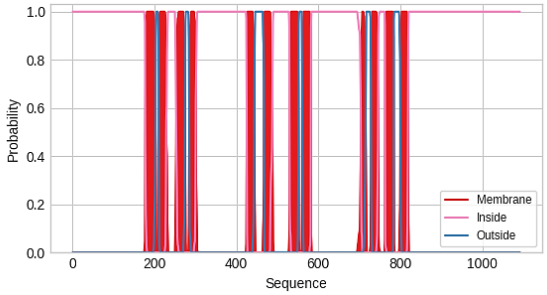

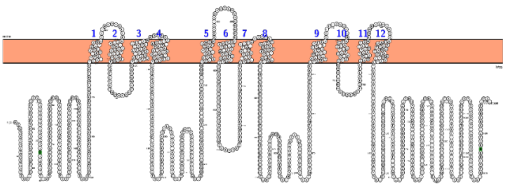

NoDGTT5
40.87 kDa

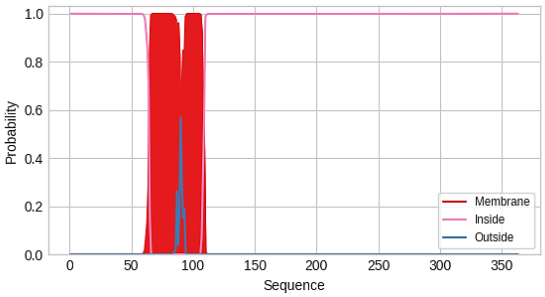

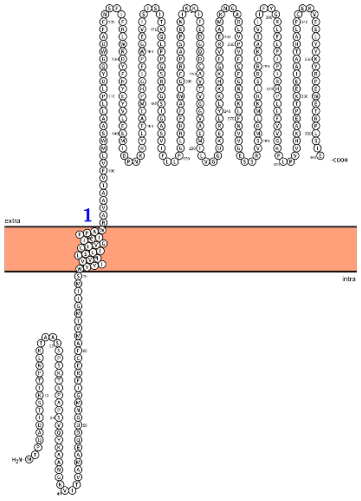

NoDGTT6
52.71 kDa

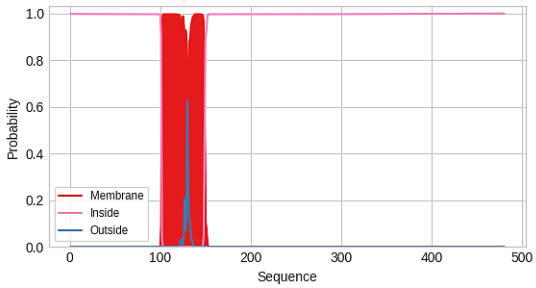

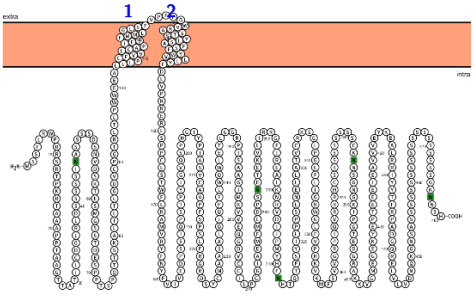

NoDGTT7
38.07 kDa

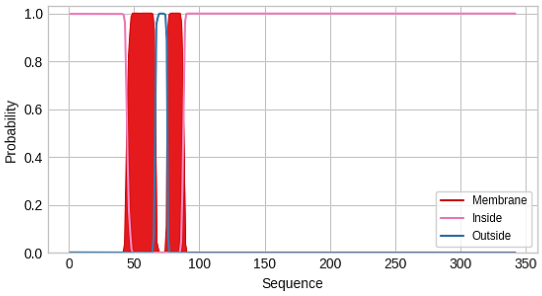

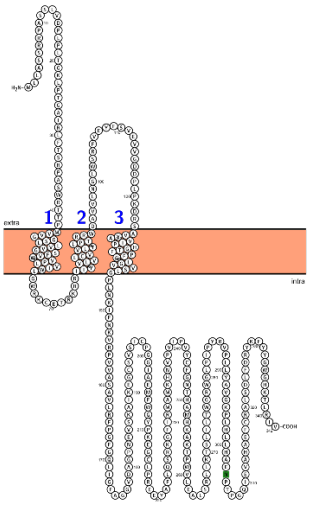

NoDGTT8
38.52 kDa

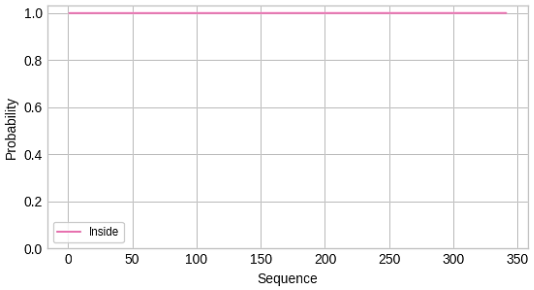

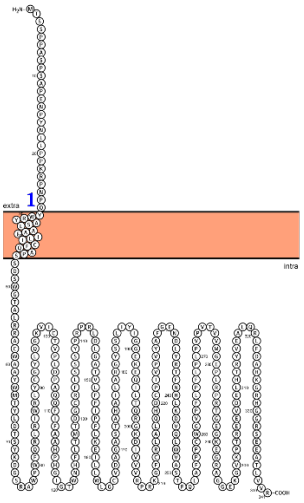

NoDGTT9
39.94 kDa

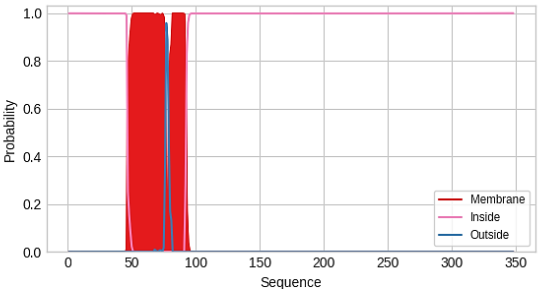

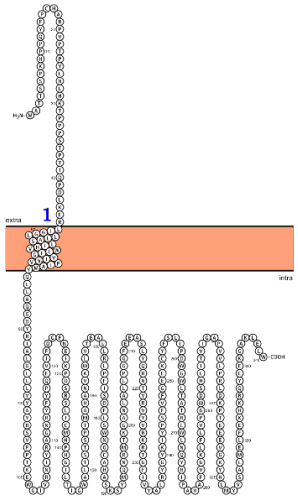

NoDGTT11
42.09 kDa

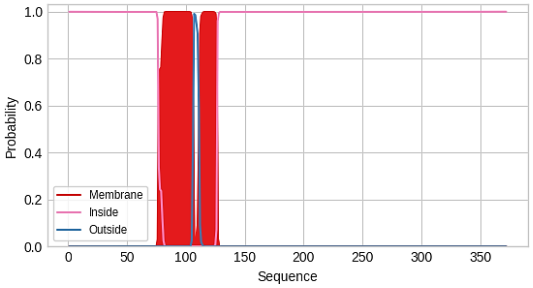

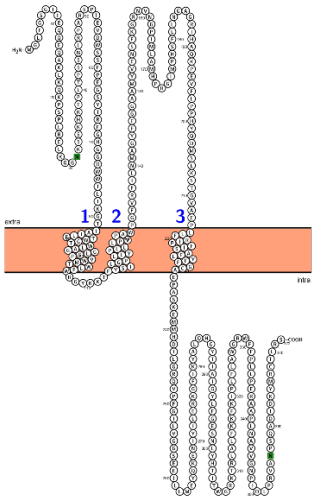

NoDGTT12
45.39 kDa

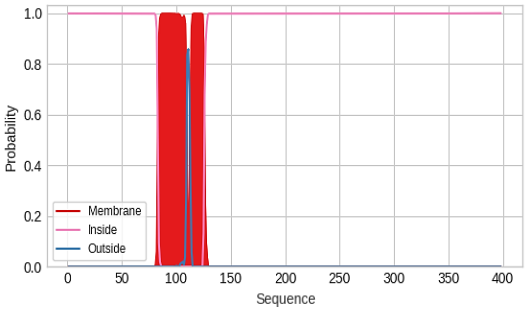

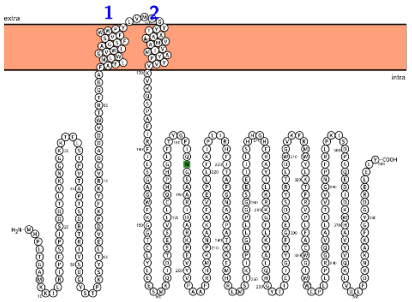

Predictions made using DeepTMHMM – 1.0 and Protter confirmed that all proteins are integral membrane enzymes characterized by multiple hydrophobic regions arranged as transmembrane helices. Considerable variation was observed in the number and distribution of these helices across the isoforms. The smallest proteins, NoDGTT7, NoDGTT8, and NoDGTT9, with molecular weights around 38–40 kDa, displayed one to three TMDs concentrated within central and C-terminal regions. Medium sized isoforms, such as NoDGTT1, NoDGTT3, NoDGTT5, NoDGTT6, NoDGTT11, and NoDGTT12, ranging between 42 and 53 kDa, exhibited one to four predicted helices, with hydrophobic clusters regularly interspersed with hydrophilic loops. The most distinct architecture was identified in NoDGTT4, which at 122.4 kDa showed the highest structural complexity, with up to twelve membrane-spanning segments predicted along its sequence. In all cases, the predicted topologies indicated a polytopic arrangement anchored in the ER membrane, with both N- and C-termini alternating between cytosolic and luminal orientations depending on the isoform.

To complement the transmembrane topology analyses, the probable subcellular localizations of all identified DGTT isoforms were predicted using the DeepLoc – 2.0 algorithm. This tool applies deep learning–based classification to assign localization probabilities across major eukaryotic compartments. The full probability distributions are summarized in Table 26.

Table 26. Subcellular localization of NoDGTTs predicted by DeepLoc – 2.0 software. Given values correspond to probabilities ranging from 0 to 1, where 0 indicates the lowest and 1 the highest likelihood. The most probable subcellular localizations are shown in green.

Localization probability / Protein name	Cytoplasm	Nucleus	Extracellular	Cell membrane	Mitochondrion	Plastid	Endoplasmic reticulum	Lysosome/ vacuole	Golgi apparatus	Peroxisome
NoDGTT1	0.2140	0.1978	0.0732	0.2267	0.1660	0.0679	0.7669	0.1624	0.2022	0.0072
NoDGTT2	0.1717	0.1317	0.0246	0.1784	0.1969	0.0723	0.7909	0.1682	0.2456	0.0190
NoDGTT3	0.2006	0.1456	0.0546	0.1582	0.2288	0.1105	0.8386	0.1581	0.3098	0.0046
NoDGTT4	0.2073	0.2223	0.0580	0.2739	0.1992	0.0818	0.6997	0.3464	0.3030	0.0343
NoDGTT5	0.1722	0.1316	0.0317	0.1587	0.1941	0.0461	0.8347	0.1775	0.2795	0.0065
NoDGTT6	0.2046	0.1745	0.0727	0.1785	0.2003	0.0757	0.7078	0.1102	0.1868	0.0077
NoDGTT7	0.1999	0.1587	0.0528	0.1369	0.2516	0.1937	0.7715	0.2409	0.2195	0.0294
NoDGTT8	0.1489	0.1476	0.0448	0.0836	0.1984	0.0733	0.8065	0.1508	0.2317	0.0147
NoDGTT9	0.1424	0.1593	0.0376	0.1505	0.2471	0.0572	0.8165	0.0666	0.1260	0.0275
NoDGTT11	0.2077	0.1417	0.0298	0.2159	0.3037	0.0901	0.8066	0.1278	0.2303	0.0119
NoDGTT12	0.2093	0.1127	0.0444	0.2421	0.2932	0.0572	0.8307	0.1290	0.2706	0.0057

Cellular localization was further assessed using DeepLoc – 2.0, which consistently assigned the highest probability of localization to the ER for all isoforms, ranging from 0.70 in NoDGTT4 to values exceeding 0.83 in NoDGTT3, NoDGTT5, NoDGTT8, NoDGTT9, NoDGTT11, and NoDGTT12. These strong predictions were uniform across the dataset, confirming the ER as the principal site of residence for the DGTT family. Nonetheless, below threshold probabilities were also detected for additional compartments. Several isoforms showed minor localization likelihoods to mitochondria, with values approaching 0.25 in NoDGTT7, NoDGTT9, NoDGTT11, and NoDGTT12. Plastid localization was also weakly represented, with probabilities reaching 0.19 in NoDGTT7. Golgi apparatus signals were more evident in some isoforms, particularly NoDGTT3, NoDGTT4, and NoDGTT5, with values between 0.27 and 0.31, suggesting potential alternative targeting or partial overlap with ER-Golgi trafficking. NoDGTT4 showed the most complex prediction pattern, combining a relatively lower ER score with elevated probabilities for Golgi (0.30) and vacuolar (0.35) localization, distinguishing it from the other isoforms. Collectively, the combined membrane topology and localization analyses characterized the DGTT proteins as a family of ER – associated enzymes, all bearing multiple predicted transmembrane segments but differing in size, architecture, and secondary localization probabilities.

4.2 Heterologous expression of *Nannochloropsis oceanica* CCMP1779 *DGTT* genes in *Saccharomyces cerevisiae* H1246

In order to functionally characterize *DGTT*s encoded by *N. oceanica* CCMP1779 genome, in the first step their heterologous expression in the yeast system was performed. All putative membrane-bound DGTTs

were transformed into the TAG deficient yeast strain H1246 to test their ability to synthesize TAG in heterologous yeast system (see point 2.1.2 for yeast characteristics). All the PCR primers used in this study for amplification of full-length coding sequences were designed using Oligo Evaluator™ and are listed under point 2.7.

4.2.1 Acquisition of *Nannochloropsis oceanica DGTT* genes for H1246 yeast transformation

To obtain templates for amplification of the DGTTs full-length sequences, *N. oceanica* CCMP1779 cultures were grown under sterile conditions in three different variants (Figure 13):

- standard conditions (N+) – medium containing a nitrogen source, under optimal light
- nitrogen deprivation (N−) – medium lacking a nitrogen source, under optimal light
- high light (HL) – medium containing a nitrogen source and exposed to increased light intensity

The culture variants were selected based on earlier studies analyzing *NoDGTT* expression profiles under different stress conditions (partially published data, Zienkiewicz *et al*., 2017 and 2020). To capture the full spectrum of stress-responsive changes in *NoDGTT* expression, it was necessary to include all three treatments (N+, N−, and HL). Detailed culture conditions are described in Section 3.2.1.

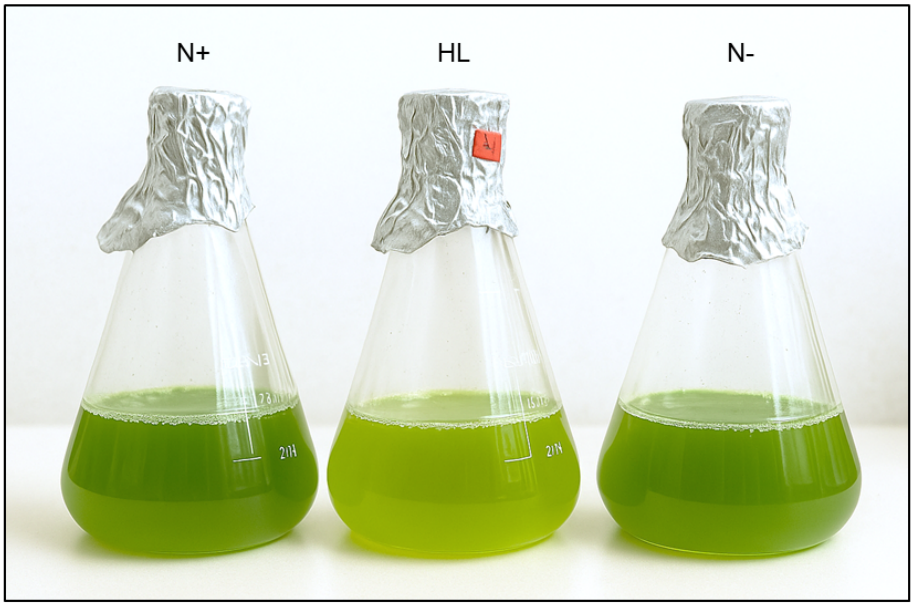

Figure 13. *N. oceanica* CCMP1779 cultures grown under different conditions. (N+) standard conditions, with a nitrogen source and optimal light. (HL) high light, with a nitrogen source and increased light intensity. (N−) nitrogen deprivation, medium lacking a nitrogen source, under optimal light.

Total RNA was extracted from the abovementioned cultures and transcribed into cDNA (see point 3.1.2), followed by evaluation of the quality of the cDNA. One gene was selected to serve as reference gene – elongation factor (*EF*) – due to its consistently high constitutive expression in algal cells (Zienkiewicz *et al*., 2017; Du *et al*., 2023). As shown in Figure 14, short fragment of ~110 bp length was amplified using primers for *NoEF* (see point 3.1.2) on the cDNA matrix obtained for N+ (Figure 14 A) and N- (Figure 14 B), verifying that in both cases the quality of the RNA isolated from the algal cells met the required standards.

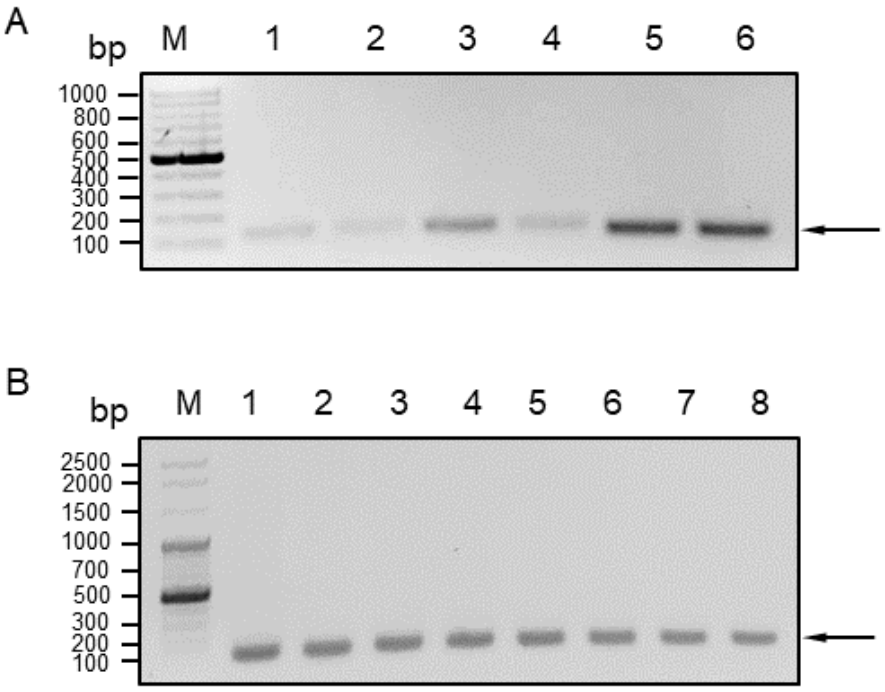

Figure 14. Expression of *NoEF* reference gene in *N. oceanic*a CCMP1779 under N- (A) and HL (B) conditions. Total cDNA was used as template for PCR amplification. (A) Lane M: DNA ladder for size estimation. Lanes 1–6: amplification of the *NoEF* gene. (B) Lane M: DNA ladder for size estimation. Lanes 1–8: amplification of the *NoEF* gene. The arrow indicates the correct PCR products (~110 bp). PCR products were resolved on a 1% agarose gel in 1× TAE buffer.

The full-length sequence of *NoDGTT5* was amplified first using primers listed in Table 1 and served as a reference, given that it has been confirmed to have a significant impact on lipid synthesis in *N. oceanica* CCMP1779 (Zienkiewicz *et al.*, 2017). After gradient PCR, the corresponding band of 1092 bp was observed only at 60 °C (Figure 15).

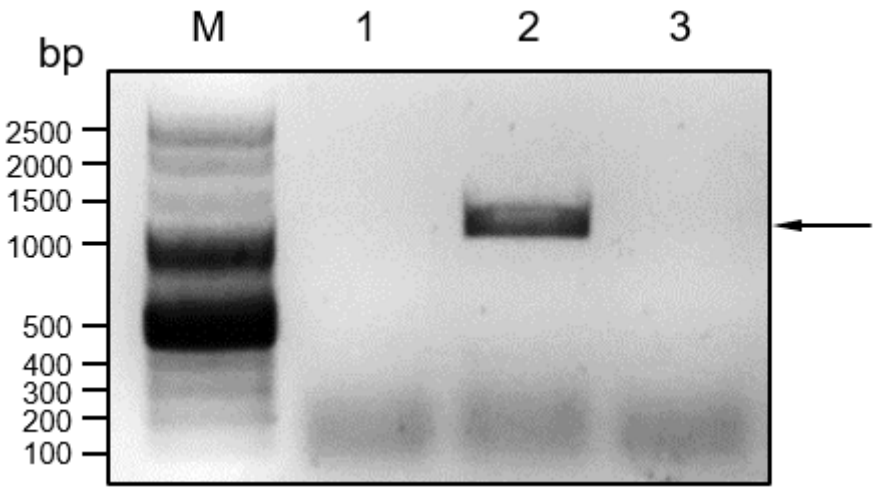

Figure 15. Amplification of full-length sequence of *NoDGTT5* on the total cDNA isolated from *N. oceanica* CCMP1779 grown under N- conditions. M - DNA ladder. Lanes 1-3 - Gradient PCR with specific primers at 58 °C (line 1), 60 °C (line 2) and 62 °C (line 3). The arrow indicates correct *NoDGTT5*-corresponding PCR product of 1092 bp. Agarose gel electrophoresis in 1% agarose gel in 1x TAE buffer.

The obtained PCR product was then cloned into a high copy *pJET1.2*/blunt vector (as described under point 3.1.3) to obtain sufficient concentration of desired gene for further cloning into pYES2.1 vector. Subcloning Efficiency™ DH5α Competent Cells of *E. coli* were then transformed with the *NoDGTT5*-containing construct *via* heat shock transformation, as described in point 3.1.3 The efficiency of cloning was estimated by a colony PCR (Figure 16).

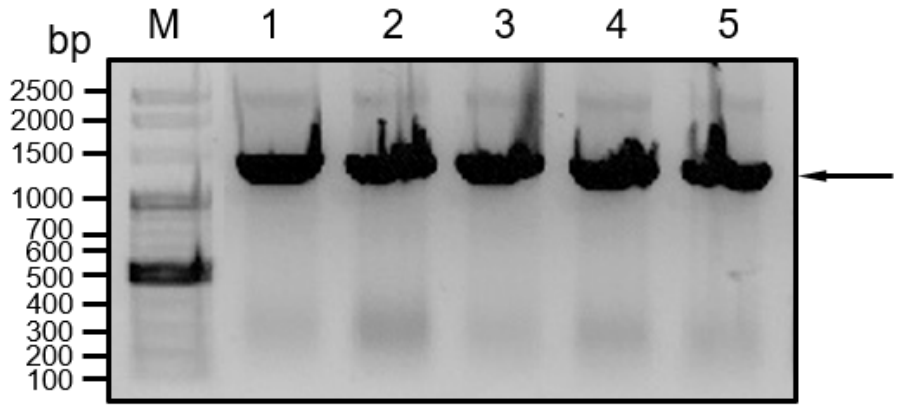

Figure 16. *NoDGTT5* colony PCR, pJET1.2/blunt vector. M - DNA ladder. (1-5) pJET1.2-*NoDGTT5* constructs. The arrow indicates the correct PCR product of size 1092 bp. Agarose gel electrophoresis in 1% agarose gel in 1x TAE buffer.

Following verification of the correct colony PCR products, the *pJET1.2-NoDGTT5* construct was extracted from the selected colonies of *E. coli* transformants and resulting DNA samples were sent for sequencing. Sequence validated DNA samples were subsequently cloned into the pYES2.1 vector and One Shot™ TOP10 Chemically Competent *E. coli* were transformed with this construct, as described under the point 3.1.4. The selected TOP10 *E. coli* colonies were further screened for the presence of pYES2.1-*NoDGTT5* construct by the colony PCR, using the primers listed in the Table 6 (Figure 17).

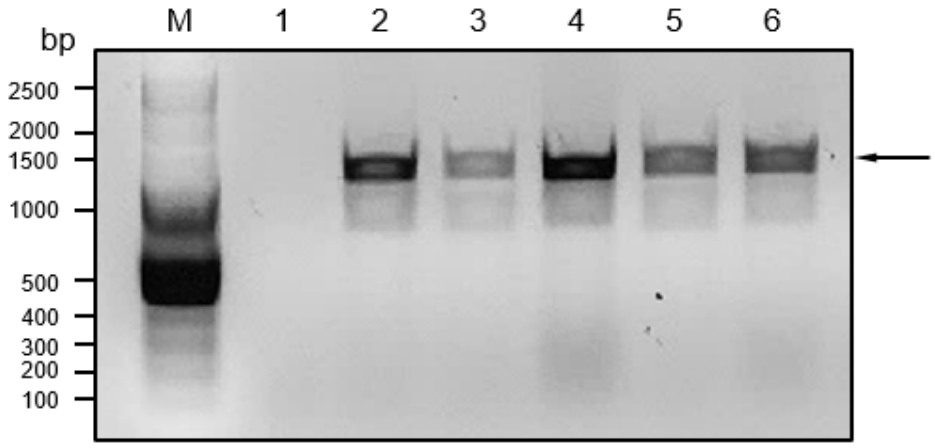

Figure 17. *NoDGTT5* colony PCR, pYES2.1 vector. M - DNA ladder. (1-8) p YES2.1-*NoDGTT5* constructs. The arrow indicates the correct PCR product of size 1092 bp. Agarose gel electrophoresis in 1% agarose gel.

Analogous steps were carried out for heterologous expression of NoDGTT7, NoDGTT8, NoDGTT11 and NoDGTT12-encoding genes in H1246 strain and are summarized in Figures 18 to 21. As accurate DNA sequences were not successfully obtained for *NoDGTT9*, and *NoDGTT10* following cloning into the pJET1.2/blunt vector, these genes were excluded from subsequent experimental analyses.

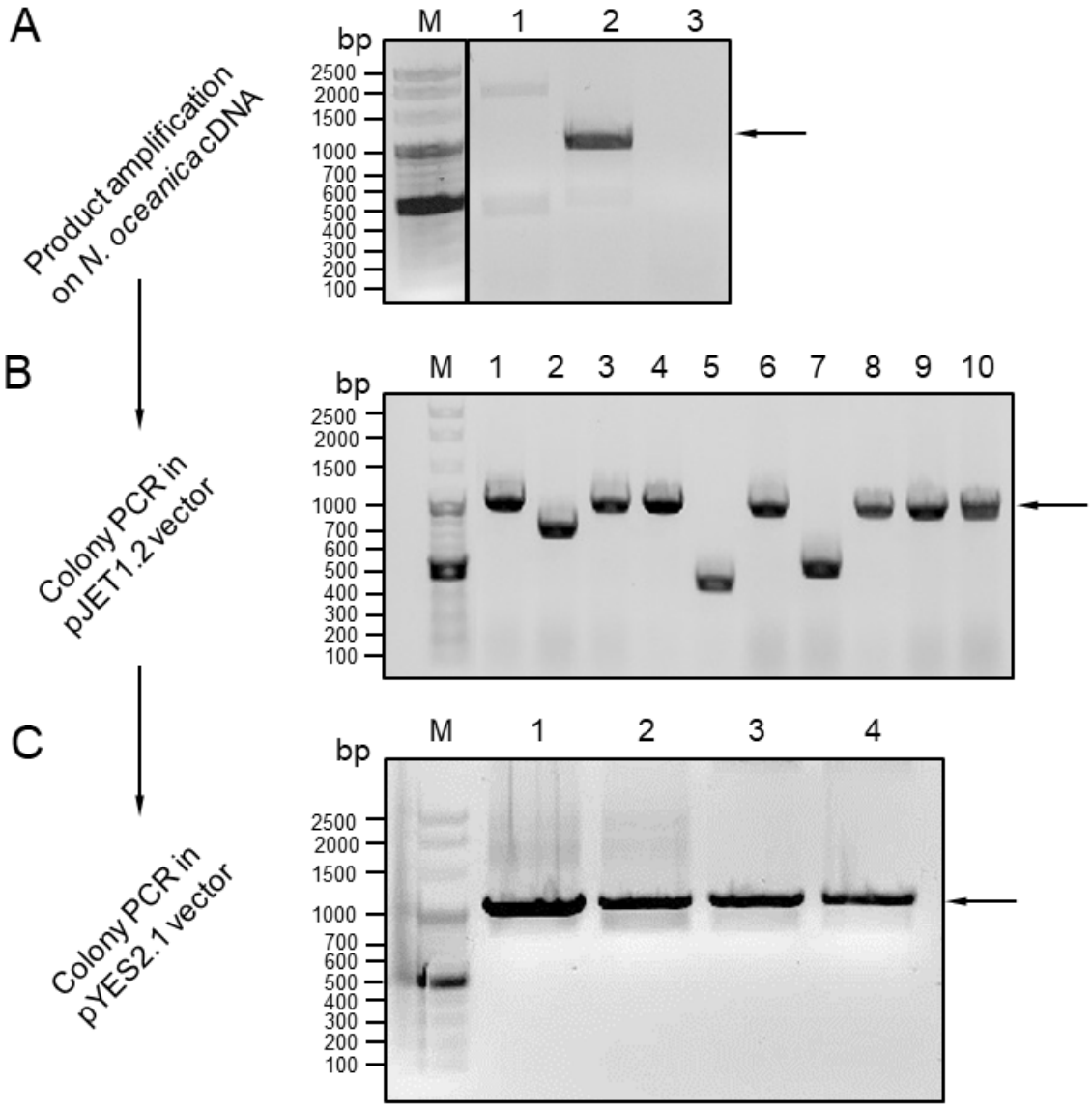

Figure 18. Steps of cloning *NoDGTT7* into pYES2.1 vector. (A) *NoDGTT7* amplified on total cDNA isolated from *N. oceanica* CCMP1779 grown under N- conditions. (A) M - DNA ladder. Lines 1-3 - gradient PCR. The arrow indicates the correct PCR product of size 1029 bp. Agarose gel electrophoresis in 1% agarose gel in 1x TAE buffer. (B) Colony PCR on *E. coli* DH5 transformed with pJET1.2/blunt vector. M - DNA ladder. Lines 1-10 - amplification of pJET1.2-*NoDGTT7* constructs. The arrow indicates the correct PCR product of size 1029 bp. Agarose gel electrophoresis in 1% agarose gel in 1x TAE buffer. (C) Colony PCR of *E. coli* One Shot™TOP10 transformed with pYES2.1+*NoDGTT7* construct. M - DNA ladder. Lines 1-4 - amplification of YES2.1- constructs. The arrow indicates the correct PCR product of size 1029 bp. Agarose gel electrophoresis in 1% agarose gel in 1x TAE buffer.

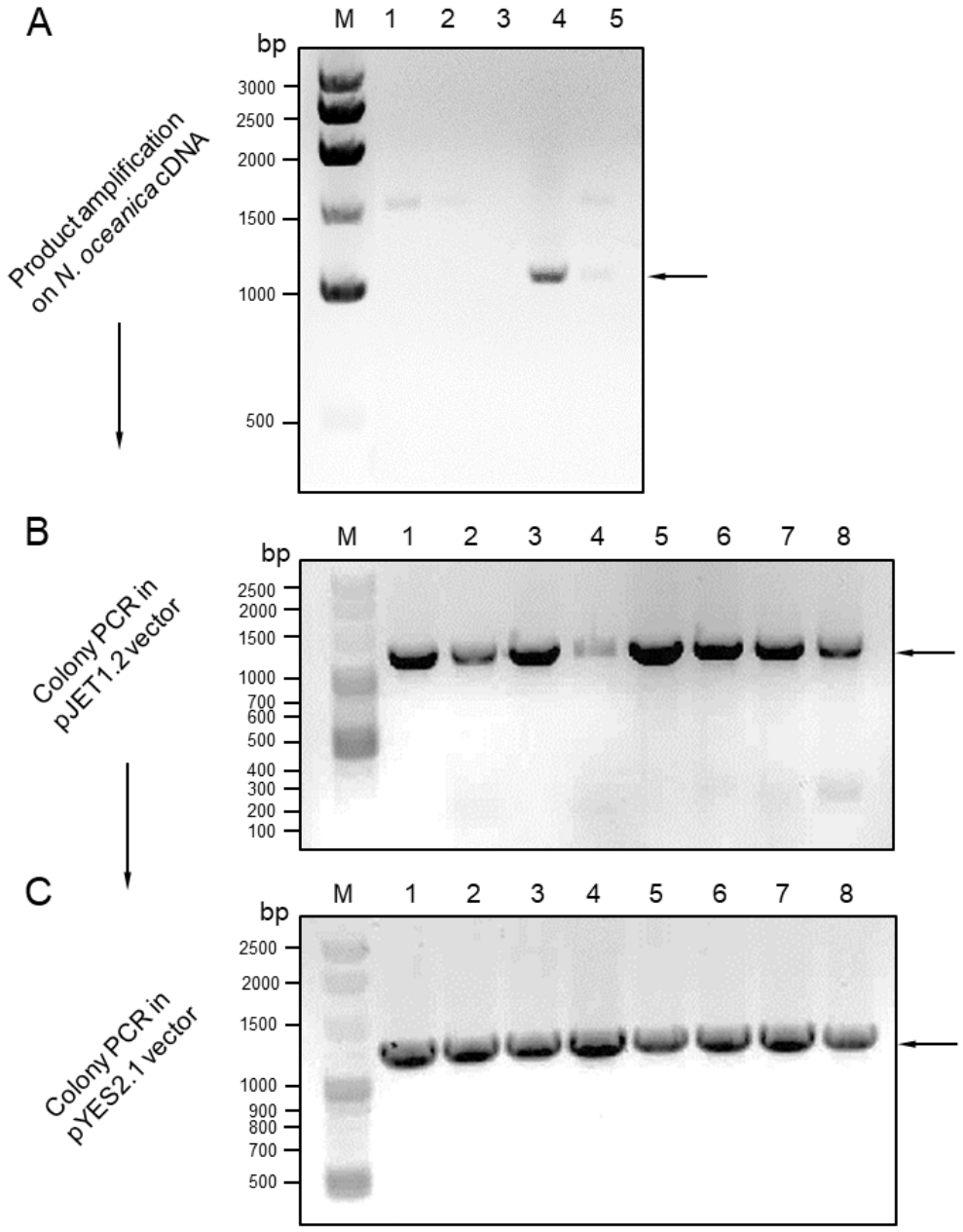

Figure 19. Steps of cloning *NoDGTT8* into pYES2.1 vector. (A) *NoDGTT8* amplified on total cDNA isolated from *N. oceanica* CCMP1779 grown under N- conditions. (A) M - DNA ladder. Lines 1-5 - gradient PCR. The arrow indicates the correct PCR product of size 1140 bp. Agarose gel electrophoresis in 1% agarose gel in 1x TAE buffer. (B) Colony PCR on *E. coli* DH5 transformed with pJET1.2/blunt vector. M - DNA ladder. Lines 1-8 - amplification of pJET1.2-*NoDGTT8* constructs. The arrow indicates the correct PCR product of size 1140 bp. Agarose gel electrophoresis in 1% agarose gel in 1x TAE buffer. (C) Colony PCR of *E. coli* One Shot™TOP10 transformed with pYES2.1+*NoDGTT8* construct. M - DNA ladder. Lines 1-8 - amplification of YES2.1-*NoDGTT8* constructs. The arrow indicates the correct PCR product of size 1140 bp. Agarose gel electrophoresis in 1% agarose gel in 1x TAE buffer.

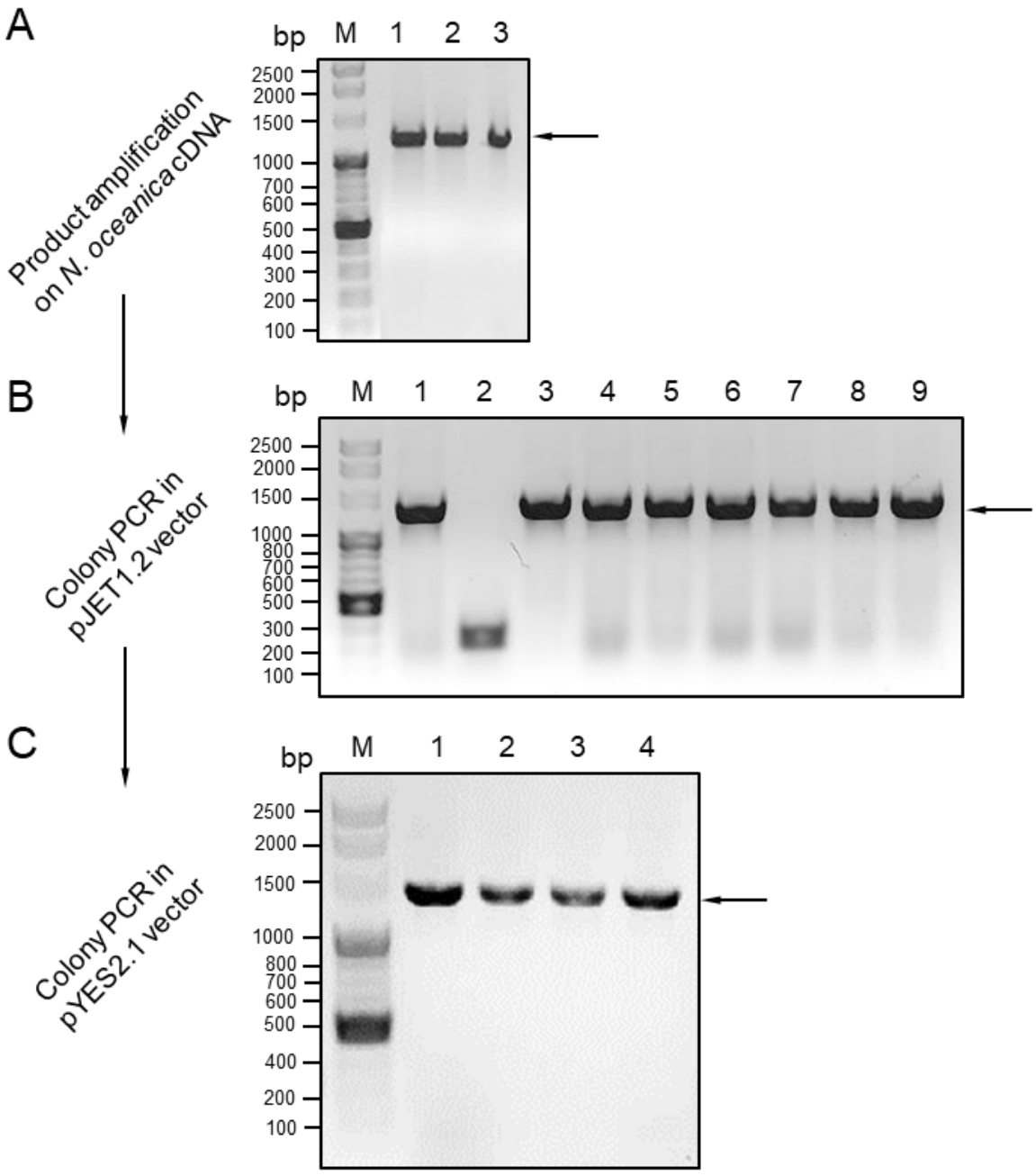

Figure 20. Steps of cloning *NoDGTT11* into pYES2.1 vector. (A) *NoDGTT11* amplified on total cDNA isolated from *N. oceanica* CCMP1779 grown under N- conditions. (A) M - DNA ladder. Lines 1-3 - PCR reaction. The arrow indicates the correct PCR product of size 1185 bp. Agarose gel electrophoresis in 1% agarose gel in 1x TAE buffer. (B) Colony PCR on *E. coli* DH5 transformed with pJET1.2/blunt vector. M - DNA ladder. Lines 1-9 - amplification of pJET1.2-*NoDGTT11* constructs. The arrow indicates the correct PCR product of size of 1185 bp. Agarose gel electrophoresis in 1% agarose gel in 1x TAE buffer. (C) Colony PCR of *E. coli* One Shot™TOP10 transformed with pYES2.1+*NoDGTT11* construct. M - DNA ladder. Lines 1-4 - amplification of YES2.1-NoDGTT11 constructs. The arrow indicates the correct PCR product of size 1185 bp. Agarose gel electrophoresis in 1% agarose gel in 1x TAE buffer.

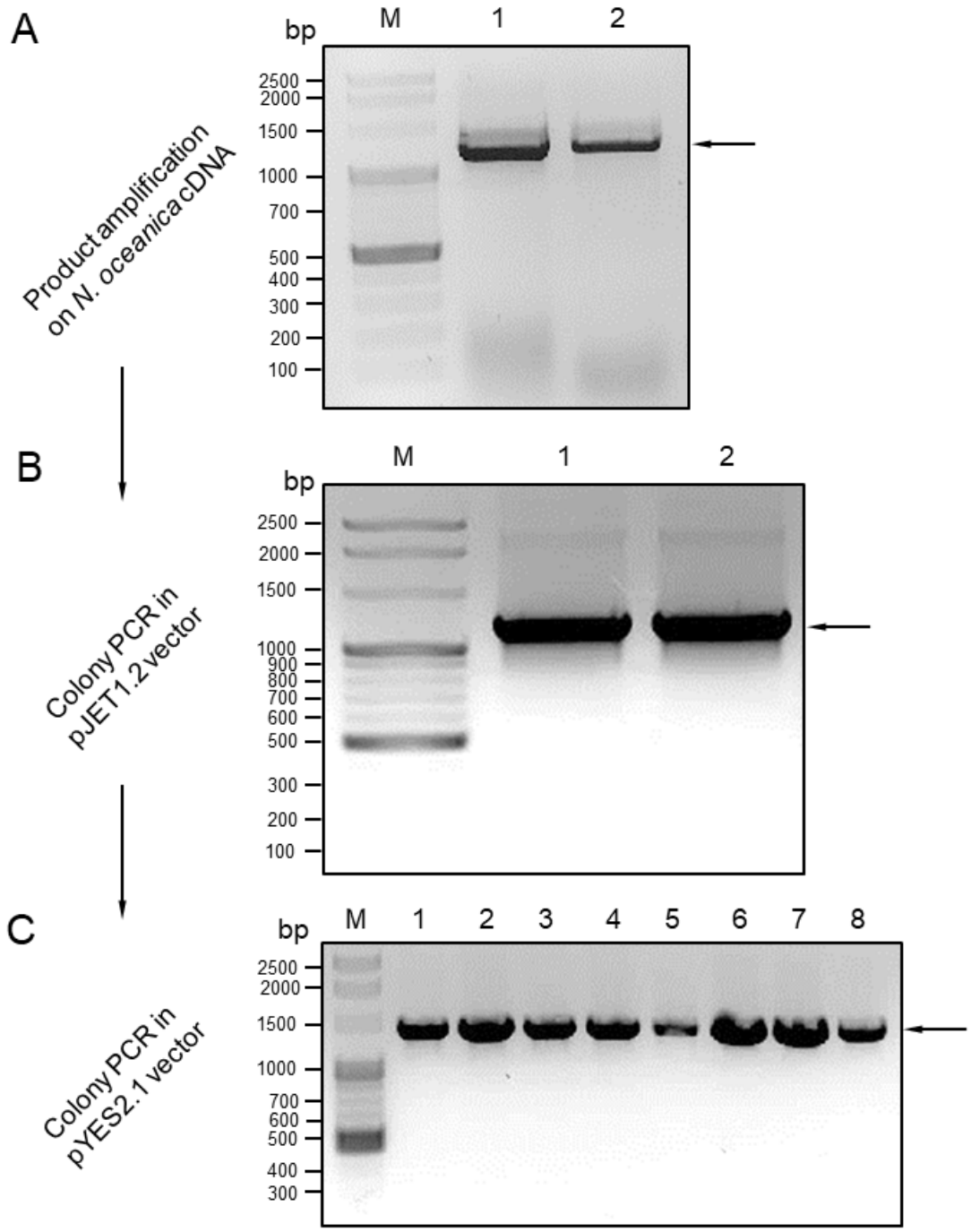

Figure 21. Steps of cloning *NoDGTT12* into pYES2.1 vector. (A) *NoDGTT12* amplified on total cDNA isolated from *N. oceanica* CCMP1779 grown under HL conditions. (A) M - DNA ladder. Lines 1-2 - PCR reaction. The arrow indicates the correct PCR product of size 1197 bp. Agarose gel electrophoresis in 1% agarose gel in 1x TAE buffer. (B) Colony PCR on *E. coli* DH5 transformed with pJET1.2/blunt vector. M - DNA ladder. Lines 1-2 - amplification of pJET1.2-*NoDGTT12* constructs. The arrow indicates the correct PCR product of size of 1197 bp. Agarose gel electrophoresis in 1% agarose gel in 1x TAE buffer. (C) Colony PCR of *E. coli* One Shot™TOP10 transformed with pYES2.1+*NoDGTT12* construct. M - DNA ladder. Lines 1-8 - amplification of YES2.1-*NoDGTT12* constructs. The arrow indicates the correct PCR product of size 1197 bp. Agarose gel electrophoresis in 1% agarose gel in 1x TAE buffer.

The *S. cerevisiae* strain H1246, used for the heterologous expression of algal transgenes, were initially cultured under sterile conditions on solid YPD medium as described under point 3.1.1. Subsequently, liquid YPD medium was inoculated with the H1246 mutant strains in separate culture tubes, following the procedure described in section 3.1.5. The pYES2.1 constructs carrying target full-length sequences of *NoDGTT*s described above, were introduced into the H1246 yeast mutant using the "*lazy bones*" transformation method, as detailed under point 3.1.5.

Transgene expression was induced by activating the GAL1 promoter, which is galactose-inducible, in accordance with the protocol outlined in section 3.1.6. Positively transformed yeast cultures were then harvested and processed for microscopic analysis of restored TAG synthesis, following the procedures described under point 3.1.7.

4.2.2. Microscopic analysis of TAG accumulation in transgenic H1246 yeast cells

As the initial stage of screening the obtained H1246 transformants, TAG accumulation was evaluated by staining with the fluorescent dye BODIPY™ 505/515 followed by visualization using a CLSM, as detailed in section 3.1.7 (Figures 23 – 27). The H1246 strain transformed with empty pYES2.1 vector served as a negative control and displayed only minimal neutral lipid staining, with no detectable LD formation (Figure 22). As a positive control for the heterologous expression system, H1246 expressing *NoDGTT5* was used, based on previous findings in *N. oceanica* CCMP1779 (Zienkiewicz *et al.*, 2017). As expected, this line exhibited a strong BODIPY™ 505/515 fluorescence signal, characterized by numerous, well-defined LDs (Figure 23, arrowheads). In contrast, heterologous expression of *NoDGTT7*, *NoDGTT8* and *NoDGTT11* in H1246 resulted in noticeably weaker neutral lipid accumulation, reflected by lower fluorescence intensity and relatively few LDs (Figures 23 – 26). Strikingly, the H1246 strain expressing *NoDGTT12* showed by far the strongest response among all analysed lines. This transformant displayed the most intense BODIPY™ 505/515 fluorescence signal, clearly exceeding both the positive control and all other NoDGTT-expressing lines. The signal was accompanied by abundant, large, and highly fluorescent LDs, highlighting a pronounced stimulation of TAG biosynthesis mediated specifically by NoDGTT12 (Figure 27). Because of this exceptionally strong phenotype, The *NoDGTT12*-expressing lines were selected for further in-depth characterization.

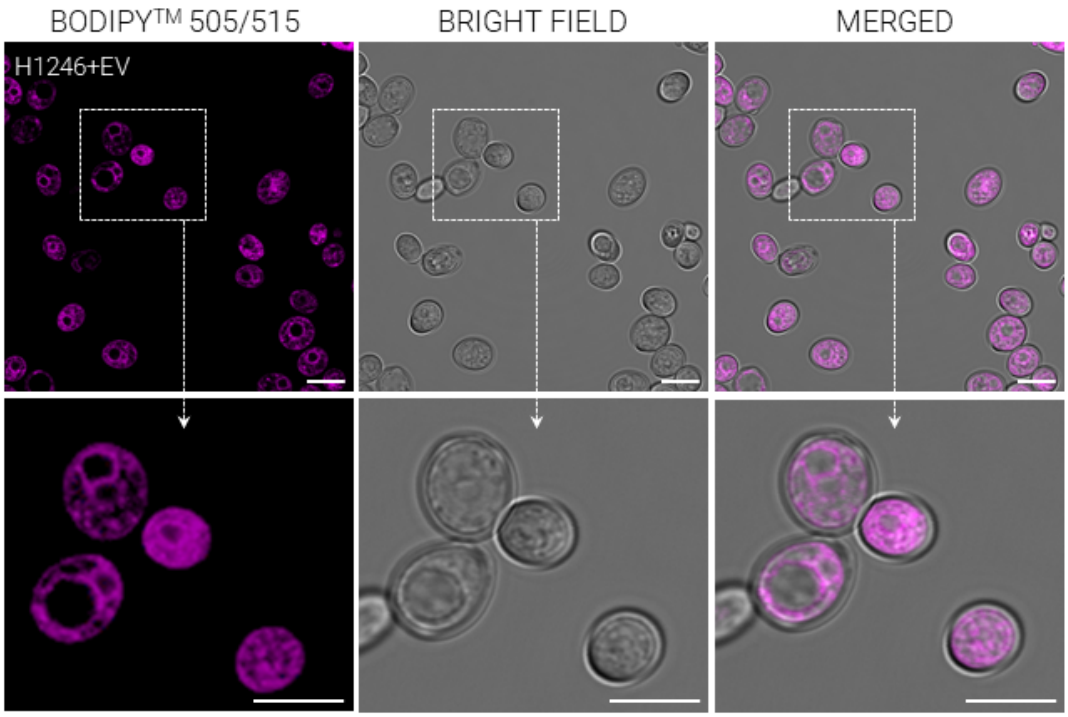

Figure 22. BODIPY™ 505/515 staining of neutral lipids (magenta) in H1246 yeast strain transformed with pYES2.1+EV construct. The area marked with dashed line indicates zoomed area showed in the lower panel. Bars = 5 µm.

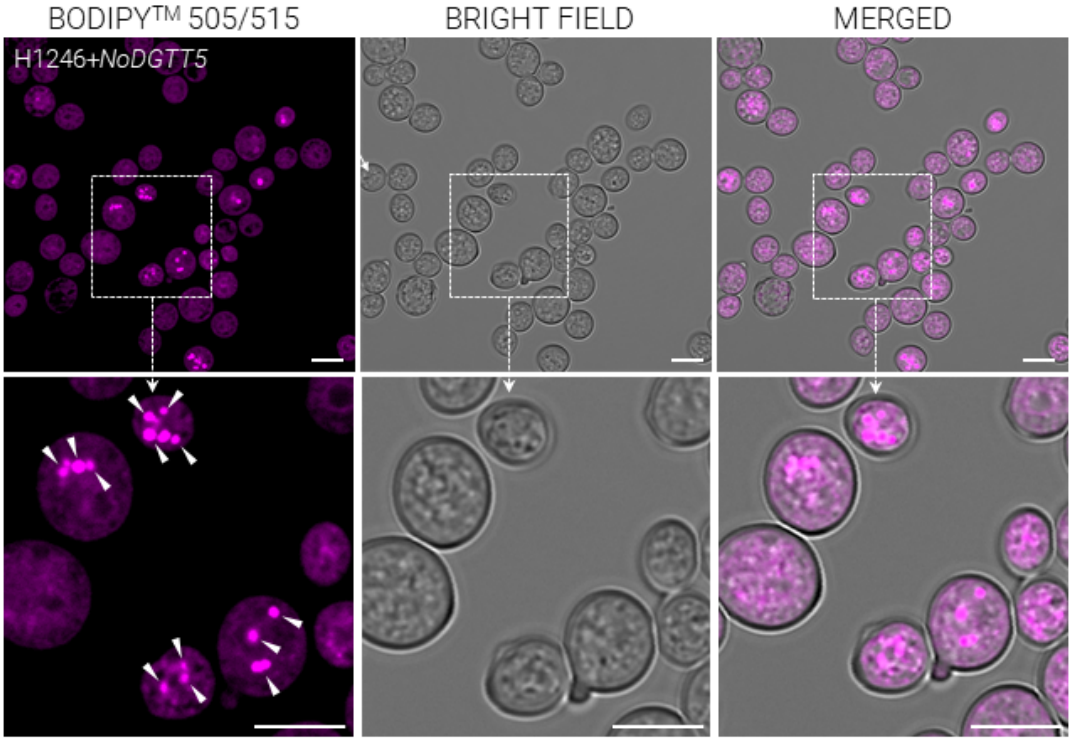

Figure 23. BODIPY™ 505/515 staining of neutral lipids (magenta) in H1246 yeast strain transformed with pYES2.1+*NoDGTT5* construct. Arrowheads indicate lipid droplets (LDs). The area marked with dashed line indicates zoomed area showed in the lower panel. Bars = 5 µm.

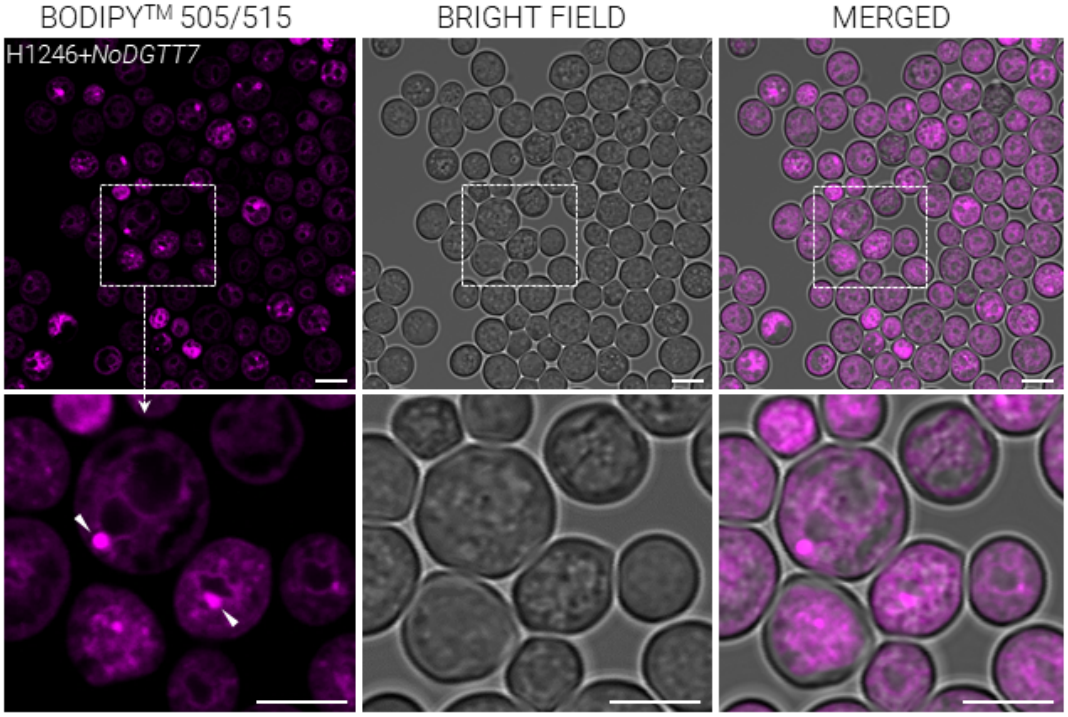

Figure 24. BODIPY™ 505/515 staining of neutral lipids (magenta) in H1246 yeast strain transformed with pYES2.1+*NoDGTT7* construct Arrowheads indicate lipid droplets (LDs). The area marked with dashed line indicates zoomed area showed in the lower panel. Bars = 5 µm.

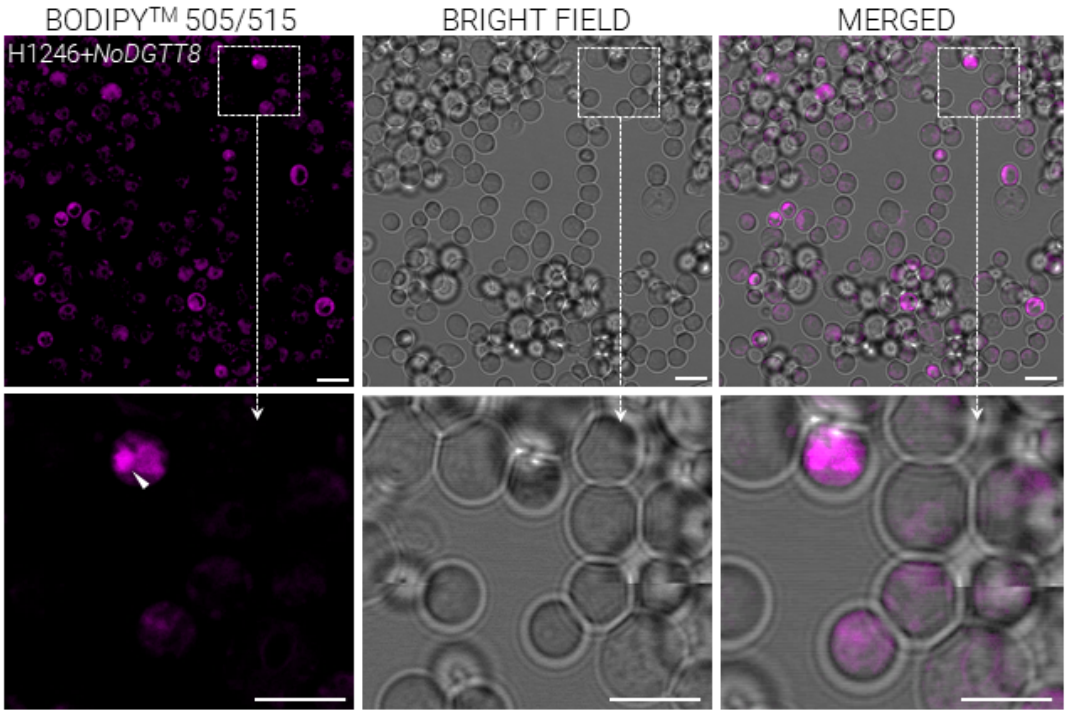

Figure 25. BODIPY™ 505/515 staining of neutral lipids (magenta) in H1246 yeast strain transformed with pYES2.1+*NoDGTT8* construct. Arrowheads indicate lipid droplets (LDs). The area marked with dashed line indicates zoomed area showed in the lower panel. Bars = 5 µm.

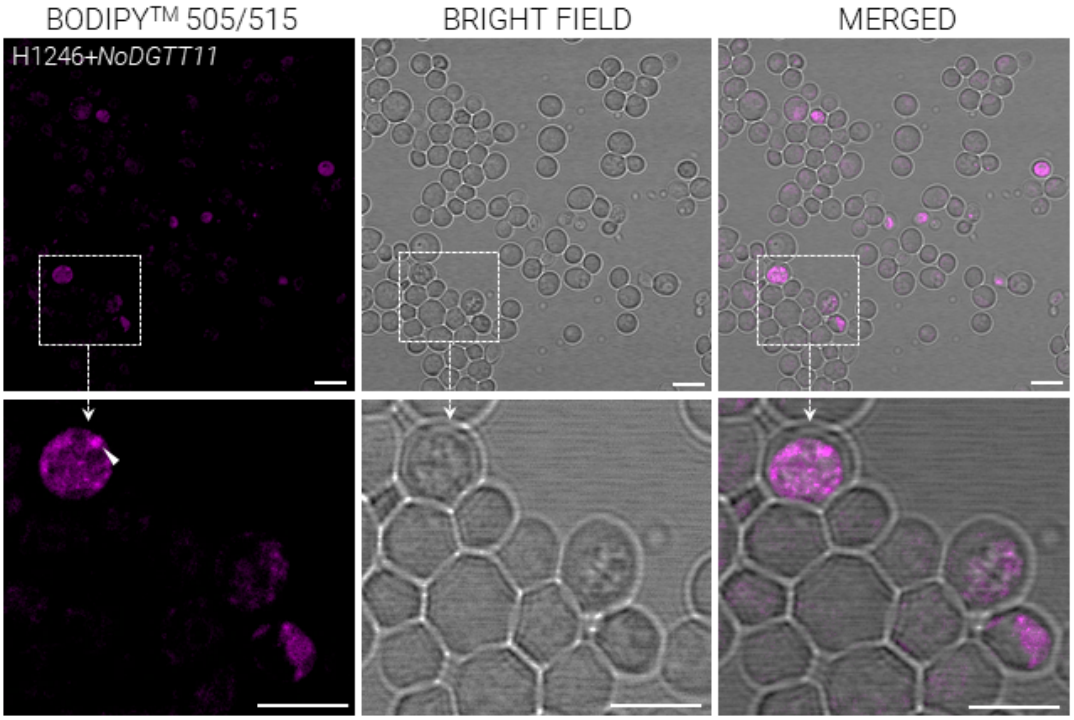

Figure 26. BODIPY™ 505/515 staining of neutral lipids (magenta) in H1246 yeast strain transformed with pYES2.1+*NoDGTT11* construct. Arrowheads indicate lipid droplets (LDs). The area marked with dashed line indicates zoomed area showed in the lower panel. Bars = 5 µm.

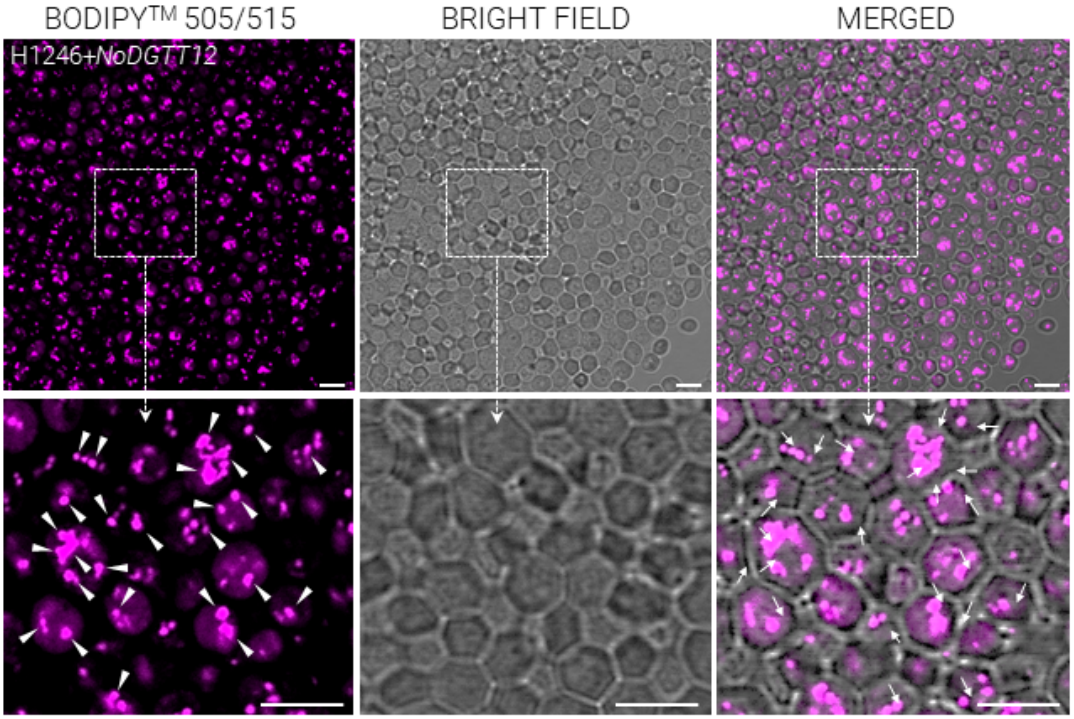

Figure 27. BODIPY™ 505/515 staining of neutral lipids (magenta) in H1246 yeast strain transformed with pYES2.1+*NoDGTT12* construct. Arrowheads indicate lipid droplets (LDs). The area marked with dashed line indicates zoomed area showed in the lower panel. Bars = 5 µm.

4.2.3. Characterization of lipid content and FA composition in H1246 yeast mutant transformed with *NoDGTT12*

Based on the initial screening, the best-performing H1246 transformants expressing pYES2.1-*NoDGTT12* construct were selected for subsequent quantitative and qualitative analyses using GC-FID. Prior to these analyses, the stability and expression of the NoDGTT12-His-tagged fusion protein were verified by western blotting (as described in Section 3.1.9.2) and the corresponding yeast lines were examined for LD formation (Figure 28).

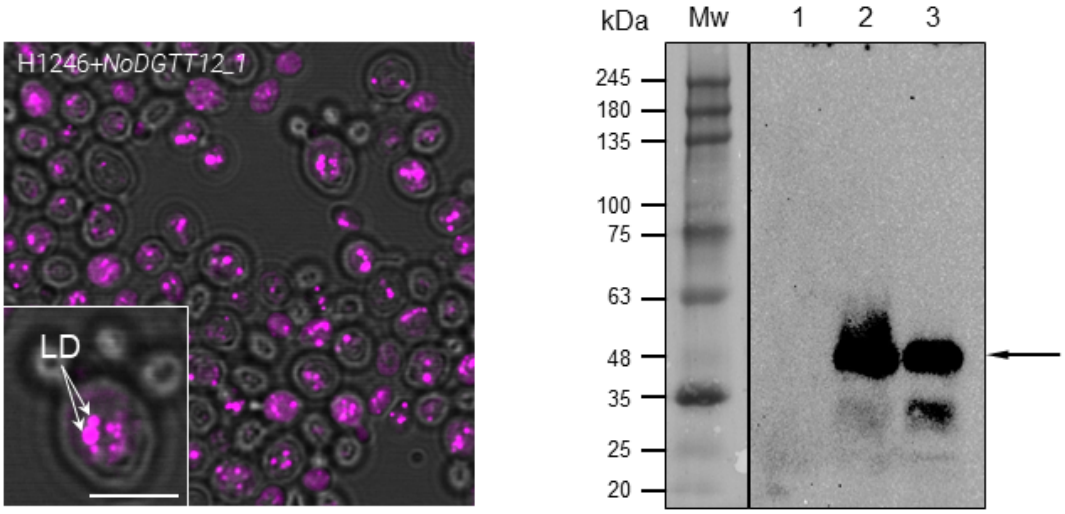

Figure 28. (A) Representative images of CLSM analysis of LD formation (magenta) in NoDGTT12 line no 1, and (B) western blotting analysis of pYES-NoDGTT12-His-tagged protein in this line. Mw - protein ladder. Line 1 - Protein expression without *NoDGTT12* transgene induction, line 2 - Protein expression after 6 hours of *NoDGTT12* transgene induction, and line 3 - Protein expression after 12 hours of *NoDGTT12* transgene induction. The arrow indicates protein product of size ~ 47 kDa.

Expression of the pYES-NoDGTT12-His-tagged protein in *S. cerevisiae* was verified by immunoblotting following SDS-PAGE separation and transfer to a PVDF membrane. The NoDGTT12 protein was fused with His affinity tag of approximately 2 kDa, allowing specific detection using anti-His antibodies in western blotting, as described in Section 3.1.9.2 (Figure 7). Given that the predicted molecular weight od NoDGTT12 is ~45 kDa (see Section 4.1), the expected size of the NDGTT12-His tagged fusion protein was ~47 kDa. A band corresponding to this molecular weight was detected in the analysed transformants after both 6 and 12 hours of induction, achieved by transferring H1246 cultures from glucose-containing medium to medium supplemented with galactose and raffinose (Figure 28 B).

To characterize lipid content and FA composition of TAGs in yeast transformed with pYES2.1-*NoDGTT12*-His-tag, lipid extraction and GC analysis was performed on five independent lines of H1246 expressing *NoDGTT12* (Figure 29), as described in Section 3.1.8. Thin-layer chromatography (TLC) analysis confirmed the absence of TAGs in mutant yeast transformed with the empty pYES2.1 vector (H1246+EV), whereas TAGs were detected in H1246 lines expressing *NoDGTT12* (Figure 29 A). Quantification showed that *NoDGTT12* expression resulted in TAG levels exceeding 30% of the total lipid fraction (Figure 29 B).

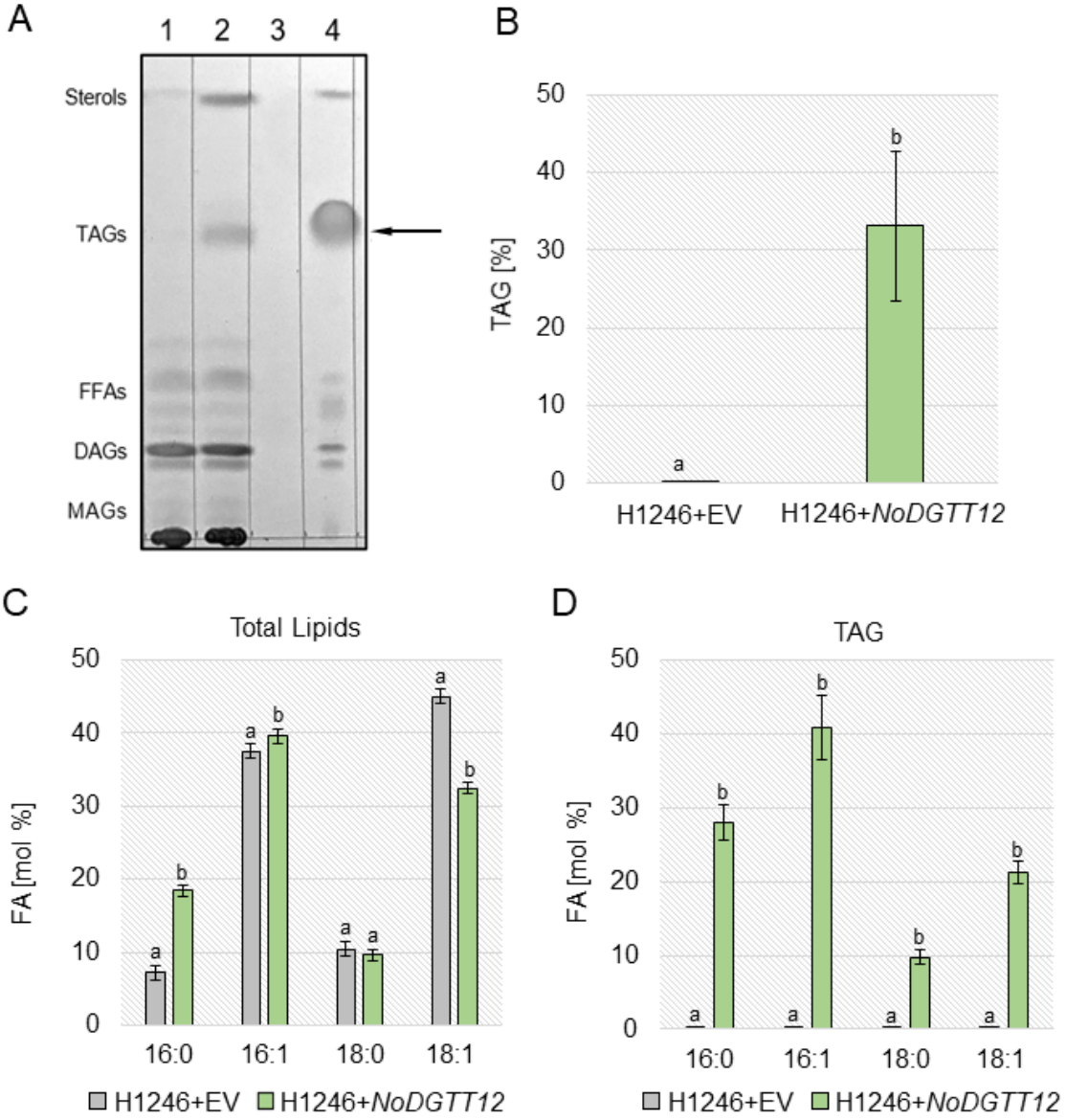

Figure 29. Lipid content and FA composition of total lipids and TAGs in H1246 yeast transformed with *NoDGTT12*. (A) Representative TLC analysis of lipid extracts from H1246 yeast mutant lines. (1) H1246 yeast transformed with empty pYES2.1 vector. (2) H1246 yeast transformed with *NoDGTT12*. (3) Empty lane. (4) Olive oil used as a TAG standard. MAGs – monoacylglycerols, DAGs – diacylglycerols, FFAs – free fatty acids, TAGs – triacylglycerols. Black arrow indicates TAGs corresponding bands. (B) Quantification of TAG in total lipid fraction in H1246 lines expressing *NoDGTT12* used for GC analysis. (C and D) Comparison of FA profiles from total lipids (C) and TAGs (D) extracted from H1246 transformed with empty vector (H1246+EV) and H1246 expressing No*DGTT12* (H1246+DGTT12). FAs are reported by number of carbons : number of double bonds. Values represent the mean of ± SD of five biological replicates (n=5). Statistical analysis was performed by one-way ANOVA with Tukey's post hoc test. Different letters indicate significant differences.

FA profiles of total lipids and TAG fractions were analysed to assess the effect of *NoDGTT12* expression on lipid composition in transgenic *S. cerevisiae* H1246. In the total lipid fraction, both H1246 and five H1246 lines expressing *NoDGTT12* contained primarily C16 and C18 FAs, with 16:0, 16:1, 18:0, and 18:1 as the dominant components. Expression of *NoDGTT12* did not markedly alter the overall FA composition of total lipid fraction compared to the empty vector control. In contrast, analysis of the TAG fraction revealed changes associated with expression of *NoDGTT12*. The TAGs accumulated in response in

NoDGTT12 expression were enriched in monounsaturated FAs, particularly 18:1, while showing a relative decrease in saturated species such as 16:0 and 18:0. Statistical analysis confirmed significant differences ($p < 0.05$) in the proportions of 18:1 and 16:0 between control and transgenic strains (Figure 29, B and C).

4.3 *In vitro* NoDGTT12 enzyme activity

Bioinformatic analysis predicted that NoDGTT enzymes localize to the ER (see Section 4.1). Therefore, for the enzymatic activity assays of NoDGTT12, the microsomal fraction, predominantly derived from the ER, was isolated from transgenic *S. cerevisiae* H1246 expressing *NoDGTT12*, previously used for GC-FID analysis. All steps in the preparation of the microsomal fraction were performed on ice or at 4 °C to maintain protein integrity and activity, as described in Section 3.1.9.1.

The substrate specificity assays were performed in the frame of collaboration with the Centre for Modern Interdisciplinary Technologies of Nicolaus Copernicus University in Toruń (Poland) and the laboratory of dr Ida Lager (Swedish University of Agricultural Sciences, Malmö, Sweden). Detailed experimental procedures are presented in Section 3.1.10. Preliminary tests conducted in the host laboratory indicated that NoDGTT12 exhibits a higher catalytic efficiency toward 18:1-DAG than 22:1-DAG as the acyl acceptor (Figure 30).

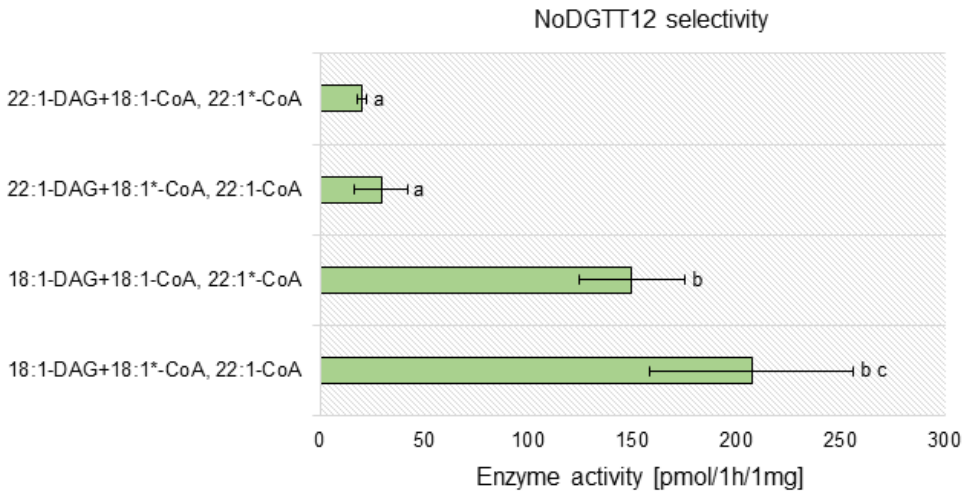

Figure 30. Enzyme selectivity analysis of NoDGTT12 in the microsomal fraction of H1246 yeast. Selectivity assays were performed using substrate mixtures containing either 22:1-DAG or 18:1-DAG in combination with 18:1-CoA and 22:1-CoA. Asterisks denote isotopically labeled substrates. Enzyme activity was expressed as pmol h^{-1} μg^{-1}. Data represent mean ± SD (n = 3). Statistical analysis was performed using one-way ANOVA followed by Tukey's post hoc test; different letters indicate significant differences.

Further experiments revealed that NoDGTT12 possesses measurable activity toward a wide range of acyl-CoA substrates, including 16:0-CoA, 16:1-CoA, 18:0-CoA, 18:1-CoA, 18:2-CoA, 18:3-CoA, 20:0-CoA, 20:4-CoA, and 22:1-CoA (Figure 31).

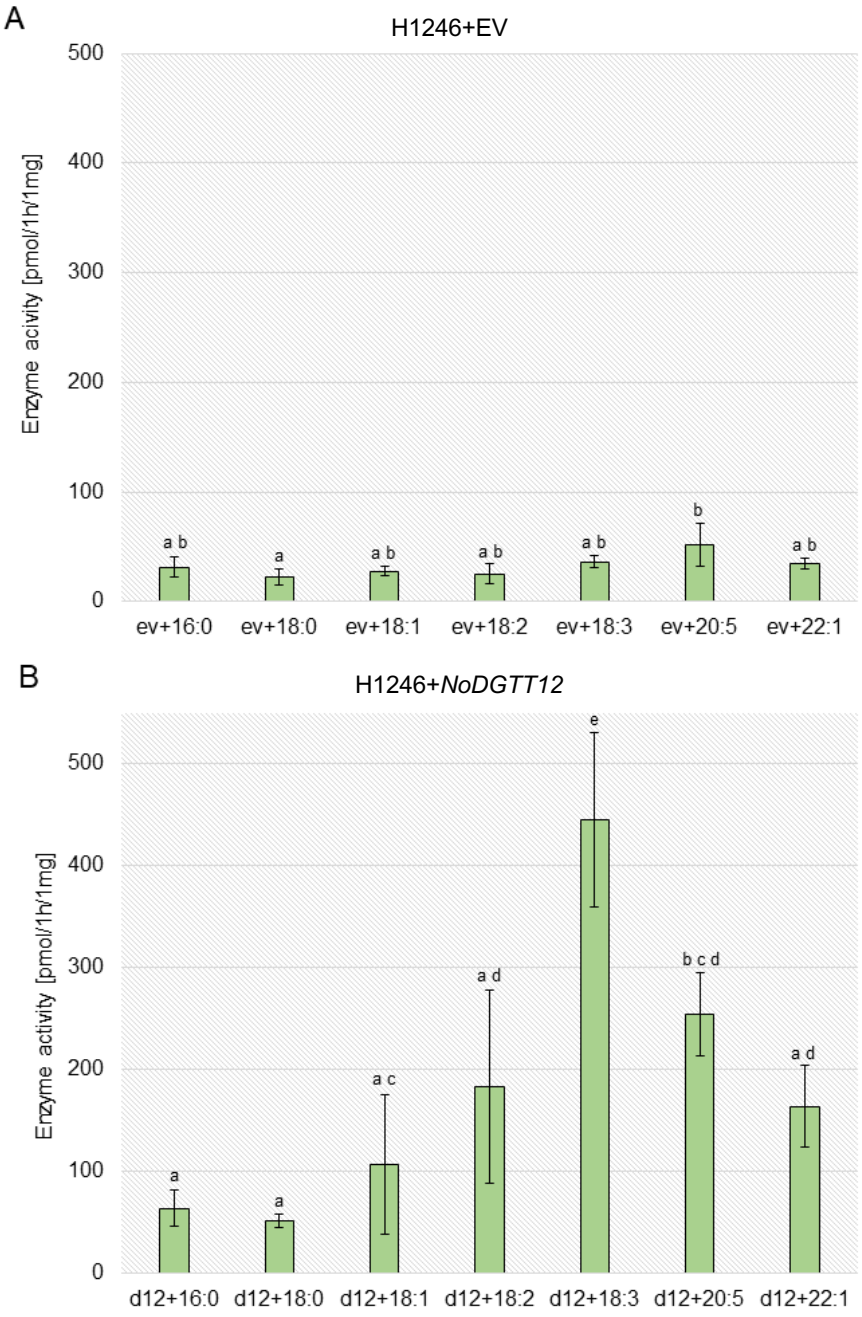

Figure 31. Comparison of microsomal NoDGTT activity in H1246 yeast transformed with (A) empty pYES2.1 vector and (B) pYES2.1-*NoDGTT12* construct toward various acyl-CoA substrates. Enzyme activity is expressed as pmol h^{-1} μg^{-1}. Data represent mean ± SD (n = 3). Statistical differences were assessed by one-way ANOVA with Tukey's post hoc test; distinct letters denote significant differences.

These analyses showed that NoDGTT12 exhibits distinct substrate preferences. The enzyme displayed the highest activity toward unsaturated acyl-CoAs such as 18:3-CoA, 20:5-CoA, 18:2-CoA, and 22:1-CoA, whereas activity toward saturated substrates (16:0-CoA, 18:0-CoA, 20:0-CoA) was markedly lower. The enzyme also demonstrated a clear preference for 18:1-DAG as an acyl acceptor. A low level of background activity was observed in the microsomal fraction from H1246 cells transformed with the empty pYES2.1 vector; this was taken into account in the subsequent analyses.

4.4 Overexpression of *NoDGTT12* in *Nannochloropsis oceanica* CCMP1779

4.4.1 *Nannochloropsis oceanica* CCMP1779 transformation with *NoDGTT12*

Based on the results described above, NoDGTT12 emerged as the most functionally robust candidate, displaying the highest TAG-accumulating capacity in the heterologous yeast system. Its markedly superior performance, both in terms of LDs formation and TAG content, strongly indicated that NoDTT12 may represent a key enzyme in TAG biosynthesis in *N. oceanica* CCMP1779. Therefore, this gene was selected for further overexpression in *N. oceanica* CCMP1779 to assess whether increasing its gene dosage could enhance TAG synthesis and overall lipid productivity in its native host.

As a first step towards constructing overexpression lines, the full coding sequence of *NoDGTT12* was amplified from the *NoDGTT12*-pYES2.1 construct previously used for heterologous expression in yeast (see Section 3.1.4). Primers containing flanking *Asc*I and *Hpa*I restriction sites were designed to facilitate subsequent cloning steps. The amplified fragment of ~1200 kb was first inserted into the pJET1.2/blunt vector and transformed into *E. coli* DH5α cells for propagation. Plasmid DNA was then isolated as described previously (Section 3.1.3). The resulting plasmid was subsequently digested with *Asc*I and *Hpa*I, and the target fragment was purified by agarose gel electrophoresis (Figure 32).

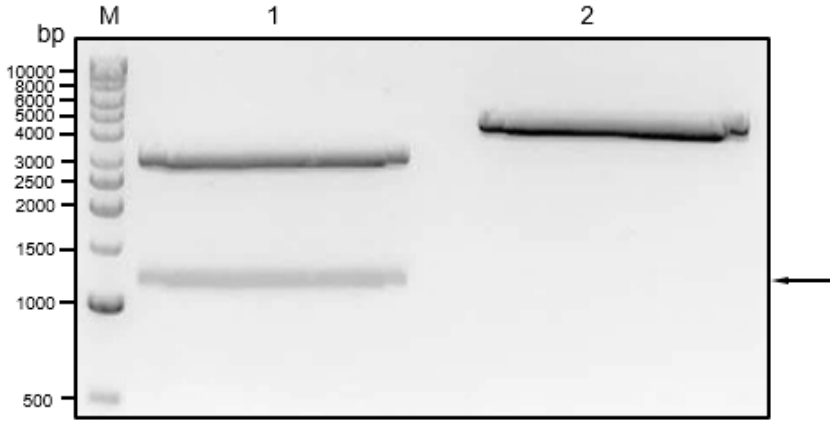

Figure 32. Digestion of *NoDGTT12*-pJET1.2/blunt vector with *Asc*I and *Hpa*I restriction enzymes. M – DNA ladder; (1) partially digested *NoDGTT12* product; (2) undigested *NoDGTT12*-pJET1.2/blunt plasmid. The arrow indicates the excised fragment of approximately 1.2 kb used for subsequent cloning steps. Agarose gel electrophoresis was performed on a 1% agarose gel in 1× TAE buffer.

In parallel, the pNOC-OX destination vector, designed for overexpression in *N. oceanica* CCMP1779 cells, was digested with the same restriction enzymes (*Asc*I and *Hpa*I) and subsequently purified by agarose gel electrophoresis (Figure 33).

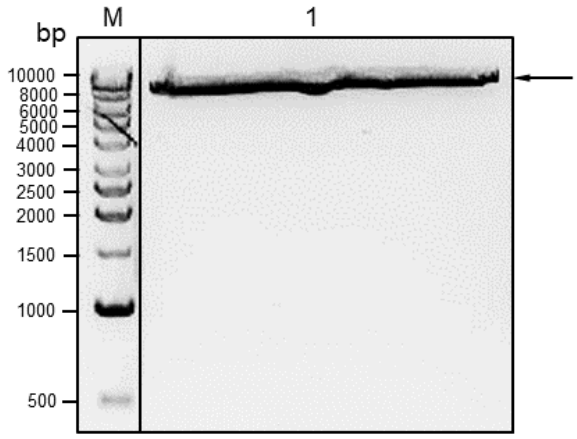

Figure 33. Digestion of the pNOC-OX-*CFP* vector with *Asc*I and *Hpa*I restriction enzymes. M – DNA ladder; (1) linearized pNOC-OX-*CFP* vector. The arrow indicates the linearized product of approximately 8.3 kb used for subsequent cloning steps. Agarose gel electrophoresis was performed on a 1% agarose gel in 1× TAE buffer.

Finally, the *NoDGTT12* transgene was ligated into the prepared pNOC-OX-*CFP* vector, and the resulting construct was used to transform *N. oceanica* CCMP1779, as described in detail in Section 3.2.5.

To verify expression of the pNOC-NoDGTT12-CFP fusion protein in *N. oceanica* CCMP1779, immunoblot analysis was performed following SDS-PAGE separation and electrotransfer onto a PVDF membrane, as described under Section 3.2.4.3.2 (Figure 34). The NoDGTT12 protein was fused to CFP, a derivative of GFP (~27 kDa), enabling detection using anti-GFP antibodies. Specifically, a primary mouse anti-GFP antibody and an HRP-conjugated secondary anti-mouse antibody were employed, both capable of recognizing GFP and its fluorescent derivatives, including CFP. Bioinformatic predictions (for details see Section 4.1) indicated a molecular weight of approximately 45 kDa for NoDGTT12 alone, corresponding to an expected size of ~72 kDa for the NoDGTT12-CFP fusion protein. Immunoblot analysis confirmed the presence of a distinct protein band at the expected molecular weight, consistent with successful expression of the *NoDGTT12-CFP* construct in *N. oceanica* CCMP1779.

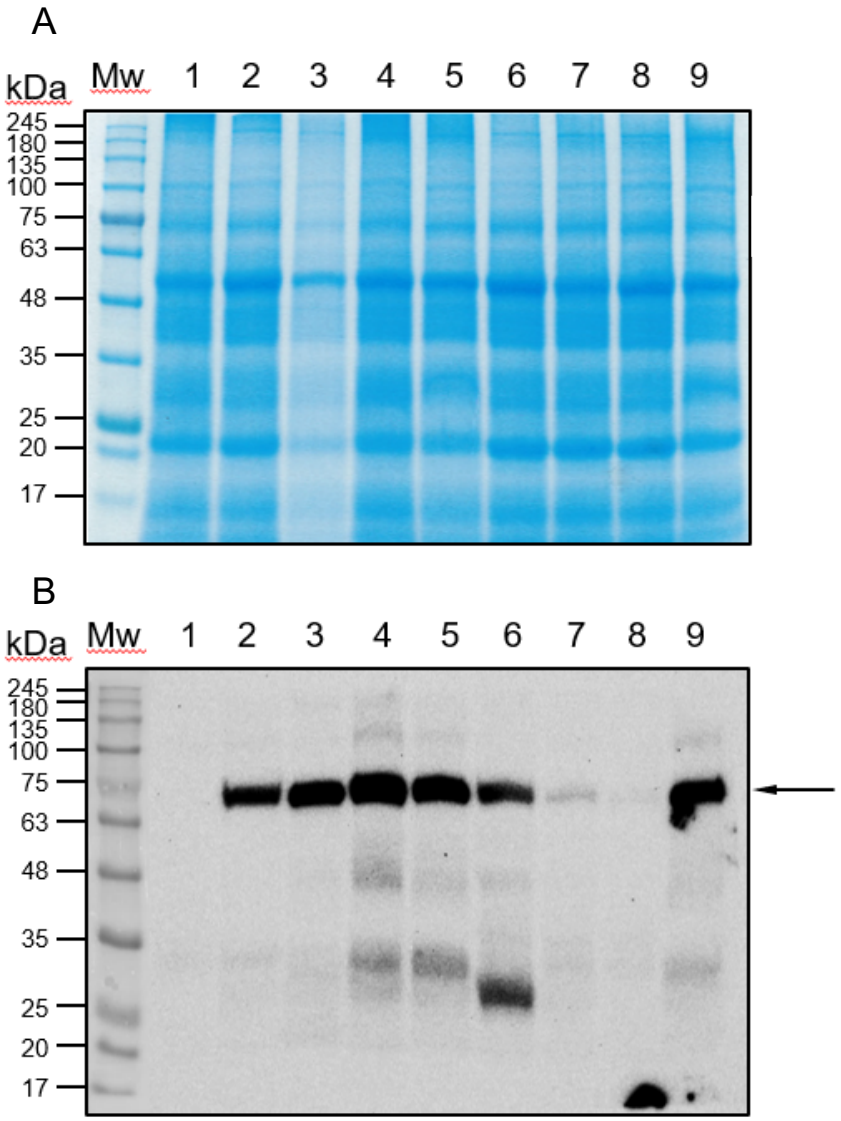

Figure 34. Western blot analysis of the pNOC-NoDGTT12-CFP fusion protein expressed in *N. oceanica* CCMP1779. (A) Coomassie-stained SDS-PAGE gel. (B) PVDF membrane after immunoblotting. Mw – protein ladder; lane 1 – *N. oceanica* CCMP1779 wild type; lanes 2–8 – transgenic *N. oceanica* CCMP1779 lines overexpressing *NoDGTT12*. The arrow indicates the detected NoDGTT12-CFP fusion protein band at approximately 72 kDa.

4.4.2 Cellular analysis of *Nannochloropsis oceanica* CCMP1779 lines expressing *NoDGTT12-CFP* fusion construct

To assess whether overexpression of *NoDGTT12* influences TAG accumulation and LD formation, *N. oceanica* CCMP1779 transformants were stained with BODIPY™ 505/515 and visualized using CLSM, as described in Section 3.2.4.3.3. *N. oceanica* CCMP1779 cells transformed with the empty *pNOC-OX* vector served as the control (Figure 35, A and B).

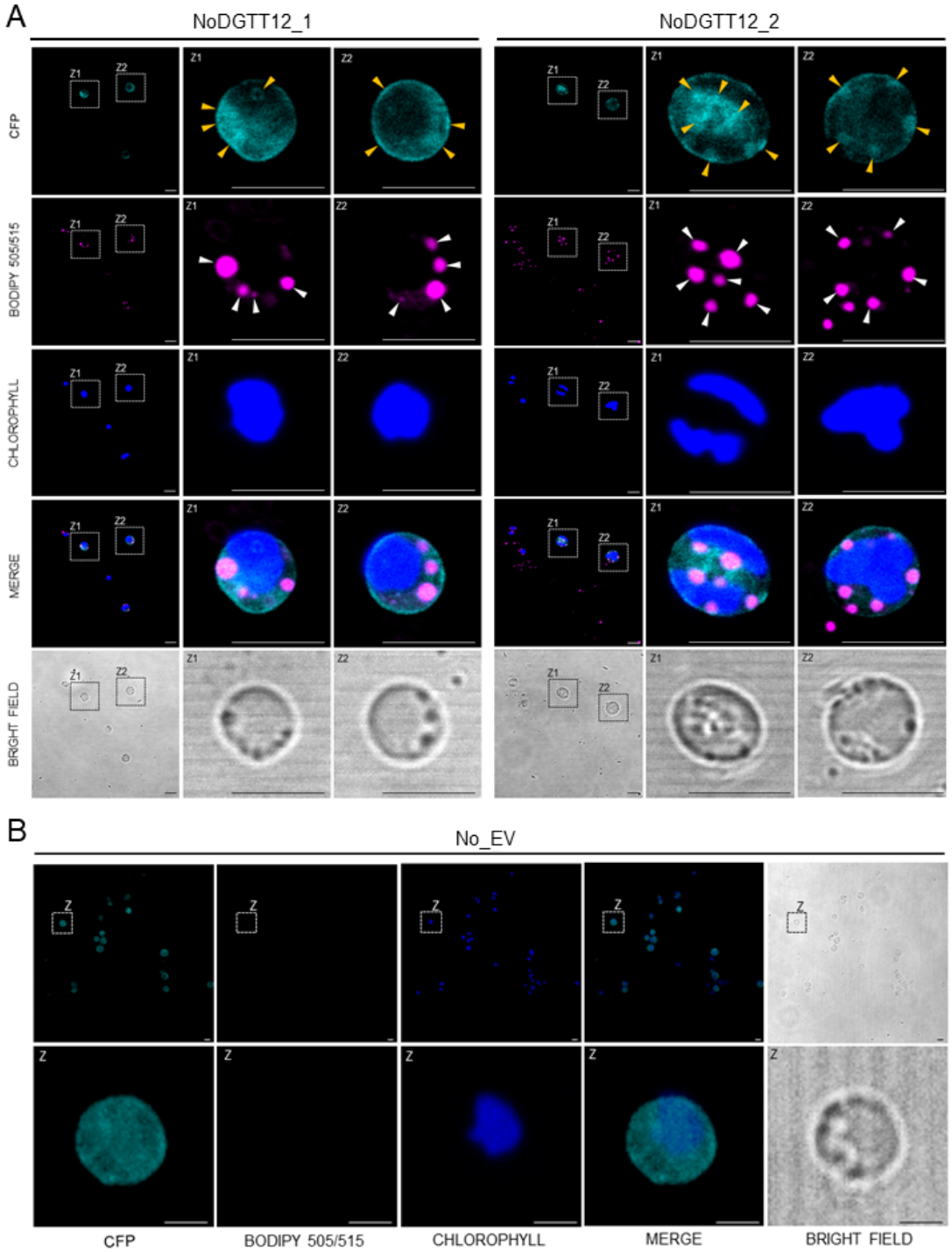

Figure 35. Visualization of LDs and *NoDGTT12-CFP* construct expression in *N. oceanica* CCMP1779 transformed with the *pNOC-NoDGTT12-CFP* fusion construct under N+ conditions. (A) Representative confocal fluorescence micrographs of two independent *N. oceanica* CCMP1779 transgenic lines expressing *NoDGTT12-CFP* fusion construct. Dashed boxes (Z1 and Z2) indicate distinct optical sections through individual cells. Cyan fluorescence corresponds to the CFP signal, representing the NoDGTT12-CFP fusion protein. Yellow arrowheads highlight regions of DGTT12-CFP accumulation within the cells. Magenta fluorescence represents neutral lipid staining with BODIPY™ 505/515, and white arrowheads indicate LDs. Blue fluorescence corresponds to chlorophyll autofluorescence. Merged images show the spatial relationship among CFP, BODIPY™, and chlorophyll signals. Bright field images depict the corresponding cellular morphology for the same focal planes. Scale bars = 5 µm. (B) Control cells transformed with the *pNOC-CFP* empty vector (No_EV) under N+ conditions. Cyan fluorescence represents CFP alone, while blue fluorescence corresponds to chlorophyll autofluorescence. Merged images illustrate the localization of CFP relative to chloroplasts. Bright field images show the overall morphology of the cells. Scale bars = 5 µm.

In the two independent transgenic lines, NoDGTT12_1 and NoDGTT12_2, a strong cyan fluorescence corresponding to the NoDGTT12-CFP fusion protein was observed throughout the cytoplasm. In addition to the diffuse signal, localized accumulations of fluorescence (Figure 35, B – yellow arrowheads) were evident at specific regions of the cells, occupied by LDs stained with BODIPY™ 505/515 (Figure 35A – white arrowheads). Such localization patterns were also accompanied by the presence of blue autofluorescence derived from chlorophyll, suggesting the presence of organized chloroplasts. In contrast, control cells transformed with the empty *pNOC-CFP* vector (No_EV) exhibited only diffuse and rather uniform cytoplasmic CFP fluorescence (Figure 35, B). Blue chlorophyll-derived fluorescence and no BODIPY™ signal were detected in the controls.

4.4.3 Characterization of lipid content and FA composition in *Nannochloropsis oceanica* CCMP1779 expressing *NoDGTT12-CFP* fusion construct

To gain further insight into the lipid metabolism of transgenic *N. oceanica* CCMP1779 lines, lipid content and composition were analysed by GC-FID, as described in Section 3.2.4.4. TLC analysis revealed distinct bands corresponding to TAGs in transgenic *N. oceanica* CCMP1779 lines expressing the NoDGTT12-CFP fusion protein (Figure 36, lines 1-3). In contrast, control cultures transformed with the empty pNOC-*CFP* construct displayed considerably weaker TAG bands (Figure 36, lines 4-6).

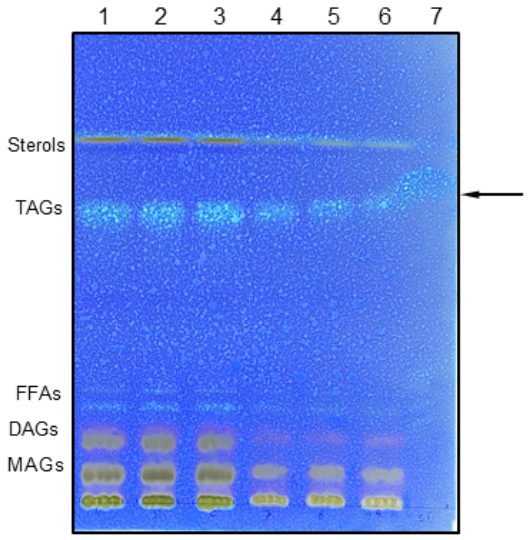

Figure 36. Representative image of TLC separation of lipid extracts from transgenic *N. oceanica* CCMP1779 lines expressing *NoDGTT12-CFP* fusion construct (lines 1-3) and *pNOC-CFP* empty vector (lines 4-6). Line 7 - Olive oil used as a TAG standard. MAGs – monoacylglycerols, DAGs – diacylglycerols, FFAs – free fatty acids, TAGs – triacylglycerols. Black arrow indicates TAGs corresponding bands.

To address the impact of NoDGTT12-CFP fusion protein expression on lipid metabolism in transgenic *N. oceanica* CCMP1779 cells, the content and composition of total lipid and TAG fraction were measured under N+ conditions in WT, EV control and four independent transgenic *N. oceanica* CCMP1779 lines (Figure 37).

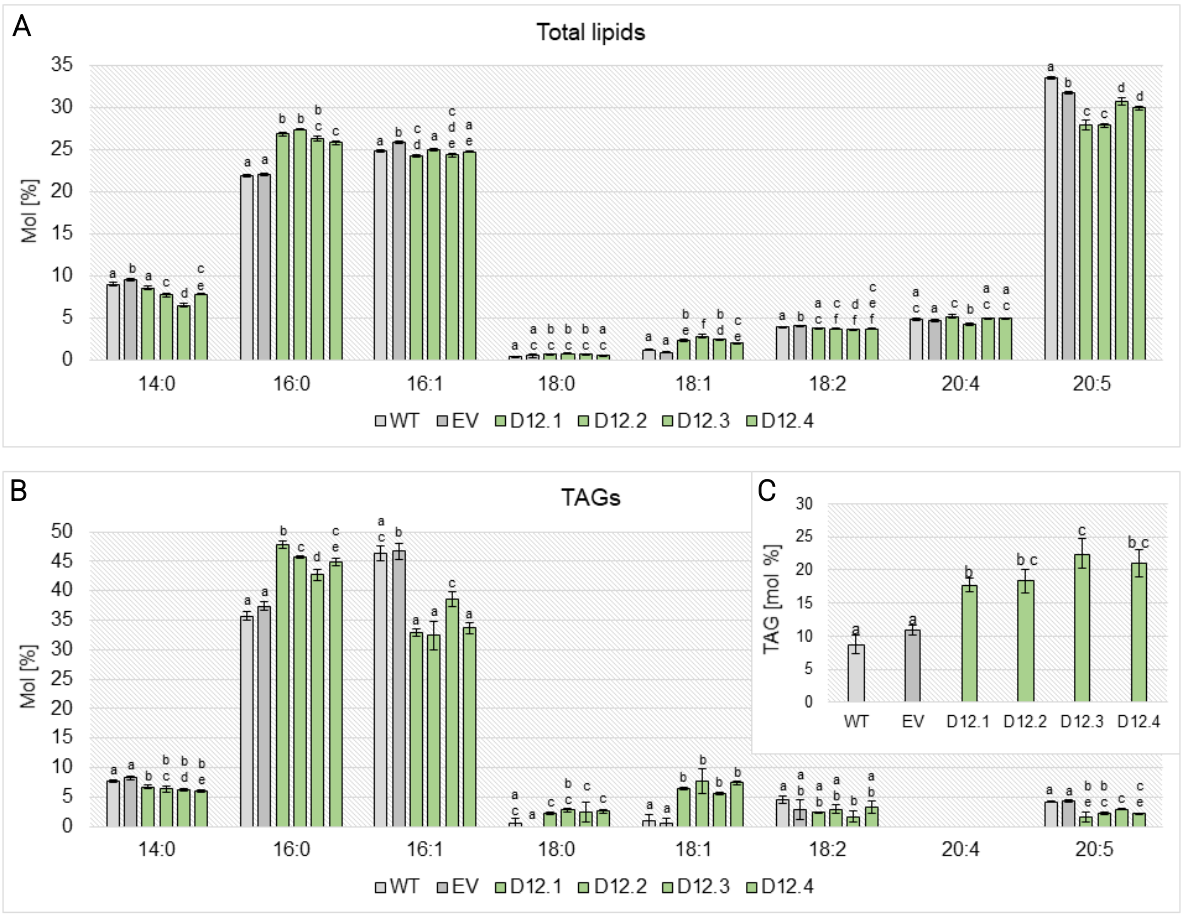

Figure 37. Comparison of FA profiles from total lipids (A) and TAGs (B) extracted from wild type (WT), empty vector control (EV), and transgenic lines of *N. oceanica* CCMP1779 transformed with *NoDGTT12-CFP* construct (D12.1 – D12.4). The small inserted panel (C) displays the proportion of total TAGs relative to total lipids. FAs are reported by number of carbons (C) : number of double bonds. Values represent the mean of ± SD of four biological replicates (n=4). Statistical analysis was performed by one-way ANOVA with Tukey's post hoc test. Different letters indicate significant differences.

Expression of the NoDGTT12-CFP fusion protein in *N. oceanica* CCMP1779 resulted in clear changes in FA composition within both the total lipid and TAG fractions compared to the WT and empty vector EV control cells under N+ conditions. In the total lipid fraction (Figure 37A), transgenic lines (D12.1–D12.4) showed a general shift toward higher proportions of medium-chain saturated (16:0) and monounsaturated (16:1) FAs, while the relative abundance of long-chain polyunsaturated FAs (PUFAs), such as 20:4 and 20:5, was notably reduced compared with WT and EV. In the TAG fraction (Figure 37B), similar alterations in FA composition were observed. The transgenic lines accumulated significantly higher proportions of 16:0 and 16:1 FAs, while the proportions of 20:5 decreased relative to WT and EV. This pattern indicates a remodeling of the TAG pool toward more saturated and monounsaturated FAs, consistent with increased TAG synthesis activity. The inset (Figure 37C) further demonstrates that the proportion of TAGs relative to total lipids was significantly higher in all transgenic lines compared to WT and EV controls.

4.5 Heterologous expression of *NoDGTT12* in *Arabidopsis thaliana* AS11 (*tag1-1*)

4.5.1 *Arabidopsis thaliana* genotyping

In order to test whether *NoDGTT12* is effective in restoring TAG synthesis in a plant heterologous system, its expression was analysed in the *A. thaliana* AS11 (*tag1-1*) mutant, which carries a disruption in the endogenous DGAT1-encoding gene (Katavic *et al*., 1995). Col-0 (WT) plants were used as controls. In the first step, all experimental plants were genotyped to confirm their genetic identity and to exclude any possibility of seed contamination or mixed lines (Figure 38). Genotyping was performed as described in Section 3.3.1.3.1. The AS11 (*tag1-1*) mutant contains a 147 bp insertion within intron 2 of the *TAG1* gene encoding DGAT1 (Zou *et al*., 1999; Bai *et al*., 2023). To exclude potential PCR artifacts, two primer sets were used. Primers A (located in exon 1) and B (in exon 3) amplified a fragment approximately 150 bp longer in AS11 (*tag1-1*) than in the wild type, reflecting the presence of the insertion (Figure 38, A). Since primers A and B only revealed a size difference, an additional Primer C, designed within the inserted sequence, was used together with Primer B as a specific diagnostic test to confirm the identity and orientation of the insertion (Figure 38, B and C). The obtained results confirmed that the inserted sequence corresponded to the duplicated region described previously, verifying its presence independently of PCR size differences. In conclusion, homozygosity of the *A. thaliana* AS11 (*tag1-1*) plants was confirmed, and these plants were subsequently used for further experimental procedures.

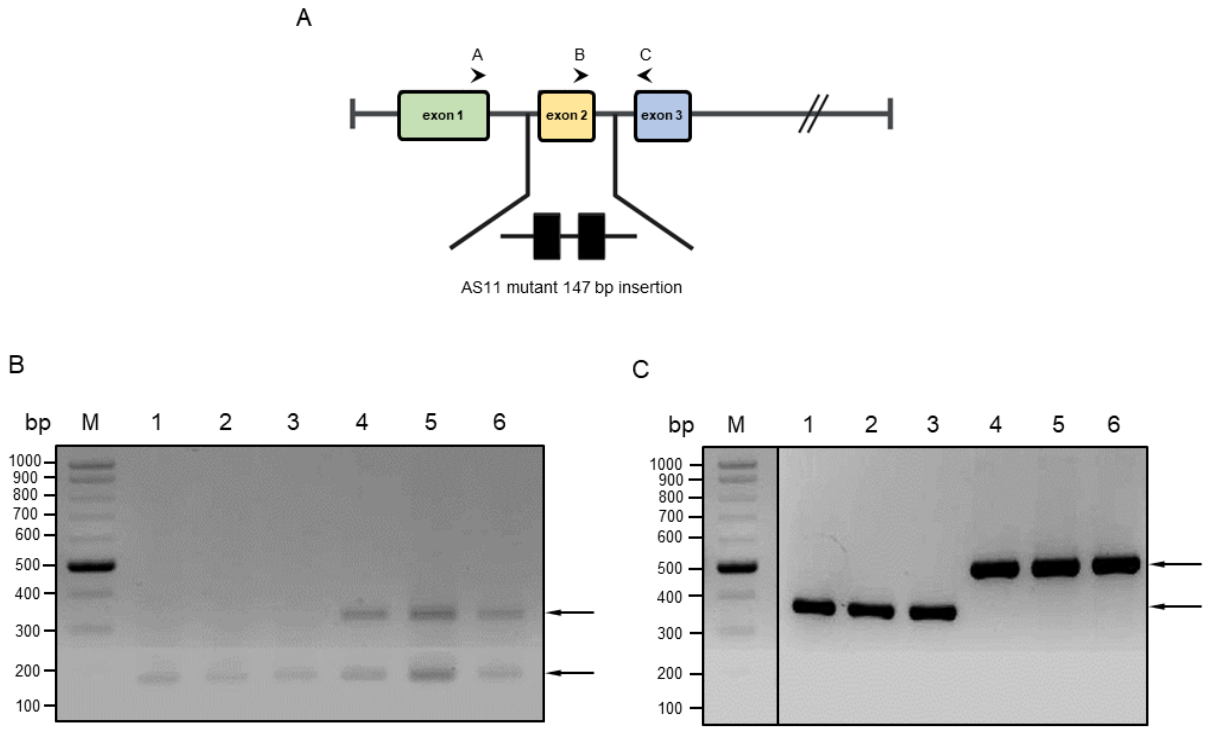

Figure 38. *A. thaliana* genotyping. A) Schematic diagram of the *TAG1* gene showing exons 1-3 and the locations of primers A, B, and C. The AS11 (*tag1-1*) mutant contains a 147 bp insertion within intron 2. B) PCR amplification using primers A and B. The AS11 (*tag1-1*) mutant (lanes 4-6) shows the presence of a fragment approximately 150 bp larger than the wild type (lanes 1-3), consistent with the insertion. M - DNA ladder. C) PCR amplification using primers C and B yielded two fragments in AS11 (lanes 4–6) but only one in the wild type (lanes 1–3), confirming the presence of the 147 bp insertion. The arrows indicate the correct PCR products of size ~150 and 350 bp. Agarose gel electrophoresis in 1% agarose gel in 1x TAE buffer.

4.5.2 Gateway cloning™ strategy

Gateway cloning™ was employed for transfer of full-length coding sequence for *NoDGTT12* from pDONR™221 vector to pUBC-*CFP* destination vector for the final expression in *A. thaliana* AS11 (*tag1-1*), as described in sections 3.3.1.1 and 3.3.1.2. The *NoDGTT12* full-length sequence was first amplified on previously sequenced *pYES2.1-NoDGTT12* cDNA construct (see points 3.1 and 4.2.1) using primers to *NoDGTT12* with *att* flanking sites. The following cloning procedure consisted of three main steps: 1) generation of entry clones through BP recombination, 2) integration into destination vectors *via* LR recombination, and 3) subsequent expression of the resulting constructs in the target system (Figure 10). The entry clone was generated in BP reaction by cloning *NoDGTT12+att* flanking sites into pDONR™221 vector and transformed into One Shot™ *E. coli*, as described under point 3.3.1. The positive transformants were screened by colony PCR (Figure 39). The correctly assembled plasmids obtained from successful transformations were then extracted and confirmed by sequencing. Only the correct plasmids were proceeded to the LR recombination reaction.

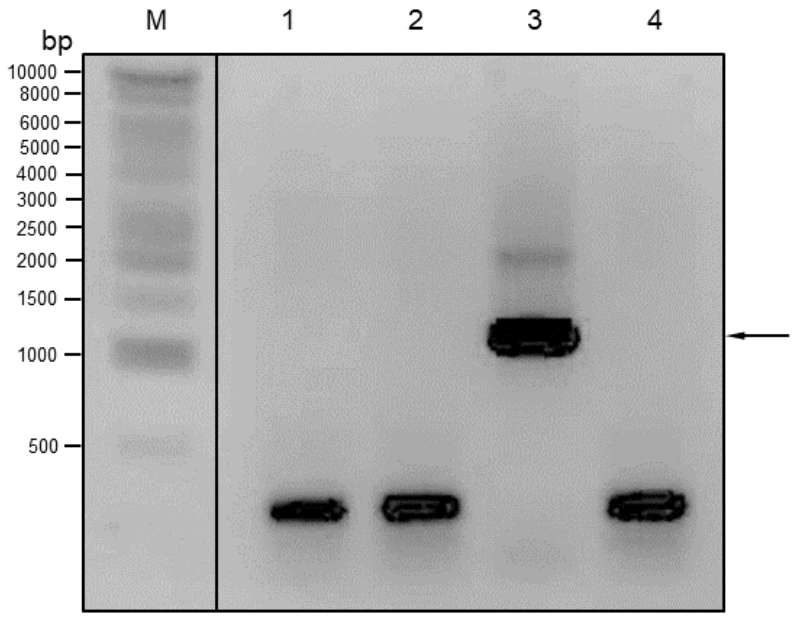

Figure 39. BP reaction with pDONR™221 vector, colony PCR. M - DNA ladder. (1-4) pDONR™221-NoDGTT12 constructs in One Shot™ TOP10 Chemically Competent *E. coli* cells. The arrow indicates the correct PCR product of size ~1200 bp. Agarose gel electrophoresis in 1% agarose gel in 1x TAE buffer.

The full coding sequence of NoDGTT12 flanked with *att* sites was then transferred from pDONR™221 vector into the *pUBC-CFP* destination vector *via* site-specific recombination in LR reaction and subsequently transformed into One Shot™ *E. coli* cells for cloning. Positive transformants were screened by colony PCR using primers for *NoDGTT12* (Figure 40). The *pUBC-CFP* plasmids carrying *NoDGTT12+att* sites were extracted from successfully transformed colonies, sequenced and used for *A. tumefaciens* GV3101 transformation.

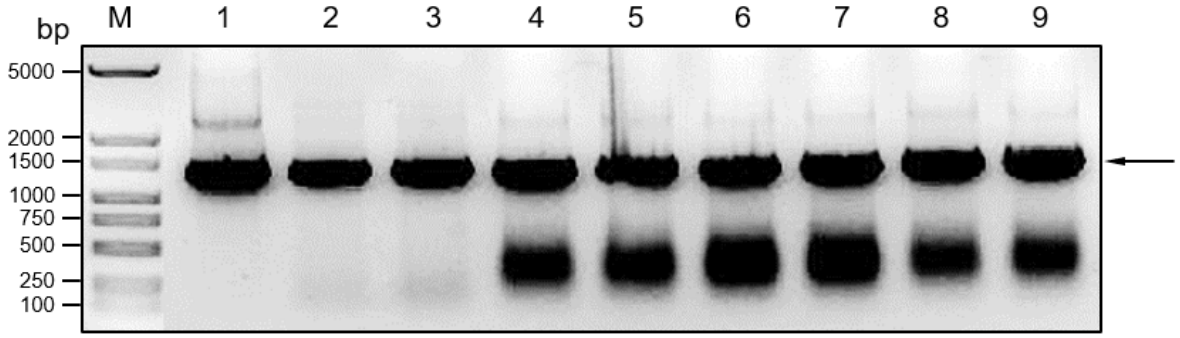

Figure 40. LR reaction with *pUBC-CFP* vector, colony PCR. M - DNA ladder. (1-9) pUBC-*NoDGTT12-CFP* constructs in One Shot™ TOP10 Chemically Competent *E. coli* cells. The arrow indicates the correct PCR product of size ~1200 bp. Agarose gel electrophoresis in 1% agarose gel in 1x TAE buffer.

A. tumefaciens GV3101 competent cells were transformed with the obtained pUBC-*NoDGTT12*-CFP construct DNA and colony PCR was performed to check the transformation efficiency before the floral dip transformation of *Arabidopsis thaliana* AS11 (*tag1-1*) (Figure 41).

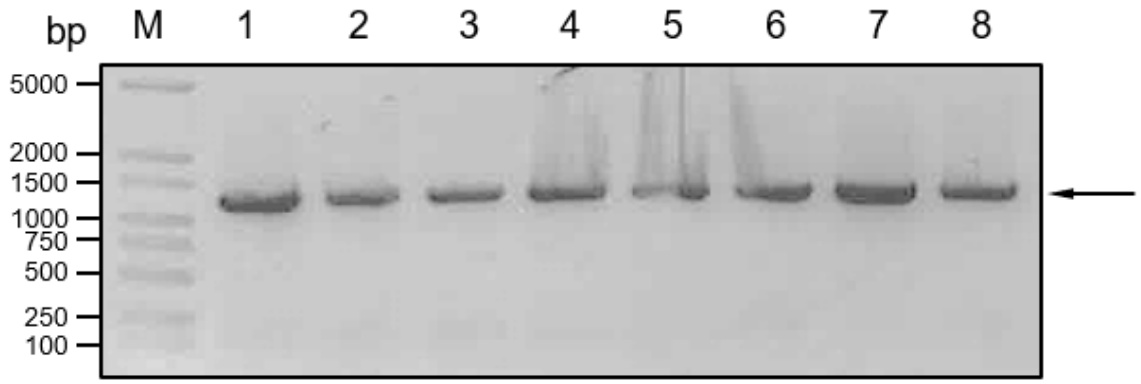

Figure 41. *A. tumefaciens* GV3101 transformation with *pUBC-NoDGTT12*-CFP construct, colony PCR. M - DNA ladder. (1-8) pUBC-*NoDGTT12*-CFP constructs in *A. tumefaciens* GV3101 cells. The arrow indicates the correct PCR product of size ~1200 bp. Agarose gel electrophoresis in 1% agarose gel in 1x TAE buffer.

4.5.3 *Arabidopsis thaliana* AS11 (*tag1-1*) floral dip transformation

The floral dip method was employed to generate transgenic AS11 (*tag1-1*) *A. thaliana* lines expressing pUBC-*NoDGTT12-CFP* construct, as described under point 3.3.1.3.2. After transformation, *A. thaliana* AS11 (*tag1-1*) plants were grown until seed maturation. The mature seeds of F1 were harvested, sowed and grown as described under point 3.3.2. The treatment with BASTA selected positive transformants, as shown in Figure 42.

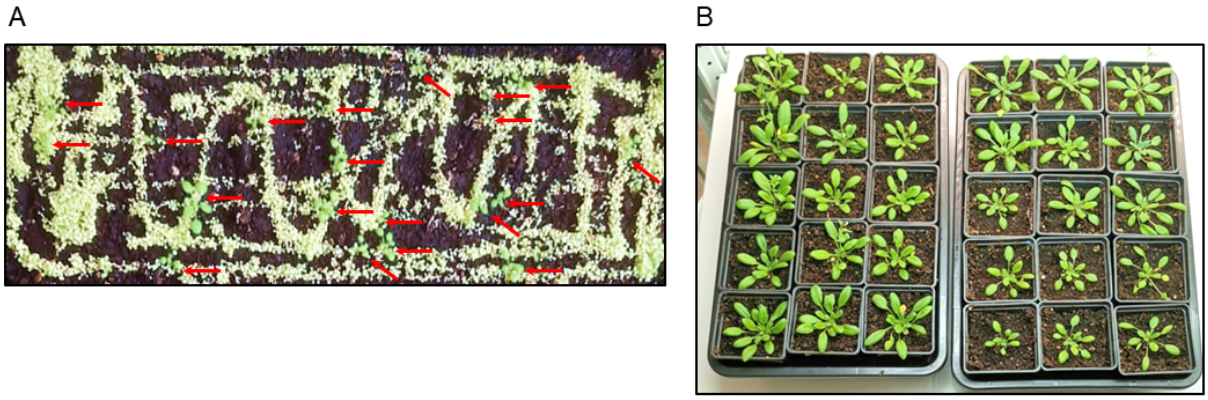

Figure 42. Selection of BASTA resistant *A. thaliana* AS11 (*tag1-1*) expressing pUBC-*NoDGTT12-CFP* construct. (A) Seeds sown on soil and treated with BASTA. Red arrows indicate successfully transformed individuals resistant to BASTA. (B) Positive transformants exhibiting resistance to BASTA, grown individually in separate pots.

4.5.4 Detection of NoDGTT12-CFP fusion construct expression in *Arabidopsis thaliana* plants

All the BASTA-resistant plants of F1 generation were analysed for the presence of pUBC-*NoDGTT12-CFP* construct by western blotting with anti-GFP antibody, as describe in details under point 3.3.3.1 (Figure 43). Bioinformatic predictions (see point 4.1) estimated the molecular weight of approximately 45 kDa for NoDGTT12 alone, and ~27 kDA for CFP which corresponding to an expected size of ~72 kDa for the whole NoDGTT12-CFP fusion protein. Immunoblot analysis confirmed the presence of a distinct protein band of this size in analysed plants (Figure 43 A). The same strategy was implemented for F2 generation of transformants (see point 3.3.3.2), allowing for a comprehensive assessment of transgene expression stability across generations (Figure 43 B).

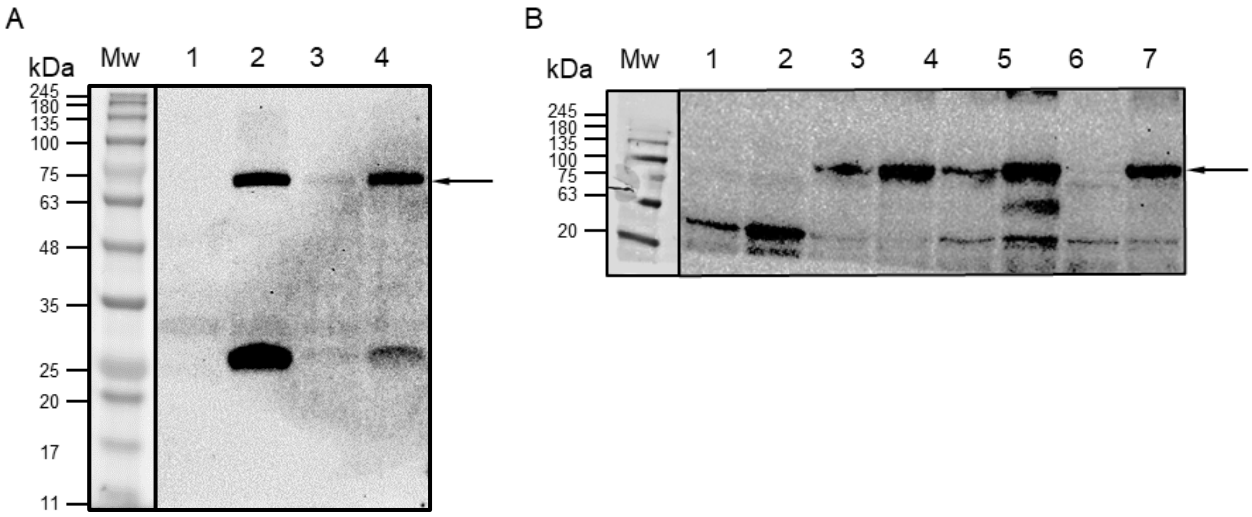

Figure 43. Western blot analysis of the pUBC-NoDGTT12-CFP fusion protein expressed in *A. thaliana* across F1 (A) and F2 (B) generations. (A) PVDF membrane after immunoblotting. Mw – protein ladder; lane 1 – *A. thaliana* Col-0 wild type; lanes 2-4 – transgenic *A. thaliana* AS11 (*tag1-1*) mutant expressing pUBC-NoDGTT12-CFP fusion protein (B) PVDF membrane after immunoblotting. Mw – protein ladder; lane 1 – *A. thaliana* Col-0 wild type; lanes 2-7 – transgenic *A. thaliana* AS11 (*tag1-1*) mutant expressing pUBC-NoDGTT12-CFP fusion protein Arrows indicate the detected NoDGTT12-CFP fusion protein band at approximately 72 kDa.

4.5.5 Characterization of lipid content and fatty acid composition in *Arabidopsis thaliana* plants

To investigate the lipid content and composition in wild type, AS11 (*tag1-1*), and *NoDGTT12*-expressing *A. thaliana* AS11 (*tag1-1*) during seed germination and early seedling development, a series of systematic lipid extractions were conducted (Figure 44 and 45). Samples were prepared in batches, each comprising 30 seeds/seedlings, at the following developmental stages: (1) dry seeds (prior to germination), (2) germinating seeds after 24 hours of growth, (3) seedlings after 48 hours of growth, (4) seedlings after 72 hours of growth, and (5) seedlings after 92 hours of growth. All samples were subsequently subjected to lipid isolation and GC-FID analysis as explained in sections 3.3.7.1 and 3.3.7.2.

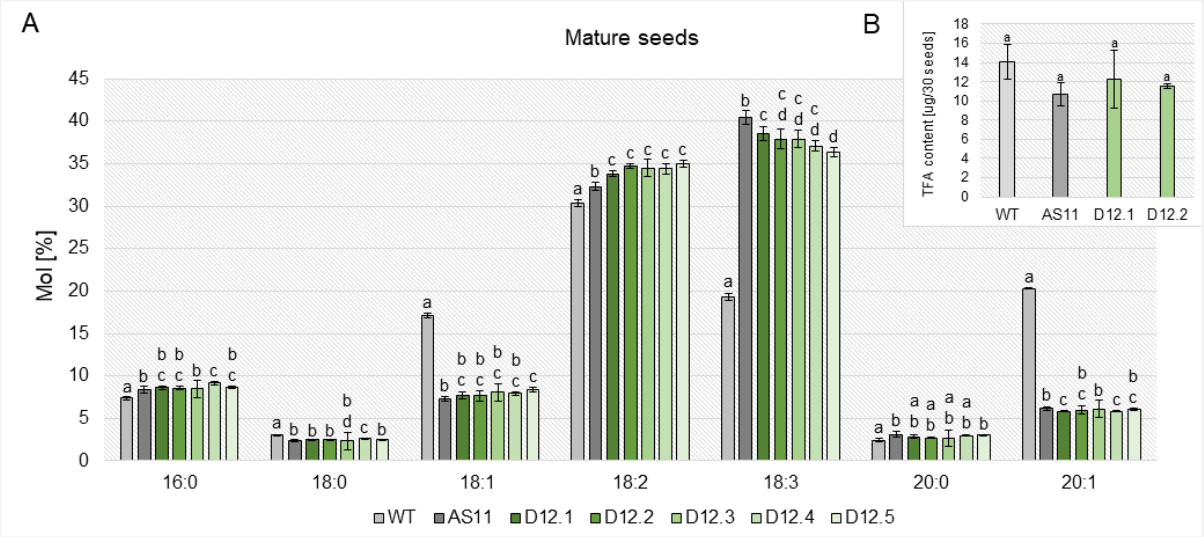

Figure 44. (A) Comparison of FA profiles from mature seeds extracted from wild type (WT), mutant line (AS11), and transgenic lines of *A. thaliana* transformed with NoDGTT12-CFP protein construct (D12.1-D12.5). The small inserted panel (B) displays the total FAs (TFA) content in representative lines. FAs are reported by number of carbons (C) : number of double bonds. Values represent the mean of ± SD of four biological replicates (n=4). Statistical analysis was performed by one-way ANOVA with Tukey's post hoc test. Different letters indicate significant differences.

Across all genotypes, the major FAs detected in mature seeds were 18:2 and 18:3, together accounting for the largest proportion of total FAs (Figure 44, A). The overall distribution of saturated FAs (16:0, 18:0 and 20:0) was similar among WT, AS11, and D12 lines, with only minor variations. A significant decrease in 18:1 and 20:1 was observed in AS11 and D12 lines when compared to WT. Also, a significant increase of PUFAs (18:2 and 18:3) was found for AS11 and D12 lines alongside the WT line. Total FA content varied among the wild type, mutant, and transgenic *A. thaliana* lines (Figure 44B). WT seeds exhibited the highest TFA content, significantly exceeding that of AS11 (*tag1-1*). Both D12.1 and D12.2 showed reduced TFA content relative to WT, yet displayed higher TFA levels than AS11 (*tag1-1*).

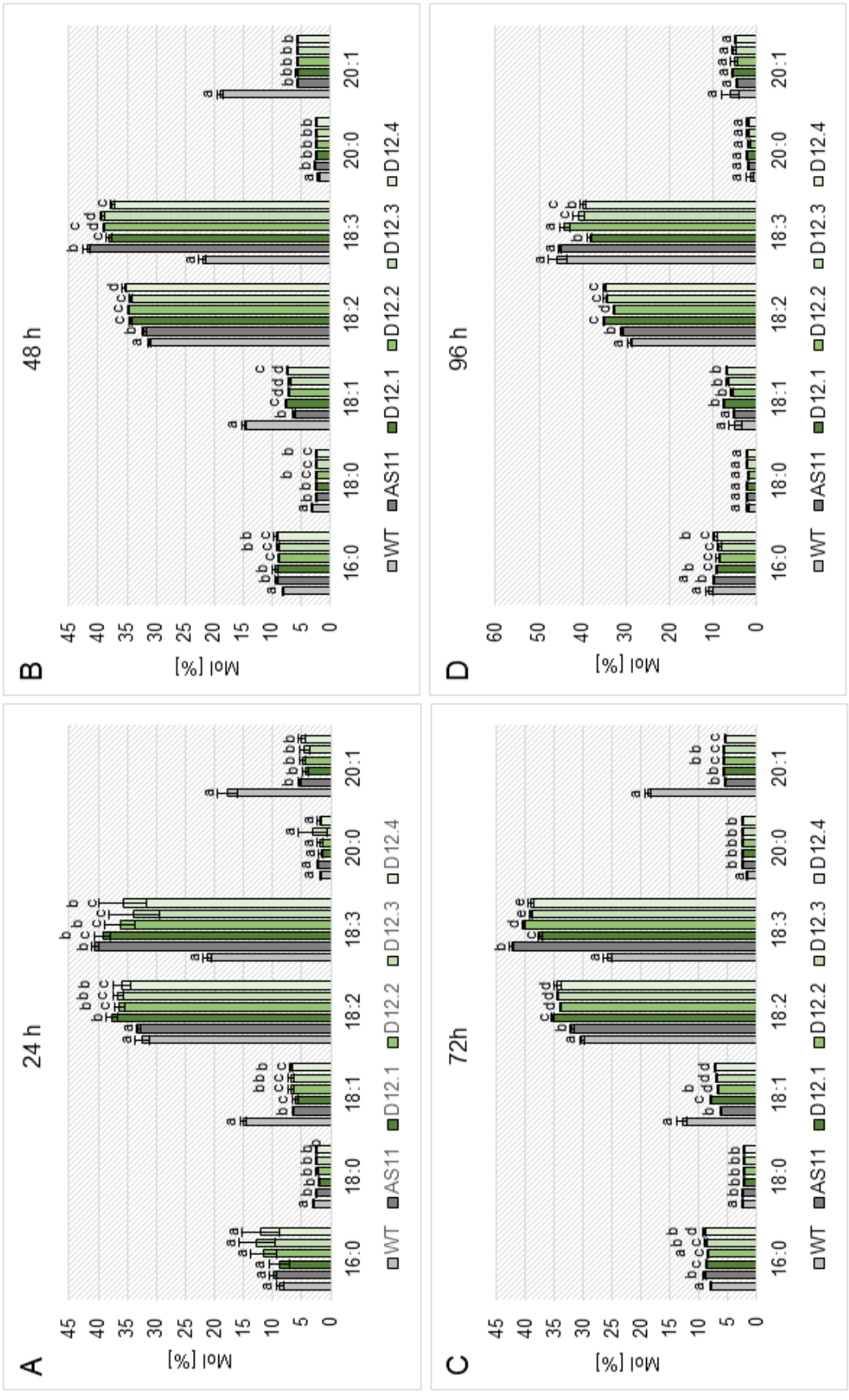

Figure 45. Comparison of FA profiles from germinating seeds of *A. thaliana* wild type (WT), mutant line (AS11), and transgenic lines of *A. thaliana* mutant line transformed with NoDGTT12-CFP protein construct (D12.1-D12.4) after 24 hours (A), 48 hours (B), 72 hours (C) and 96 hours (D) of germination. FAs are reported by number of carbons : number of double bonds. Values represent the mean of ± SD of six biological replicates (n=6). Statistical analysis was performed by one-way ANOVA with Tukey's post hoc test. Different letters indicate significant differences.

Across all time points, PUFAs (18:2 and 18:3) dominated the lipid profiles of all analysed lines of *A. thaliana*, accounting for the largest proportion of total fatty acids (Figure 45). Compared with WT, the AS11 mutant showed reduced levels of 18:1 and 20:1, accompanied by a relative increase in 18:2 and 18:3, a trend that was maintained or further enhanced in the D12 transgenic lines. Expression of NoDGTT12 partially restored lipid profiles toward WT levels, with D12 lines displaying consistently elevated PUFAs over time while saturated fatty acids (16:0 and 18:0) remained largely unchanged. These effects were most pronounced at 48–72 h, indicating a time-dependent impact of NoDGTT12 on FA remodelling rather than on saturated FA accumulation.

4.5.6 CLSM analysis of LD formation in seeds of transgenic *Arabidopsis thaliana* AS11 (*tag1-1*) expressing *NoDGTT12*

To investigate the effect of *TAG1* disruption on LD formation in AS11 (*tag1-1*) mutant of *A. thaliana* and to assess the possible functional complementation by *NoDGTT12*, CLSM analysis was performed as described under point 3.3.5 (Figure 46).

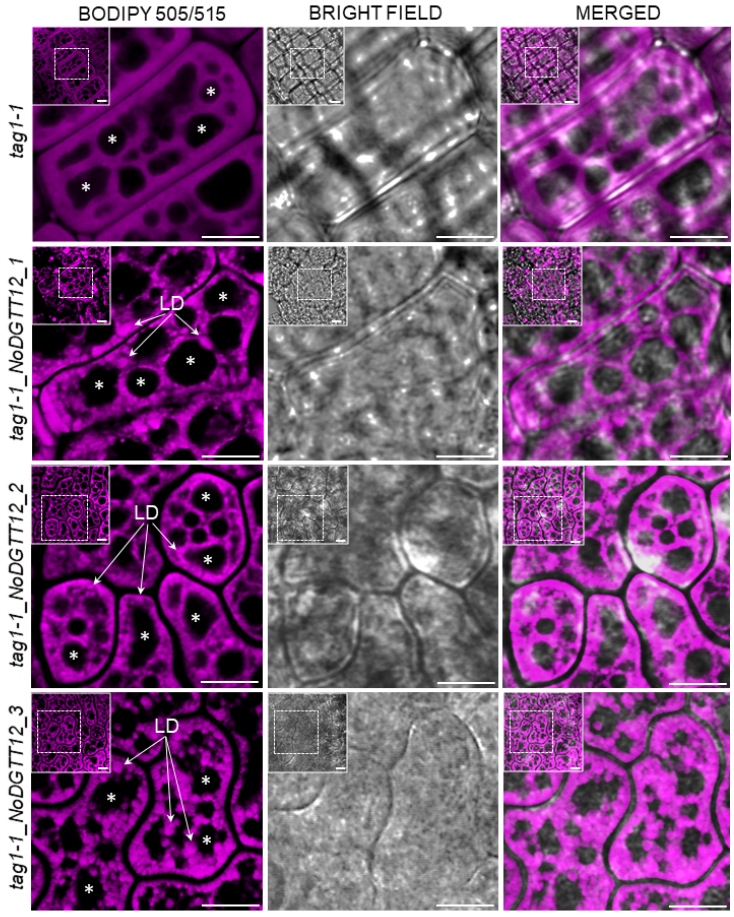

Figure 46. BODIPY™ 505/515 staining of neutral lipids (magenta) in *A. thaliana* AS11 (*tag1-1*) transformed with pUBC-*NoDGTT12-CFP* construct. Representative micrographs of AS11 (*tag1-1*) mutant line (control) and three independent *A. thaliana* AS11 (*tag1-1*) transgenic lines expressing *NoDGTT12-CFP* fusion construct. Dashed boxes indicate zoomed area showed in the panels. White asterisks represent protein bodies. Scale bars = 5 µm.

CLSM seed analysis revealed the absence of lipid droplets in the AS11 (*tag1-1*) mutant. BODIPY™ fluorescence signal was weak and diffuse, indicating a low level of neutral lipid accumulation. In contrast,

the AS11 (*tag1-1*) mutant lines complemented with *NoDGTT12* exhibited numerous bright BODIPY™-stained LDs distributed throughout the cytoplasm. LDs were mainly localized surrounding the protein bodies (marked with asterisks) and positioned at the peripherical regions of the cell. The restored LD formation in these lines demonstrates that introduction of *NoDGTT12* into the AS11 (*tag1-1*) mutant rescues the defects in TAG synthesis and lipid droplet formation caused by the loss of *TAG1* gene.

4.5.7 Seed morphometrics

Morphometric analyses (as described in Section 3.3.6) revealed that complementation of the seed TAG phenotype in AS11 (*tag1-1*) plants by expression of *NoDGTT12* was accompanied by an increase in seed size (Figure 47A–C). The AS11 (*tag1-1*) plants expressing *NoDGTT12* reached seed sizes even greater than those observed in WT plants. Panels A–C in Figure 47 illustrate the morphological differences among seeds of the WT, the AS11 (*tag1-1*) mutant, and the AS11 (*tag1-1*) line complemented with *NoDGTT12*. WT seeds (Figure 47A) were uniformly sized, well filled, and displayed the characteristic elongated shape associated with normal maturation. In contrast, seeds from the AS11 (*tag1-1*) mutant were visibly smaller, less expanded, and often irregular in shape (Figure 47B). Introduction of *NoDGTT12* into the AS11 (*tag1-1*) background resulted in fuller, more regularly shaped seeds that closely resemble wild type morphology (Figure 47C).

These visual observations were supported by quantitative measurements of seed area, length, and width (Figure 47D–F). As expected, seeds of the AS11 (*tag1-1*) mutant displayed a marked reduction in all three parameters relative to the WT. Complementation with *NoDGTT12* significantly increased these values, restoring them to levels comparable to, or even surpassing, those of WT seeds. This high-throughput statistical analysis, which included more than 7000 seeds per line, confirms the robustness of these differences and highlights the significant variation among the analysed genotypes.

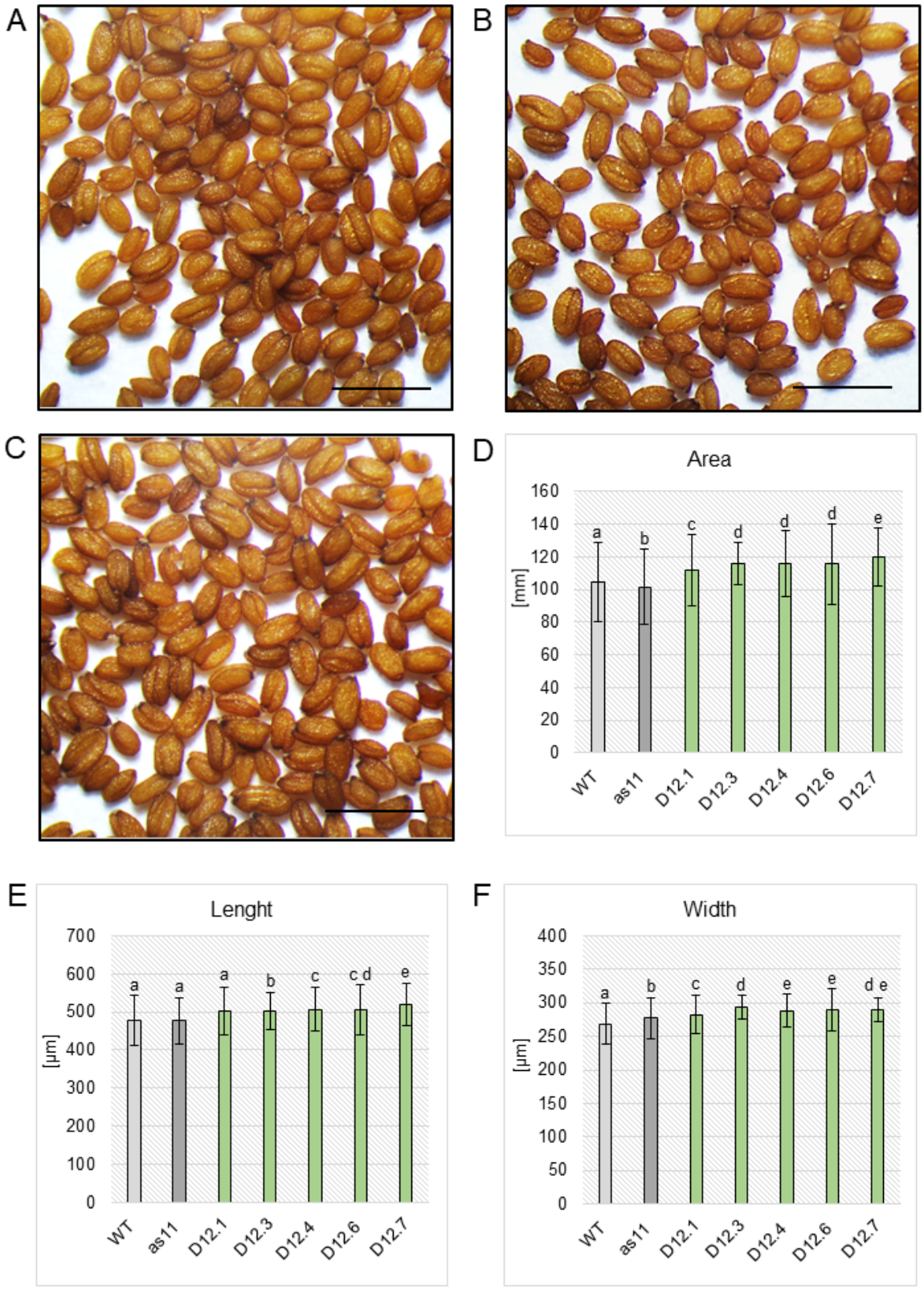

Figure 47. Seed morphology (A-C) and size parameters (D-F) of *A. thaliana* seeds. Representative seeds from the WT of *A. thaliana* (A), AS11 (*tag1-1*) mutant of *A. thaliana* (B) and AS11 (*tag1-1*) mutant line complemented with *NoDGTT12* (C). Bars = 1mm. (D–F) Quantification of seed area (D), length (E), and width (F) across genotypes. WT – wild type of *A. thaliana*, as11 – AS11 (*tag1-1*) mutant line of *A. thaliana*, D12.1 - 5 – separate lines of AS11 (*tag1-1*) *A. thaliana* complemented with *NoDGTT12*. Statistical differences were assessed by one-way ANOVA with Tukey's post hoc test; distinct letters denote significant differences.

4.6 *In silico* analysis of NoDGTT5 and NoDGTT12 amino acid sequences

Having the exceptionally high TAG-synthesizing activity of NoDGTT12 observed in both the native *N. oceanica* CCMP1779 background and heterologous systems, a comparative analysis of its amino acid sequence was performed to identify structural features potentially underlying its superior performance. Given that NoDGTT5 was previously characterized as a highly efficient TAG synthase in the same experimental models (Zienkiewicz et al., 2017), similarities and differences between these two proteins were analysed specifically at the level of their primary protein sequence (Figure 48).

NoDGTT5 consists of 375 amino acids, whereas NoDGTT12 comprises 402 amino acids. Multiple sequence alignment using PRALINE online tool revealed a moderate level of primary sequence similarity between the two proteins, with 86 identical residues corresponding to approximately 24% sequence identity across an alignment length of 405 amino acids. The alignment score and residue-pair score indicated statistically meaningful similarity despite substantial sequence divergence, consistent with their classification as paralogous members of the expanded NoDGTT family.

Analysis of amino acid conservation patterns demonstrated that conserved residues are unevenly distributed along the sequences. Clusters of high conservation were predominantly located in the central and C-terminal regions, whereas the N-terminal regions exhibited low conservation and numerous gaps. The N-terminal domains of both proteins were enriched in polar and charged residues, including lysine, arginine, serine, and threonine, and lacked extended hydrophobic segments. These regions contained multiple low-complexity regions enriched in polar and charged residues. As shown on Figure 48, several conserved segments corresponded to regions previously identified as harbouring characteristic DGAT type 2 motifs, including PH, PR, GGE, RGFA, VPFG, ang G motifs involved in substrate binding (Liu *et al*., 2012; Zienkiewicz *et al*., 2017; Xu *et al*., 2018).

Hydrophobicity profiling revealed similar distributions of hydrophobic and hydrophilic residues in both sequences (Figure 49). Multiple extended hydrophobic segments were aligned between the two proteins, corresponding to predicted transmembrane domains. Each protein contained four to six hydrophobic regions of sufficient length to span lipid bilayers. These transmembrane segments were primarily distributed throughout the central and C-terminal regions and were enriched in leucine, isoleucine, valine, phenylalanine, and tryptophan residues. Both sequences exhibited extended hydrophilic regions separating predicted transmembrane helices. These regions were enriched in glycine, serine, asparagine, and charged amino acids. Several aromatic residues, including tryptophan, phenylalanine, and tyrosine, were clustered within membrane-associated regions in both proteins.

Comparison of terminal regions revealed notable differences in length and composition. NoDGTT12 contained several insertions and extended segments, particularly in the N-terminal and C-terminal regions, resulting in an increased number of alignment gaps relative to NoDGTT5. These regions were characterized by lower conservation scores and higher proportions of charged and polar residues. The C- terminal region of NoDGTT12 was longer than that of NoDGTT5 and lacked extended hydrophobic segments.

Overall, the alignment revealed a mosaic pattern of sequence conservation, in which catalytic and membrane-associated regions were strongly preserved, whereas terminal and inter-helical regions exhibited pronounced divergence. NoDGTT5 and NoDGTT12 share conserved structural features, including comparable overall length, similar transmembrane organization, conservation of characteristic DGTT motifs, and analogous distributions of hydrophilic and hydrophobic domains.

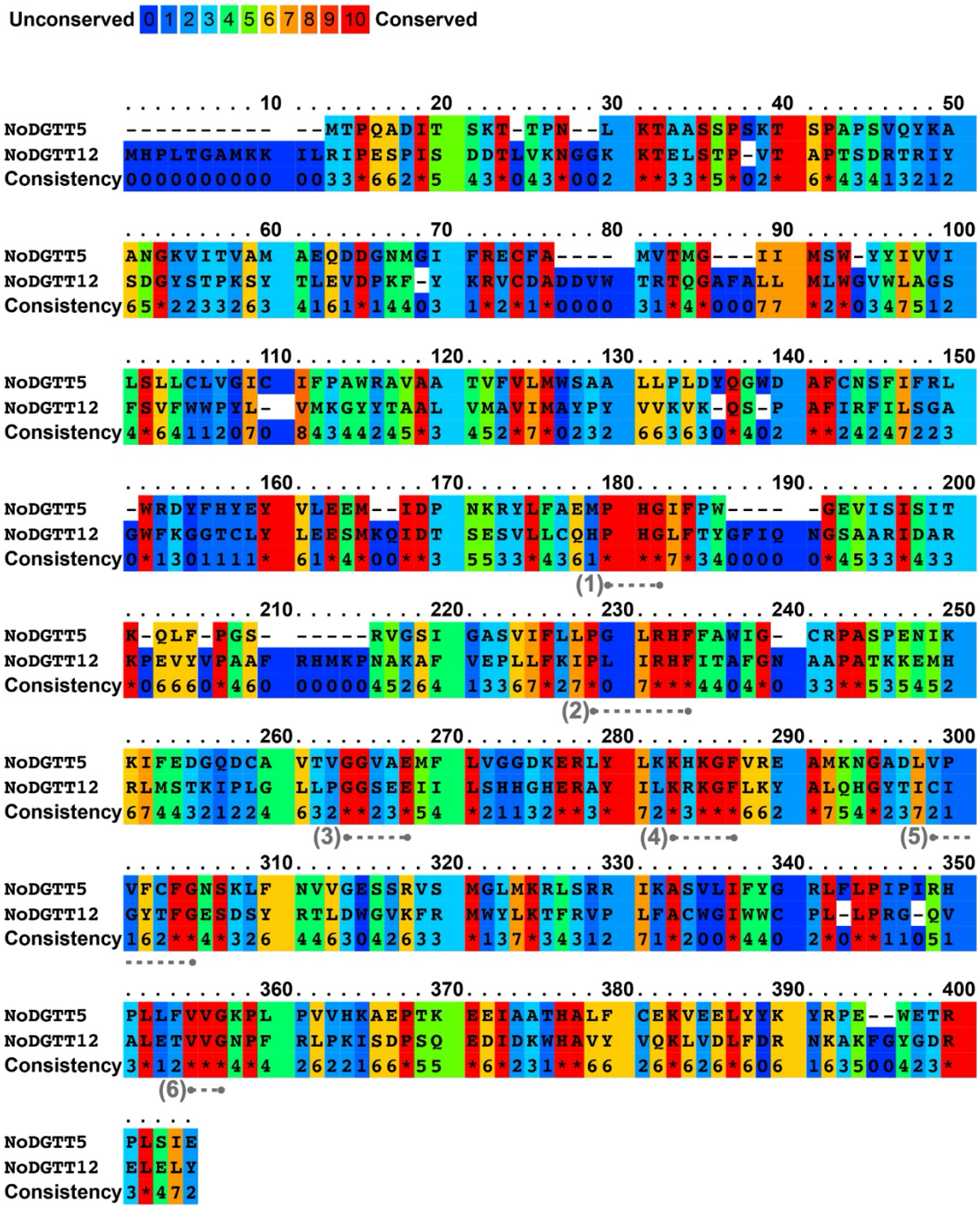

Figure 48. Conservation and motif architecture of NoDGTT5 and NoDGTT12 amino acid sequences. Sequence alignment of NoDGTT5 and NoDGTT12 highlighting conserved amino acid sequence motifs and overall residue conservation. Conserved blocks are indicated as: (1) PH block, (2) PR block, (3) GGE block, (4) RGFA block, (5) VPGF block, and (6) G block. Amino acid positions are numbered above the alignment. The "Consistency" line represents the conservation score at each position (0–10), where blue (0) indicates unconserved residues and red (10) indicates highly conserved residues across the aligned sequences. Asterisks (*) denote fully conserved positions, and dashes indicate alignment gaps introduced to optimize sequence similarity.

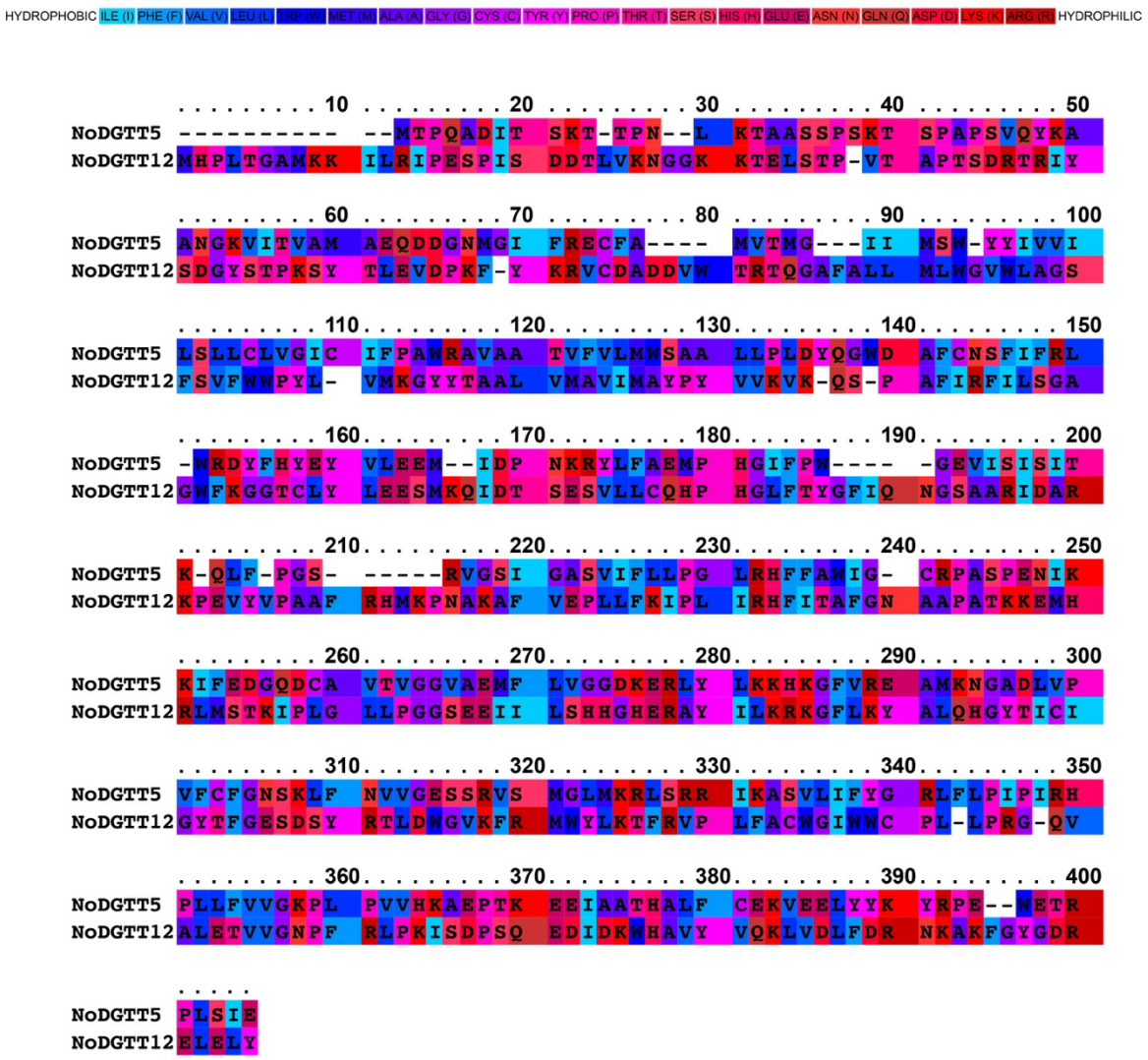

Figure 49. Hydrophobicity-based sequence alignment of NoDGT5 and NoDGT12 proteins. Multiple sequence alignment of the amino acid sequences of NoDGT5 and NoDGT12 is shown from residues 1–400. Amino acids are color-coded according to physicochemical properties, with a gradient from hydrophobic (blue/cyan) to hydrophilic (red) as indicated in the legend above the alignment. Residue numbers are shown above each block in increments of 10. Identical and conserved residues are aligned vertically, while dashes indicate gaps introduced to optimize the alignment. Conserved regions and stretches of hydrophobic residues are evident throughout the sequences, highlighting shared structural features between NoDGT5 and NoDGT12.

5 Discussion

5.1 Extensive structural diversification defines the DGTT protein family of *Nannochloropsis oceanica* CCMP1779

The present study provides the comprehensive structural and functional overview of the complete DGTT gene family encoded in the genome of *N. oceanica* CCMP1779. *In silico* analyses, based on sequences originally annotated in the genome of this strain by Vieler *et al*. (2012) showed the presence of twelve putative *DGTT* genes, designated *NoDGTT1–NoDGTT12*, encoding proteins with predicted molecular weights ranging from approximately 38 kDa to over 122 kDa and exhibiting substantial variation in membrane topology and domain organization. Similar to other DGAT/DGTT proteins commonly found in eukaryotic cells, TMD predictions using DeepTMHMM and Protter online tools demonstrated that all the NoDGTT isoforms represent integral membrane proteins. However, the number, distribution, and orientation of predicted transmembrane helices differed markedly among family members. The smallest isoforms, including NoDGTT7, NoDGTT8, and NoDGTT9, displayed compact architectures with one to three membrane-spanning regions, whereas intermediate-sized proteins such as NoDGTT1, NoDGTT3, NoDGTT5, NoDGTT6, NoDGTT11, and NoDGTT12 contained one to four helices interspersed with extended hydrophilic loops. In contrast, NoDGTT4 exhibited an unusually complex topology with up to twelve predicted TMDs and an extended polytopic arrangement. Comparable structural heterogeneity has been reported for DGTT families in other microalgal species, including model *C. reinhardtii* (Liu *et al.,* 2016; Bagnato *et al.,* 2017), *C. zofingiensis* (Mao *et al.,* 2019), *L. incisa* (Zienkiewicz *et al.,* 2018), *H. pluvialis* (Ma *et al.,* 2021), and *C. zofingiensis* (Mao *et al.,* 2019). These studies consistently demonstrate that DGTT protein families are characterized by extensive variation in size and topology, suggesting that structural diversification represents a conserved feature associated with functional differentiation in algal lipid metabolism.

The exceptional size and complexity of NoDGTT4 are particularly noteworthy. Similar large and highly polytopic DGTT-like proteins are rare in algae and have not been reported in detail for most model species. This distinctive architecture suggests that NoDGTT4 may not function primarily as a conventional terminal acyltransferase but may instead participate in auxiliary processes such as lipid remodeling, membrane reorganization, or metabolic channeling, as proposed previously by Zienkiewicz *et al*. (2017).

5.2 Conserved ER localization supports a central role of NoDGTTs in TAG assembly

Subcellular localization predictions using DeepLoc 2.0 assigned all NoDGTT isoforms predominantly to the ER, with probability values exceeding 0.70 for all family members and surpassing 0.83 for most isoforms. These results are fully consistent with experimental evidence demonstrating ER localization of DGAT and DGTT enzymes in diverse algal systems (Liu *et al.,* 2016; Zienkiewicz *et al.,* 2017; Wei *et al.,* 2017; Mao *et al.,* 2019). The ER represents the principal site of TAG assembly and LD biogenesis in microalgae, providing physical proximity to acyl-CoA pools, DAG substrates, and LDs formation machinery (Chapman and Ohlrogge, 2012; Li-Beisson *et al.,* 2019). The uniform ER targeting of NoDGTT isoforms therefore supports their direct involvement in the terminal step of TAG biosynthesis.

In addition to dominant ER localization, several isoforms displayed minor predicted associations with other cellular compartments, including mitochondria, plastids, Golgi apparatus, and vacuoles. Notably, NoDGTT4 exhibited elevated probabilities for Golgi and vacuolar localization relative to other family members. Similar secondary targeting patterns have been reported for DGTTs in *L. incisa* and *C. zofingiensis* and may reflect partial involvement in lipid trafficking or turnover pathways (Zienkiewicz *et al.,* 2018; Mao *et al.,* 2019).

Interestingly, unlike higher plants, which possess cytosolic DGAT type 3 enzymes (Ayme *et al.,* 2018; Han *et al.,* 2022), and *C. reinhardtii*, which encodes a functional DGAT type 3 homolog (Bagnato *et al.,* 2017; Carro *et al.,* 2022), *Nannochloropsis* species appear to rely almost exclusively on ER-localized DGTT and DGAT1-type enzymes for TAG synthesis. This compartmental specialization may enhance metabolic efficiency and facilitate rapid TAG accumulation under stress conditions.

5.3 Structural diversification reflects functional specialization within the NoDGTT family

The pronounced heterogeneity in molecular size, membrane topology, and predicted domain organization strongly suggests that the NoDGTT family is functionally stratified rather than redundant. Similar conclusions have been drawn from comparative analyses of DGTT families in *C. reinhardtii*, *C. zofingiensis*, and *L. incisa*, where only subsets of isoforms exhibit strong TAG-synthesizing activity in heterologous systems (Sanjaya *et al.,* 2013; Liu *et al.,* 2016; Mao *et al.,* 2019; Zienkiewicz *et al.,* 2017, 2018). Smaller NoDGTT isoforms with compact architectures may represent streamlined catalytic units optimized for basal TAG turnover or rapid deployment under specific physiological conditions. In contrast, intermediate-sized proteins with extended loop regions may provide increased conformational flexibility and regulatory capacity, facilitating integration of TAG synthesis with cellular signalling and metabolic control. The presence of large hydrophilic regions in these isoforms is consistent with proposed regulatory functions of DGTT loops observed in other algal systems (Mao *et al.,* 2019; Ma *et al.,* 2021).

The exceptionally complex NoDGTT4 likely represents a specialized evolutionary innovation. Its extensive membrane embedding and unusual topology suggest potential involvement in multi-enzyme complexes or LD-ER contact sites, which have been implicated in efficient TAG packaging and remodeling (Zienkiewicz *et al.,* 2016; Wei *et al.,* 2017). Such structural specialization may allow NoDGTT4 to participate in processes beside simple TAG synthesis, including lipid recycling during stress recovery.

Importantly, the structural stratification observed *in silico* is reflected in the functional heterogeneity revealed by heterologous expression experiments presented in this study. Only a subset of structurally intermediate isoforms, most notably NoDGTT5 and NoDGTT12, exhibited strong TAG-synthesizing activity in yeast, whereas compact isoforms such as NoDGTT7, NoDGTT8, and NoDGTT11 showed limited functionality. This correspondence between architecture and activity supports the hypothesis that structural diversification underpins enzymatic specialization within the NoDGTT family.

5.4 *NoDGTT* gene family expansion as an adaptive strategy for metabolic flexibility of *Nannochloropsis oceanica* CCMP1779

The expansion and diversification of the *DGTT* gene family in *N. oceanica* CCMP1779 represent a distinctive genomic feature that reinforces the exceptional oleaginous capacity of this species. Comparative genomic analyses have demonstrated that *Nannochloropsis* genomes are characterized by compact size, high coding density, and extensive enrichment of lipid biosynthesis-related genes, including an unusually large repertoire of *DGTT*s (Vieler *et al.,* 2012; Wang *et al.,* 2014; Li *et al*., 2016). Phylogenomic reconstruction indicates that these *DGTT* genes originated from multiple ancestral sources associated with secondary endosymbiosis and ancient genome pooling events, followed by selective retention and diversification (Wang *et al.,* 2014). Horizontal gene transfer and lineage-specific duplication have further contributed to the expansion of lipid-related gene families in *Nannochloropsis* species, creating a mosaic genomic architecture that favors metabolic innovation (Wang *et al.,* 2014; Zienkiewicz *et al.,* 2016). Such genomic plasticity provides a structural basis for the evolution of complex regulatory networks capable of supporting rapid metabolic reprogramming in response to environmental stress. So far obtained results as well as the results of this study support the hypothesis that following gene duplication, *DGTT* paralogs in *N. oceanica* species appear to have undergone extensive subfunctionalization and neofunctionalization, resulting in enzymes with distinct regulatory profiles, substrate preferences, and catalytic properties (Wang *et al*., 2014). Similar evolutionary trajectories have been documented for DGAT families in higher plants and oleaginous fungi, where duplication events facilitate specialization toward stress-responsive, developmental, or tissue-specific functions (Turchetto-Zolet *et al.,* 2011; Chapman and Ohlrogge, 2012). In microalgae, this process is particularly pronounced, reflecting the strong selective pressure imposed by fluctuating nutrient and light regimes in aquatic environments.

Transcriptomic studies provide further evidence that diversification of NoDGTT-encoding genes in *N. oceanica* CCMP1779 is associated with differential regulatory integration. Time-resolved transcriptome and lipidome analyses demonstrated that only a subset of these genes is strongly induced during nitrogen deprivation, while others remain constitutively expressed or display complex temporal patterns (Li *et al.*, 2014; Zienkiewicz *et al*., 2020). These observations indicate that individual DGTT paralogs are embedded within distinct regulatory circuits that respond to specific metabolic and environmental cues. Detailed expression profiling by Zienkiewicz *et al*. (2017, 2020) further revealed that *NoDGTT1–NoDGTT6* are strongly upregulated under nitrogen deprivation, whereas *NoDGTT7–NoDGTT12* show relatively stable expression under both N+ and N- conditions. Such transcriptional profiles suggest functional partitioning between stress-inducible and housekeeping-like *NoDGTT* isoforms. The stress-responsive *NoDGTT*s appear to support rapid TAG accumulation during growth arrest, while constitutively expressed isoforms may contribute to basal lipid turnover and metabolic buffering during active growth. Comparable regulatory diversification has been observed in *C. reinhardtii*, where only selected *DGTT* genes respond strongly to nitrogen limitation (Miller *et al.,* 2010; Deng *et al.,* 2012), and in other oleaginous algae such as *C. zofingiensis* and *L. incisa* (Zienkiewicz *et al.,* 2018; Mao *et al.,* 2019). These parallels indicate that transcriptional specialization of DGAT/DGTT families represents a conserved evolutionary strategy for optimizing lipid storage under variable environmental conditions.

At the metabolic level, the expanded DGTT family most likely enables to coordinate TAG biosynthesis with large-scale remodeling of central carbon metabolism in *N. oceanica* cells. Under nitrogen deprivation, carbon flux is redirected from protein and carbohydrate pools toward glycerolipid synthesis through coordinated regulation of glycolysis, pyruvate dehydrogenase, β-oxidation, and transport systems (Li *et al.,* 2014; Banerjee *et al.,* 2017; Zienkiewicz *et al*., 2020). The induction of *NoDGTT* expression most probably forms a critical downstream effector of this reprogramming, converting redistributed carbon into stable storage lipids.

The presence of multiple NoDGTT isoforms may also facilitate efficient regulation of fatty acid channeling into TAGs. Lipidomic analyses in *N. oceanica* IMET1 strain have shown that early TAG species accumulating during nitrogen stress are enriched in saturated and monounsaturated FAs, whereas polyunsaturated TAG species increase at later stages (Li *et al.,* 2014). This temporal pattern suggests that different DGTT isoforms may preferentially utilize distinct DAG and acyl-CoA pools, thereby shaping TAG composition during stress progression. Functional divergence among DGTT-encoding genes may therefore contribute not only to quantitative regulation of TAG synthesis but also to qualitative control of lipid composition in *N. oceanica* strains. From an evolutionary perspective, the maintenance of an unusually large *DGTT* gene family in *Nannochloropsis* genus implies strong selective advantages associated with metabolic flexibility. Marine environments are characterized by frequent fluctuations in nutrient availability, light intensity, temperature, and salinity. Under such conditions, organisms capable of rapidly adjusting carbon partitioning and energy storage gain a substantial fitness advantage. Expansion of DGTT paralogs enables *N. oceanica* to deploy specialized enzymes optimized for distinct physiological states, thereby ensuring efficient TAG synthesis across a wide range of environmental scenarios. This adaptive significance is further supported by comparative genomic evidence showing that gene dose expansion in lipid biosynthesis pathways is a defining feature of diverse *Nannochloropsis* species (Wang *et al.,* 2014; Zienkiewicz *et al*., 2016). Rather than relying on a single dominant acyltransferase, these organisms utilize a diversified enzymatic toolkit that enhances robustness and resilience of lipid metabolism. Importantly, the functional analyses presented in this thesis seem to support this evolutionary model. The strong divergence in catalytic performance observed among NoDGTT isoforms in heterologous and native systems reflects underlying specialization shaped by long-term selection. High-performance enzymes such as NoDGTT5 reported by Zienkiewicz *et al*. (2017) and NoDGTT12 showed in this study likely represent evolutionary solutions optimized for high-flux TAG synthesis, whereas weaker isoforms may fulfill auxiliary or condition-specific roles.

5.5 Functional divergence of NoDGTT isoforms revealed by TAG-less yeast complementation

Heterologous expression of microalgal DGTT-encoding genes in the TAG-deficient *S. cerevisiae* H1246 strains has become an established experimental strategy for dissecting DGAT functionality, substrate specificity, and regulatory potential in a simplified and genetically tractable background (Liu *et al*., 2016; Zienkiewicz *et al*., 2018; Mao *et al*., 2019; Cui *et al*., 2021; Ma *et al*., 2021). This system eliminates endogenous DGAT and PDAT activities and therefore enables direct attribution of TAG accumulation to the introduced heterologous enzyme. Previous studies employing this platform have successfully

characterized DGTTs from such key model microalgae like *C. reinhardtii* (Liu *et al*., 2016), *H. pluvialis* (Ma *et al*., 2021), *C. zofingiensis* (Mao *et al*., 2019) or *L. incisa* (Zienkiewicz *et al*., 2018), demonstrating its robustness and comparability across phylogenetically distant algae.

Consequently, in the present study, multiple *DGTT* genes from *N. oceanica* CCMP1779 were successfully expressed in H1246 yeast mutant under control of the galactose-inducible GAL1 promoter. This approach was designed to maximize transcript diversity and to ensure representation of selected *NoDGTT* isoforms. Initial functional screening using BODIPY™ 505/515 staining revealed substantial differences in the ability of individual *NoDGTT*s to restore TAG biosynthesis in the transgenic H1246 lines. Transformants expressing *NoDGTT5* exhibited strong TAG accumulation and numerous well-defined LDs, confirming previous findings that identified this isoform as a major contributor to TAG synthesis in heterologous systems (Zienkiewicz *et al.,* 2017). Accordingly, *NoDGTT5* served as the positive control in this study. In contrast, transformants expressing *NoDGTT7*, *NoDGTT8*, and *NoDGTT11* produced only sparse LDs, indicating limited TAG-forming activity under the applied experimental conditions. Most strikingly, expression of *NoDGTT12* resulted in the highest BODIPY™ fluorescence intensity and the formation of large, abundant LDs, exceeding even the levels observed for the *NoDGTT5*-expressing positive control. This pronounced phenotypic variability among closely related *NoDGTT* family members reflects functional specialization that has been consistently observed in microalgal *DGAT*/*DGTT* families. Similar divergence was reported for *DGTTs* from *C. reinhardtii*, where only expression of *CrDGTT1*, *CrDGTT2*, and *CrDGTT3* resulted in complementation of TAG-less phenotype of yeast mutants, whereas *CrDGTT4* and *CrDGTT5* were largely inactive (Sanjaya *et al*., 2013; Liu *et al*., 2016). In *C. zofingiensis*, *CzDGTT5* exhibited the highest complementation efficiency, while several other DGTTs showed marginal activity (Mao *et al*., 2019). Similar functional divergence has been reported for DGTT families in *N. oceanica* and *L. incisa* (Zienkiewicz *et al*. 2017, 2018).

The limited phenotype observed in H1246 yeast transformants expressing certain *NoDGTT* isoforms does not necessarily indicate a lack of function in their native algal context, as heterologous systems may not fully recapitulate algal regulatory or metabolic environments. Instead, several factors may contribute to the apparent inactivity observed in yeast. First, inappropriate substrate availability. *S. cerevisiae* predominantly synthesizes C16:0, C16:1, C18:0, and C18:1 FAs, whereas *N. oceanica* produces substantial amounts of long-chain FAs and PUFAs, including EPA (C20:5). DGTTs that evolved to preferentially utilize such substrates may therefore exhibit low activity in yeast due to substrate mismatch. This limitation has been demonstrated, for example, for DGAT1 from *H. pluvialis*, whose activity in the H1246 background was constrained by the absence of preferred polyunsaturated FAs and could be enhanced by FAs feeding (Ma *et al.,* 2021). Consistent with this, DGTTs adapted to long-chain or polyunsaturated substrates may display reduced activity in yeast, particularly in the absence of exogenous FAs supplementation (Liu *et al.,* 2016; Mao *et al.,* 2019; Cui *et al.,* 2021; Ma *et al.,* 2021). Second, improper folding, membrane insertion, or targeting of microalgal DGTT proteins in yeast which may compromise their enzymatic activity. DGTT proteins are membrane-associated enzymes that localize to specialized ER subdomains closely associated with LDs biogenesis (Liu *et al*., 2016; Zienkiewicz *et al*., 2017). Differences in ER architecture and LDs formation between algae and yeast may therefore influence protein functionality. Third, post-

translational regulation and protein–protein interactions may also be required for full DGTT activity *in vivo*. Functional divergence within the DGTT family, including neofunctionalization toward alternative acyltransferase activities, has been reported in microalgae, exemplified by the conversion of HpDGTT2 into a lysophosphatidic acid acyltransferase (Ma *et al*., 2021). Such divergence suggests that some DGTT isoforms no longer function primarily as TAG synthases (Mao *et al*., 2019, Ma *et al*., 2021;). Fourth, sequence variation within conserved DGTT motifs may further contribute to functional differences. Previous analyses highlighted partial divergence of the YFH and HPHG motifs in DGTT proteins from *N. oceanica* as well as other microalgal species (Zienkiewicz *et al*., 2017), and suggested that variation in these regions may affect enzyme activity. In addition, comparative analyses revealed extensive amino acid substitutions among DGTT isoforms that correlate with functional divergence (Ma *et al*., 2019), indicating that even subtle sequence changes can influence catalytic efficiency and heterologous performance.

Collectively, the heterogeneous phenotypes observed in the TAG-deficient yeast strain H1246 likely reflect a combination of intrinsic enzymatic specialization, host-dependent substrate availability, and evolutionary divergence within the DGAT/DGTT family (Liu *et al.,* 2016; Zienkiewicz *et al.,* 2017, 2018; Ma *et al.,* 2021). Functional complementation performed in thus study consistently demonstrate that individual DGTT isoforms from *N. oceanica* most probably differ in their substrate preferences and catalytic efficiency, and that their apparent activities in yeast might be influenced by the limited acyl-CoA and DAG pools of the host. This is also supported by previous reports, where only a subset of *N. oceanica* DGTTs, particularly NoDGTT5 and NoDGAT1A, displayed robust activity in heterologous systems, whereas several paralogs show weak or no detectable function, consistent with their divergent evolutionary origins and regulatory patterns (Wei *et al.,* 2017; Zienkiewicz *et al.,* 2017). These observations suggest also that superior performance in yeast likely reflects a favorable match between enzyme substrate specificity and host lipid metabolism, rather than a universal property of individual DGTT members.

5.6 NoDGTT12 is a high-efficiency TAG synthase in *Saccharomyces cerevisiae*

The most remarkable finding of this study is the exceptionally strong phenotype induced by *NoDGTT12* expression in the TAG-deficient yeast strain H1246. Microscopic analyses revealed extensive formation of LDs throughout the cytoplasm, while TLC confirmed robust restoration of TAG biosynthesis. Quantitative lipid profiling further demonstrated that TAG accounted for more than 30% of total cellular lipids in *NoDGTT12*-expressing lines, compared with approximately 1% in empty-vector controls. This level of accumulation represents one of the highest TAG contents reported for microalgal *DGAT*s/*DGTT*s expressed in yeast and exceeds those observed for many previously characterized enzymes of this family. Comparable high-efficiency complementation has been reported for *NoDGTT5*, *CzDGTT5*, and *CrDGTT2/3* (Liu *et al.,* 2016; Zienkiewicz *et al.,* 2017; Mao *et al.,* 2019). However, the extent of TAG accumulation in H1246 yeast mutant varies substantially among studies and enzymes. While expression of some *DGAT*s/*DGTT*s, such as *CzDGTT5*, promote moderate TAG levels (approximately 10–15% of TFAs), others, including *NoDGTT5* and *CzDGAT1A*, support substantially higher accumulation, reaching ~27–

53% of total FAs (Sanjaya *et al.,* 2013; Liu *et al.,* 2016; Zienkiewicz *et al.,* 2017; Mao *et al.,* 2019). The performance of *NoDGTT12* therefore places this enzyme among the most potent microalgal *DGAT*s/*DGTT*s identified to date. Moreover, the formation of numerous large and well-defined LDs indicates that expression of *NoDGTT12* not only enhances TAG synthesis but also facilitates efficient lipid packaging and storage within yeast cells.

Interestingly, as mentioned above, previous transcriptomic analyses in *N. oceanica* CCMP1779 indicated that *NoDGTT7–NoDGTT12* are not strongly induced under N deprivation (Zienkiewicz *et al*., 2017, 2020). Thus, *NoDGTT12* does not belong to the classical stress-responsive *DGTT* cluster, which includes *NoDGTT1–NoDGTT6*. Its strong activity in yeast therefore suggests that transcriptional regulation in the native host does not necessarily reflect intrinsic catalytic potential. Instead, *NoDGTT12* may function under specific physiological conditions, developmental stages, or subcellular contexts that were not fully captured in available transcriptomic datasets. The ability of *NoDGTT12* to induce high TAG accumulation in H1246 yeast mutant suggests also that this enzyme possesses high intrinsic catalytic efficiency and broad compatibility with eukaryotic DAG and acyl-CoA pools. Such properties resemble those of *C. reinhardtii CrDGTT2* and *CrDGTT3*, which were shown to efficiently restore TAG synthesis and to function across multiple host systems (Sanjaya *et al*., 2013; Liu *et al*., 2016). Likewise, *CzDGTT5* has been reported to display strong cross-species functionality in yeast and microalgal hosts (Mao *et al*., 2019). These observations indicate that a subset of microalgal DGTT-encoding genes has evolved structural features that enable robust activity of their protein products across divergent cellular environments.

A key strength of this work is its direct connection to previous functional studies of the *DGTT* gene family in *N. oceanica* CCMP1779. Previous research found that *NoDGTT5* was the most effective of the nitrogen stress–induced *NoDGTT* enzymes (*NoDGTT1–NoDGTT6*) in restoring TAG biosynthesis in H1246 yeast strain (Zienkiewicz *et al*., 2017). That study was consistent with the finding that *NoDGTT5* promotes LDs formation, enhances TAG accumulation in algae and plants, and preferentially incorporates unsaturated FAs into TAGs. The expression of *NoDGTT12* resulted in an even more pronounced phenotype than that observed for *NoDGTT5*. TAG levels exceeded 30% of total cellular lipids, and LDs were larger and more abundant. Thus, although *NoDGTT5* remains a highly efficient *DGTT*, these data indicate that *NoDGTT12* surpasses *NoDGTT5* in its capacity to stimulate TAG accumulation under the applied experimental conditions. Importantly, this difference is quantitative rather than qualitative, as both enzymes are clearly functional and highly active in *S. cerevisiae* H1246 expression system. This observation refines rather than contradicts previous conclusions regarding *NoDGTT5* made by Zienkiewicz *et al*. (2017).

As proposed above, this diversification likely reflects adaptation to the unique evolutionary history of *Nannochloropsis* genus, which arose through secondary endosymbiosis within the heterokont lineage, resulting in a mosaic genome that provided abundant raw material for gene duplication and subsequent functional divergence (Wang *et al*., 2014). As consequence of duplication, *NoDGTT* paralogs appear to have divided their original roles and gained new functions, resulting in enzymes with distinct catalytic properties, regulatory features, and substrate preferences. The exceptional activity of NoDGTT12

suggests that certain members of this enzymatic family have evolved specialized roles in TAG biosynthesis, possibly optimized for rapid lipid accumulation under specific environmental or physiological conditions such as nitrogen deprivation, high light stress, or nutrient imbalance (Zienkiewicz *et al*., 2016, 2020). Meanwhile, different NoDGTT isoforms appear to be optimized for distinct regulatory regimes, substrate pools, and cellular environments. For example, NoDGTT5 may function primarily as a stress-responsive enzyme that promotes TAG accumulation during nutrient deprivation, whereas NoDGTT12 may serve as a high-throughput acyltransferase operating under alternative physiological conditions.

Detailed biochemical characterization of NoDGTT12 presented here showed that possesses a broad substrate spectrum combined with distinct substrate preferences. *In vitro* assays using microsomal fractions demonstrated measurable activity toward saturated, monounsaturated, and polyunsaturated acyl-CoAs, including C16:0-CoA, C18:1-CoA, C18:2-CoA, C18:3-CoA, C20:4-CoA, and C22:1-CoA. Notably, the highest catalytic activities were consistently observed with unsaturated substrates, particularly C18:3-CoA, C20:5-CoA, C18:2-CoA, and C22:1-CoA. In parallel, DAG selectivity assays revealed a clear preference for C18:1-DAG over C22:1-DAG, indicating that NoDGTT12 exhibits specificity at both the acyl donor and acyl acceptor levels. Similar biochemical approaches have been successfully applied to characterize substrate preferences of diverse microalgal DGTT and DGAT proteins using yeast heterologous systems and *in vitro* assays (Liu *et al*., 2016; Wei *et al*., 2017; Zienkiewicz *et al*., 2017; Mao *et al*., 2019; Cui *et al*., 2021). For example, CrDGTT1 from *C. reinhardtii* has been shown to preferentially utilize polyunsaturated acyl-CoAs, whereas CrDGTT2 showed preference towards monounsaturated substrates and CrDGTT3 for C16 acyl-CoAs (Liu *et al*., 2016). Similarly, in *C. zofingiensis*, CzDGAT1A and CzDGTT5 displayed overlapping but distinct acyl-CoA and DAG specificities (Mao *et al*., 2019). Finally, in *N. oceanica*, NoDGTT5 exhibited broad substrate specificity with a strong preference toward unsaturated C18 acyl-CoAs, whereas NoDGAT1A preferentially incorporates saturated and monounsaturated acyl-CoAs into TAGs (Wei *et al*., 2017; Zienkiewicz *et al*., 2017).

Selectivity of algal DGATs/DGTTs is further reflected in TAG composition in heterologous hosts. Expression of *CrDGTTs*, *CzDGAT1A*, *CzDGTT5*, *NoDGTT5*, and *NoDGAT1A* in yeast or plants results in selective enrichment of unsaturated FAs, C18:1 and C18:3, accompanied by reduced proportions of saturated species (Sanjaya *et al*., 2013; Wei *et al*., 2017; Zienkiewicz *et al*., 2017; Mao *et al*., 2019). These observations indicate that many algal DGATs/DGTTs actively reshape TAG composition rather than merely increasing TAG abundance. Consistent with this trend, the pronounced preference of NoDGTT12 for unsaturated acyl-CoAs suggests that it similarly contributes to the formation of TAGs enriched in MUFAs and PUFAs.

Beside acyl-CoA selectivity, utilization of specific DAG species represents another important layer of regulation in TAG biosynthesis. Studies on CrDGTTs and CzDGAT1A have shown a preference for eukaryotic-type DAGs enriched in C18 acyl chains, whereas NoDGAT1A favors C16:0/C18:1 and C18:1/C18:1 DAG species (Liu *et al*., 2016; Wei *et al*., 2017; Mao *et al*., 2019). In agreement with these

findings, NoDGTT12 displays a clear preference for C18:1-DAG over C22:1-DAG species. Such coordinated preferences for both acyl donors and acceptors are characteristic of ER-localized TAG biosynthesis and are consistent with models in which acyl flux from membrane phospholipids is redirected toward storage lipid formation (Liu *et al*., 2016; Zienkiewicz *et al*., 2018).

The functional properties of NoDGTT12 seem also to be reflected in its primary amino acid sequence and predicted structural organization. At the sequence level, NoDGTT12 shares the characteristic architecture of type 2 DGATs, including multiple predicted TMDs and conserved acyltransferase motifs concentrated in the C-terminal region (Liu *et al*., 2016; Zienkiewicz *et al*., 2017; Ma *et al*., 2021). Comparative analyses have revealed conserved PH and HPHG-related motifs that are thought to be critical for catalytic activity (Zienkiewicz *et al*., 2017; Mao *et al*., 2019). Similar motifs are present also in DGATs/DGTTs from *H. pluvialis* and *L. incisa*, indicating strong evolutionary conservation (Zienkiewicz *et al*., 2018; Ma *et al*., 2021). DGTT proteins are also enriched in hydrophobic amino acids and contain multiple membrane-spanning regions that promote stable integration into the ER and appropriate positioning of the catalytic domain toward cytosolic substrate pools (Liu *et al*., 2016; Zienkiewicz *et al*., 2018). Variations in terminal regions and hydrophobic segment distribution among algal DGTTs are proposed to influence enzyme stability, membrane topology, and substrate accessibility (Zienkiewicz *et al*., 2018; Ma *et al*., 2021). In NoDGTT12, these features likely contribute to efficient membrane anchoring and high catalytic efficiency. Beside overall topology, increasing evidence suggests that conformational flexibility is an important determinant of enzyme activity performance. Regions enriched in charged, glycine, or histidine residues may facilitate conformational dynamics, substrate channeling, and protein - protein interactions (Cui *et al*., 2021; Ma *et al*., 2021). In NoDGTT12, comparable regions may enhance catalytic adaptability and regulatory potential, although their precise roles remain to be elucidated.

Taken together, the combined biochemical, metabolic, and structural evidence indicates that DGTTs integrate conserved catalytic machinery with variable membrane topology and substrate-binding features, enabling functional specialization within expanded algal DGTT families. The demonstrated broad substrate spectrum, strong preference for unsaturated acyl-CoAs, and selective utilization of 18:1-DAG establish NoDGTT12 as a versatile and efficient TAG-synthesizing enzyme. Its functional properties closely resemble those of CrDGTT2, NoDGTT5, and HpDGAT1, while also displaying distinctive features that may confer enhanced adaptability (Liu *et al*., 2016; Wei *et al*., 2017; Zienkiewicz *et al*., 2017; Cui *et al*., 2021).

5.7. Functional validation of *NoDGTT12* by its overexpression in *Nannochloropsis oceanica* CCMP1779

In this study, NoDGTT12 was identified as a highly active DGAT based on its strong performance in heterologous yeast assays and was subsequently overexpressed in *N. oceanica* CCMP1779 to evaluate its native function in TAG biosynthesis. Successful cloning, transformation, and expression of the *NoDGTT12-CFP* fusion construct were confirmed by immunoblotting and confocal microscopy, demonstrating stable accumulation of the recombinant protein in multiple independent lines.

At cellular level, NoDGTT12-CFP fusion protein localized predominantly in the cytoplasm and in close proximity to LDs stained by BODIPY™ 505/515, suggesting a close spatial association between the enzyme and sites of TAG deposition. This subcellular localization is consistent with the expected role of DGTTs, which are generally associated with ER membranes and LDs biogenesis in microalgae and other eukaryotic cells (Liu and Benning 2013; Farese and Walther 2023). Interestingly, the observed localization pattern of the NoDGTT12-CFP fusion protein is similar to that previously reported for the NoDGTT5-CFP construct in *N. oceanica* CCMP1779 cells by Zienkiewicz *et al*. (2017). These findings support the functional involvement of NoDGTT12 in TAG assembly and LDs formation, further confirming its prominent role in TAG biosynthesis in *N. oceanica* CCMP1779.

Biochemical analyses further demonstrated that *NoDGTT12* overexpression resulted in enhanced TAG accumulation under N-replete conditions, as evidenced by stronger TAG bands in TLC and increased TAG proportions relative to total lipids. These results indicate that increasing *NoDGTT* gene dosage can partially decouple TAG synthesis from nutrient stress, a major bottleneck in microalgal lipid production. The observed enhancement of TAG accumulation observed in *NoDGTT12*-overexpressing *N. oceanica CCMP1779* lines is consistent with previous studies in which DGTT-encoding genes were overexpressed in diverse microalgal species. In *P. tricornutum*, overexpression of *PtDGAT2D* resulted in a twofold increase in lipid content and enhanced carbon flux toward TAG synthesis (Dinamarca *et al*., 2017). Similarly, overexpression of other gene from this family in the same microalga increased TAG accumulation by approximately 35% (Niu *et al*., 2013). In another oleaginous microalga *Neochloris oleoabundans*, overexpression of endogenous *NeoDGAT2* led to 1.8- to 3.2-fold increases in TAG content and productivity (Klaitong *et al*., 2017), with long-term genetic stability over several years. Moreover, co-overexpression of *NeoDGAT2* with another Kennedy pathway gene, *NeoLPAT1* further enhanced TAG productivity and total lipid accumulation (Chungjatupornchai and Fa-Aroonsawat 2021). In contrast, in *C. reinhardtii*, constitutive *DGTT* overexpression often failed to significantly increase TAG levels unless driven by inducible promoters or combined with stress treatments (La Russa *et al*., 2012; Wang *et al*., 2018). These findings highlight species-specific differences in metabolic regulation and indicate that oleaginous algae such as *N. oceanica* and *N. oleoabundans* are more suitable to *DGTT*-based engineering. Collectively, the results presented in the frame of this study confirm that *NoDGTT12* belongs to a subset of highly active *DGTT* isoforms capable of substantially enhancing TAG accumulation, similar to *NoDGTT5* in *N. oceanica* (Zienkiewicz *et al*., 2017) or *PtDGAT2B* in *P. tricornutum* (Haslam *et al*., 2020).

Overexpression of *NoDGTT12* in *N. oceanica* CCMP1779 resulted in marked alterations in FAs profiles in both total lipid and TAG fractions in transgenic lines. Specifically, they showed increased proportions of C16:0 and C16:1 FAs and reduced levels of long-chain PUFAs, including C20:5 (EPA). Similar shifts toward saturated and monounsaturated FAs have been reported in *DGTT*-overexpressing *N. oleoabundans* (Klaitong *et al*., 2017) and *P. tricornutum* (Niu *et al*., 2013), suggesting that many DGTTs preferentially utilize C16 acyl-CoA substrates in microalgal expression systems. Indeed, this substrate preference is also supported by the present results, which show a significant enrichment of C16:0 and C16:1 and a simultaneous reduction of EPA in the TAG fraction of *NoDGTT12*-overexpressing lines of *N. oceanica*

CCMP1779, and likely contributes to the remodeling of TAG pools observed in this study. By contrast, some microalgal *DGTT* isoforms, such as *PtDGAT2B* from diatom *P. tricornutum* show broader substrate specificity and promote incorporation of long-chain PUFAs into TAG (Haslam *et al*., 2020). It can't be excluded, that the reduction in EPA observed in *NoDGTT12*-overexpressing lines of *N. oceanica* CCMP1779 lines therefore suggests that this enzyme favors medium-chain saturated and monounsaturated acyl-CoAs over highly unsaturated substrates.

Interestingly, the substrate specificity of NoDGTT12 observed in this study in heterologous yeast system differed from that deduced from *in vivo* analyses in *N. oceanica* CCMP1779 transgenic lines. In microsomal fractions isolated from transgenic *S. cerevisiae* H1246, NoDGTT12 displayed broad substrate tolerance and showed highest catalytic activity toward unsaturated acyl-CoAs, including C18:3-CoA, C20:5-CoA, C18:2-CoA, and C22:1-CoA, while exhibiting comparatively lower activity toward saturated substrates. Moreover, the enzyme preferentially utilized C18:1-DAG as an acyl acceptor *in vitro*. In contrast, expression of *NoDGTT12-CFP* fusion construct in its native algal host resulted in preferential accumulation of C16:0 and C16:1 in the TAG fraction and a concomitant reduction in C20:5, indicating an apparent *in vivo* preference toward medium-chain saturated and monounsaturated FAs. This discrepancy suggests that substrate selectivity of NoDGTT12 is strongly influenced by the cellular context, including differences in acyl-CoA pool composition, membrane lipid environment, and availability of competing metabolic pathways between yeast and microalgal cells. In yeast, the artificial expression system and simplified lipid metabolism may allow NoDGTT12 to access a wider range of substrates, thereby revealing its intrinsic catalytic flexibility. In contrast, in *N. oceanica* cells, substrate utilization is likely constrained by endogenous lipid fluxes, compartmentalization, and regulatory mechanisms that favor incorporation of abundant C16 acyl-CoAs into TAG. Similar context-dependent differences in DGAT substrate utilization have been reported for other microalgal and plant enzymes expressed in heterologous systems (Zienkiewicz *et al*., 2017; Haslam *et al*., 2020). These findings indicate that *in vitro* and heterologous assays reflect the inherent catalytic potential of NoDGTT12, whereas *in vivo* substrate incorporation in *N. oceanica* CCMP1779 is primarily shaped by host-specific metabolic networks, emphasizing the importance of evaluating DGTT function within its native cellular environment.

Nevertheless, from an applied perspective, such FA remodeling may be advantageous for biodiesel production, as higher proportions of C16:0 and C16:1 improve cetane number and oxidative stability (Klaitong *et al*., 2017). However, for nutraceutical applications targeting omega-3 FAs, the observed decrease in EPA represents a limitation that must be addressed through complementary metabolic engineering strategies.

The enhanced TAG accumulation observed in *NoDGTT12*-overexpressing lines under N-replete conditions suggests also a redirection of cellular carbon flux from growth-associated pathways toward TAG synthesis. Such metabolic reprogramming is consistent with previous reports in *P. tricornutum*, in which overexpression of *PtDGAT2D* increased carbon flux through central metabolic intermediates, including pyruvate and acetyl-CoA, thereby promoting enhanced lipid biosynthesis (Dinamarca *et al*., 2017). These

findings indicate that increased DGTT activity can effectively act as a metabolic sink, stimulating upstream pathways to supply precursors for TAG formation. However, excessive or unbalanced diversion of carbon toward storage lipids may also impose metabolic stress and disrupt cellular homeostasis. In *N. oceanica* CCMP1779, constitutive overexpression of *NoDGTT5* has been shown to induce a quiescence-like physiological state characterized by chloroplast degradation, reduced photosynthetic capacity, and markedly impaired growth, even under nutrient-replete conditions (Zienkiewicz *et al*. 2017). This suggests that while enhanced DGTT activity can promote TAG accumulation, its physiological consequences depend on the extent and regulation of carbon reallocation. Excessive diversion of carbon and energy toward TAG synthesis may therefore trigger stress-associated metabolic remodeling resembling nitrogen starvation. In the present study, although detailed growth and physiological analyses were not the primary focus, the increased TAG accumulation in *NoDGTT12*-overexpressing lines was not accompanied by pronounced morphological abnormalities or overt signs of cellular degeneration. This observation indicates that *NoDGTT12* overexpression may promote TAG accumulation through a more balanced and physiologically sustainable metabolic shift. through a more moderate and balanced metabolic shift than that induced by the action of *NoDGTT5*.

The contrasting physiological outcomes associated with *NoDGTT12* and *NoDGTT5* overexpression suggest functional specialization among *DGTT* isoforms in *N. oceanica* CCMP1779. As it has been mentioned above, transcriptomic analyses by Zienkiewicz *et al*. (2020) demonstrated that only a subset of *NoDGTT* genes (*NoDGTT1–NoDGTT6*) is strongly induced in response to nitrogen deprivation, whereas the remaining once, including *NoDGTT12* exhibit relatively stable, constitutive expression patterns under such conditions. The stress-responsive *NoDGTTs*, such as *NoDGTT5*, may therefore be tightly integrated into nutrient-sensing and survival pathways, and their forced overexpression may prematurely activate quiescence-related programs. In contrast, constitutively expressed *NoDGTTs*, like *NoDGTT12*, may primarily function in basal TAG turnover and lipid homeostasis, enabling enhanced TAG synthesis without severely disrupting cellular physiology.

From a metabolic engineering perspective, these findings highlight the importance of isoform selection for optimizing lipid productivity. While stress-inducible *DGTT*s can drive strong TAG accumulation, they may compromise growth and photosynthetic performance. In contrast, constitutively expressed *DGTT*s with high catalytic activity, such as *NoDGTT12*, appear better suited for sustained lipid production under favorable growth conditions. The successful exploitation of *NoDGTT12* in this study therefore demonstrates that targeting non-stress-responsive *NoDGTTs* isoforms represents a promising strategy for enhancing TAG accumulation while preserving cellular fitness. Future engineering efforts combining such isoforms with controlled expression systems and upstream pathway optimization may further improve the balance between biomass formation and lipid productivity in *N. oceanica* CCMP1779.

5.8. Cross-kingdom functionality of *NoDGTT12* in land plants

Heterologous expression of *NoDGTT12* in *A. thaliana* AS11 (*tag1-1*) provided an effective system for evaluating the functional conservation of microalgal *DGTT*s in a higher plant context. Transcriptomic analyses, overexpression studies, and mutational approaches have consistently demonstrated that in this

model land plant DGAT of type 1 represents the principal contributor to TAG accumulation in seeds, whereas DGAT of type 2 plays a more limited and context-dependent role (Jako *et al*., 2001; Zhang *et al*., 2009). Consequently, the use of the *A. thaliana* AS11 (*tag1-1*) mutant, which carries a disruption in the endogenous DGAT1-encoding gene and displays severely reduced TAG accumulation, therefore represents a highly sensitive genetic background for assessing DGAT activity *in planta* (Katavic *et al*., 1995; Routaboul *et al.,* 1999; Zou *et al*., 1999). Restoration of TAG synthesis in this mutant provides a reliable test of whether heterologous enzymes, including those belonging to the DGAT2/DGTT family, can substitute for the dominant DGAT type 1-mediated pathway in seed tissues. Rigorous genotyping and molecular validation of homozygous *A. thaliana* AS11 (*tag 1-1*) lines ensured that phenotypic variation observed in this study could be confidently attributed to *NoDGTT12* heterologous expression. The presence of the diagnostic 147 bp insertion within intron 2 of *TAG1* locus shown to encode AtDGAT1, confirmed the mutant genotype (Zou *et al*., 1999; Bai *et al*., 2023). This careful validation is particularly important in cross-kingdom engineering studies, where unintended genetic variation may obscure functional interpretation.

Partial restoration of TAG accumulation in *NoDGTT12*-expressing plants demonstrates that this microalgal DGTT retains catalytic competence in the plant ER environment. Importantly, despite belonging to the type 2 *DGAT* family, *NoDGTT12* was able to compensate, at least partially, for the loss of the dominant *AtDGAT1* activity in developing seeds. This finding indicates that under appropriate expression conditions, DGTT-type enzymes can substitute for DGAT1 in directing acyl flux toward TAG assembly in seed tissues. This functional substitution is particularly important given that endogenous *AtDGAT2* does not normally play a major role in seed oil biosynthesis. The ability of *NoDGTT12* to complement the *A. thaliana* AS11 (*tag1-1*) phenotype therefore suggests that the limited contribution of *AtDGAT2* in *A. thaliana* is not primarily due to inherent catalytic constraints of *DGAT*s type 2, but rather reflects differences in expression patterns, regulation, or metabolic integration. When expressed ectopically, microalgal *DGTTs* such as *NoDGTT12* can bypass these endogenous limitations and participate effectively in storage lipid synthesis. These findings are consistent with previous studies demonstrating that algal DGTT enzymes can operate within the plant Kennedy pathway. Expression of *CrDGTT2* from *C. reinhardtii* and *NoDGTT5* from *N. oceanica* CCMP1779 in *A. thaliana* restored TAG accumulation in mutant backgrounds and enhanced TAG in seeds as well as in leaves (Sanjaya *et al*., 2013; Zienkiewicz *et al*., 2017). Together, these results indicate that the fundamental biochemical machinery underlying acyl-CoA-dependent TAG synthesis is highly conserved and that functional specialization of DGAT and DGTT isoforms in plants arises primarily from regulatory and developmental constraints rather than from strict enzymatic incompatibility.

Despite its demonstrated functionality, expression of *NoDGTT12* resulted only in partial restoration of seed TAG content in *A. thaliana* AS11 (*tag1-1*) transgenic lines, when compared with ectopically expressed endogenous *AtDGAT1* (Jako *et al*., 2001) or highly active algal isoforms such as *NoDGTT5* (Zienkiewicz *et al*., 2017). Consistent with observations in H1246 yeast expressing *NoDGTT12*, this difference likely reflects biochemical and regulatory diversity within algal DGTT families, whose members often show

distinct substrate preferences, catalytic efficiencies, and stress responses (Mao *et al*., 2019; Haslam *et al*., 2020). In *N. oceanica* CCMP1779, transcriptomic data indicate that *NoDGTT12* is stably expressed under both N+ and N- conditions, unlike stress-induced isoforms such as *NoDGTT5* (Zienkiewicz *et al*., 2017, 2020), suggesting a primary role of *NoDGTT12* in basal lipid metabolism rather than stress-induced lipid storage. When expressed in *A. thaliana*, such constitutively active isoforms may support moderate TAG synthesis but lack the capacity to drive maximal oil accumulation. Moreover, heterologous DGATs of any origin may not fully engage with plant-specific regulatory mechanisms, including phosphorylation, transcriptional coordination, and metabolic channeling, which are known to modulate *AtDGAT1* activity during seed development (Chapman and Ohlrogge, 2012; Li-Beisson *et al*., 2013). These factors may further limit the effectiveness of *NoDGTT12* in restoring WT lipid levels.

In higher plants, TAG biosynthesis is closely integrated with carbon assimilation, plastidial FA synthesis, membrane lipid remodeling, and TAG packaging. During seed development, coordinated regulation of these processes ensures efficient conversion of photoassimilates into storage lipids (Bates *et al*., 2013; Li-Beisson *et al*., 2013). Heterologously expressed *NoDGTT12* is unlikely to be fully embedded within these regulatory and structural networks in *A. thaliana*. Its activity may therefore be limited by restricted access to appropriate acyl-CoA substrates, reduced interaction with endogenous lipid biosynthetic complexes, and lack of developmental regulation synchronized with seed maturation. In addition, competition with alternative TAG-forming pathways, particularly PDAT-mediated acyl transfer from phosphatidylcholine, may further restrict the contribution of NoDGTT12 to overall TAG flux (Bates *et al*., 2013). These limitations highlight the importance of metabolic context in determining the outcome of lipid engineering strategies. While NoDGTT12 is catalytically competent, its performance *in planta* reflects not only its intrinsic enzymatic properties but also its ability to integrate into host metabolic networks.

In the present study, expression of *NoDGTT12* did not lead to major qualitative changes in FAs profiles of seed TAGs. The relative proportions of dominant FAs, including C18;1, C18: and C18:3 remained largely comparable to those of control plants, indicating that *NoDGTT12* primarily enhanced TAG accumulation without substantially altering acyl composition. This observation suggests that NoDGTT12 exhibits broad substrate tolerance and utilizes the endogenous acyl-CoA pool in a largely non-selective manner. Similar findings were reported for *CeDGAT1* from *Chlorella ellipsoidea*, which increased oil content in *A. thaliana* and *Brassica napus* without significantly affecting FA composition (Guo *et al*., 2017). These results indicate that many heterologous DGATs act mainly as metabolic flux enhancers rather than as determinants of acyl specificity. In contrast, some algal DGATs have been shown to preferentially incorporate unusual or long-chain fatty acids into TAGs. Expression of *CrDGTT2* from *C. reinhardtii* promoted accumulation of very-long-chain fatty acids in leaf TAGs (Sanjaya *et al*., 2013), while PtDGAT2b from *P. tricornutum* efficiently incorporated omega-3 PUFAs when combined with upstream biosynthetic pathways (Klińska-Bąchor *et al*., 2024). The absence of such effects in *NoDGTT12*-expressing seeds suggests that this enzyme lacks strong intrinsic acyl preference or that its specificity is overridden by substrate availability in *A. thaliana* seeds. The stability of FA profiles further implies that NoDGTT12 does not strongly perturb upstream FA synthesis or acyl editing pathways. Instead, it appears to channel

existing acyl-CoA pools more efficiently into TAG, thereby increasing TAG content while preserving endogenous compositional patterns. From an applied perspective, this property may be advantageous for enhancing oil yield without compromising oil quality.

Enhanced TAG synthesis in developing seeds has the potential to influence carbon partitioning between storage lipids, proteins, and carbohydrates. In *Arabidopsis*, mutations affecting DGAT1-encoding gene alter not only oil content but also seed size, FA composition, and developmental timing (Routaboul *et al*., 1999; Zou *et al*., 1999). Restoration of TAG synthesis by *NoDGTT12* partially alleviated the lipid deficiency of the *A. thaliana* AS11 (*tag1-1*) mutant, indicating improved allocation of carbon toward storage lipids. However, the moderate level of complementation suggests that carbon flux into TAG remained suboptimal compared with WT plants. This may reflect limitations in precursor supply, particularly malonyl-CoA and acetyl-CoA, as well as competition with starch and protein biosynthesis pathways.

Previous studies demonstrated that strong overexpression of *DGAT1* or stress-induced algal *DGAT*s can redirect carbon away from structural and metabolic pools, sometimes resulting in growth penalties (Zienkiewicz *et al*., 2017; Vanhercke *et al*., 2019). In this context, the moderate activity of *NoDGTT12* may represent a favorable compromise between enhanced lipid accumulation and maintenance of normal seed development. The absence of pronounced morphological or developmental defects in transgenic lines supports this interpretation and suggests that *NoDGTT12*-mediated TAG enhancement does not impose excessive metabolic cost. The successful functional expression of *NoDGTT12* in *Arabidopsis* contributes to a growing body of evidence supporting the feasibility of cross-kingdom lipid pathway engineering.

5.9. Comparative structural basis of superior performance of NoDGTT12 and NoDGTT5

To elucidate the molecular basis of the superior TAG-synthesizing capacity of NoDGTT12, a detailed comparative analysis of its amino acid sequence was performed with NoDGTT5, previously identified as a highly efficient DGTT isoform in *N. oceanica* CCMP1779 as well as in heterologous yeast and plant hosts (Zienkiewicz *et al.,* 2017). This comparison provides insight into the shared structural features that underlie high enzymatic activity as well as the sequence differences that may contribute to functional divergence between the two enzymes.

NoDGTT5 and NoDGTT12 proteins exhibit comparable overall lengths and similar distributions of hydrophobic and hydrophilic regions. Both enzymes contain multiple predicted TMDs located primarily in the central and C-terminal regions, consistent with stable integration into the ER membrane. Hydrophobicity profiling indicates strong conservation of membrane-spanning segments, suggesting that both enzymes adopt similar membrane topologies and are positioned in comparable cellular environments. Balanced membrane topology has been recognized as a critical determinant of DGAT2-type enzyme activity, as it enables efficient coupling between cytosolic acyl-CoA pools and membrane-associated DAG substrates (Liu *et al.,* 2012; Xu *et al.,* 2018; Sui *et al.,* 2020). The shared membrane architecture of NoDGTT5 and NoDGTT12 therefore provides a common structural framework supporting high TAG-synthesizing capacity.

Moreover, both NoDGTT5 and NoDGTT12 retain all six conserved DGTT motifs, including the PH, PR, GGE, RGFA, VPFG, and G blocks, previously identified in *N. oceanica* DGTTs by Zienkiewicz *et al*. (2017). These motifs are concentrated in the central and C-terminal regions and form the catalytic core responsible for acyl transfer. The PH block, containing a conserved proline–histidine pair, is fully preserved in both proteins. This motif has been implicated in substrate positioning and stabilization of reaction intermediates (Liu *et al.,* 2012; Zienkiewicz *et al.,* 2017). Similarly, glycine-rich segments and conserved aromatic residues associated with DAG and acyl-CoA binding are maintained in both sequences and have been shown to contribute to catalytic efficiency in DGAT type 2 enzymes (Xu *et al.,* 2018; Sui *et al.,* 2020). The conservation of these motifs indicates that NoDGTT5 and NoDGTT12 possess comparable intrinsic catalytic machinery, providing a structural basis for their strong TAG-synthesizing activity in both native and heterologous systems.

Despite conservation of the catalytic core, pronounced divergence is observed in the N-terminal, C- terminal, and inter-helical regions between NoDGTT5 and NoDGTT12. These domains display lower sequence conservation, increased frequency of insertions and deletions, and enrichment in polar and charged residues. The N-terminal region of NoDGTT12 is also longer and more compositionally complex than that of NoDGTT5. N-terminal domains of DGAT type 2 enzymes have been implicated in regulating protein stability, membrane targeting, and responsiveness to cellular signals (Caldo *et al.,* 2017; Xu *et al.,* 2018). The expanded N-terminus of NoDGTT12 may therefore enhance ER retention, reduce proteolytic turnover, or modulate interactions with regulatory partners. Differences are also evident in inter-helical loop regions. NoDGTT12 contains longer and more flexible loops enriched in charged residues. Loop flexibility has been shown to facilitate substrate access and product release in membrane-associated acyltransferases (Liu *et al.,* 2012; Xu *et al.,* 2018) and thus may support better catalytic efficiency of NoDGTT12 when compared to NoDGTT5. The C-terminal region of NoDGTT12 is similarly extended relative to NoDGTT5 and contains multiple charged and aromatic residues. C-terminal domains have been generally implicated in proper folding, oligomerization, and membrane retention of lipid metabolic enzymes (Stone *et al.,* 2009; Xu *et al.,* 2018), suggesting that this region may contribute to enhanced structural stability also in NoDGTT12.

Although both proteins share comparable transmembrane organization, NoDGTT12 exhibits slightly longer and more hydrophobic segments in selected membrane-spanning regions. Increased hydrophobicity may strengthen membrane anchoring and promote localization of enzymatic proteins to lipid-synthesizing microdomains within the ER (Wilfling *et al.,* 2014; Sui *et al.,* 2020). In addition, NoDGTT12 displays a higher density of aromatic residues, particularly tryptophan and phenylalanine, within membrane-associated regions. Aromatic residues play key roles in stabilizing lipid - protein interfaces and forming hydrophobic reaction chambers (Xu *et al.,* 2018; Sui *et al.,* 2020). Enrichment of these residues in NoDGTT12 may enhance substrate retention and increase effective substrate concentration at the catalytic site.

Sequence alignment revealed also several amino acid substitutions close to the conserved catalytic motifs. Although the motifs themselves remain intact, changes in flanking residues may subtly alter active-site geometry, substrate orientation, and local flexibility. Structural and mutational analyses of DGAT type 2 enzymes from other cell types indicate that such fine-scale variations can substantially influence catalytic kinetics and substrate specificity (Liu *et al.,* 2012; Xu *et al.,* 2018). In NoDGTT12, these substitutions may confer modest kinetic advantages over NoDGTT5 while preserving overall enzymatic integrity.

Overall, the comparative analysis indicates that NoDGTT5 and NoDGTT12 share a conserved structural framework characterized by balanced membrane topology and intact catalytic motifs, which could be responsible for their high TAG-synthesizing capacity. Consequently, this shared architecture might also explain why both enzymes perform efficiently in yeast, microalgal, and plant systems (Zienkiewicz *et al.,* 2017; this study). At the same time, NoDGTT12 displays multiple structural refinements, including an expanded N-terminus, more flexible loop regions, an extended C-terminal domain, enhanced membrane anchoring, and increased aromatic content in lipid-interacting segments, when compared to NoDGTT5. Similar structural optimizations have been associated with improved performance of DGATs in plants and oleaginous microorganisms (Xu *et al.,* 2018; Cui *et al.,* 2021; Ma *et al.,* 2021). These cumulative differences likely improve protein stability, membrane localization, substrate accessibility, and integration into lipid biosynthetic complexes. While both enzymes retain the essential catalytic frame required for efficient TAG synthesis, NoDGTT12 appears to represent a functionally optimized variant in which regulatory and structural are more optimal and enhance robustness and versatility. This structural refinement likely underlies the superior and broader performance of NoDGTT12 observed in this study and explains its emergence as the dominant TAG synthase across diverse cellular environments.

5.10. Biotechnological potential of *NoDGTT12* for lipid engineering in microbial and plant systems

The results obtained in *S. cerevisiae*, *N. oceanica*, and *A. thaliana* collectively identify NoDGTT12 as a highly efficient, robust, and versatile TAG synthase with exceptional cross-system functionality. Heterologous expression in the TAG-deficient H1246 yeast strain demonstrated that *NoDGTT12* is capable of restoring TAG biosynthesis to levels exceeding 30% of total cellular lipids, placing it among the most active microalgal *DGTT*s reported to date. This outstanding performance contrasts with the weaker phenotypes observed for several other *NoDGTT* isoforms and highlights the importance of substrate availability and host metabolic context in functional complementation assays (Liu *et al*., 2016; Zienkiewicz *et al*., 2017; Mao *et al*., 2019; Cui *et al*., 2021). As it has been mentioned earlier, *S. cerevisiae* predominantly synthesizes C16 and C18 saturated and monounsaturated FAs, resulting in a restricted acyl-CoA pool. In contrast, microalgae and plants generate diverse long-chain and PUFAs (Wei *et al*., 2017; Zienkiewicz *et al*., 2018; Ma *et al*., 2021). Many algal DGTTs appear adapted to these native substrate environments and therefore show limited activity in yeast. The exceptional performance of NoDGTT12 in this system indicates a high degree of substrate tolerance and compatibility with dominant yeast acyl-CoA species, particularly unsaturated C18 derivatives. *In vitro* substrate preference assays confirmed high catalytic activity of

NoDGTT12 toward unsaturated acyl-CoAs and a strong preference for C18:1-DAG, closely matching the major substrates available in yeast.

Furthermore, *NoDGTT12* displayed stable expression and sustained activity over extended induction periods, indicating limited sensitivity to host-specific regulatory limitations. Many heterologous DGATs suffer from improper folding, suboptimal membrane insertion, or incompatibility with host lipid networks (Liu *et al*., 2016; Mao *et al*., 2019). In contrast, NoDGTT12 exhibited likely favorable structural compatibility with yeast ER membranes, supporting efficient LDs formation and intracellular TAG packaging. Importantly, the high TAG yields observed in *NoDGTT12*-expressing yeast suggest also that this enzyme functions as an effective metabolic sink for acyl-CoA and DAG pools. By strengthening the terminal step of TAG biosynthesis, NoDGTT12 likely modulates feedback inhibition on upstream FAs synthesis and enhances overall lipid flux. Such "pull" strategies are widely recognized as powerful tools in metabolic engineering (Vanhercke *et al*., 2019; Haslam *et al*., 2020).

Overall, similar to NoDGFTT5 (Zienkiewicz *et al*. 2017), NoDGTT12 represents an example of a DGTT isoform with pronounced catalytic plasticity, capable of functioning efficiently in metabolically constrained heterologous environments. All these observations emphasize also that the H1246 yeast platform should be regarded as a context-dependent screening tool rather than a universal predictor of native enzyme performance (Zienkiewicz *et al*., 2017; Ma *et al*., 2021). Nevertheless, strong activity in this system, as observed for NoDGTT12, is indicative of broad applicability in synthetic biology and metabolic engineering.

Overexpression of *NoDGTT12* in *N. oceanica* CCMP1779 demonstrated that its high catalytic potential can be effectively exploited also in its native metabolic context. Transgenic microalgal lines accumulated significantly higher TAG levels under N+ conditions, indicating that enhancement of terminal acyltransferase activity alone is sufficient to stimulate TAG synthesis and storage in actively growing cells of *N. oceanica* CCMP1779. This finding is particularly relevant for industrial microalgal cultivation, where traditional nitrogen-starvation strategies often reduce biomass productivity and prolong cultivation cycles (Zienkiewicz *et al*., 2016; Janssen *et al*., 2020). NoDGTT12-mediated TAG accumulation under N+ conditions offers a potential route to decouple oil production from severe stress responses, thereby improving overall productivity.

However, *NoDGTT12* overexpression was associated with substantial remodeling of FA composition, characterized by increased proportions of C16:0 and C16:1 and reduced levels of long-chain PUFAs, particularly EPA (C20:5) (Li *et al*., 2016; Zienkiewicz *et al*., 2017; Janssen *et al*., 2020). This shift likely reflects enhanced channeling of newly synthesized FAs into TAG at the expense of PUFAs biosynthesis and membrane lipid remodeling. From an applied perspective, this compositional change represents both an opportunity and a limitation. Increased saturation and monounsaturation improve oxidative stability and suitability for biodiesel production, whereas reduced EPA content may limit applications in nutraceutical markets. Consequently, commercial use of *NoDGTT12* would require careful balancing of lipid quantity and quality. Future strategies should therefore combine *NoDGTT12* overexpression with

targeted enhancement of PUFAs biosynthesis pathways through co-expression of elongases and desaturases. Such combinatorial approaches have shown promise for example in *P. tricornutum* as well as in *Nannochloropsis* species (Wei *et al*., 2017; Klińska-Bąchor *et al*., 2024) and represent a logical extension of the present work.

Long-term genetic stability is essential for industrial strain development. Although extended stability assays were beyond the scope of this study, the consistent expression of *NoDGTT12-CFP* fusion construct in multiple independent lines of *N. oceanica* CCMP1779 suggests promising robustness. Similar long-term stability has been reported for other *DGAT*-overexpressing microalgae (Klaitong *et al*., 2017; Chungjatupornchai and Fa-Aroonsawat, 2021). Evidence from these studies indicates that multigene approaches often outperform single-gene strategies. Co-expression of *LPAAT* and *DGAT* in *N. oleoabundans* and combined expression of *NoDGAT*2B with elongases in diatoms resulted in superior lipid productivity and improved FA profiles (Haslam *et al*., 2020Chungjatupornchai and Fa-Aroonsawat, 2021). In this context, *NoDGTT12* represents a valuable building block for future multigene engineering in *N. oceanica*. Combining NoDGTT12 with upstream enzymes such as GPAT or LPAAT, or with PUFA biosynthesis genes, may further enhance both TAG quantity and quality.

Partial complementation of the *A. thaliana* AS11 (*tag1-1*) mutant phenotype by *NoDGTT12* demonstrates strong evolutionary conservation of DGTT catalytic mechanisms and highlights the potential of microalgal enzymes for plant lipid engineering. Despite belonging to the DGAT type 2 (DGTT) family, *NoDGTT12* was able to substitute, at least in part, for the dominant DGAT type 1 pathway of TAG synthesis in developing *A. thaliana* AS11 (*tag1-1*) seeds, restoring TAG accumulation, LDs formation, and seed size. This cross-kingdom functionality is consistent with previous reports showing that algal DGTTs can operate within the plant Kennedy pathway (Sanjaya *et al*., 2013; Guo *et al*., 2017; Zienkiewicz *et al*., 2017). The moderate degree of complementation observed in this study suggests that maximal oil production in plants requires integration with endogenous regulatory networks controlling carbon allocation, seed development, and storage compound synthesis (Chapman and Ohlrogge, 2012; Li-Beisson *et al*., 2019).

Importantly, *NoDGTT12* expression did not cause major alterations in seed FAs composition, indicating that it primarily enhances metabolic flux rather than imposing strong substrate selectivity. This property is advantageous for breeding and engineering programs aiming to increase oil yield without compromising oil quality or agronomic performance. Moreover, restoration of seed size and morphology indicates the close coupling between lipid storage and developmental processes. By improving TAG synthesis, *NoDGTT12* indirectly supports cellular expansion and reserve accumulation during seed maturation.

Collectively, the results presented in this thesis identify NoDGTT12 from *N. oceanica* CCMP1779 as a versatile and robust DGTT enzyme with exceptional cross-system functionality for TAG synthesis. Its broad substrate tolerance, high catalytic efficiency, stable membrane integration, and genetic robustness make it well suited for incorporation into synthetic lipid biosynthesis modules. Such modules could be employed in diverse hosts to generate customized lipid profiles, support carbon sequestration strategies,

and produce high-value oleochemicals. The ability of NoDGTT12 to function effectively in metabolically constrained backgrounds suggests that it may serve as a quasi-universal TAG synthase capable of buffering metabolic fluctuations and stabilizing engineered pathways. This property is particularly valuable in multigene engineering approaches, where imbalances in precursor supply frequently limit productivity. By acting as a strong metabolic sink, NoDGTT12 can enhance pathway robustness and predictability, key requirements for industrial biotechnology.

6. CONCLUSIONS

Taken together, the research presented in this thesis demonstrates that systematic functional and structural analysis of the *NoDGTT* gene family from *N. oceanica* CCMP1779 provides fundamental insights into the regulation of TAG biosynthesis and identifies enzymes with exceptional biotechnological potential. By integrating *in silico* characterization, heterologous expression, biochemical profiling, native overexpression, and cross-kingdom functional validation, this work elucidates how diversification of *NoDGTTs* reflects metabolic specialization and lipid homeostasis. In particular, the identification and detailed characterization of NoDGTT12 as a highly efficient and broadly compatible DGTT represents a central outcome of this thesis. The main conclusions of this research can be summarized as follows:

1. The *DGTT* gene family of *N. oceanica* CCMP1779 represents a structurally and functionally diversified enzymatic system central to TAG biosynthesis. Through integrated computational, biochemical, and genetic approaches, this work extends previous comprehensive characterization of all *DGTT* isoforms in this microalga, demonstrating their extensive variation in molecular architecture and membrane topology while confirming conserved ER localization. These findings highlight also the evolutionary conservation of spatial organization of TAG metabolism and emphasize the ER as the primary hub of TAG assembly in oleaginous microalgae.
2. The expansion of the *DGTT* gene family in *N. oceanica* CCMP1779 reflects functional specialization rather than genetic redundancy**.** Functional screening in the TAG-deficient *S. cerevisiae* H1246 system revealed pronounced divergence in catalytic performance among *NoDGTT* isoforms, with only a limited subset exhibiting strong TAG-synthesizing activity. This demonstrates that gene family expansion has enabled enzymatic specialization and regulatory differentiation, supporting metabolic flexibility under diverse physiological conditions.
3. NoDGTT12 is identified as a highly efficient and broadly compatible TAG synthase optimized for activity across diverse cellular environments. Among all analyzed isoforms, NoDGTT12 showed exceptional performance in yeast, restoring TAG levels to more than 30% of total cellular lipids and promoting efficient LDs formation. Biochemical analyses revealed broad acyl-CoA tolerance, preference for unsaturated substrates, and selective utilization of 18:1-diacylglycerol, providing a mechanistic basis for its superior catalytic efficiency and cross-system functionality.
4. The high catalytic potential of *NoDGTT12* can be effectively exploited in its native microalgal host to enhance TAG accumulation under non-stress conditions. Overexpression of *NoDGTT12* in *N. oceanica* CCMP1779 significantly increased TAG content during growth under optimal culture conditions, demonstrating that reinforcement of key DGAT activity alone is sufficient to stimulate TAG

accumulation. However, the associated shift toward saturated and monounsaturated FAs and reduction of EPA (C20:5) reveals an inherent trade-off between TAG quantity and quality that must be considered in future engineering strategies.

5. Microalgal DGTT enzymes, exemplified by NoDGTT12, exhibit strong evolutionary conservation that enables functional integration into plant TAG biosynthesis pathways. Partial complementation of the *A. thaliana* AS11 (*tag1-1*) mutant by expression of *NoDGTT12* restored TAG accumulation, LDs formation, and seed morphology, demonstrating effective operation within plant metabolic networks. At the same time, moderate complementation levels indicate that maximal oil production in plants depends on coordinated interaction with endogenous regulatory and developmental systems.
6. *NoDGTT12* represents a versatile molecular tool for next-generation TAG biotechnology, while also defining key directions for future research. Its robust activity in yeast, microalgae, and plants supports its potential application in microbial fermentation platforms, algal production systems, and crop improvement programs. Nevertheless, limitations related to incomplete structural information, regulatory complexity, and large-scale stability highlight the need for future studies integrating structural biology, systems-level analyses, and multigene engineering.

7. REFERENCES

Alboresi, A., Perin, G., Vitulo, N., Diretto, G., Block, M., Jouhet, J., ... and Morosinotto, T. (2016). Light remodels lipid biosynthesis in Nannochloropsis gaditana by modulating carbon partitioning between organelles. *Plant Physiology*, *171*(4), 2468-2482.

Ali, O., and Szabó, A. (2023). Review of eukaryote cellular membrane lipid composition, with special attention to the fatty acids. *International journal of molecular sciences*, 24(21), 15693.

Amari, C., Carletti, M., Yan, S., Michaud, M., and Salvaing, J. (2024). Lipid droplets degradation mechanisms from microalgae to mammals, a comparative overview. *Biochimie*, *227*, 19-34.

Arhar, S., Gogg-Fassolter, G., Ogrizović, M., Pačnik, K., Schwaiger, K., Žganjar, M., ... and Natter, K. (2021). Engineering of Saccharomyces cerevisiae for the accumulation of high amounts of triacylglycerol. *Microbial Cell Factories*, *20*(1), 147.

Aymé, L., Arragain, S., Canonge, M., Baud, S., Touati, N., Bimai, O., ... and Chardot, T. (2018). Arabidopsis thaliana DGAT3 is a [2Fe-2S] protein involved in TAG biosynthesis. *Scientific Reports*, *8*(1), 17254.

Bagnato, C., Prados, M. B., Franchini, G. R., Scaglia, N., Miranda, S. E., and Beligni, M. V. (2017). Analysis of triglyceride synthesis unveils a green algal soluble diacylglycerol acyltransferase and provides clues to potential enzymatic components of the chloroplast pathway. *BMC genomics*, *18*(1), 223.

Bai, F., Zhang, Y., and Liu, J. (2021). A bZIP transcription factor is involved in regulating lipid and pigment metabolisms in the green alga Chlamydomonas reinhardtii. *Algal Research*, *59*, 102450.

Banerjee, A., Maiti, S. K., Guria, C., and Banerjee, C. (2017). Metabolic pathways for lipid synthesis under nitrogen stress in Chlamydomonas and Nannochloropsis. *Biotechnology letters*, *39*(1), 1-11.

Bates, P. D., Stymne, S., and Ohlrogge, J. (2013). Biochemical pathways in seed oil synthesis. Current opinion in plant biology, 16(3), 358-364.

Beacham, T. A., and Ali, S. T. (2016). Growth dependent silencing and resetting of DGA1 transgene in Nannochloropsis salina. *Algal research*, *14*, 65-71.

Bouchnak, I., Coulon, D., Salis, V., D'andrea, S., and Bréhélin, C. (2023). Lipid droplets are versatile organelles involved in plant development and plant response to environmental changes. *Frontiers in Plant Science*, *14*, 1193905.

Cai, W. L., Yu, S. Y., and Hu, Y. H. (2025). Synergistic mechanisms of DGAT and PDAT in shaping triacylglycerol diversity: evolutionary insights and metabolic engineering strategies. *Frontiers in Plant Science*, *16*, 1598815.

Canini, D., Ceschi, E., and Perozeni, F. (2024). Toward the Exploitation of Sustainable Green Factory: Biotechnology Use of Nannochloropsis spp. *Biology*, *13*(5), 292.

Carro, M. D. L. M., Gonorazky, G., Soto, D., Mamone, L., Bagnato, C., Pagnussat, L. A., and Beligni, M. V. (2022). Expression of Chlamydomonas reinhardtii chloroplast diacylglycerol acyltransferase 3 is induced by light in concert with triacylglycerol accumulation. *The Plant Journal*, *110*(1), 262-276.

Chapman, K. D., and Ohlrogge, J. B. (2012). Compartmentation of triacylglycerol accumulation in plants. *Journal of Biological Chemistry*, *287*(4), 2288-2294.

Chapman, K. D., Aziz, M., Dyer, J. M., and Mullen, R. T. (2019). Mechanisms of lipid droplet biogenesis. *Biochemical Journal*, *476*(13), 1929-1942.

Chen, J. E., and Smith, A. G. (2012). A look at diacylglycerol acyltransferases (DGATs) in algae. *Journal of biotechnology*, *162*(1), 28-39.

Chi, X., Hu, R., Zhang, X., Chen, M., Chen, N., Pan, L., Wang, T., Wang, M., Yang, Z., Wang, Q., Yu, S. (2014). Cloning and functional analysis of three diacylglycerol acyltransferase genes from peanut (Arachis hypogaea L.). *PloS one*, *9*(9), e105834.

Choudhary, V., and Schneiter, R. (2021). A unique junctional interface at contact sites between the endoplasmic reticulum and lipid droplets. *Frontiers in cell and developmental biology*, *9*, 650186.

Chouhan, N., Devadasu, E., Yadav, R. M., and Subramanyam, R. (2022). Autophagy induced accumulation of lipids in pgrl1 and pgr5 of Chlamydomonas reinhardtii under high light. *Frontiers in plant science*, *12*, 752634.

Chungjatupornchai, W., and Fa-Aroonsawat, S. (2021). Enhanced triacylglycerol production in oleaginous microalga Neochloris oleoabundans by co-overexpression of lipogenic genes: Plastidial LPAAT1 and ER-located DGAT2. *Journal of bioscience and bioengineering*, *131*(2), 124-130.

Cohen, P., and Spiegelman, B. M. (2016). Cell biology of fat storage. *Molecular biology of the cell*, *27*(16), 2523-2527.

Conroy, M. J., Andrews, R. M., Andrews, S., Cockayne, L., Dennis, E. A., Fahy, E., Gaud, C., Griffiths, W.J., Jukes, G., Kolchin, M., Mendivelso, K., Lopez-Clavijo, A.F., Ready, C., Subramaniam, S., O'Donnell, V.B. (2024). LIPID MAPS: update to databases and tools for the lipidomics community. *Nucleic Acids Research*, *52*(D1), D1677-D1682.

Cui, H., Zhao, C., Xu, W., Zhang, H., Hang, W., Zhu, X., Ji, C., Xue, J., Zhang, C., Li, R. (2021). Characterization of type-2 diacylglycerol acyltransferases in Haematococcus lacustris reveals their functions and engineering potential in triacylglycerol biosynthesis. *BMC Plant Biology*, *21*(1), 20.

Cui, Y., Zhao, J., Wang, Y., Qin, S., and Lu, Y. (2018). Characterization and engineering of a dual-function diacylglycerol acyltransferase in the oleaginous marine diatom Phaeodactylum tricornutum. *Biotechnology for Biofuels*, *11*(1), 32.

Diaz, M. (2019). Arabidopsis Thaliana: From weed to model organism. *Current Protocols Essential Laboratory Techniques*, *19*(1), e38.

Dinamarca, J., Levitan, O., Kumaraswamy, G. K., Lun, D. S., and Falkowski, P. G. (2017). Overexpression of a diacylglycerol acyltransferase gene in Phaeodactylum tricornutum directs carbon towards lipid biosynthesis. Journal of phycology, 53(2), 405-414.

Ding, W., Ye, Y., Yu, L., Liu, M., and Liu, J. (2023). Physiochemical and molecular responses of the diatom Phaeodactylum tricornutum to illumination transitions. *Biotechnology for biofuels and bioproducts*, *16*(1), 103.

Du, Z. Y., and Benning, C. (2016). Triacylglycerol accumulation in photosynthetic cells in plants and algae. *Lipids in plant and algae development*, 179-205.

Einhaus, A., Baier, T., and Kruse, O. (2024). Molecular design of microalgae as sustainable cell factories. *Trends in Biotechnology*, *42*(6), 728-738.

Farese Jr, R. V., and Walther, T. C. (2025). Essential Biology of Lipid Droplets. *Annual Review of Biochemistry*, *94*.

Farese, R. V., and Walther, T. C. (2023). Glycerolipid synthesis and lipid droplet formation in the endoplasmic reticulum. Cold Spring Harbor Perspectives in Biology, 15(5), a041246.

Feng, Y., Ge, J., Show, P. L., Song, C., Wu, L., Ma, Z., and Gao, G. (2025). Using high CO2 concentrations to culture microalgae for lipid and fatty acid production: synthesis based on a meta-analysis. *Aquaculture*, *594*, 741386.

Gaikani, H. K., Stolar, M., Kriti, D., Nislow, C., and Giaever, G. (2024). From beer to breadboards: yeast as a force for biological innovation. *Genome Biology*, *25*(1), 10.

Gao, B., Hong, J., Chen, J., Zhang, H., Hu, R., and Zhang, C. (2023). The growth, lipid accumulation and adaptation mechanism in response to variation of temperature and nitrogen supply in psychrotrophic filamentous microalga Xanthonema hormidioides (Xanthophyceae). *Biotechnology for Biofuels and Bioproducts*, *16*(1), 12.

Gargouri, M., Bates, P. D., Park, J. J., Kirchhoff, H., and Gang, D. R. (2017). Functional photosystem I maintains proper energy balance during nitrogen depletion in Chlamydomonas reinhardtii, promoting triacylglycerol accumulation. *Biotechnology for biofuels*, *10*(1), 89.

Gidda, S. K., Park, S., Pyc, M., Yurchenko, O., Cai, Y., Wu, P., Andrews, D.W., Chapman, K.D., Dyer, J.M., Mullen, R. T. (2016). Lipid droplet-associated proteins (LDAPs) are required for the dynamic regulation of neutral lipid compartmentation in plant cells. *Plant Physiology*, *170*(4), 2052-2071.

Gimpel, J. A., Henríquez, V., and Mayfield, S. P. (2015). In metabolic engineering of eukaryotic microalgae: potential and challenges come with great diversity. *Frontiers in microbiology*, *6*, 1376.

Goffeau, A., Barrell, B. G., Bussey, H., Davis, R. W., Dujon, B., Feldmann, H., Galibert, F., Hoheisel, J.D., Jacq, C., Johnston, M., Louis, E.J., Mewes, H.W., Murakami, Y., Philippsen, P., Tettelin, H., Oliver, S.G. (1996). Life with 6000 genes. *Science*, *274*(5287), 546-567.

Gong, Y., Zhang, J., Guo, X., Wan, X., Liang, Z., Hu, C. J., and Jiang, M. (2013). Identification and characterization of PtDGAT2B, an acyltransferase of the DGAT2 acyl-coenzyme A: diacylglycerol acyltransferase family in the diatom Phaeodactylum tricornutum. *FEBS letters*, *587*(5), 481-487.

Grama, S. B., Liu, Z., and Li, J. (2022). Emerging trends in genetic engineering of microalgae for commercial applications. *Marine Drugs*, *20*(5), 285.

Guéguen, N., Le Moigne, D., Amato, A., Salvaing, J., and Maréchal, E. (2021). Lipid droplets in unicellular photosynthetic stramenopiles. *Frontiers in Plant Science*, *12*, 639276.

Guo, X., Fan, C., Chen, Y., Wang, J., Yin, W., Wang, R. R., and Hu, Z. (2017). Identification and characterization of an efficient acyl-CoA: diacylglycerol acyltransferase 1 (DGAT1) gene from the microalga Chlorella ellipsoidea. *BMC Plant Biology*, *17*(1), 48.

Guzha, A., Whitehead, P., Ischebeck, T., and Chapman, K. D. (2023). Lipid droplets: packing hydrophobic molecules within the aqueous cytoplasm. *Annual review of plant biology*, *74*(1), 195-223.

Han, L., Zhai, Y., Wang, Y., Shi, X., Xu, Y., Gao, S., Zhang, M., Luo, J., Zhang, Q. (2022). Diacylglycerol acyltransferase 3 (DGAT3) is responsible for the biosynthesis of unsaturated fatty acids in vegetative organs of Paeonia rockii. *International Journal of Molecular Sciences*, *23*(22), 14390.

Harayama, T., and Riezman, H. (2018). Understanding the diversity of membrane lipid composition. *Nature reviews Molecular cell biology*, *19*(5), 281-296.

Haslam, R. P., Hamilton, M. L., Economou, C. K., Smith, R., Hassall, K. L., Napier, J. A., and Sayanova, O. (2020). Overexpression of an endogenous type 2 diacylglycerol acyltransferase in the marine diatom Phaeodactylum tricornutum enhances lipid production and omega-3 long-chain polyunsaturated fatty acid content. *Biotechnology for biofuels*, *13*(1), 87.

Holechek, J. L., Geli, H. M., Sawalhah, M. N., and Valdez, R. (2022). A global assessment: can renewable energy replace fossil fuels by 2050?. *Sustainability*, *14*(8), 4792.

Hu, Z., Hao, X., Pan, Y., and Hu, H. (2025). Heterologous phospholipid: diacylglycerol acyltransferase enhances triacylglycerol accumulation without compromising growth in Nannochloropsis oceanica. *Algal Research*, *86*, 103902.

Huang, B., Mimouni, V., Lukomska, E., Morant-Manceau, A., and Bougaran, G. (2020). Carbon partitioning and lipid remodeling during phosphorus and nitrogen starvation in the marine microalga Diacronema lutheri (Haptophyta). Journal of Phycology, 56(4), 908-922.

Hulatt, C. J., Smolina, I., Dowle, A., Kopp, M., Vasanth, G. K., Hoarau, G. G., Wijffels, R.H., Kiron, V. (2020). Proteomic and transcriptomic patterns during lipid remodeling in Nannochloropsis gaditana. *International Journal of Molecular Sciences*, *21*(18), 6946.

Hung, C. H., Ho, M. Y., Kanehara, K., and Nakamura, Y. (2013). Functional study of diacylglycerol acyltransferase type 2 family in Chlamydomonas reinhardtii. *FEBS letters*, *587*(15), 2364-2370.

Iwai, M., Hori, K., Sasaki-Sekimoto, Y., Shimojima, M., and Ohta, H. (2015). Manipulation of oil synthesis in Nannochloropsis strain NIES-2145 with a phosphorus starvation–inducible promoter from Chlamydomonas reinhardtii. *Frontiers in Microbiology*, *6*, 912.

Jako, C., Kumar, A., Wei, Y., Zou, J., Barton, D. L., Giblin, E. M., Covello, P.S., Taylor, D. C. (2001). Seed-specific over-expression of an Arabidopsis cDNA encoding a diacylglycerol acyltransferase enhances seed oil content and seed weight. Plant physiology, 126(2), 861-874.

Janssen, J. H., Spoelder, J., Koehorst, J. J., Schaap, P. J., Wijffels, R. H., and Barbosa, M. J. (2020). Time-dependent transcriptome profile of genes involved in triacylglycerol (TAG) and polyunsaturated fatty acid synthesis in Nannochloropsis gaditana during nitrogen starvation. *Journal of applied phycology*, *32*(2), 1153-1164.

Jeong, S. W., Nam, S. W., HwangBo, K., Jeong, W. J., Jeong, B. R., Chang, Y. K., and Park, Y. I. (2017). Transcriptional regulation of cellulose biosynthesis during the early phase of nitrogen deprivation in Nannochloropsis salina. *Scientific reports*, *7*(1), 5264.

Jeppson, S., Demski, K., Carlsson, A. S., Zhu, L. H., Banaś, A., Stymne, S., and Lager, I. (2019). Crambe hispanica subsp. abyssinica diacylglycerol acyltransferase specificities towards diacylglycerols and acyl-CoA reveal combinatorial effects that greatly affect enzymatic activity and specificity. *Frontiers in Plant Science*, *10*, 1442.

Jia, S., Wu, S., Liu, X., Gu, W., and Wang, G. (2023). Appropriate carbon–nitrogen ratio is beneficial to the accumulation of 9-cis-β-carotene during Dunaliella salina cultivation. *Journal of Applied Phycology*, *35*(4), 1537-1552.

Juergens, M. T., Disbrow, B., and Shachar-Hill, Y. (2016). The relationship of triacylglycerol and starch accumulation to carbon and energy flows during nutrient deprivation in Chlamydomonas reinhardtii. *Plant physiology*, *171*(4), 2445-2457.

Kang, N. K., Baek, K., Koh, H. G., Atkinson, C. A., Ort, D. R., and Jin, Y. S. (2022). Microalgal metabolic engineering strategies for the production of fuels and chemicals. *Bioresource technology*, *345*, 126529.

Katavic, V., Reed, D. W., Taylor, D. C., Giblin, E. M., Barton, D. L., Zou, J., Mackenzie, S.L., Covello, P.S., Kunst, L. (1995). Alteration of seed fatty acid composition by an ethyl methanesulfonate-induced mutation in Arabidopsis thaliana affecting diacylglycerol acyltransferase activity. *Plant physiology*, *108*(1), 399-409.

Klaitong, P., Fa-Aroonsawat, S., and Chungjatupornchai, W. (2017). Accelerated triacylglycerol production and altered fatty acid composition in oleaginous microalga Neochloris oleoabundans by overexpression of diacylglycerol acyltransferase 2. Microbial cell factories, 16(1), 61.

Klińska-Bąchor, S., Demski, K., Gong, Y., and Banaś, A. (2024). Biochemical characterization of acyl-CoA: diacylglycerol acyltransferase2 from the diatom Phaeodactylum tricornutum and its potential effect on LC-PUFAs biosynthesis in planta. *BMC Plant Biology*, *24*(1), 309.

Kohlwein, S. D. (2010). Triacylglycerol homeostasis: insights from yeast. *Journal of Biological Chemistry*, *285*(21), 15663-15667.

Kokabi, K., Gorelova, O., Zorin, B., Didi-Cohen, S., Itkin, M., Malitsky, S., Solovchenko, A., Boussiba, S., Khozin-Goldberg, I. (2020). Lipidome remodeling and autophagic respose in the arachidonic-acid-rich microalga Lobosphaera incisa under nitrogen and phosphorous deprivation. *Frontiers in plant science*, *11*, 614846.

Koornneef, M., and Meinke, D. (2010). The development of Arabidopsis as a model plant. *The plant journal*, *61*(6), 909-921.

Kou, Y., Liu, M., Sun, P., Dong, Z., and Liu, J. (2020). High light boosts salinity stress-induced biosynthesis of astaxanthin and lipids in the green alga Chromochloris zofingiensis. *Algal Research*, *50*, 101976.

Kumar, G., Shekh, A., Jakhu, S., Sharma, Y., Kapoor, R., and Sharma, T. R. (2020). Bioengineering of microalgae: recent advances, perspectives, and regulatory challenges for industrial application. *Frontiers in Bioengineering and Biotechnology*, *8*, 914.

La Russa, M., Bogen, C., Uhmeyer, A., Doebbe, A., Filippone, E., Kruse, O., and Mussgnug, J. H. (2012). Functional analysis of three type-2 DGAT homologue genes for triacylglycerol production in the green microalga Chlamydomonas reinhardtii. Journal of biotechnology, 162(1), 13-20.

Lee, J., Yamaoka, Y., Kong, F., Cagnon, C., Beyly-Adriano, A., Jang, S., Gao, P., Kang, B.H., Li-Beisson, Y., Lee, Y. (2020). The phosphatidylethanolamine-binding protein DTH1 mediates degradation of lipid droplets in Chlamydomonas reinhardtii. *Proceedings of the National Academy of Sciences*, *117*(37), 23131-23139.

Lee, K. R., Kim, Y. M., Yeo, Y., Kim, S., and Suh, M. C. (2022a). Camelina cytosol-localized diacylglycerol acyltransferase 3 contributes to the accumulation of seed storage oils. *Industrial Crops and Products*, *189*, 115808.

Lenka, S. K., Carbonaro, N., Park, R., Miller, S. M., Thorpe, I., and Li, Y. (2016). Current advances in molecular, biochemical, and computational modeling analysis of microalgal triacylglycerol biosynthesis. *Biotechnology advances*, *34*(5), 1046-1063.

Li, D. W., Cen, S. Y., Liu, Y. H., Balamurugan, S., Zheng, X. Y., Alimujiang, A., Yang, W.D., Liu, J.S., Li, H. Y. (2016). A type 2 diacylglycerol acyltransferase accelerates the triacylglycerol biosynthesis in heterokont oleaginous microalga Nannochloropsis oceanica. *Journal of biotechnology*, *229*, 65-71.

Li, J., Chen, H., Chang, L., Wu, C., Zhang, H., Chen, Y. Q., and Chen, W. (2023). Functions and substrate selectivity of diacylglycerol acyltransferases from Mortierella alpina. *Applied Microbiology and Biotechnology*, *107*(18), 5761-5774.

Li, J., Han, D., Wang, D., Ning, K., Jia, J., Wei, L., Jing X, Huang, S., Chen, J., Li, Y., Hu, Q., Xu, J. (2014). Choreography of transcriptomes and lipidomes of Nannochloropsis reveals the mechanisms of oil synthesis in microalgae. *The Plant Cell*, *26*(4), 1645-1665.

Liang, Y., Huang, Y., Liu, C., Chen, K., and Li, M. (2023). Functions and interaction of plant lipid signalling under abiotic stresses. *Plant Biology*, *25*(3), 361-378.

Li-Beisson, Y., Shorrosh, B., Beisson, F., Andersson, M. X., Arondel, V., Bates, P. D., Baud, S., Bird, D., Debono, A., Durrett, T.P., Franke, R.B., Graham, I.A., Katayama, K., Kelly, A.A., Larson, T., Markham, J.E., Miquel, M., Molina, I., Nishida, I., Rowland, O., Samuels, L., Schmid, K.M., Wada, H., Welti, R., Xu, C., Zallot, R., Ohlrogge, J. (2013). Acyl-lipid metabolism. The Arabidopsis book/American Society of Plant Biologists, 11, e0161.

Li-Beisson, Y., Thelen, J. J., Fedosejevs, E., and Harwood, J. L. (2019). The lipid biochemistry of eukaryotic algae. *Progress in lipid research*, *74*, 31-68.

Liu, B., and Benning, C. (2013). Lipid metabolism in microalgae distinguishes itself. Current opinion in biotechnology, 24(2), 300-309.

Liu, J., Han, D., Yoon, K., Hu, Q., and Li, Y. (2016). Characterization of type 2 diacylglycerol acyltransferases in Chlamydomonas reinhardtii reveals their distinct substrate specificities and functions in triacylglycerol biosynthesis. *The Plant Journal*, *86*(1), 3-19.

Liu, J., Liu, M., Pan, Y., Shi, Y., and Hu, H. (2022). Metabolic engineering of the oleaginous alga Nannochloropsis for enriching eicosapentaenoic acid in triacylglycerol by combined pulling and pushing strategies. *Metabolic Engineering*, *69*, 163-174.

Liu, Q., Siloto, R. M., Lehner, R., Stone, S. J., and Weselake, R. J. (2012). Acyl-CoA: diacylglycerol acyltransferase: molecular biology, biochemistry and biotechnology. *Progress in lipid research*, *51*(4), 350-377.

Liu, Q., Siloto, R. M., Lehner, R., Stone, S. J., and Weselake, R. J. (2012). Acyl-CoA: diacylglycerol acyltransferase: molecular biology, biochemistry and biotechnology. *Progress in lipid research*, *51*(4), 350-377.

Liu, X. Y., Ouyang, L. L., and Zhou, Z. G. (2016a). Phospholipid: diacylglycerol acyltransferase contributes to the conversion of membrane lipids into triacylglycerol in Myrmecia incisa during the nitrogen starvation stress. *Scientific Reports*, *6*(1), 26610.

Lundquist, P. K., Shivaiah, K. K., and Espinoza-Corral, R. (2020). Lipid droplets throughout the evolutionary tree. *Progress in Lipid Research*, *78*, 101029.

Ma, H., Wu, X., Wei, Z., Zhao, L., Li, Z., Liang, Q., Zheng, J., Wang, Y., Li, Y., Huang, L., Hu, Q., Han, D. (2021). Functional divergence of diacylglycerol acyltransferases in the unicellular green alga Haematococcus pluvialis. *Journal of Experimental Botany*, *72*(2), 510-524.

Maltsev, Y., Maltseva, K., Kulikovskiy, M., and Maltseva, S. (2021). Influence of light conditions on microalgae growth and content of lipids, carotenoids, and fatty acid composition. *Biology*, *10*(10), 1060.

Manoyan, J., Hakobyan, L., Samovich, T., Kozel, N., Sahakyan, N., Muravitskaya, H., Demidchik, V., Gabrielyan, L. (2024). Comparison of sulfur and nitrogen deprivation effects on photosynthetic pigments, polyphenols, photosystems activity and H2 generation in Chlorella vulgaris and Parachlorella kessleri. *International Journal of Hydrogen Energy*, *59*, 408-418.

Mao, X., Wu, T., Kou, Y., Shi, Y., Zhang, Y., and Liu, J. (2019). Characterization of type I and type II diacylglycerol acyltransferases from the emerging model alga Chlorella zofingiensis reveals their functional complementarity and engineering potential. *Biotechnology for Biofuels*, *12*(1), 28.

McFie, P. J., Chumala, P., Katselis, G. S., and Stone, S. J. (2021). DGAT2 stability is increased in response to DGAT1 inhibition in gene edited HepG2 cells. *Biochimica et Biophysica Acta (BBA)-Molecular and Cell Biology of Lipids*, *1866*(9), 158991.

Milrad, Y., Mosebach, L., and Buchert, F. (2024). Regulation of Microalgal Photosynthetic Electron Transfer. *Plants*, *13*(15), 2103.

Moog, D., Stork, S., Reislöhner, S., Grosche, C., and Maier, U. G. (2015). *In vivo* localization studies in the stramenopile alga Nannochloropsis oceanica. *Protist*, *166*(1), 161-171.

Morales, M., Aflalo, C., and Bernard, O. (2021). Microalgal lipids: A review of lipids potential and quantification for 95 phytoplankton species. *Biomass and Bioenergy*, *150*, 106108.

Murison, V., Hérault, J., Marchand, J., and Ulmann, L. (2025). Diatom triacylglycerol metabolism: from carbon fixation to lipid droplet degradation. *Biological Reviews*.

Naduthodi, M. I. S., Mohanraju, P., Südfeld, C., D'Adamo, S., Barbosa, M. J., and Van Der Oost, J. (2019). CRISPR–Cas ribonucleoprotein mediated homology-directed repair for efficient targeted genome editing in microalgae Nannochloropsis oceanica IMET1. *Biotechnology for biofuels*, *12*(1), 66.

Naduthodi, M. I. S., Suɗfeld, C., Avitzigiannis, E. K., Trevisan, N., van Lith, E., Alcaide Sancho, J., ... and van der Oost, J. (2021). Comprehensive genome engineering toolbox for microalgae Nannochloropsis oceanica based on CRISPR-Cas systems. *ACS synthetic biology*, *10*(12), 3369-3378.

Naselli-Flores, L., and Padisák, J. (2023). Ecosystem services provided by marine and freshwater phytoplankton. *Hydrobiologia*, *850*(12), 2691-2706.

Nawkarkar, P., Kapase, V. U., Chaudhary, S., Kajla, S., and Kumar, S. (2023). Heterogeneous diacylglycerol acyltransferase expression enhances lipids and PUFA in Chlorella species. *GCB Bioenergy*, *15*(10), 1240-1254.

Niu, Y. F., Zhang, M. H., Li, D. W., Yang, W. D., Liu, J. S., Bai, W. B., and Li, H. Y. (2013). Improvement of neutral lipid and polyunsaturated fatty acid biosynthesis by overexpressing a type 2 diacylglycerol acyltransferase in marine diatom Phaeodactylum tricornutum. Marine drugs, 11(11), 4558-4569.

Otaki, R., Oishi, Y., Abe, S., Fujiwara, S., and Sato, N. (2019). Regulatory carbon metabolism underlying seawater-based promotion of triacylglycerol accumulation in Chlorella kessleri. *Bioresource Technology*, *289*, 121686.

Oyama, K., Matsuwaki, I., Ito, M., Iwahori, R., Nagata, H., Nakamura, I., Kondo, A., Kodaka, A., Fuseya, Y., Yamamoto, H., Ueyama, Y., Ide, Y., Kasai, Y., Harayama, S., Kato, M., Kato, M. (2022). Limited fatty-acid supply from the plastid and active catabolism of triacylglycerol prevent the accumulation of triacylglycerol in Coccomyxa sp. strain Obi grown under nitrogen-replete conditions. *Algal Research*, *62*, 102620.

Pandey, M., Ganotra, J., Singh, A., Parchuri, P., and Giri, J. (2025). Lipid-mediated responses to nutrient and other stresses: Roles in plant adaptation and signaling. *Journal of Experimental Botany*, eraf482.

Pavia, N., Potenza, A., Hornos, F., Poveda, J. A., Gonorazky, G., Neira, J. L., Giudici, A.M., Beligni, M. V. (2025). The Diacylglycerol Acyltransferase 3 of Chlamydomonas reinhardtii Is a Disordered Protein Capable of Binding to Lipids Derived from Chloroplasts. *Biomolecules*, *15*(2), 245.

Peregrín-Alvarez, J. M., Sanford, C., and Parkinson, J. (2009). The conservation and evolutionary modularity of metabolism. *Genome biology*, *10*(6), R63.

Poliner, E., Farré, E. M., and Benning, C. (2018a). Advanced genetic tools enable synthetic biology in the oleaginous microalgae Nannochloropsis sp. *Plant cell reports*, *37*(10), 1383-1399.

Poliner, E., Pulman, J. A., Zienkiewicz, K., Childs, K., Benning, C., and Farré, E. M. (2018). A toolkit for Nannochloropsis oceanica CCMP 1779 enables gene stacking and genetic engineering of the eicosapentaenoic acid pathway for enhanced long-chain polyunsaturated fatty acid production. *Plant biotechnology journal*, *16*(1), 298-309.

Radakovits, R., Jinkerson, R. E., Darzins, A., and Posewitz, M. C. (2010). Genetic engineering of algae for enhanced biofuel production. *Eukaryotic cell*, *9*(4), 486-501.

Ratledge, C., and Wynn, J. P. (2002). The biochemistry and molecular biology of lipid accumulation in oleaginous microorganisms. *Advances in applied microbiology*, *51*, 1-52.

Remmers, I. M., D'Adamo, S., Martens, D. E., de Vos, R. C., Mumm, R., America, A. H., Cordewener, J. H.G., Bakker, L.V., Peters, S.A., Wijffels, R.H., Lamers, P. P. (2018). Orchestration of transcriptome, proteome and metabolome in the diatom Phaeodactylum tricornutum during nitrogen limitation. *Algal research*, *35*, 33-49.

Rodolfi, L., Chini Zittelli, G., Bassi, N., Padovani, G., Biondi, N., Bonini, G., and Tredici, M. R. (2009). Microalgae for oil: Strain selection, induction of lipid synthesis and outdoor mass cultivation in a low-cost photobioreactor. *Biotechnology and bioengineering*, *102*(1), 100-112.

Routaboul, J. M., Benning, C., Bechtold, N., Caboche, M., and Lepiniec, L. (1999). The TAG1 locus of Arabidopsis encodes for a diacylglycerol acyltransferase. Plant Physiology and Biochemistry, 37(11), 831-840.

Sandager, L., Gustavsson, M. H., Ståhl, U., Dahlqvist, A., Wiberg, E., Banas, A., Lenman, M., Ronne, H., Stymne, S. (2002). Storage lipid synthesis is non-essential in yeast. *Journal of Biological Chemistry*, *277*(8), 6478-6482.

Sanjaya, Miller, R., Durrett, T. P., Kosma, D. K., Lydic, T. A., Muthan, B., Koo, A.J., Bukhman, Y.V., Reid, G.E., Howe, G. A., Ohlrogge, J., Benning, C. (2013). Altered lipid composition and enhanced nutritional value of Arabidopsis leaves following introduction of an algal diacylglycerol acyltransferase 2. The Plant Cell, 25(2), 677-693.

Scarsini, M., Thiriet-Rupert, S., Veidl, B., Mondeguer, F., Hu, H., Marchand, J., and Schoefs, B. (2022). The transition toward nitrogen deprivation in diatoms requires chloroplast stand-by and deep metabolic reshuffling. *Frontiers in Plant Science*, *12*, 760516.

Shi, T. Q., Wang, L. R., Zhang, Z. X., Sun, X. M., and Huang, H. (2020). Stresses as first-line tools for enhancing lipid and carotenoid production in microalgae. *Frontiers in bioengineering and biotechnology*, *8*, 610.

Shi, X., Xiao, Y., Liu, L., Xie, Y., Ma, R., and Chen, J. (2021). Transcriptome responses of the dinoflagellate Karenia mikimotoi driven by nitrogen deficiency. *Harmful Algae*, *103*, 101977.

Simionato, D., Block, M. A., La Rocca, N., Jouhet, J., Maréchal, E., Finazzi, G., and Morosinotto, T. (2013). The response of Nannochloropsis gaditana to nitrogen starvation includes de novo biosynthesis of triacylglycerols, a decrease of chloroplast galactolipids, and reorganization of the photosynthetic apparatus. *Eukaryotic cell*, *12*(5), 665-676.

Smythers, A. L., McConnell, E. W., Lewis, H. C., Mubarek, S. N., and Hicks, L. M. (2020). Photosynthetic metabolism and nitrogen reshuffling are regulated by reversible cysteine thiol oxidation following nitrogen deprivation in chlamydomonas. *Plants*, *9*(6), 784.

Song, X., Liu, B. F., Kong, F., Ren, N. Q., and Ren, H. Y. (2022). Overview on stress-induced strategies for enhanced microalgae lipid production: Application, mechanisms and challenges. *Resources, Conservation and Recycling*, *183*, 106355.

Song, Y., Wang, F., Chen, L., and Zhang, W. (2024). Engineering fatty acid biosynthesis in microalgae: recent progress and perspectives. *Marine Drugs*, *22*(5), 216.

Sreenikethanam, A., Raj, S., Gugulothu, P., and Bajhaiya, A. K. (2022). Genetic engineering of microalgae for secondary metabolite production: Recent developments, challenges, and future prospects. *Frontiers in bioengineering and biotechnology*, *10*, 836056.

Stone, S. J., Levin, M. C., Zhou, P., Han, J., Walther, T. C., and Farese, R. V. (2009). The endoplasmic reticulum enzyme DGAT2 is found in mitochondria-associated membranes and has a mitochondrial targeting signal that promotes its association with mitochondria. *Journal of Biological Chemistry*, *284*(8), 5352-5361.

Sui, X., Wang, K., Gluchowski, N. L., Elliott, S. D., Liao, M., Walther, T. C., and Farese Jr, R. V. (2020). Structure and catalytic mechanism of a human triacylglycerol-synthesis enzyme. *Nature*, *581*(7808), 323-328.

Sui, X., Wang, K., Song, K., Xu, C., Song, J., Lee, C. W., Liao, M., Farese Jr., R. V., Walther, T. C. (2023). Mechanism of action for small-molecule inhibitors of triacylglycerol synthesis. *Nature Communications*, *14*(1), 3100.

Sun, X. M., Ren, L. J., Zhao, Q. Y., Ji, X. J., and Huang, H. (2018). Microalgae for the production of lipid and carotenoids: a review with focus on stress regulation and adaptation. *Biotechnology for biofuels*, *11*(1), 272.

Thiam, A. R., and Ikonen, E. (2021). Lipid droplet nucleation. *Trends in Cell Biology*, *31*(2), 108-118.

Tran, Q. G., Cho, K., Park, S. B., Kim, U., Lee, Y. J., and Kim, H. S. (2019). Impairment of starch biosynthesis results in elevated oxidative stress and autophagy activity in Chlamydomonas reinhardtii. *Scientific reports*, *9*(1), 9856.

Turchetto-Zolet, A. C., Maraschin, F. S., de Morais, G. L., Cagliari, A., Andrade, C. M., Margis-Pinheiro, M., and Margis, R. (2011). Evolutionary view of acyl-CoA diacylglycerol acyltransferase (DGAT), a key enzyme in neutral lipid biosynthesis. *BMC evolutionary biology*, *11*(1), 263.

Vanhercke, T., Dyer, J. M., Mullen, R. T., Kilaru, A., Rahman, M. M., Petrie, J. R., Green, A. G., Yurchenko, O., Singh, S. P. (2019). Metabolic engineering for enhanced oil in biomass. Progress in lipid research, 74, 103-129.

Van Meer, G. (2010). Membrane lipids, where they are and how they behave: Sphingolipids on the move. *The FASEB Journal*, *24*, 312-1.

Van Vooren, G., Le Grand, F., Legrand, J., Cuiné, S., Peltier, G., and Pruvost, J. (2012). Investigation of fatty acids accumulation in Nannochloropsis oculata for biodiesel application. *Bioresource Technology*, *124*, 421-432.

Vanderwaeren, L., Dok, R., Voordeckers, K., Nuyts, S., and Verstrepen, K. J. (2022). Saccharomyces cerevisiae as a model system for eukaryotic cell biology, from cell cycle control to DNA damage response. *International Journal of Molecular Sciences*, *23*(19), 11665.

Vieler, A., Wu, G., Tsai, C. H., Bullard, B., Cornish, A. J., Harvey, C., ... and Benning, C. (2012). Genome, functional gene annotation, and nuclear transformation of the heterokont oleaginous alga Nannochloropsis oceanica CCMP1779. *PLoS genetics*, *8*(11), e1003064.

Wakao, S., and Niyogi, K. K. (2021). Chlamydomonas as a model for reactive oxygen species signaling and thiol redox regulation in the green lineage. *Plant Physiology*, *187*(2), 687-698.

Walther, T. C., and Farese Jr, R. V. (2012). Lipid droplets and cellular lipid metabolism. Annual review of biochemistry, 81(1), 687-714.

Wang DongMei, W. D., Ning Kang, N. K., Li Jing, L. J., Hu JianQiang, H. J., Han DanXiang, H. D., Wang Hui, W. H., ... and Xu Jian, X. J. (2014). Nannochloropsis genomes reveal evolution of microalgal oleaginous traits.

Wang, B., and Jia, J. (2020). Photoprotection mechanisms of Nannochloropsis oceanica in response to light stress. *Algal Research*, *46*, 101784.

Wang, J., Wang, Y., Wu, Y., Fan, Y., Zhu, C., Fu, X., Chu, Y., Chen, F., Sun, H., Mou, H. (2021). Application of microalgal stress responses in industrial microalgal production systems. *Marine Drugs*, *20*(1), 30.

Wang, L., Qian, H., Nian, Y., Han, Y., Ren, Z., Zhang, H., Hu, L., Prasad, B. V. V., Laganowsky, A., Yan, N., Zhou, M. (2020). Structure and mechanism of human diacylglycerol O-acyltransferase 1. *Nature*, *581*(7808), 329-332.

Wang, M., Ye, X., Bi, H., and Shen, Z. (2024). Microalgae biofuels: illuminating the path to a sustainable future amidst challenges and opportunities. *Biotechnology for Biofuels and Bioproducts*, *17*(1), 10.

Wang, X., Fosse, H. K., Li, K., Chauton, M. S., Vadstein, O., and Reitan, K. I. (2019). Influence of nitrogen limitation on lipid accumulation and EPA and DHA content in four marine microalgae for possible use in aquafeed. *Frontiers in Marine Science*, *6*, 95.

Wei, H., Shi, Y., Ma, X., Pan, Y., Hu, H., Li, Y., Luo, M., Gerken, H., Liu, J. (2017). A type-I diacylglycerol acyltransferase modulates triacylglycerol biosynthesis and fatty acid composition in the oleaginous microalga, Nannochloropsis oceanica. *Biotechnology for biofuels*, *10*(1), 174.

Wilfling, F., Haas, J. T., Walther, T. C., and Farese Jr, R. V. (2014). Lipid droplet biogenesis. *Current opinion in cell biology*, *29*, 39-45.

Xin, Y., Lu, Y., Lee, Y. Y., Wei, L., Jia, J., Wang, Q., Wang, D., Bai, F., Hu, H., Hu, Q., Liu, J., Li, Y., Xu, J. (2017). Producing designer oils in industrial microalgae by rational modulation of co-evolving type-2 diacylglycerol acyltransferases. *Molecular plant*, *10*(12), 1523-1539.

Xin, Y., Wu, S., Miao, C., Xu, T., and Lu, Y. (2024). Towards lipid from microalgae: Products, biosynthesis, and genetic engineering. *Life*, *14*(4), 447.

Xu, K., Zou, W., Peng, B., Guo, C., and Zou, X. (2023). Lipid droplets from plants and microalgae: characteristics, extractions, and applications. *Biology*, *12*(4), 594.

Xu, Y. (2022). Biochemistry and biotechnology of lipid accumulation in the microalga Nannochloropsis oceanica. *Journal of agricultural and food chemistry*, *70*(37), 11500-11509.

Xu, Y., Falarz, L., and Chen, G. (2018). Characterization of type-2 diacylglycerol acyltransferases in the green microalga Chromochloris zofingiensis. *Journal of Agricultural and Food Chemistry*, *67*(1), 291-298.

Xue, J., Gao, H., Xue, Y., Shi, R., Liu, M., Han, L., Gao, Y., Zhou, Y., Zhang, F., Zhang, H., Jia, X., Li, R. (2022). Functional characterization of soybean diacylglycerol acyltransferase 3 in yeast and soybean. *Frontiers in Plant Science*, *13*, 854103.

Yang, Z., Zhang, M., and Du, C. (2025). A novel mechanism promoting lipid droplet formation. *Trends in Plant Science*.

Yao, H., Dahal, S., and Yang, L. (2023). Novel context-specific genome-scale modelling explores the potential of triacylglycerol production by Chlamydomonas reinhardtii. *Microbial Cell Factories*, *22*(1), 13.

Yen, C. L. E., Stone, S. J., Koliwad, S., Harris, C., and Farese Jr, R. V. (2008). Thematic review series: glycerolipids. DGAT enzymes and triacylglycerol biosynthesis. *Journal of lipid research*, *49*(11), 2283-2301.

Young, D. Y., and Shachar-Hill, Y. (2021). Large fluxes of fatty acids from membranes to triacylglycerol and back during N-deprivation and recovery in Chlamydomonas. *Plant Physiology*, *185*(3), 796-814.

Zhang, H., Zhao, L., Chen, Y., Zhu, M., Xu, Q., Wu, M., Han, D., Hu, Q. (2021). Trophic transition enhanced biomass and lipid production of the unicellular green alga Scenedesmus acuminatus. *Frontiers in Bioengineering and Biotechnology*, *9*, 638726.

Zhang, L., Wang, S., Han, J. C., Yang, G. P., Pan, K. H., and Xu, J. L. (2022). Manipulation of triacylglycerol biosynthesis in Nannochloropsis oceanica by overexpressing an Arabidopsis thaliana diacylglycerol acyltransferase gene. *Algal Research*, *61*, 102590.

Zhang, M., Fan, J., Taylor, D. C., and Ohlrogge, J. B. (2009). DGAT1 and PDAT1 acyltransferases have overlapping functions in Arabidopsis triacylglycerol biosynthesis and are essential for normal pollen and seed development. The Plant Cell, 21(12), 3885-3901.

Zhang, Y., Pan, Y., Ding, W., Hu, H., and Liu, J. (2021). Lipid production is more than doubled by manipulating a diacylglycerol acyltransferase in algae. *GCB Bioenergy*, *13*(1), 185-200.

Zhu, Z., Sun, J., Fa, Y., Liu, X., and Lindblad, P. (2022). Enhancing microalgal lipid accumulation for biofuel production. *Frontiers in microbiology*, *13*, 1024441.

Zienkiewicz, A., Zienkiewicz, K., Poliner, E., Pulman, J. A., Du, Z. Y., Stefano, G., Tsai, C. H., Horn, P., Feussner, I., Farre, E. M., Childs, K. L., Brandizzi, F., Benning, C. (2020). The microalga Nannochloropsis during transition from quiescence to autotrophy in response to nitrogen availability. *Plant physiology*, *182*(2), 819-839.

Zienkiewicz, K., and Zienkiewicz, A. (2020). Degradation of lipid droplets in plants and algae—right time, many paths, one goal. *Frontiers in Plant Science*, *11*, 579019.

Zienkiewicz, K., Benning, U., Siegler, H., and Feussner, I. (2018). The type 2 acyl-CoA: diacylglycerol acyltransferase family of the oleaginous microalga Lobosphaera incisa. *BMC Plant Biology*, *18*(1), 298.

Zienkiewicz, K., Zienkiewicz, A., Poliner, E., Du, Z. Y., Vollheyde, K., Herrfurth, C., Farré, E. M., Feussner, I., Benning, C. (2017). Nannochloropsis, a rich source of diacylglycerol acyltransferases for engineering of triacylglycerol content in different hosts. *Biotechnology for biofuels*, *10*(1), 8.

Zou, J., Wei, Y., Jako, C., Kumar, A., Selvaraj, G., and Taylor, D. C. (1999). The Arabidopsis thaliana TAG1 mutant has a mutation in a diacylglycerol acyltransferase gene. The Plant Journal, 19(6), 645-653.

Supplementary Table 1. *Nannochloropsis oceanica* CCMP1779 *DGTT* genes nucleotide and amino acid sequences.

Gene	Nucleotide sequence	Amino acid sequence
NoDGTT1	ATGTACCCAATCAAGCTGTGCTTCCTCTTCATCTTGAC AATCCCACCTTATGCTCACGTGCGCACACGTACCCCA CACAGAAGAGGCACCACAAGCAAAATGGCCAAGGCCA ACTTCCCACCCTCGGCACGCTATGTTAATATGACGCA GGTCTATGCGACAGGTGCTCACAATATGCCGGACGAG GACCGTCTCAAGGTGATGAATGGACTTTCCAAGCCCT TGACGGAGGCCAAGCCCGGTGATTTGGGGTTTGGGG ATGTGGAGTCCATGACGTTCTGTGAAGAGTTTGTAGC GATTATGTTCTTATTGATCATTGTCGGGAGCATGCTTT GGATACCGATTGCAGTGTTGGGTTTCGCCCTGTATGT CCGCAGCGCAATGGCGTGGGTGGTGATGCTCATCGTG TTCTTCACCCTGAGCCTGCACCCAGTCCCGCGCATCC ATGATATGGTTCATTCCCCATTGAATCACTTCATATTCA AGTACTTCAGTCTAAAAATGGCGAGTGATGCACCACTT GATAGTGCTGGGCGCTATATTTTTGTCGCTCCGCCAC ATGGCGTGCTGCCTATGGGGAATCTTATGACGGTGCA CGCGATGAAGGCGTGTGGTGGATTGGAGTTCCGTGG GCTGACGACTGATGTCGCGCTTAGGCTGCCTTTGTTT CGACACTATTTAGGCGCCATTGGTACTATTGCCGCGA CGAGGCACGTGGCGAAGCAGTACCTCGACAAAGGATG GTCAATAGGTATATCTTCGGGCGGAGTCGCGGAGATT TTCGAAGTTAACAATAAGGATGAGGTGGTGTTGATGA AGGAGCGAAAGGGCTTTGTGAAGCTTGCCCTTCGCAC GGGGACTCCGTTGGTAGCTTGTTATATTTTTGGGAATA CCAAGCTGTTGTCGGCGTGGTATGATGATGGGGGGGT GTTGGAGGGCCTGTCGCGTTATTTGAAATGTGGTGTA TTGCCACTTTGGGGTCGCTTTGGTTTGCCGCTTATGC ACCGTCATCCTGTATTGGGCGCGATGGCAAAGCCGAT CGTAGTTCCCAAGGTGGAGGGAGAGCCCACGCAGGA GATGATTGATGAGTACCATAGTCTCTTCTGTCAGACGC TGGTCGATCTATTTGATAGATACAAGACCTTGTATGGC TGGCCGGACAAGAAGCTGCTTATTAAGTGA	MYPIKLCFLFILTIPPYAHVRTRTPHRRG TTSKMAKANFPPSARYVNMTQVYATG AHNMPDEDRLKVMNGLSKPLTEAKPG DLGFGDVESMTFCEEFVAIMFLLIIVGS MLWIPIAVLGFALYVRSAMAWVVMLIVF FTLSLHPVPRIHDMVHSPLNHFIFKYFS LKMASDAPLDSAGRYIFVAPPHGVLPM GNLMTVHAMKACGGLEFRGLTTDVAL RLPLFRHYLGAIGTIAATRHVAKQYLDK GWSIGISSGGVAEIFEVNNKDEVVLMKE RKGFVKLALRTGTPLVACYIFGNTKLLS AWYDDGGVLEGLSRYLKCGVLPLWGR FGLPLMHRHPVLGAMAKPIVVPKVEGE PTQEMIDEYHSLFCQTLVDLFDRYKTLY GWPDKKLLIK
NoDGTT2	ATGGCTCACCTCTTCCGTCGTAGAAGCAAAGGCGAGG GCAACAGCACTAGCAGCCGCTGCTTATCTTTATCGGAA GGCAATAAGGCCATGTTAATCCTCTCATCCGAAATCGA GCCGCCCGCTTCCGCCACGTCCAAAGCCGCGACAAGC GGCATCAAAGAGATTGGGGACCCGTCATTGCCCACCG TCGCACTATTATCACTACCTAGCATAAGCAAGGCAGAT ACAAATTCCGCCACTGCTGCAGTAGCAGCAGGAACAC TGGAGGATGCAGCAGCAGGCGCCCTGACAGCTCCATT CGCCGACCGATCTGTGAAGAAGCAATACGGGCAGGAT GGTGATGGGGCGCAGTGTAAGGAGGCAGAAGGTGGA CGAAAACGCAGTGGAAGCGTTGGTAATCTCCTACTGT CTTCTATGACTTCGTTTTCTAAAGGCACGTCCCTTTCC TTCTTGACCGGCGAGGACAAGACACCGTCTCCTCCTG AGACAGGGCCTGCTGGGATTGATTTCTCGACACCGGC GCACCCAACGATGCAATTCGTGGACTTTATCATCACCT TTCTCTTGGTGCACTACATTCAAGTCTTCTACTCCCTC GTGTTCCTCTTCATCTACCTCGTCAAGCACGGTCACCG ATGGCCGTATTTCCTCGCTGCCATCTACGCGCCTTCCT ACTTCATTCCTTTGCAGCGCTTGGGGGGATGGCCGTT CAAAGGATTCATGCGCCGCCCCTTCTGGCGGTGTGTG CAGCGGACCCTTGCTCTCCAGGTGGAGAGAGAGGTTG AGCTAAGCCCGGACGAACAATACATCTTTGGTTGGCA CCCCCACGGGATCTTGCTGTTGTCCCGGTTTGCCATC TATGGGGGTCTGTGGGAGAAGCTCTTTCCGGGTATAC ATTTTAAGACGCTGGCTGCAAGTCCTCTATTTTGGATT CCACCTATTCGCGAGGTGTCGATCTTGCTGGGGGGGG TAGATGCAGGCAGGGCATCCGCAGCACGGGCGCTTAC GGACGGCTACTCCGTTTCTCTTTATCCGGGGGGAAGC AAGGAAATCTACACCACCGACCCCTACACTCCTGAAAC GACCCTGGTCCTTAAAATCCGCAAAGGCTTCATTCGCA	MAHLFRRRSKGEGNSTSSRCLSLSEG NKAMLILSSEIEPPASATSKAATSGIKEI GDPSLPTVALLSLPSISKADTNSATAAV AAGTLEDAAAGALTAPFADRSVKKQYG QDGDGAQCKEAEGGRKRSGSVGNLLL SSMTSFSKGTSLSFLTGEDKTPSPPET GPAGIDFSTPAHPTMQFVDFIITFLLVHY IQVFYSLVFLFIYLVKHGHRWPYFLAAIY APSYFIPLQRLGGWPFKGFMRRPFWR CVQRTLALQVEREVELSPDEQYIFGWH PHGILLLSRFAIYGGLWEKLFPGIHFKTL AASPLFWIPPIREVSILLGGVDAGRASA ARALTDGYSVSLYPGGSKEIYTTDPYTP ETTLVLKIRKGFIRMALRYGCALVPVYTF GEKYAYHRLGQATGFARWLLAVLKVPF LIFWGRWGTFMPLKETQVSVVVGTPLR VPKIEGEPSPEVVEEWLQKYCDEVQALF RRHKHKYAKPEEFVAIS

	TGGCCCTCCGGTATGGCTGTGCCCTTGTCCCGGTGTA CACGTTTGGAGAAAAATATGCCTATCATCGTCTAGGGC AAGCCACAGGCTTCGCGCGCTGGCTGCTGGCGGTGCT AAAAGTGCCATTTTTGATCTTTTGGGGACGATGGGGAA CGTTCATGCCGCTCAAGGAGACGCAGGTATCGGTGGT GGTGGGCACGCCGTTGCGGGTGCCCAAAATCGAGGG AGAACCCTCCCCGGAGGTGGTGGAAGAGTGGCTGCAG AAATACTGTGATGAAGTCCAAGCACTGTTCAGGCGGC ACAAGCATAAATACGCGAAGCCCGAGGAGTTCGTTGC GATCTCTTGA	
NoDGTT3	ATGGGCGCTACCACCGAGACCCAGACTAAAAAGACGT TTGTAATGCGGACAGTCGCAGTACGAAACGAGGATATA GCGCTGGAAGCAGCGACAGGAGACGGGGCAGCAGGG GATGCAACTGCTGGTGGCCTTTCACGCTCGATACTAAC AGAGGCTCCGGCGGCGTCCACTTCACTTTCATCGCGA CTGGCACCGTCCTCAGCACAAGCTTCAGCTTCGCCTA TAATGGTTCGGCCCGAAGCACGCCCCCCAGGTCTACT AGGCCGTCTACAAACGTTAGGTGCGGTGGTATTTTTG GGGCTCATGGGATCCTCGCTGTACCTAGTGATAGCGTC TGCGCTTTACATCGTGATTGGTTTCGGCGTATTGGGCC ACCGTATTTGCCCTTCGATCTTACTGGGGGTTTGGGTA GGACAAGGTCTAATTTCTGTCAAGGTGCTGCACCAAG ACCCGGAAGGTATCAAGCGGTCGTGGCTCTTCCGAGA AATGGCTAACTTTTTTGATGTGACATTGGTGATGGAGC AGAAATTGGACACTTCCAAGAAGTACTTGTTCGCACAG CATCCGCACGGTATCCTTCCTCTCGCCCCCGTGTTGTC CGCTTACTTTATCTCGGACGTGGTGCCCGGCGGAGGC AAGATTTTCTGTTTGATACATAGCGGAATGTTCTACTT GCCCATCGTCCGATTTTTCATGGGCGAATGGGGTGCG CTCCCCGCAAACAAGGAGTCTGTCGCCGAAGCCAAGC AACAAGGACAGCATTGCTCCATCGTCGTCGGCGGGGT CGCAGAGATTTTCCTTCAAAACGGAGAGACCGAACAA CTGCAACTCAGGAAGGGTTTTATTCGTGAGGCGATTC GCAACGGATATGACCTTGTGCCCATGTTCCATTTTGGA GCCACGCGCATGTATAATTTTATCGGCCCCGCCTCATT TTGGCGGTCCTTGTCAAACCGCCTGCCGTTTCCCTTC TTTCTGATTGGGGGATGGGGGAAAGGAATGACCCTGC TTCCCAAACCCGTGCGTATCGTTATTGCTGTTGGCTCA CCAATAGGTCTGGCGGCTCTGTATGGCGTGCCGGAAG GACAGTCGGTGCCTGATCCAGACCCGGCGAAGGTGGA TTTGATTTATGAGGAGTGGAAGAAGCATTTGGCAGGC CTTTATTATCGGCAGCGACCTGAGTGGGAGACGCGAG AGTTGGAGATTTGGGACTGTCCGAAGTCGTGA	MGATTETQTKKTFVMRTVAVRNEDIAL EAATGDGAAGDATAGGLSRSILTEAPAA STSLSSRLAPSSAQASASPIMVRPEARP PGLLGRLQTLGAVVFLGLMGSSLYLVIA SALYIVIGFGVLGHRICPSILLGVWVGQG LISVKVLHQDPEGIKRSWLFREMANFF DVTLVMEQKLDTSKKYLFAQHPHGILPL APVLSAYFISDVVPGGGKIFCLIHSGMF YLPIVRFFMGEWGALPANKESVAEAKQ QGQHCSIVVGGVAEIFLQNGETEQLQLR KGFIREAIRNGYDLVPMFHFGATRMYN FIGPASFWRSLSNRLPFPFFLIGGWGK GMTLLPKPVRIVIAVGSPIGLAALYGVPE GQSVPDPDPAKVDLIYEEWKKHLAGLY YRQRPEWETRELEIWDCPKS
NoDGTT4	ATGAAACGACGACGGCCCCACATAGAAAACGCACC GTCACCTGCTGCGGGAATACCACTCCCGGACGCAT CACACCGTTCCACCCTTCCGTCTCGTACCAAGACGT TCTCCATCTCCTCCTCCTACTCGTACTTCCCCACCT CATCCCTCTCCTCAAATTCCTCTGCCTCTTTCCCTA TCGCGTCATGGGCAAGGAAACCCTCCAACTTCTTTC GACGCCGGTGGAGGAAGTTCAAGCAACGTAAGTGG AGAGATCCAGCCGAGGCGAGCTCAGCATGGACCCC TGAAGGAGAGGATGACGAGGAAGAGGAAGACGACA CAGACATTGGACTTCCCCCGCCCGAACGACGTCCA CGATCCATTATTTCAATGCCAAGGCAACAGCCAATG GAAGTTGCTGCCTTCATTTCTGCTGATGCAGGTGCC GGATCACTTTCAGCAGTAGCAGCGGCAGCAGCCAC AGTCGCCTCGCGTCGTGCCAAAGAGGCAGGGGAAG CGACTGTACGGCGGCAACAACTATGGAAATTGAAG GGTTTTTTAGCGCTGTACACCACGCTACTAGTCGTG AGTTTTGCTCTTACGGTTTGGGCGGATTTGACGTGG TTGGTGCCGCAATTACTCAAGGTGTCCCTAGCACTA CAAGCGACTTCTGCCGTGTTTTTCTGCTTGGTCGTA CCTTTGACCCATTTCTCCGGGACTTTTTTCTTTCGG	MKRRRPHIENAPSPAAGIPLPDASHRS TLPSRTKTFSISSSYSYFPTSSLSSNSS ASFPIASWARKPSNFFRRRWRKFKQRK WRDPAEASSAWTPEGEDDEEEEDDTDI GLPPPERRPRSIISMPRQQPMEVAAFIS ADAGAGSLSAVAAAAATVASRRAKEAG EATVRRQQLWKLKGFLALYTTLLVVSFA LTVWADLTWLVPQLLKVSLALQATSAVF FCLVVPLTHFSGTFFFRQWRFWQPFQG GARFIVFQAISWTFYALCLVLAVCCLLF WARLAKYTFGLITSFGVFGVLSQVFMV TSLVVYERQQHKQWLRREKDEDEKMIG KKRKNEEERIEEEEKKEKKESSHLPICP STAAGGRKIPLSETAATTAAEDEEGKKN NDDGNHHVQQLQQQDEEEKAGGGLIR LLQSLYKEIFFQHHLALAIVAVGLAILAEC LWTMEEGGTVGVWGGMVEGHQKDFA RAAGLLSVLLFAVVVFSTYGIGGQVAGG REGRREGGREGRAHQKAVRKQWRFW QPFLGGAKFMLLQGLSWSFLTLSIVVEI

	CAATGGAGGTTCTGGCAGCCTTTTCAGGGCGGGGC GCGCTTCATTGTGTTCCAGGCGATTAGCTGGACGTT CTACGCCTTGTGCCTTGTCCTTGCTGTGTGTTGCTT GCTGTTTTGGGCGCGTCTGGCCAAGTACACTTTCG GCCTGATCACGTCTTTTGGTGTCTTTGGTGTGCTAT CGCAGGTTTTCATGGTGACGAGCTTGGTAGTATATG AACGACAGCAGCATAAGCAGTGGTTGCGGCGGGAG AAGGACGAGGACGAGAAGATGATAGGGAAAAAGAG AAAGAATGAGGAGGAACGGATAGAGGAAGAGGAGA AGAAGGAGAAGAAGGAATCCTCACACTTGCCGATA TGTCCATCAACAGCAGCCGGAGGACGAAAAATACC TCTCTCAGAAACGGCAGCAACAACAGCAGCGGAGG ACGAGGAAGGAAAAAAGAACAACGATGACGGCAAT CACCATGTGCAGCAGCTGCAACAACAAGATGAAGA AGAAAAAGCAGGTGGAGGATTGATCCGTCTGCTTC AAAGTCTGTACAAAGAGATATTTTTCCAGCATCACT TGGCCTTGGCAATCGTGGCCGTGGGCCTGGCCATA CTGGCGGAGTGTCTATGGACGATGGAGGAGGGGGG AACGGTGGGAGTGTGGGGTGGGATGGTTGAGGGTC ATCAAAAGGATTTCGCAAGGGCCGCAGGACTGCTG TCGGTGTTGTTGTTTGCTGTTGTTGTCTTTAGCACG TACGGGATAGGTGGACAGGTGGCTGGTGGAAGGGA GGGAAGGCGAGAGGGAGGGAGGGAAGGTAGAGCG CACCAAAAGGCCGTACGAAAGCAATGGCGCTTTTG GCAGCCATTTTTAGGAGGGGCCAAGTTTATGCTATT GCAGGGATTAAGCTGGTCTTTTTTGACGCTGTCCAT TGTGGTAGAAATCTTGTTTGTTATCTCGACGTTTGC GGTGGGGTTTGAGTTGTTTGTGGGAGCGGCTGTGG TAGCGGGCGGCTTCTTTTTGGTCTCGGAAGTGTTG ATGATTGTGAGCTTGCATTTTTACATGCCTACGACG ACTACGACTGTGACCACTACGGGATTGACGGTGAT GGAGAAGAAGGTGGAGGAGGTGGAGGAGATGTTGG TGGAGAGGGAGGGAGTGGAGAAGGACGAGATGATG ATGGAGGAAAAGGTGGACGTGACGACAGCGGCGAC GACAAACGCTCTCCTAAGAACCGGAAAGCAGCGGC TGCTCTTGGCCAAAGAAAGTGCTACGACAACTACTA CTACCGTGACAATGACCACGGAGCAGACCAGCAAG ACGTCTACTTCATTTATGCCTGTCCGGGTCGACGAG GCTTCCCTTGAGCAATTCCGCCGGCTCACCGTTATA ACCGTTCTGAGCAACATGCAATACCTGCCCTTCCTC CTTCCCATCCTTCCCTTTATTCTCTCCGGTCTCCCT CTCCCTGTGGCATCTTTGCACTGGTTCGGGGCTTTT TGTTGTCTGACATCAGCAGTCGTTTTGAATGCCTAT GTCAAAACCACGTTGGCCAAAGCGGGGCATCGTCT TAACTCCTTCCAGCGCTCCCTTCTTCATGCCCTCCC CTCGCTCATTTATGCAGCCCCGGGCGTTATTTGCTT TTTTGCGTGGAAGCAACACCAAGGTGGGAGGGGGG ACGGGAAGCAGGGCGCGGTGTCCGCGTTCCCGGCT TGGGCGGTGCTCACGGCCATGCATTATCTGTACCT TTTTCTCACGTTTCGCGGAAAACCGGAAGTGACGG GAGAGAGATATTTGGGCGAAAAGTTAGAGTTGTGG AAAGGCGGTTGGTCTCTTTACTATTTTTTGGAAGGG ATAGATCAATATTTTCAGGCGAGGTTTGTTTTTATG GACCCGAATCTGGATCTGAAGGGGAAACCGCATGT GTTGGCGTTTCACCCGCATGGAGTTCAGCCATTTAC GACGTGTTGGATTCAACTTTCGCGGGCCTGGAGAG AGGGGGTGGGGAAAGGACAGAGGTTTTGTGTAATG ACTGCGAGTGTCATGCACTATGTGCCTTTGATGCGC GATATTCTACAGTGGCTCGGGGGGCGGGAAGTGAG CAGGGAAGCCATTTCGTACGCACTGGGCCGTCGAG AGTCTGTGCTATTGGTCCCAGGCGGACAGCAAGAG ATGATGGAGTCCCAATCTCAGATGGGCGAAATTCG GATCATCACGAAGCACGTCGGCTTTATTAGATTAGC GCTCCAAACAGGCGCACCGCTCGTGCCTGTGCTCT CATTTGGCGAAGTTGAAGTGATGGACTTTGTCCGGT	LFVISTFAVGFELFVGAAVVAGGFFLVSE VLMIVSLHFYMPTTTTTVTTTGLTVME KKVEEVEEMLVEREGVEKDEMMMEEK VDVTTAATTNALLRTGKQRLLLAKESAT TTTTTVTMTTEQTSKTSTSFMPVRVDE ASLEQFRRLTVITVLSNMQYLPFLLPILP FILSGLPLPVASLHWFGAFCCLTSAVVL NAYVKTTLAKAGHRLNSFQRSLLHALP SLIYAAPGVICFFAWKQHQGGRGDGKQ GAVSAFPAWAVLTAMHYLYLFLTFRGKP EVTGERYLGEKLELWKGGWSLYYFLEGI DQYFQARFVFMDPNLDLKGKPHVLAF HPHGVQPFTTCWIQLSRAWREGVGKG QRFCVMTASVMHYVPLMRDILQWLGG REVSREAISYALGRRESVLLVPGGQQEM MESQSQMGEIRIITKHVGFIRLALQTGA PLVPVLSFGEVEVMDFVRYPRLQRFFIS RIGIPVPFFPYGLFGFPIPRPVPVTVVFG RPIPVEKVEQPTQEEVRKLSKKYFESIQ EVFDKNKTEALGHGNHRLVLL

	ACCCGCGTCTACAGCGTTTCTTTATCTCGCGCATTG GTATCCCGGTTCCCTTCTTTCCATACGGATTGTTTG GATTTCCCATCCCGAGGCCCGTGCCCGTGACGGTC GTATTTGGCCGGCCCATTCCAGTGGAGAAGGTTGA GCAGCCGACGCAGGAAGAGGTTCGAAAATTGTCGA AAAAGTACTTTGAAAGTATTCAGGAGGTGTTTGATA AAAATAAGACTGAGGCCCTAGGGCATGGGAATCAT AGGCTGGTCCTGTTGTAA	
NoDGTT5	ATGACGCCGCAAGCCGACATCACCAGCAAGACGACAC CCAACCTCAAGACGGCTGCGTCATCCCCCTCCAAGAC CTCGCCCGCCCCCTCCGTTCAATACAAGGCGGCGAAT GGCAAGGTGATCACGGTGGCCATGGCCGAGCAAGAC GACGGGAACATGGGCATTTTCCGCGAGTGTTTTGCAA TGGTGACAATGGGCATAATTATGTCGTGGTATTACAT CGTCGTCATTCTCTCCCTCCTCTGCTTGGTGGGGATC TGCATCTTCCCTGCCTGGCGGGCGGTAGCGGCCACG GTTTTTGTGCTTATGTGGAGTGCGGCGCTATTGCCGC TTGACTACCAGGGATGGGATGCTTTCTGCAACTCCTT TATCTTCAGGCTGTGGCGGGACTACTTCCACTATGAA TACGTCCTGGAGGAGATGATCGACCCAAACAAGCGCT ACCTCTTTGCTGAGATGCCTCACGGTATCTTCCCCTG GGGAGAGGTGATTTCCATTTCGATCACCAAACAGCTT TTTCCCGGGAGCCGCGTAGGCTCCATCGGTGCGAGTG TCATCTTCCTCCTTCCCGGTCTCAGGCACTTCTTCGC TTGGATCGGGTGTCGGCCCGCGAGCCCAGAGAACATC AAAAAGATTTTTGAGGATGGGCAGGACTGTGCCGTGA CGGTGGGGGGGGTCGCCGAGATGTTTCTAGTCGGAG GAGACAAGGAACGACTGTACCTGAAGAAGCACAAGGG TTTCGTTCGAGAAGCCATGAAGAATGGGGCGGACCTG GTTCCTGTCTTCTGCTTCGGCAACAGCAAACTGTTCA ATGTGGTGGGGGAGAGCAGTCGGGTTTCTATGGGCCT GATGAAGCGCCTCTCAAGGAGGATTAAGGCCAGCGTC CTCATCTTTTACGGCCGTCTCTTCCTGCCCATTCCGA TTCGACACCCGCTCTTGTTCGTGGTGGGGAAGCCCCT GCCGGTCGTGCACAAGGCAGAGCCGACCAAGGAGGA GATCGCGGCAACGCACGCACTCTTTTGCGAGAAGGTC GAGGAGCTTTACTACAAATACAGGCCGGAGTGGGAGA CGCGCCCGTTGTCCATTGAGTAA	MTPQADITSKTTPNLKTAASSPSKTSP APSVQYKAANGKVITVAMAEQDDGNM GIFRECFAMVTMGIIMSWYYIVVILSLLC LVGICIFPAWRAVAATVFVLMWSAALLP LDYQGWDAFCNSFIFRLWRDYFHYEYV LEEMIDPNKRYLFAEMPHGIFPWGEVIS ISITKQLFPGSRVGSIGASVIFLLPGLRHF FAWIGCRPASPENIKKIFEDGQDCAVTV GGVAEMFLVGGDKERLYLKKHKGFVRE AMKNGADLVPVFCFGNSKLFNVVGES SRVSMGLMKRLSRRIKASVLIFYGRLFL PIPIRHPLLFVVGKPLPVVHKAEPTKEEI AATHALFCEKVEELYYKYRPEWETRPL SIE
NoDGTT6	ATGTCCTCCTTCTTGCGTTGGCCTCGTCGCTCCAGGA CTCCTAAACGTACTGCCGCTGCACCTCCCACCGCAGC AGGCACCACGGCCACCATCCTGTGCGATGGCCTGCGC CTTGACAGCAGCAGCAGTAGCATCAACGCCAGCAGTA GCAGTGACAGCAACGTCGACAGCAAGACCGAATCGAT GGGGAGCAGCACCGACGAGAGCCCCCCGACTTCCCC CCAGACCACCTCCAAAGCTCTCACGCTCACCCTTGGC GACGTCTGCCCCGGCACTCGCCTAACCTTGCCTTGGT GGGAAGAAGCACTGCTCCTCCCCTGCTTCGTTGTGCT GTGTGCCCCCATCTTTTCATTTATGATGCTTGGCCTAT CGTTTGTGCCATTTTTCGGGTGGGTGAGGGCCAGCAC TAGCTACCTCTCCGCATTCTCCTTCTACTGGGTCCTGC TATACTTCGACCTCGTCCCTCGCCGGGAACGCCTTAGT CCTCCCTGCCTCTCTACCTGGTTCCTGCGGGCCATGG TGCGGTACTTCAACTATTTTGTCATTGTCGAAGATCCT TCCTCCATCCAGCCCTCCACTCCCTACATCGGTGTGCA GAGCCCGCACGGCATTTATCCCATTGCAAGCGTCTGT GCCGCTCCCTTCAGCCCCAGTCTCTTCCGAGGCCGCG ATTCATATTGTATGGCGGCGTCGGCGTTGCAGTTGCAG CCTTTTTTGTGGCAATGGCTGGAGACACTGGGGGGGC GACCGATATCGGCGGCAGGGATCATGAAGGTGGTGGA GCAGGGAGACGTATGTTGTATTCTACCGGGAGGAATC GCAGAAATGTTCATGCTGGATCCATCAAACGAGACGGA GAAGGTCCTGATTCGACGGGGTTTCATACGCGAAGCG TTGAAGAACCGTGTGGATATCATCCCGATGTATCACTT	MSSFLRWPRRSRTPKRTAAAPPTAAG TTATILCDGLRLDSSSSSINASSSSDSN VDSKTESMGSSTDESPPTSPQTTSKAL TLTLGDVCPGTRLTLPWWEEALLLPCF VVLCAPIFSFMMLGLSFVPFFGWVRAS TSYLSAFSFYWVLLYFDLVPRRERLSPP CLSTWFLRAMVRYFNYFVIVEDPSSIQP STPYIGVQSPHGIYPIASVCAAPFSPSLF RGRDSYCMAASALQLQPFLWQWLETL GGRPISAAGIMKVVEQGDVCCILPGGIA EMFMLDPSNETEKVLIRRGFIREALKNR VDIIPMYHFNHTQTFSYILPPSLNELLAT VCRKSGLPGCFLIGRWGLFVPHKVKMF SVVGRPIQVRRRHCSSSSSSSSSCKNN SGNGKIPGTEDGRAKKVGMEGEKYEPT EEEIEAVVVEYKEALRRIYYTFRPADGQR ELVLVDNQKGNSASSSSSSSSSSSSSS SSSSSGKNNSH

	TAACCACACGCAGACGTTCAGCTACATCCTTCCTCCTT CGCTCAATGAACTGTTGGCAACCGTGTGTCGGAAGAG TGGGTTGCCTGGCTGCTTTTTGATCGGACGATGGGGA TTATTTGTCCCTCATAAGGTCAAGATGTTCTCGGTTGT GGGGAGGCCGATTCAGGTGCGGCGACGCCACTGCAG CAGCAGCAGCAGCAGCAGCAGCAGCTGCAAAAACAAC AGTGGGAATGGGAAGATTCCGGGGACGGAGGATGGAA GGGCGAAGAAGGTAGGCATGGAGGGAGAGAAGTATGA GCCAACGGAGGAGGAGATTGAGGCAGTGGTTGTGGAG TACAAGGAGGCACTACGCCGCATTTATTACACTTTTCG ACCGGCGGATGGACAGCGGGAGCTGGTGCTGGTGGAT AACCAGAAGGGGAATAGCGCTAGCAGCAGCAGCAGCA GCAGCAGCAGCAGCAGCAGCAGCAGCAGCAGCAGCA GTAGCAGCGGTAAGAATAATAGCCATTAG	
NoDGTT7	ATGTTGCTGGCGTCGTCTCGGCGGCCGGCATCGTCCT TGGTGGATCCTTTGCCATTAACGGGGAAACTGCCTAC CGGGGCAATCAGGCTTTTCACGTCCCGGCCTGCTTCC TGGCGTACAACTCCCATGGTGGTGGGCGGGTCCTTGC TGGTGGTGGGATCATTCGTCTGGGTACCCCTAGTTAT CTGGCTGGGTTGGAGGAAATGTGAGACACGGAAGCG ACGCATCATCTATGTCCTTGTTTTGTGTGTTGTTCTGA CTCTACCTACACGACGGTGGGACGCGGTGGTCTTGAA CGGCCTCTGGAGCCGTTTTGTGGAATATTTTTCAGTC GAGGTGGTGGGGGACGACCCCTTGCCCAAGGACCGC TCTGCGGTCTACGCCGTCATTCCTCACGGCACCTTCC CCTTTGGTCTCGGCGTGGTCTCCCTCGGTCCCTTGAA CAAGATCTTCAATAAGGTTCGGCCCGTGGTGGCCTCG GCCGTCTTGCGCTTTCCGGGCTTCGGCCAACTTATAG GCTTCGCCGGCGGGGTAGATGCAGGGCCTAATGAAG TAAGCAAGGCCATCAAGGAGGGCTGTTCAGTGAGTAT CTGTCCGGGGGGCATCGCAGAGATGTTCTGGGGATAT CCAAAGGAGGGCTGCTTACCGCGGGAGGAATACGCG TTCTTGCAGTCGAGGAAAGGGTTTATACGAATGGCCA TGAAACATAATGTGCCTGTGATCCCTGTATACTGTTTT GGTAACACCCATGCGATGCATAAGGCTAAGACGCCTT GGGTCTTGGAGGCGCTCTCAAGGCTTCTGAAGACCTC TCTCATATTGACTTGGGGCCGGTGGGGGCTGCCCATT CCCTACCGTGTGCCTCTCCTCTATGCCGTCGGCAAGC CCCTCCACCTCCTGCATGCTGAAAATCCAACCCCTGG TCAGATTGAGGTGGCGCACGCCGAGTTCTGCAGGGC CCTTTCGGATTTGTTCGATCGGTACAAGTTTTATTATG GATGGGGGCACAAGACGCTTCGCATCGTCTGA	MLLASSRRPASSLVDPLPLTGKLPTGAI RLFTSRPASWRTTPMVVGGSLLVVGSF VWVPLVIWLGWRKCETRKRRIIYVLVLC VVLTLPTRRWDAVVLNGLWSRFVEYFS VEVVGDDPLPKDRSAVYAVIPHGTFPF GLGVVSLGPLNKIFNKVRPVVASAVLRF PGFGQLIGFAGGVDAGPNEVSKAIKEGC SVSICPGGIAEMFWGYPKEGCLPREEY AFLQSRKGFIRMAMKHNVPVIPVYCFG NTHAMHKAKTPWVLEALSRLLKTSLIL TWGRWGLPIPYRVPLLYAVGKPLHLLH AENPTPGQIEVAHAEFCRALSDLFDRYK FYYGWGHKTLRIV
NoDGTT8	ATGACATCCTCCCCACCAGCCTCACCATCTGCACCTGA GAATCCCTATAACCTATTGCCACCTAAGCGGCCAAATC CGCAGTACTGGCGGTATGCAAGCCTGGCCGCTTTCAT TCTCATTTGCTTCCAAGCCCCTTCAAGTGACTCGTGGG GCACCGCCCTCCGCCGCGCCTGCTGGGCGGCGTACT GGATGACCTACCTGGACACAAGCTATAAGGATGGCTCA CGGGCCTGGCCCTGGTTTCAGCGCTTAAGGATCTGGC GTTTGTACTGCGGCTATTTACAGGGCAAAGTAATTTGT ACGGTGCCCTTGGACCCGGCACAGCAATTCATCTTCG CAGCTCATCCCCACGGCATTGGCACCTGGAATCATTTT CTAACCATGACTGACGGCTGTCGCTTCCTCTCCTCATC CTACCCCCGCCCGCGGCTCGACCTGGGTGCGACGGTA CTTTTCTTCATCCCCTTCTTAAAGGAAATTCTGCTCTG GCTGGGCTGTGTGGATGCTGGAGCGTCCACGGCCCAC GCAATCTTGGCGCGGGGCTACTCATCCCTCATTTACAT TGGTGGAGAAAAGGAGCAGATTTTAACGCAGCGAGGC AAAGACATCGTGGTGGTACGTCCCCGCAAGGGTTTTT GCAGGCTGGCCCTGCAACATGACTGCCCCATCGTACC CGTCTACGCGTTTGGGGAGAACGATCTCTATCGCACAT TCAACCACCTGAAGGACGTCCAACTGTGGGTGGCCAG CACCTTCCAGCTGGCTTTTCCTCCTTGTTGGGGCGTC	MTSSPPASPSAPENPYNLLPPKRPNPQ YWRYASLAAFILICFQAPSSDSWGTALR RACWAAYWMTYLDTSYKDGSRAWPW FQRLRIWRLYCGYLQGKVICTVPLDPAQ QFIFAAHPHGIGTWNHFLTMTDGCRFL SSSYPRPRLDLGATVLFFIPFLKEILLWL GCVDAGASTAHAILARGYSSLIYIGGEK EQILTQRGKDIVVVRPRKGFCRLALQHD CPIVPVYAFGENDLYRTFNHLKDVQLW VASTFQLAFPPCWGVPFLPFLPLPVPV TVVMGEPLRPRTGEGKEGRAGGEKGV KPTREEVDELHTRYVEALQRLFDAHKG RHGGRSEEATLVVR

	CCCTTCCTCCCCTTCCTCCCTCTGCCAGTCCCCGTCA CGGTGGTGATGGGCGAACCCTTGCGGCCCAGAACAGG AGAAGGAAAGGAGGGAAGGGCTGGTGGAGAAAAAGG AGTGAAGCCCACAAGGGAGGAGGTGGACGAGCTGCA CACCCGGTACGTGGAGGCCCTGCAGAGGTTGTTCGAC GCACACAAGGGCAGGCACGGGGGGAGGAGCGAAGAG GCCACCTTAGTGGTCAGGTGA	
NoDGTT9	ATGGCCACAACCTCGTCGCCTAAACATCCTCCGCAGTA CTTCCCTTGTCACGCTCGTCCGGTCCCAACTCCATACC TCAACTTACACAAAACCCCTCCTCCTTCAACCCCAACC ACGCAGCCTGATCTGAAGGAACGCCTTATTGGGGGGT TACTCCTCGCTTCGCTAATCCATGTATGGCTCTTTGGT GTCATCGTTGTACCCTTGGCCATGTACCAGTTGCTGGC ACAGGGCGACTACCGCATCGCCCTTGGCCTCCTCCTT TATTACGCCTACCGCTCGGTCTTTCCGACGAAGGAATG GGGCATCGTTCGCAACATCTATAGAGCAGGCAACCGAT ATTTCTACCCACAAGAGGTCATTTTTGATGGCTTCAAT GAGATCAAACCCGATTCGAGGTCATTGATTTGCATGCA CCCGCACGGGATCTTGACGATTGGTTGGGCGTTGACC AGCACGAGTCCGACCATGGCGCACGCCAACGTGAAGT GGCTGGTGACAGAAGCTTTGTTGCGGCTGCCTTTTAT CAGCGACTTCCTCTCCTGGAACGGTTGTGCACACGCC AGCAAGAGCTACATGCAAAATCGTATGACGAAGGGTG CGAATCTTGCTCTGCTCCCCGGCGGATTTGAAGAGGC TTCTCTCTATCAACGCAACACTTATCGTGTTTACGTCA GAAAGCGCACAGGCTTTATTGTGTATGCCCTCAGGTAT GGGTACAAGATTTACCCATCGTTCGTCTTTGGGGAGG AAAAGTGTTATTTCTCCTTGATACCCGACTGGGGTTGG CTGACAGCGACCAGGTTATGGTTGAACCAGTACCGGA TACCGGCAGTTGCGTTCGTCGGAAAGTTATTTTTGGTT CCTGGTTGGGATTCACATTTGATAACGGTGATCGGCGC CCCCGTGGTGTTGCCGAGGCTGGACAAGCCGACTGAG GAGGAGGTGGGGAAATACCATTTAATGTATGTGAGTGC ATTGATGGAATTATTCGAGAAGCACAAACGGCAATATT GTGAAAAGGGGGCGAAGTTGGAGTTGTGGTAG	MATTSSPKHPPQYFPCHARPVPTPYL NLHKTPPPSTPTTQPDLKERLIGGLLLA SLIHVWLFGVIVVPLAMYQLLAQGDYRI ALGLLLYYAYRSVFPTKEWGIVRNIYRA GNRYFYPQEVIFDGFNEIKPDSRSLICM HPHGILTIGWALTSTSPTMAHANVKWL VTEALLRLPFISDFLSWNGCAHASKSY MQNRMTKGANLALLPGGFEEASLYQR NTYRVYVRKRTGFIVYALRYGYKIYPSF VFGEEKCYFSLIPDWGWLTATRLWLNQ YRIPAVAFVGKLFLVPGWDSHLITVIGAP VVLPRLDKPTEEEVGKYHLMYVSALME LFEKHKRQYCEKGAKLELW
NoDGTT11	ATGGGTCTATTTGGCAGTGGGATCATCGAGCAGCAAG AGCAGGCGAAGCTGAAGCAGAAACCGTCTCCGCTGCG GGAGCTCAAGGGAGGCAATAAAAGCAGCAAGCACAAG GAACCCCTGACGCCCTCCAGTAATCTGAGGCCGGCCC GCTCCCCGACCGAGGTAGACTGGAGCTCTTTTCCCGA GGGCAGCTACACGCGCTTCGGGCATGGCGGGGATTGG TGGACGCTGATCAAGGGGACGATAGCCATTTTGTTCA CGTGGGGAACCTGGCTGGCCGGCGGCTTGTCTCCCGT TTGGATGACTTGGTTGTTTTGGCACGGATACAAAAAGA CGTTTTATTCGATCTTGGGCCCTTTGCTCTATCCGCTT TTGTTGCCAGTGCCGGCCTGGCCTGGATTCGTCCGAT TCATTCTAAACATGGCTGGGTATTTTGAGGGCGGTGCA GCGATGTACGTTGAAAACTCCTTCAAAGGCCGCAACG TGAACGGCCCTATCATGTTGGCCATGCATCCCCACGG CATCATGCCTCACTCTTTCCTTCTCAACGGTGCCGGGC GGATCCACGCGCAGAAACCAGAGGTATTCCTCCCTCC ACACTATCAAGATATGTCTCTCAAATCGACGGGCGTAG CGGAGCCTTTGTTGTTTCGGATTCCGTTTATCTCGGCG TTTCTATACTTTTTCGGATGTGCCGAACCAGCGTCAAA GGAGATGATGCACGACATCTTGGGGAGGCAGGTGCCG TTTGGGATTCTGGTTGGTGGCTCAGAAGAAATTCTCCT CATGGAGTACCAGAAGGAAAACATCTACATCCTGGAAC GCAAAGGCTTCATCAAATACGCCCTCCAACACGGCTAC ACCATTGCTATTGGCTATCTGTTCGGGGAATCCAACCT CTACCACACCATCACCTGGGGCCGCAAGACCCGCCTC GCTCTCTTCAAAAAATTCAAGATCCCCCTCTTCTTGGC TTGGGGGCGTTGGTTCTTCCCCTTACTTCCTGAGCGA GCCGCGCCTTTGAATGCTGTCGTAGGTAACCCGATAG	MGLFGSGIIEQQEQAKLKQKPSPLRELK GGNKSSKHKEPLTPSSNLRPARSPTEV DWSSFPEGSYTRFGHGGDWWTLIKGT IAILFTWGTWLAGGLSPVWMTWLFWH GYKKTFYSILGPLLYPLLLPVPAWPGFV RFILNMAGYFEGGAAMYVENSFKGRN VNGPIMLAMHPHGIMPHSFLLNGAGRI HAQKPEVFLPPHYQDMSLKSTGVAEPL LFRIPFISAFLYFFGCAEPASKEMMHDIL GRQVPFGILVGGSEEILLMEYQKENIYIL ERKGFIKYALQHGYTIAIGYLFGESNLYH TITWGRKTRLALFKKFKIPLFLAWGRW FFPLLPERAAPLNAVVGNPIDLPRVANP SQADIDKYMRCTLRS

	ATTTGCCCAGGGTAGCTAACCCAAGCCAGGCCGACAT TGACAAATACATGCGTTGTACATTGAGAAGTTGACAGA CTTGTTCGAACGGAATAAGGCGGCCTTCGGGTATTCT GATCGGACGTTGAATTTCTTTTAG	
NoDGTT12	ATGCATCCTCTAACAGGTGCTATGAAGAAAATCTTGCG CATCCCGGAGTCGCCCATCTCGGACGACACCCTGGTG AAGAATGGAGGCAAGAAGACCGAGCTCTCCACGCCGG TCACCGCTCCTACGTCGGACCGCACGCGCATCTACAG TGATGGCTATTCGACCCCCAAGTCCTACACATTGGAAG TCGATCCAAAATTTTACAAGCGAGTATGTGATGCTGAC GATGTGTGGACACGCACACAGGGGGCCTTTGCTCTCC TCATGCTCTGGGGCGTTTGGCTTGCCGGGTCCTTTTC TGTGTTTTGGTGGCCCTATTTAGTAATGAAGGGGTACT ACACTGCAGCCCTTGTCATGGCAGTGATCATGGCATAT CCGTATGTTGTCAAGGTCAAGCAAAGCCCGGCATTTAT TCGGTTCATCTTGAGCGGCGCGGGTTGGTTTAAGGGC GGGACTTGTTTGTATTTGGAGGAGTCGATGAAGCAGA TCGACACCAGCGAGTCTGTCCTCCTCTGCCAGCATCC GCACGGTCTCTTCACCTACGGCTTCATTCAGAACGGG TCCGCCGCCCGCATCGATGCCCGCAAACCAGAGGTTT ATGTGCCTGCCGCATTTCGTCACATGAAACCCAACGCC AAGGCCTTCGTGGAGCCCTTGCTTTTCAAAATCCCGC TCATCCGTCACTTCATTACCGCCTTCGGCAATGCCGCT CCGGCGACAAAGAAAGAAATGCACCGGCTCATGTCCA CCAAAATTCCCCTGGGGCTTCTACCCGGTGGGTCGGA AGAGATCATACTAAGCCACCACGGCCATGAGCGGGCC TACATACTTAAACGGAAAGGCTTCCTCAAGTACGCATT ACAACATGGCTACACGATTTGCATTGGATACACGTTCG GGGAGTCCGACTCGTACCGCACCTTGGACTGGGGCGT GAAGTTTCGTATGTGGTATCTGAAAACCTTCCGTGTTC CACTTTTCGCGTGCTGGGGGATTTGGTGGTGTCCCCT CTTGCCGCGGGGGCAGGTGGCGCTTGAGACAGTCGTT GGGAACCCGTTTCGGTTGCCCAAGATCTCAGATCCGA GCCAGGAGGATATTGACAAGTGGCATGCGGTGTATGT GCAAAAACTTGTGGATCTGTTTGATCGGAACAAAGCCA AGTTCGGGTATGGGGACAGGGAGCTGGAGCTTTATTA G	MHPLTGAMKKILRIPESPISDDTLVKNG GKKTELSTPVTAPTSDRTRIYSDGYSTP KSYTLEVDPKFYKRVCDADDVWTRTQ GAFALLMLWGVWLAGSFSVFWWPYLV MKGYYTAALVMAVIMAYPYVVKVKQSP AFIRFILSGAGWFKGGTCLYLEESMKQI DTSESVLLCQHPHGLFTYGFIQNGSAA RIDARKPEVYVPAAFRHMKPNAKAFVE PLLFKIPLIRHFITAFGNAAPATKKEMHR LMSTKIPLGLLPGGSEEIILSHHGHERAY ILKRKGFLKYALQHGYTICIGYTFGESDS YRTLDWGVKFRMWYLKTFRVPLFACW GIWWCPLLPRGQVALETVVGNPFRLPK ISDPSQEDIDKWHAVYVQKLVDLFDRN KAKFGYGDRELELY